INSIGHTS IN CARDIOVASCULAR THERAPEUTICS: 2021

EDITED BY: Xiaofeng Yang
PUBLISHED IN: Frontiers in Cardiovascular Medicine

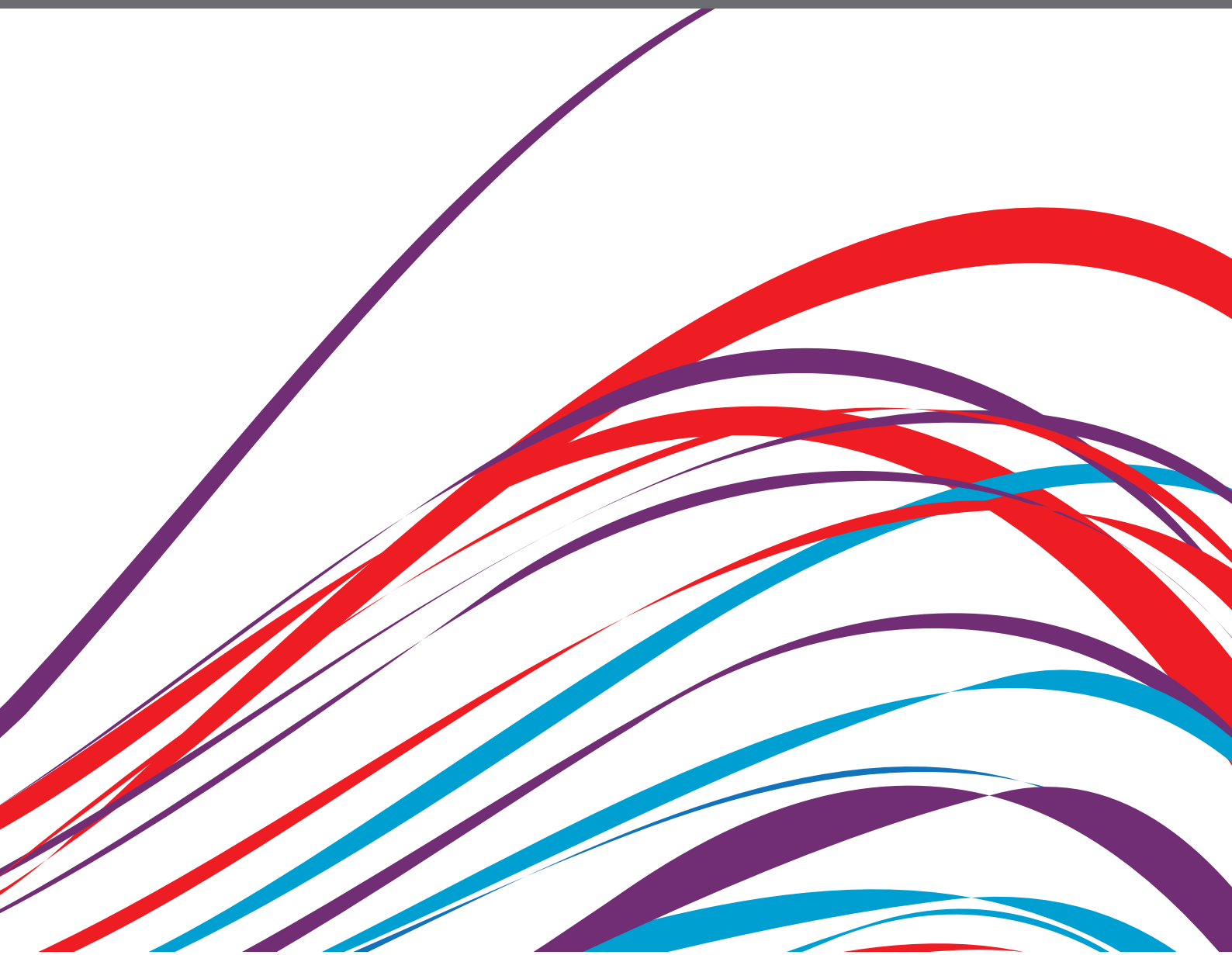

frontiers Research Topics

ISSN 1664-8714
ISBN 978-2-88976-870-7
DOI 10.3389/978-2-88976-870-7

About Frontiers

Frontiers is more than just an open-access publisher of scholarly articles: it is a pioneering approach to the world of academia, radically improving the way scholarly research is managed. The grand vision of Frontiers is a world where all people have an equal opportunity to seek, share and generate knowledge. Frontiers provides immediate and permanent online open access to all its publications, but this alone is not enough to realize our grand goals.

Frontiers Journal Series

The Frontiers Journal Series is a multi-tier and interdisciplinary set of open-access, online journals, promising a paradigm shift from the current review, selection and dissemination processes in academic publishing. All Frontiers journals are driven by researchers for researchers; therefore, they constitute a service to the scholarly community. At the same time, the Frontiers Journal Series operates on a revolutionary invention, the tiered publishing system, initially addressing specific communities of scholars, and gradually climbing up to broader public understanding, thus serving the interests of the lay society, too.

Dedication to Quality

Each Frontiers article is a landmark of the highest quality, thanks to genuinely collaborative interactions between authors and review editors, who include some of the world's best academicians. Research must be certified by peers before entering a stream of knowledge that may eventually reach the public - and shape society; therefore, Frontiers only applies the most rigorous and unbiased reviews.
Frontiers revolutionizes research publishing by freely delivering the most outstanding research, evaluated with no bias from both the academic and social point of view. By applying the most advanced information technologies, Frontiers is catapulting scholarly publishing into a new generation.

What are Frontiers Research Topics?

Frontiers Research Topics are very popular trademarks of the Frontiers Journals Series: they are collections of at least ten articles, all centered on a particular subject. With their unique mix of varied contributions from Original Research to Review Articles, Frontiers Research Topics unify the most influential researchers, the latest key findings and historical advances in a hot research area! Find out more on how to host your own Frontiers Research Topic or contribute to one as an author by contacting the Frontiers Editorial Office: frontiersin.org/about/contact

INSIGHTS IN CARDIOVASCULAR THERAPEUTICS: 2021

Topic Editor:
Xiaofeng Yang, Temple University, United States

Citation: Yang, X., ed. (2022). Insights in Cardiovascular Therapeutics: 2021. Lausanne: Frontiers Media SA.
doi: 10.3389/978-2-88976-870-7

Table of Contents

frontiers | Frontiers in Cardiovascular Medicine

TYPE Editorial
PUBLISHED 26 July 2022
DOI 10.3389/fcvm.2022.981544

OPEN ACCESS

EDITED AND REVIEWED BY
Masanori Aikawa,
Harvard Medical School, United States

*CORRESPONDENCE
Xiaofeng Yang
xfyang@temple.edu

SPECIALTY SECTION
This article was submitted to Cardiovascular Therapeutics, a section of the journal Frontiers in Cardiovascular Medicine

RECEIVED 29 June 2022
ACCEPTED 11 July 2022
PUBLISHED 26 July 2022

CITATION
Xu K, Khan M, Yu J, Snyder NW, Wu S, Vazquez-Padron RI, Wang H and Yang X (2022) Editorial: Insights in cardiovascular therapeutics: 2021 – cell death, cardiovascular injuries, and novel targets of cardiovascular therapeutics.
Front. Cardiovasc. Med. 9:981544.
doi: 10.3389/fcvm.2022.981544

Editorial: Insights in cardiovascular therapeutics: 2021 – cell death, cardiovascular injuries, and novel targets of cardiovascular therapeutics

Keman Xu[1], Mohsin Khan[2], Jun Yu[2], Nathaniel W. Snyder[2], Sheng Wu[2], Roberto I. Vazquez-Padron[3], Hong Wang[2] and Xiaofeng Yang[1,2]*

[1]Departments of Cardiovascular Sciences and Biomedical Education and Data Sciences, Cardiovascular Research Center, Lewis Katz School of Medicine, Temple University, Philadelphia, PA, United States, [2]Departments of Cardiovascular Sciences and Biomendical Education and Data Sciences, Centers for Metabolic Disease Research, Lewis Katz School of Medicine, Temple University, Philadelphia, PA, United States, [3]DeWitt Daughtry Family Department of Surgery, Leonard M. Miller School of Medicine, University of Miami, Miami, FL, United States

KEYWORDS

cell death, cardiovascular injuries, novel targets, cardiovascular therapeutics, inflammation

Editorial on the Research Topic
Insights in cardiovascular therapeutics: 2021

Introduction

With the effort and support of the authors, editorial office, and editorial team, the Frontiers in Cardiovascular Medicine, Cardiovascular Therapeutics Section-Research Topic "*Insights in Cardiovascular Therapeutics: 2021*" has achieved great success and is attracting interest from the cardiovascular community. Here, we spotlight 12 studies published in our section that related to cell death and cardiovascular injuries, as well as some recent advances in the field that have tremendous potential in cardiovascular therapy. In addition, these highlights may serve as the foundation for some new developments in our Cardiovascular Therapeutics areas. In 2022, we will keep working to create a fantastic platform for cardiologists, translational cardiovascular scientists, and cardiovascular pharmacological scientists to share new results and data in clinical cardiology and translational cardiovascular therapeutics.

Cell death and heart diseases

Cardiovascular diseases (CVDs) are the leading cause of morbidity and mortality worldwide. An estimated 17.9 million people live with CVDs each year with no effective cures (1). Therefore, studying the pathogenesis of heart diseases and identifying potential therapies are critical. Programmed cell death is an essential but generally detrimental

process in CVD development. Cardiomyocytes are terminally differentiated, have a limited division capacity, and serve vital functions. The death of cardiomyocytes affects hearts' ability to contract and causes adverse remodeling, and eventually lead to cardiac dysfunction and heart failure.Hence, cell death that leads to the loss of cardiomyocytes is a significant phase in the pathogenesis of cardiac diseases. Therefore, strongly suggesting that targeting cell death processes as a therapeutic approach to alleviate and reverse cardiomyopathy is a viable therapeutic strategy (2–4). In this editorial we will discuss a common molecular pathological theme related to research progresses in CVDs including heart failure reported by Wu et al., Liao et al., and Dash et al., atrial fibrillation reported by Lee et al. and Zheng Wang et al., refractory angina reported by Ambari et al., In-stent restenosis reported by Zhu et al., critical limb ischemia reported by Quiroz et al., protein conformational diseases reported by Zheng Song et al., mitochondrial dysfunction reported by Chen et al., and myocardial injury reported by Barbieri et al. and Cao et al.

In recent decades, new mechanisms that orchestrate various cell death pathways have been discovered, and this field continues to expand. The current well-established forms of cell death pathways include intrinsic or extrinsic apoptosis, necroptosis, pyroptosis, ferroptosis, mitochondrial permeability transition (MPT)-driven necrosis, autophagic cell death (autosis), lysosome-dependent cell death, immunogenic cell death (5), cellular senescence, parthanatos, mitotic catastrophe, neutrophil extracellular trap (NET)otic cell death, entosis (6, 7), anoikis (8), oxelptosis, and alkaliptosis (9). From a physiological point of view, cell death helps an organism develop, impacts morphogenesis and maintains homeostasis (10). However, pathological cell death is triggered when cells are subjected to various stimuli, including heart failure (11), myocardial injury, ischemia, ventricular remodeling (12), elevated troponins (13), energy production failure, oxidative damage, and imbalanced ion fluxes (14). As a result, pathological cell death does not maintain homeostasis but instead promotes disease progression.

Apoptosis is the most characterized form of cell death in various cardiovascular diseases. It is characterized by a process of cellular self-destruction without inflammation (15). Although apoptosis is the most studied form of cell death, few apoptotic myocytes are observed in patients with heart failure since 80–250 myocytes are found to undergo apoptosis per 1 x 10^5 myocytes (2). Moreover, immunologically silent apoptosis cannot be used to explain why vasculature or myocytes injury always accompanies the excessive inflammation and immune cell infiltration during cardiac disease progression. Another five death mechanisms have been identified in heart diseases, including necroptosis, mitochondrial-mediated necrosis, pyroptosis, ferroptosis, and autophagic cell death. Among them, lytic programmed cell death, such as necroptosis and pyroptosis (16–22), has historically received the most attention. The lytic programmed cell death pathway causes cell death by making a pore on the plasma membrane. These mechanisms of cell death are associated with release damage/danger-associated molecular patterns (DAMPs) and inflammatory cytokines, which leads to inflammation (23).

Lytic programmed cell death and its role in inflammation of heart diseases

Inflammation plays an essential role in all types of cardiac diseases. The vasculature experiences inflammation as a reaction to lipid peroxidation, damage, and possibly infection. Studies in epidemiology and medicine have consistently and strongly linked the risk of cardiovascular events to inflammation (24). In contrast, the absence of inflammatory properties of apoptosis allows us to understand the importance of lytic cell death in cardiovascular diseases (25). Previous studies reported that lysophosphatidylcholine (LPC) and oxidized low-density lipoprotein (oxLDL) induce Nod-like receptor family 3 (NLRP3) and promote endothelial cell activation (26–28) in cardiac diseases (29). Further, the activation of caspase-1 canonical inflammasome pathway and caspase-4 (human)/ caspase-11 (mice) noncanonical inflammasome pathway will lead to gasdermin D cleavage and N-terminal gasdermin D protein pore formation on the plasma membrane, which could mediate endothelial pyroptosis during atherosclerosis development (30–32). In addition to pyroptosis, necroptosis, and mitochondrially mediated necrosis are the other common cell death pathways observed in heart diseases. Necroptosis is characterized by cellular enlargement, degradation of plasma membrane integrity, DAMPs release (33), and inflammation. Necroptosis could be activated when serine/threonine kinase receptor protein kinases (RIPK) 1 binds to and activates RIPK3. Then, the activated RIPK3 further activates a pseudokinase, which leads mixed lineage kinase-like domain (MLKL) phosphorylation. Phosphorylated MLKL translocates from cytosol to plasma membrane, promoting necroptotic cell death (34). Necroptosis implicated in the pathogenesis of many heart diseases. In this Research Topic, Wu et al. reported that RIPK1-RIPK3-MLKL mediated necroptosis contributes to catecholamine-induced heart failure. Moreover, necroptosis is also related to mitochondrial-mediated necrosis. RIPK1, RIPK3, and MLKL have been shown to translocate to the mitochondrial membrane during necroptosis to promote mitochondrial dysfunction, mitochondrial reactive oxygen species (mtROS) production (35–40), and cell damage (34). Chen et al. in this Research Topic demonstrated that intracellular mitochondrial transfer has been discovered in cardiovascular diseases. In pathological situations, injured cells seek recipient cells for assistance by transferring defective mitochondria; and recipient cells accept "foreign" functional mitochondria to reduce injury. Therefore, mitochondrial-targeted therapies could be a potential menthod to treat diseases. In addition to the activity of individual cell death pathways in cardiac diseases, a growing number of

TABLE 1 Summary for 12 highlighted studies in Insights in cardiovascular therapeutics: 2021.

Disease/Patient condition	Research objectives	Therapy/therapeutic targets	Reference
Heart failure	To investigate whether necroptosis is involved in beta-adrenergic stimulation-induced cardiomyocytes injury.	RIPK1/ RIPK3 inhibitors could be used for anti-inflammatory treatments.	PMID: 34604361
Heart failure and reduced ejection fraction (HFrEF)	To investigate the cost-effectiveness of additional empagliflozin in HFrEF compared to conventional therapy alone from the standpoint of the Asia-Pacific healthcare systems.	Addition of empagliflozin to HFrEF treatment is expected to be a cost effective option among Asia-Pacific countries.	PMID: 34778407
Atrial fibrillation (AF), chronic kidney disease (CKD), coronary artery disease (CAD)	Real-world data are used to assess the efficacy and safety of antithrombotic regimens in the population with concomitant CKD, AF, and CAD.	Direct oral anticoagulants showed more favorable outcomes than warfarin.	PMID: 34692798
Refractory angina (RA), coronary artery disease (CAD)	This study seeks to assess the impact of ECP therapy on flow-sensitive miR-92a, VEGF-A, and VEGFR-2, which are markers of angiogenesis in RA patients.	External counterpulsation (ECP) may improve angiogenesis by preserving the expression of VEGF-A and VEGFR-2. No significant increased miR-92a between ECP and the control group.	PMID: 34760951
In-stent restenosis (ISR), drug-eluting stents (DES), DES-ISR	To compare the angiographic and clinical results of the two most successful therapies for the patients with DES-ISR: drug-eluting balloons (DCB) and DES.	For the patients with DES-ISR, treatment with DES, especially NG-DES/EES could reduce the risk of TLR significantly compared to DCB at long-term follow-up.	PMID: 34926617
Mitochondrial dysfunction in cardiac diseases in general	This review paper summarizes the mechanism of mitochondria transfer in the cardiovascular system and outlined donor mitochondria's fate and functional role.	EVs-based mitochondrial delivery and the polymer-coated delivery system might become a more feasible and promising strategic alternative for mitochondrial transplantation.	PMID: 34901230
Atrial fibrillation (AF)	The incidence, risk predictors, and probable mechanisms of silent cerebral embolisms (SCEs) in patients with AF ablation and the potential impact of robotic magnetic navigation on SCE rates.	AF ablation carries a low risk of symptomatic cerebral ischemia but is associated with a substantial risk of SCEs.	PMID: 34926624
Heart failure, HIV	Try to find the molecular causes of the high death rate of heart failure in HIV patients.	Glycolysis byproduct methylglyoxal (MG) increased with the time of HIV infection.	PMID: 34970611
COVID-19 patients with ST-segment-elevation myocardial infarction (STEMI)	To assess the effects of RAAS-inhibitors on the clinical outcomes and in-hospital mortality of STEMI patients during the COVID-19 pandemic.	The potential benefit of ACEi/ARB discontinuation in patients with COVID-19 may be overcome by its detrimental effect.	PMID: 35004902
Protein conformational diseases	Chaperones can be used to restore intracellular protein homeostasis. Chemical chaperones improve the treatment efficiency of protein conformational diseases.	Lumacaftor (LUM) is an excellent chemical chaperone to correct specific mutants.	PMID: 35282377
Critical limb ischemia (CLI), peripheral arterial disease (PAD)	Cell-adhesion molecule plays a vital role in angiogenesis and wound healing. To increase their therapeutic profile, the authors creates a viral vector to overexpress E-selectin on mesenchymal stem cells (MSCs).	This innovative cell therapy confers increased limb reperfusion, neovascularization, improved functional recovery, decreased muscle atrophy.	PMID: 35174227
Sleep deprivation (SD), myocardial injury	To study the protective effect of stem-leaf saponins from Panax notoginseng (SLSP) on myocardial injury in SD mice.	SLSP exerted cardiac protection in SD mice by inhibiting aberrant autophagy and apoptosis through the PI3K/Akt/mTOR signaling pathway.	PMID: 35071373

studies indicate crosstalk between three types of cell death of pyroptosis, apoptosis, and necroptosis, which is termed as PANoptosis. PANoptosis is a pro-inflammatory programmed cell death (PCD) pathway and has initially discovered in response to viral infections. Following infection with a virus such as influenza A virus (IAV), a master regulator of PANoptosis, Z-DNA-binding protein 1 (ZBP1) (41, 42), interacts with RIPK3 via RIP homotypic interaction motif (RHIM) domains and forms a multimeric protein complex, PANoptosome. This single multimeric complex can concurrently activate NLRP3-dependent pyroptosis, Caspase-8-dependent apoptosis, and MLKL-dependent necroptosis (43). It is believed that simultaneous activation of the three PCDs and PANoptosome formation indicate PANoptosis occurrence. PANoptosis can elicit dramatic host inflammation in response to IAV infection or severe acute respiratory syndrome coronavirus 2 (SARS-CoV-2) infection (22), resulting in severe lung tissue damage and other lethal consequences (44). PANoptosis is not limited to virus infection but participates in other diseases including stroke, traumatic brain injury, atherosclerosis, and cancer (45). Although there is not currently much data on the involvement in PANoptosis in heart diseases, the significance of this death pathway warrants future investigation.

Potential therapeutic studies in cardiovascular diseases

Medical experts and scientists have long searched for potential cardiac disease treatments and surviving and improving patients' lives. The Frontiers in Cardiovascular Medicine -Cardiovascular Therapeutics section has provided a platform for distinguished scientists to communicate, inspire, and seek more potential therapeutic solutions (46, 47). In Table 1, we summarized 12 significant studies Wu et al., Zheng et al., Wang et al., Liao et al., Dash et al., Lee et al., Ambari et al., Zhu et al., Quiroz et al., Zheng Song et al., Chen et al., Barbieri et al., and Cao et al. on our Research Topic to illustrate the cutting-edge treatments for different cardiovascular diseases. Readers could use Table 1 as an outline to dig out their interests.

Author contributions

KX carried out literature collections, research analyses, and drafted the manuscript. MK, JY, NS, SW, RV-P, and HW provided editing input. XY supervised and edited the manuscript. All authors listed have made a substantial, direct, and intellectual contribution to the work and approved it for publication.

Funding

This work was supported by the National Institutes of Health Grants to XY (HL132399-01A1; HL138749-01; and HL147565-01), HW (DK104116; DK113775; and HL131460), JY (HL153599), MK (HL135177), and America Heart Association Award to KX (916828).

Conflict of interest

The authors declare that the research was conducted in the absence of any commercial or financial relationships that could be construed as a potential conflict of interest.

Publisher's note

All claims expressed in this article are solely those of the authors and do not necessarily represent those of their affiliated organizations, or those of the publisher, the editors and the reviewers. Any product that may be evaluated in this article, or claim that may be made by its manufacturer, is not guaranteed or endorsed by the publisher.

References

1. Khan T. Cardiovascular disease. (2022). doi: 10.1002/jcla.24354. Available online at: https://www.who.int/news-room/fact-sheets/detail/cardiovascular-diseases-(cvds)#:~:text=Cardiovascular%20diseases%20(CVDs)%20are%20the,%2D%20and%20middle%2Dincome%20countries

2. Mishra PK, Adameova A, Hill JA, Baines CP, Kang PM, Downey JM, et al. Guidelines for evaluating myocardial cell death. *Am J Physiol Heart Circ Physiol.* (2019) 317:H891–H922. doi: 10.1152/ajpheart.00259.2019

3. Kepp O, Galluzzi L, Lipinski M, Yuan J Kroemer G. Cell death assays for drug discovery. *Nat Rev Drug Discov.* (2011) 10:221–37. doi: 10.1038/nrd3373

4. Mery B, Guy JB, Vallard A, Espenel S, Ardail D, Rodriguez-Lafrasse C, et al. In vitro cell death determination for drug discovery: a landscape review of real issues. *J Cell Death.* (2017) 10:1179670717691251. doi: 10.1177/1179670717691251

5. Jiang M, Zeng J, Zhao L, Zhang M, Ma J, Guan X Zhang W. Chemotherapeutic drug-induced immunogenic cell death for nanomedicine-based cancer chemo-immunotherapy. *Nanoscale.* (2021) 13:17218–35. doi: 10.1039/D1NR05512G

6. Galluzzi L, Vitale I, Aaronson SA, Abrams JM, Adam D, Agostinis P, et al. Molecular mechanisms of cell death: recommendations of the nomenclature committee on cell death 2018. *Cell Death Differ.* (2018) 25:486–541. doi: 10.1038/s41418-017-0012-4

7. Martens MD, Karch J Gordon JW. The molecular mosaic of regulated cell death in the cardiovascular system. *Biochim Biophys Acta Mol Basis Dis.* (2022) 1868:166297. doi: 10.1016/j.bbadis.2021.166297

8. Liao M, Qin R, Huang W, Zhu HP, Peng F, Han B Liu B. Targeting regulated cell death (RCD) with small-molecule compounds in triple-negative breast cancer:

a revisited perspective from molecular mechanisms to targeted therapies. *J Hematol Oncol.* (2022) 15:44. doi: 10.1186/s13045-022-01260-0

9. Tang D, Kang R, Berghe TV, Vandenabeele P Kroemer G. The molecular machinery of regulated cell death. *Cell Res.* (2019) 29:347–364. doi: 10.1038/s41422-019-0164-5

10. Vaux DL. Cell death in development. *Cell.* (1999) 96:245–54. doi: 10.1016/S0092-8674(00)80564-4

11. Zeglinski MR, Moghadam AR, Ande SR, Sheikholeslami K, Mokarram P, Sepehri Z, et al. Myocardial cell signaling during the transition to heart failure: cellular signaling and therapeutic approaches. *Compr Physiol.* (2018) 9:75–125. doi: 10.1002/cphy.c170053

12. Canty JM, Jr. Myocardial injury, troponin release, and cardiomyocyte death in brief ischemia, failure, and ventricular remodeling. *Am J Physiol Heart Circ Physiol.* (2022) 323:H1–H15. doi: 10.1152/ajpheart.00093.2022

13. Chaulin AM. Cardiac troponins metabolism: from biochemical mechanisms to clinical practice (literature review). *Int J Mol Sci.* (2021) 22:10928. doi: 10.3390/ijms222010928

14. Blomgren K, Leist M Groc L. Pathological apoptosis in the developing brain. *Apoptosis.* (2007) 12:993–1010. doi: 10.1007/s10495-007-0754-4

15. Sauler M, Bazan IS Lee PJ. Cell death in the lung: the apoptosis-necroptosis axis. *Annu Rev Physiol.* (2019) 81:375–402. doi: 10.1146/annurev-physiol-020518-114320

16. Yang XF, Yin Y Wang H. Vascular inflammation and atherogenesis are activated via receptors for pamps and suppressed by regulatory t cells. *Drug Discov Today Ther Strateg.* (2008) 5:125–42. doi: 10.1016/j.ddstr.2008.11.003

17. Li Y-F, Xiao Huang, Xinyuan Li, Ren Gong, Ying Yin, Jun Nelson, et al. Caspase-1 mediates hyperlipidemia-weakened progenitor cell vessel repair. *Front Biosci.* (2015) 20:178–91. doi: 10.2741/4383

18. Wang L, Fu H, Nanayakkara G, Li Y, Shao Y, Johnson C, et al. Novel extracellular and nuclear caspase-1 and inflammasomes propagate inflammation and regulate gene expression: a comprehensive database mining study. *J Hematol Oncol.* (2016) 9:122. doi: 10.1186/s13045-016-0351-5

19. Xi H, Zhang Y, Xu Y, Yang WY, Jiang X, Sha X, et al. Caspase-1 inflammasome activation mediates homocysteine-induced pyrop-apoptosis in endothelial cells. *Circ Res.* (2016) 118:1525–39. doi: 10.1161/CIRCRESAHA.116.308501

20. Li YF, Nanayakkara G, Sun Y, Li X, Wang L, Cueto R, et al. Analyses of caspase-1-regulated transcriptomes in various tissues lead to identification of novel IL-1beta-, IL-18- and sirtuin-1-independent pathways. *J Hematol Oncol.* (2017) 10:40. doi: 10.1186/s13045-017-0406-2

21. Fagenson AM, Xu K, Saaoud F, Nanayakkara G, Jhala NC, Liu L, et al. Liver ischemia reperfusion injury, enhanced by trained immunity, is attenuated in caspase 1/caspase 11 double gene knockout mice. *Pathogens.* (2020) 9:879. doi: 10.3390/pathogens9110879

22. Shao Y, Saredy J, Xu K, Sun Y, Saaoud F, Drummer CT, et al. Endothelial immunity trained by coronavirus infections, DAMP stimulations and regulated by anti-oxidant NRF2 may contribute to inflammations, myelopoiesis, COVID-19 cytokine storms and thromboembolism. *Front Immunol.* (2021) 12:653110. doi: 10.3389/fimmu.2021.653110

23. Bedient L, Pokharel SM, Chiok KR, Mohanty I, Beach SS, Miura TA Bose S. Lytic cell death mechanisms in human respiratory syncytial virus-infected macrophages: roles of pyroptosis and necroptosis. *Viruses.* (2020) 12:932. doi: 10.3390/v12090932

24. Ridker JTWaPM. Inflammation as a cardiovascular risk factor. *Circulation.* (2004) 109:II-2–II-10. doi: 10.1161/01.CIR.0000129535.04194.38

25. Wang J, Lai B, Nanayakkara G, Yang Q, Sun Y, Lu Y, et al. Experimental data-mining analyses reveal new roles of low-intensity ultrasound in differentiating cell death regulatome in cancer and non-cancer cells via potential modulation of chromatin long-range interactions. *Front Oncol.* (2019) 9:600. doi: 10.3389/fonc.2019.00600

26. Drummer Ct, Saaoud F, Shao Y, Sun Y, Xu K, Lu Y, et al. Trained immunity and reactivity of macrophages and endothelial cells. *Arterioscler Thromb Vasc Biol.* (2021) 41:1032–46. doi: 10.1161/ATVBAHA.120.315452

27. Zhong C, Yang X, Feng Y Yu J. Trained immunity: an underlying driver of inflammatory atherosclerosis. *Front Immunol.* (2020) 11:284. doi: 10.3389/fimmu.2020.00284

28. Xu K, Saaoud F, Yu S, Drummer Ct, Shao Y, Sun Y, et al. Monocyte adhesion assays for detecting endothelial cell activation in vascular inflammation and atherosclerosis. *Methods Mol Biol.* (2022) 2419:169–82. doi: 10.1007/978-1-0716-1924-7_10

29. Lu Y, Nanayakkara G, Sun Y, Liu L, Xu K, Drummer Ct, et al. Procaspase-1 patrolled to the nucleus of proatherogenic lipid LPC-activated human aortic endothelial cells induces ROS promoter CYP1B1 and strong inflammation. *Redox Biol.* (2021) 47:102142. doi: 10.1016/j.redox.2021.102142

30. Yin Y, Li X, Sha X, Xi H, Li YF, Shao Y, et al. Early hyperlipidemia promotes endothelial activation via a caspase-1-sirtuin 1 pathway. *Arterioscler Thromb Vasc Biol.* (2015) 35:804–16. doi: 10.1161/ATVBAHA.115.305282

31. Yang Q, Nanayakkara GK, Drummer C, Sun Y, Johnson C, Cueto R, et al. Low-Intensity ultrasound-induced anti-inflammatory effects are mediated by several new mechanisms including gene induction, immunosuppressor cell promotion, and enhancement of exosome biogenesis and docking. *Front Physiol.* (2017) 8:818. doi: 10.3389/fphys.2017.00818

32. Xu K, Shao Y, Saaoud F, Gillespie A, Drummer Ct, Liu L, et al. Novel knowledge-based transcriptomic profiling of lipid lysophosphatidylinositol-induced endothelial cell activation. *Front Cardiovasc Med.* (2021) 8:773473. doi: 10.3389/fcvm.2021.773473

33. Wang X, Li YF, Nanayakkara G, Shao Y, Liang B, Cole L, et al. Lysophospholipid receptors, as novel conditional danger receptors and homeostatic receptors modulate inflammation-novel paradigm and therapeutic potential. *J Cardiovasc Transl Res.* (2016) 9:343–59. doi: 10.1007/s12265-016-9700-6

34. Guo X, Chen Y Liu Q. Necroptosis in heart disease: molecular mechanisms and therapeutic implications. *J Mol Cell Cardiol.* (2022) 169:74–83. doi: 10.1016/j.yjmcc.2022.05.006

35. Li X, Fang P, Li Y, Kuo YM, Andrews AJ, Nanayakkara G, et al. Mitochondrial reactive oxygen species mediate lysophosphatidylcholine-induced endothelial cell activation. *Arterioscler Thromb Vasc Biol.* (2016) 36:1090–100. doi: 10.1161/ATVBAHA.115.306964

36. Li X, Shao Y, Sha X, Fang P, Kuo YM, Andrews AJ, et al. IL-35 (Interleukin-35) suppresses endothelial cell activation by inhibiting mitochondrial reactive oxygen species-mediated site-specific acetylation of H3K14 (Histone 3 Lysine 14). *Arterioscler Thromb Vasc Biol.* (2018) 38:599–609. doi: 10.1161/ATVBAHA.117.310626

37. Sun Y, Lu Y, Saredy J, Wang X, Drummer Iv C, Shao Y, et al. ROS systems are a new integrated network for sensing homeostasis and alarming stresses in organelle metabolic processes. *Redox Biol.* (2020) 37:101696. doi: 10.1016/j.redox.2020.101696

38. Li X, Fang P, Yang WY, Chan K, Lavallee M, Xu K, et al. Mitochondrial ROS, uncoupled from ATP synthesis, determine endothelial activation for both physiological recruitment of patrolling cells and pathological recruitment of inflammatory cells. *Can J Physiol Pharmacol.* (2017) 95:247–52. doi: 10.1139/cjpp-2016-0515

39. Cheng J, Nanayakkara G, Shao Y, Cueto R, Wang L, Yang WY, et al. Mitochondrial proton leak plays a critical role in pathogenesis of cardiovascular diseases. *Adv Exp Med Biol.* (2017) 982:359–70. doi: 10.1007/978-3-319-55330-6_20

40. Nanayakkara GK, Wang H Yang X. Proton leak regulates mitochondrial reactive oxygen species generation in endothelial cell activation and inflammation-a novel concept. *Arch Biochem Biophys.* (2019) 662:68–74. doi: 10.1016/j.abb.2018.12.002

41. Karki R, Lee S, Mall R, Pandian N, Wang Y, Sharma BR, et al. ZBP1-dependent inflammatory cell death, PANoptosis, and cytokine storm disrupt IFN therapeutic efficacy during coronavirus infection. *Sci Immunol.* (2022) 2022:eabo6294. doi: 10.1126/sciimmunol.abo6294

42. Yuan F, Cai J, Wu J, Tang Y, Zhao K, Liang F, et al. Z-DNA binding protein 1 promotes heatstroke-induced cell death. *Science.* (2022) 376:609–15. doi: 10.1126/science.abg5251

43. Christgen S, Place DE Kanneganti TD. Toward targeting inflammasomes: insights into their regulation and activation. *Cell Res.* (2020) 30:315–27. doi: 10.1038/s41422-020-0295-8

44. Karki R, Sharma BR, Tuladhar S, Williams EP, Zalduondo L, Samir P, et al. Synergism of TNF-alpha and IFN-gamma Triggers Inflammatory cell death, tissue damage, and mortality in SARS-CoV-2 infection and cytokine shock syndromes. *Cell.* (2021) 184:149–168 e17. doi: 10.1016/j.cell.2020.11.025

45. Samir P, Malireddi RKS Kanneganti TD. The PANoptosome: a deadly protein complex driving pyroptosis, apoptosis, and necroptosis (PANoptosis). *Front Cell Infect Microbiol.* (2020) 10:238. doi: 10.3389/fcimb.2020.00238

46. Diepstraten ST, Anderson MA, Czabotar PE, Lessene G, Strasser A Kelly GL. The manipulation of apoptosis for cancer therapy using BH3-mimetic drugs. *Nat Rev Cancer.* (2022) 22:45–64. doi: 10.1038/s41568-021-00407-4

47. Heusch G. Myocardial ischaemia-reperfusion injury and cardioprotection in perspective. *Nat Rev Cardiol.* (2020) 17:773–89. doi: 10.1038/s41569-020-0403-y

frontiers in Cardiovascular Medicine

ORIGINAL RESEARCH
published: 16 September 2021
doi: 10.3389/fcvm.2021.740839

Catecholamine Surges Cause Cardiomyocyte Necroptosis *via* a RIPK1–RIPK3-Dependent Pathway in Mice

Penglong Wu[1,2†], *Mingqi Cai*[1], *Jinbao Liu*[2] *and Xuejun Wang*[1*]

[1] *Division of Basic Biomedical Sciences, University of South Dakota Sanford School of Medicine, Vermillion, SD, United States,* [2] *Guangzhou Municipal and Guangdong Provincial Key Laboratory of Protein Modification and Degradation, State Key Laboratory of Respiratory Disease, School of Basic Medical Sciences, Affiliated Cancer Hospital of Guangzhou Medical University, Guangzhou, China*

OPEN ACCESS

Edited by:
Jun Yu,
Temple University, United States

Reviewed by:
Jiliang Zhou,
Georgia Health Sciences University, United States
Keman Xu,
Temple University, United States

***Correspondence:**
Xuejun Wang
xuejun.wang@usd.edu

†Present address:
Penglong Wu,
Department of Cardiology, Xiamen Cardiovascular Hospital, Xiamen University, Xiamen, China

Specialty section:
This article was submitted to Cardiovascular Therapeutics, a section of the journal Frontiers in Cardiovascular Medicine

Received: *13 July 2021*
Accepted: *16 August 2021*
Published: *16 September 2021*

Citation:
Wu P, Cai M, Liu J and Wang X (2021) Catecholamine Surges Cause Cardiomyocyte Necroptosis via a RIPK1–RIPK3-Dependent Pathway in Mice. Front. Cardiovasc. Med. 8:740839. doi: 10.3389/fcvm.2021.740839

Background: Catecholamine surges and resultant excessive β-adrenergic stimulation occur in a broad spectrum of diseases. Excessive β-adrenergic stimulation causes cardiomyocyte necrosis, but the underlying mechanism remains obscure. Necroptosis, a major form of regulated necrosis mediated by RIPK3-centered pathways, is implicated in heart failure; however, it remains unknown whether excessive β-adrenergic stimulation-induced cardiac injury involves necroptosis. Hence, we conducted the present study to address these critical gaps.

Methods and Results: Two consecutive daily injections of isoproterenol (ISO; 85 mg/kg, s.c.) or saline were administered to adult mixed-sex mice. At 24 h after the second ISO injection, cardiac area with Evans blue dye (EBD) uptake and myocardial protein levels of CD45, RIPK1, Ser166-phosphorylated RIPK1, RIPK3, and Ser345-phosphorylated MLKL (p-MLKL) were significantly greater, while Ser321-phosphorylated RIPK1 was significantly lower, in the ISO-treated than in saline-treated wild-type (WT) mice. The ISO-induced increase of EBD uptake was markedly less in *RIPK3*$^{-/-}$ mice compared with WT mice ($p = 0.016$). Pretreatment with the RIPK1-selective inhibitor necrostatin-1 diminished ISO-induced increases in RIPK3 and p-MLKL in WT mice and significantly attenuated ISO-induced increases of EBD uptake in WT but not RIPK3$^{-/-}$ mice.

Conclusions: A large proportion of cardiomyocyte necrosis induced by excessive β-adrenergic stimulation belongs to necroptosis and is mediated by a RIPK1–RIPK3-dependent pathway, identifying RIPK1 and RIPK3 as potential therapeutic targets for catecholamine surges.

Keywords: necroptosis, RIPK1, RIPK3, isoproterenol, cardiomyocyte, mice, catecholamine surge, COVID-19

INTRODUCTION

In response to physical (e.g., cardiac failure and stroke) or emotional stressors, the sympathetic nervous system and the hypothalamic–pituitary–adrenal axis become hyperactive and give rise to catecholamine surges and cardiac injury (1–3). Catecholamine surges can also occur in some of the less common clinical conditions. For example, in patients with pheochromocytoma or paraganglioma, the chromaffin cells in the tumor can secrete large amounts of adrenalin or norepinephrine into the circulation, causing hypertension, cardiac injury, and damages to other organ systems (4–6); patients with Irukandji syndrome that is caused by the sting of a type of jellyfish show symptoms of catecholamine surges (7). Catecholamine surges can also result from clinical treatment (8). The catecholamine surge condition most relevant to the current COVID-19 pandemic is arguably Takotsubo syndrome, which is often triggered by psychological and physical stressors. Takotsubo cardiomyopathy, also known as broken heart syndrome or stress cardiomyopathy, can occur in COVID-19 patients (9–11). Catecholamine surges have been proposed as an important pathogenic factor for Takotsubo cardiomyopathy, including the one associated with COVID-19 (12). Interestingly, Jabri et al. reported that the incidence of Takotsubo cardiomyopathy diagnosed in patients with acute coronary syndrome (ACS) during the COVID-19 pandemic (between March 1 and April 30, 2020) in the northeast Ohio area rose to 7.8%, compared with multiple control groups of patients with ACS presenting before the pandemic across four distinct timelines, which had showed incidences ranging from 1.5 to 1.8% (13), suggesting that psychological stress associated with the COVID-19 pandemic may increase the incidence of Takotsubo cardiomyopathy even in non-COVID-19 patients. Therefore, a better understanding of the pathogenic mechanism of catecholamine surges will help advance the pathophysiology of a broad spectrum of human diseases.

Cardiac injury has long been observed in diseases associated with catecholamine surges. As highlighted by Watkins in a review article published in 1957 (14), myocardial fibrosis and inflammatory responses were observed in patients suffering from pheochromocytoma, a rare but treacherous catecholamine-producing tumor. More than a century ago, intravenous injections of adrenalin were shown to induce myocarditis and the morphological features of cardiomyocyte degeneration and necrosis in rabbits (15). In late 1950s, Rona et al. reported an infarct-like myocardial lesion produced by subcutaneous injections of a synthetic catecholamine isoproterenol (ISO) in rats (16, 17), which recapitulates many aspects of myocardial lesions previously described for patients with pheochromocytoma or paraganglioma (5, 18). Subsequently, the induction of cardiomyocyte necrosis in rats or mice by two consecutive daily injections of high dosage ISO was used by many as a non-invasive method to model acute myocardial injury or even model myocardial infarction (MI) (19–21). Mechanisms by which ISO induces cardiac necrosis remain ill-defined, although reported studies have suggested numerous theories, such as coronary insufficiency, oxidative stress, altered metabolism, and ionic imbalance (21).

During apoptosis or non-lytic cell death, cell membrane permeability is not increased so that the cellular content of an apoptotic cell *in vivo* does not leak into the extracellular space; even the apoptotic bodies derived from disintegration of the apoptotic cell are sequestered by the membrane before they are removed by phagocytes (22). During necrotic or lytic cell death (23), however, the dying cell loses its cell membrane integrity or the control of membrane permeability, allowing free movement of water and other high-molecular-weight molecules across the cell membrane and rendering the cell to swell and ultimately burst. The leak of intracellular components into the interstitial space causes inflammation. Hence, different from apoptosis, necrosis is always accompanied by inflammatory responses (22). Recent advances in our understanding of cell death have classified necrosis into two major categories: accidental/passive necrosis and regulated necrosis. The former results from direct physical or chemical insults to the cell that directly destroy the cell membrane and break the cell; so it happens instantly and is not voluntarily controllable by the demising cell. By contrast, the regulated necrosis is triggered by biochemical changes inside or outside of the cell and takes a pathway that is intrinsically controllable by the affected cell (24). Under the category of regulated necrosis, several types have emerged, such as necroptosis, ferroptosis, pyroptosis, and mitochondrial permeability transition (MPT) pore-dependent necrosis (24). Since these pathways to regulated necrosis could potentially be intervened to prevent the necrosis from occurring, deciphering the nature of, and delineating the molecular pathways to, the necrosis in diseased organs can pave new avenues to devising new therapeutic strategies for the disease. Hence, we sought to define the nature of cardiomyocyte necrosis induced by catecholamine surges in the present study.

Upon TNFα receptor 1 (TNFR1) stimulation, most cells undergo apoptosis, but the cells with caspase 8 deficiency or caspase inhibition undergo necrosis, instead. The latter is termed necroptosis (25). The canonical pathway mediating TNFα-induced necroptosis requires the kinase activity of receptor-interacting protein kinase 1 (RIPK1) (26). RIPK1 binds and phosphorylates RIPK3, and the phosphorylated RIPK3 further phosphorylates a pseudo kinase known as mixed lineage kinase domain-like protein (MLKL) (27); then the phosphorylated MLKL (p-MLKL) is believed to translocate to the plasma membrane and oligomerize to form pores on the cell membrane (28), thereby increasing membrane permeability and causing the cell to swell and ultimately burst (29). Some more recent studies suggest that necrosomes formed by RIPK3 and p-MLKL oligomers are indispensable to necroptosis and that not all necroptosis requires RIPK1, but RIPK1 kinase activity is required for TNFα stimulation to induce necroptosis (22).

Cardiomyocyte death including apoptosis and various forms of regulated necrosis contributes to cardiac pathogenesis (22). The myocardium from humans with end-stage heart failure resulting from MI or dilated cardiomyopathy displayed elevation of necroptotic biochemical markers, indicative of an involvement of necroptosis in heart failure (30). Heart failure patients harboring a genetic variant in the promoter region of *RIPK3* gene that increases *RIPK3* gene expression

tend to exhibit poorer prognosis than those who do not carry such a variant (31). Experimental studies have demonstrated an important pathogenic role for necroptosis in common pathological processes such as post-MI remodeling (32), myocardial ischemia/reperfusion (I/R) injury, cardiotoxicity of doxorubicin treatment (33, 34), and paraquat-induced cardiac contractile dysfunction (35). Therefore, a better understanding of the cellular and molecular mechanisms that govern cardiomyocyte necroptosis or link pathological stress to cardiomyocyte necroptosis is expected to unveil new therapeutic targets to prevent or more effectively treat heart failure.

Using primarily the ISO-induced rodent models of cardiac injury since late 1950s, researchers have attributed many factors to the cardiac injury induced by catecholamine surges and excessive β-adrenergic stimulation. Elevated oxidative stress is a well-known damaging factor to the cell. Myocardial oxidative stress is drastically increased either by the myocardial I/R as a result of coronary spasm and subsequent release or by the metabolism of catecholamines, as some of the catecholamine metabolites are strong oxidants (36). Calcium overload and myofibril over-contraction, which can be a direct result of excessive β-adrenergic stimulation from catecholamines and a secondary consequence of I/R injury, may contribute to cardiac dysfunction and injury (36). Additionally, β-adrenergic stimulation appears to be able to trigger inflammatory responses by upregulating the expression and release of inflammatory cytokines (37); and many compounds with an anti-inflammatory property can protect against cardiac injury induced by catecholamine surges (21), suggesting that the secondary injury from inflammation may also play a role in the cardiac injury by catecholamine surges. Necrotic cardiomyocyte death is the most prominent pathological feature of cardiac injury induced by catecholamine surges (19). However, the nature of cardiomyocyte necrosis induced by catecholamine surges or by excessive β-adrenergic stimulation remains undefined. Hence, we conducted the present study to determine if the necroptotic pathway plays a role in mediating cardiomyocyte necrosis induced by ISO. Our findings provide compelling evidence for the first time that a large proportion of cardiomyocyte necrosis induced by catecholamine surges belongs to necroptosis and is mediated by the RIPK1–RIPK3–MLKL pathway, and we have further demonstrated that targeting RIPK1 or RIPK3 can significantly attenuate ISO-induced necrosis, providing strong evidence for targeting RIPK1 and RIPK3 to protect the heart against injury from catecholamine surges or excessive β-adrenergic stimulation.

METHODS AND MATERIALS

Animal Models

The creation of RIPK3 global knockout (*RIPK3*$^{-/-}$) mice was previously described (38). The *RIPK3*$^{-/-}$ mice used in this study had undergone more than nine generations of back-crossing into the C57BL/6J inbred background. All mice used here are in the C57BL/6J inbred background. A recent report has documented that there is no sex difference in the induction of cardiac dysfunction by an ISO treatment regime in mice (39). Hence, young adult age- and sex-matched wild-type (WT) or *RIPK3*$^{-/-}$ mice were randomly divided into two groups and subjected to two consecutive subcutaneous injections of ISO (#I6504, Sigma-Aldrich, St. Louis, MO, USA; 85 mg/kg) or an equivalent amount of vehicle control [saline (SAL)], with an interval of 24 h between the two injections. The rationale for choosing this ISO dosage and treatment regime is that it has been extensively used in prior studies by others to induce MI-like cardiac injury reproducibly, although two consecutive daily injections of ISO at a dose as low as 0.33 mg/kg could induce cardiomyocyte necrosis in rats (21). To test the effect of RIPK1-selective inhibition, necrostatin-1 (NEC-1; BML-AP309-0020, Enzo Life Sciences, Inc., Farmingdale, NY, USA; 4 mg/kg, i.p.) was administered 10 min before each injection of ISO (or saline). For further protein biochemistry and histopathology analyses, the ventricular myocardium was collected 24 h after the second ISO injection. The animal care and use protocol for this study was approved by the Institutional Animal Care and Use Committee of the University of South Dakota.

Evans Blue Dye Uptake Assays

The *in vivo* Evans blue dye (EBD) uptake assay was performed to detect cardiomyocyte necrosis as we reported (40, 41). After it is absorbed into the circulatory system, EBD is bound by albumin. Therefore, in this assay, EBD does not enter cells with an intact plasma membrane (40). EBD (#314-13-6, Sigma-Aldrich) was dissolved in saline (10 mg/ml). Mice were intraperitoneally injected with EBD (100 μg/g body weight) 18 h before tissue collection. To flush out EBD in the vasculature and the interstitial space, the heart was retrogradely perfused *via* the abdominal aorta (distal end ligated) first with phosphate-buffered saline (PBS; pH 7.4) for 5 min; and for *in situ* fixation, the PBS was then replaced with 4% paraformaldehyde. The fixed ventricular myocardium was equilibrated with 50% sucrose for 4 h before being embedded in O.C.T. (Sakura Finetek USA, Inc., Torrance, CA, USA); the tissue block was then frozen in liquid nitrogen and stored in a −80°C freezer until being sectioned. Cryosections (7 μm) were collected, washed with PBS, and counterstained with Alexa Fluor™ 488 Phalloidin and DAPI (4′,6-diamidino-2-phenylindole) to reveal F-actin (green) and nuclei (blue), respectively. Stained sections were imaged using a Leica TCS SP8 STED 3X White Light Laser and Super-Resolution Confocal Imaging System (Leica Microsystem, Buffalo Grove, IL, USA). Cells that have taken up EBD show red auto-fluorescence and are readily identifiable. An image of the whole section was generated with the tiling function of the built-in imaging software. The percentage of the EBD positive area (red) over the total myocardial area (green and red) was measured by ImagePro Plus 6.0 software from representative sections from each mouse.

Co-Immunoprecipitation

Co-immunoprecipitation (Co-IP) was done with the Pierce Co-IP Kit (Catalog 26149, Thermo Fisher Scientific, Waltham, MA, USA), which provides covalent antibody immobilization so that

potential interference of the immunoprecipitation antibodies is completely avoided. The mouse monoclonal antibody against RIPK1 (#610459; BD Biosciences, San Jose, CA, USA) was used for IP and immunoblot of RIPK1; immunoblot for RIPK3 used the rabbit polyclonal anti-RIPK3 (ADI-905-242-100; Enzo).

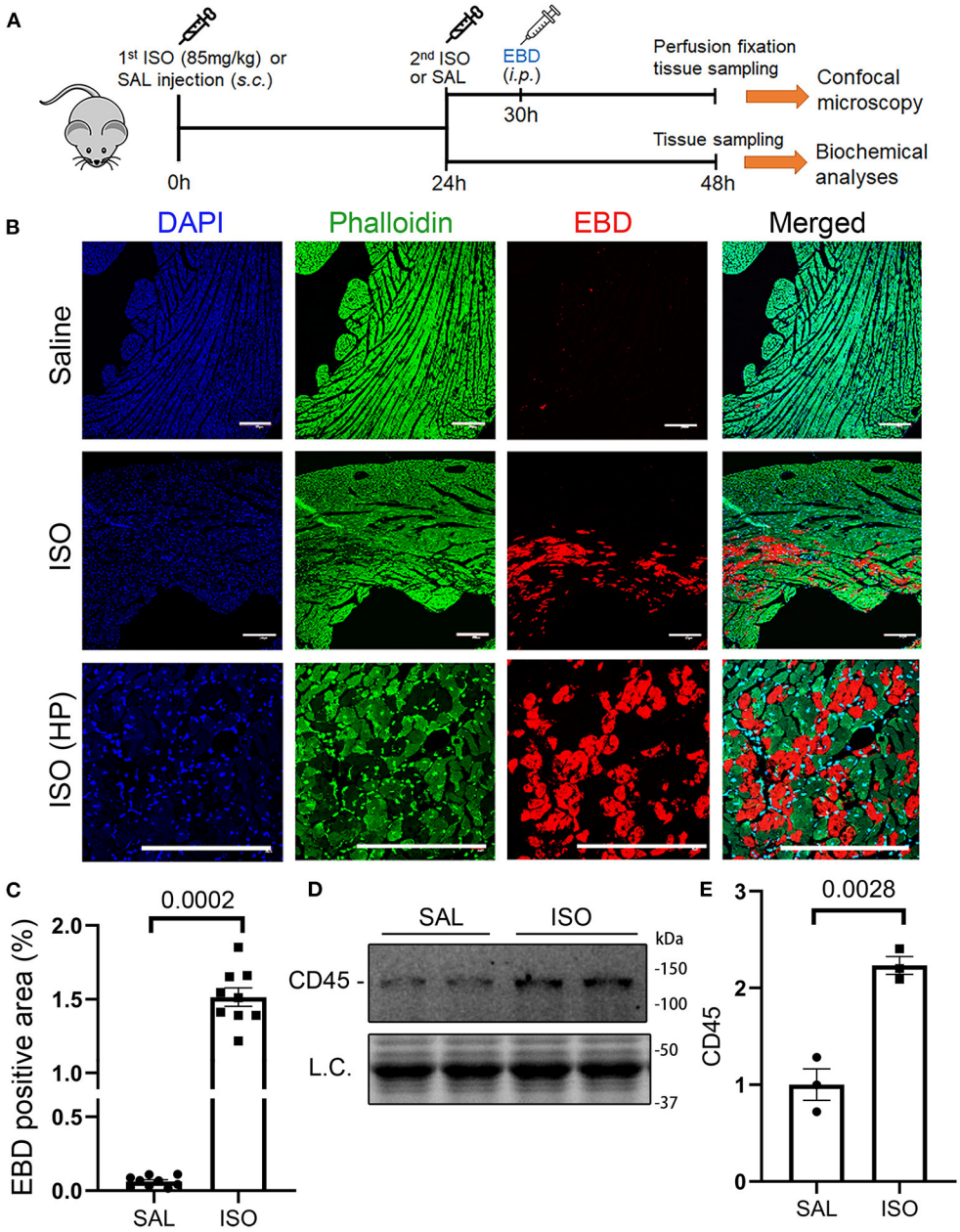

FIGURE 1 | Isoproterenol (ISO) treatment induced cardiomyocyte necrosis in wild-type mice. **(A)** A schematic for the design of experiments presented in this figure and in **Figures 2**, **3**. Adult mice of both sexes were subjected to two daily subcutaneous injections of ISO (85 mg/kg) or vehicle control [saline (SAL)] with an interval of 24 h. Myocardial tissue was collected at 24 h after the second dose of ISO. Evans blue dye (EBD) was injected 18 h before tissue collection. EBD in the vasculature and extracellular space was flushed out through retrograde perfusion with saline *via* the abdominal aorta immediately before tissue collection. A separate cohort without EBD injection and perfusion fixation was used for biochemical analyses. **(B,C)** *in vivo* EBD uptake assays. Cryosections were used for staining with Alexa 488-conjugated phalloidin and DAPI before imaging with a multicolor confocal microscope. Shown are confocal micrographs centered on an EBD positive area in the ISO-treated heart or the corresponding region of a saline-treated heart **(B)** and a graph summarizing the percentage EBD-positive area from three mice (two males and one female) per group **(C)**. Scale bar = 200 μm; mean ± SEM; three sections/mouse and three mice/group were included; nested *t*-test. HP, higher magnification. **(D,E)** Representative image **(D)** and pooled densitometry data **(E)** of Western blotting analyses for myocardial CD45. $N = 3$ mice (two males and one female) per group; the *p*-value shown in panel E is derived from two-sided unpaired *t*-test with Welch's correction. L.C. (loading control) used total protein images obtained with the stain-free total protein imaging technology.

Protein Extraction and Western Blotting Analyses

The extraction of total proteins from ventricular myocardial samples was done using 1× loading buffer containing 41 mM of Tris-HCl, 1.2% sodium dodecyl sulfate (SDS), and 8% glycerol. A protease inhibitor cocktail (#P-1540; AG Scientific, San Diego, CA, USA) was added to the extraction buffer to inhibit protein degradation. Protein concentration was determined using bicinchoninic acid reagents (#23225; Thermo Fisher Scientific, Waltham, MA, USA). Equal amounts of proteins loaded to different lanes were fractionated *via* 8–14% SDS–polyacrylamide gel electrophoresis (SDS-PAGE), and the separated proteins were transferred onto a polyvinylidene difluoride (PVDF) membrane using a trans-blot apparatus (Bio-Rad, Hercules, CA, USA). The PVDF membranes were then sequentially subjected to blocking, incubation with the primary antibodies against the protein of interest, washing with the TBST (Tris-buffered saline with 0.1% Tween® 20 detergent) buffer to remove unbound primary antibodies, incubation with horseradish peroxidase (HRP)-conjugated secondary antibodies (Santa Cruz Biotechnology, Dallas, TX, USA), and washing to remove unbound antibodies. The secondary antibodies bound to the PVDF membrane were then detected using enhanced chemiluminescence reagents (GE Healthcare, South Plainfield, NJ, USA); the chemiluminescence was digitally imaged and analyzed with the ChemiDoc™ MP imaging system and associated software (Bio-Rad, Hercules, CA, USA) as we previously reported (42). The stain-free total protein imaging technology was used as described to obtain the image from the gel and PVDF membrane to be used as loading controls (43).

Statistical Methods

GraphPad Prism software (Version 8.4; GraphPad Software, San Diego, CA, USA) was used. All continuous variables are presented as scatter dot plots with mean ± SEM superimposed. All data were examined for normality with the Shapiro–Wilk test prior to application of parametric statistical tests. Tests used for statistical significance evaluations of each dataset are specified in the figure legends. The difference between the two groups was evaluated using two-tailed unpaired *t*-test with Welch's correction to address the potential issues associated with small sample size or, where technical repeats are involved, nested *t*-test. One-way ANOVA or nested one-way ANOVA or when appropriate, two-way ANOVA, followed by Tukey's multiple comparisons test was used to evaluate the difference among three or more groups. A *p*-value or, where applicable, adjusted *p*-value < 0.05 is considered statistically significant.

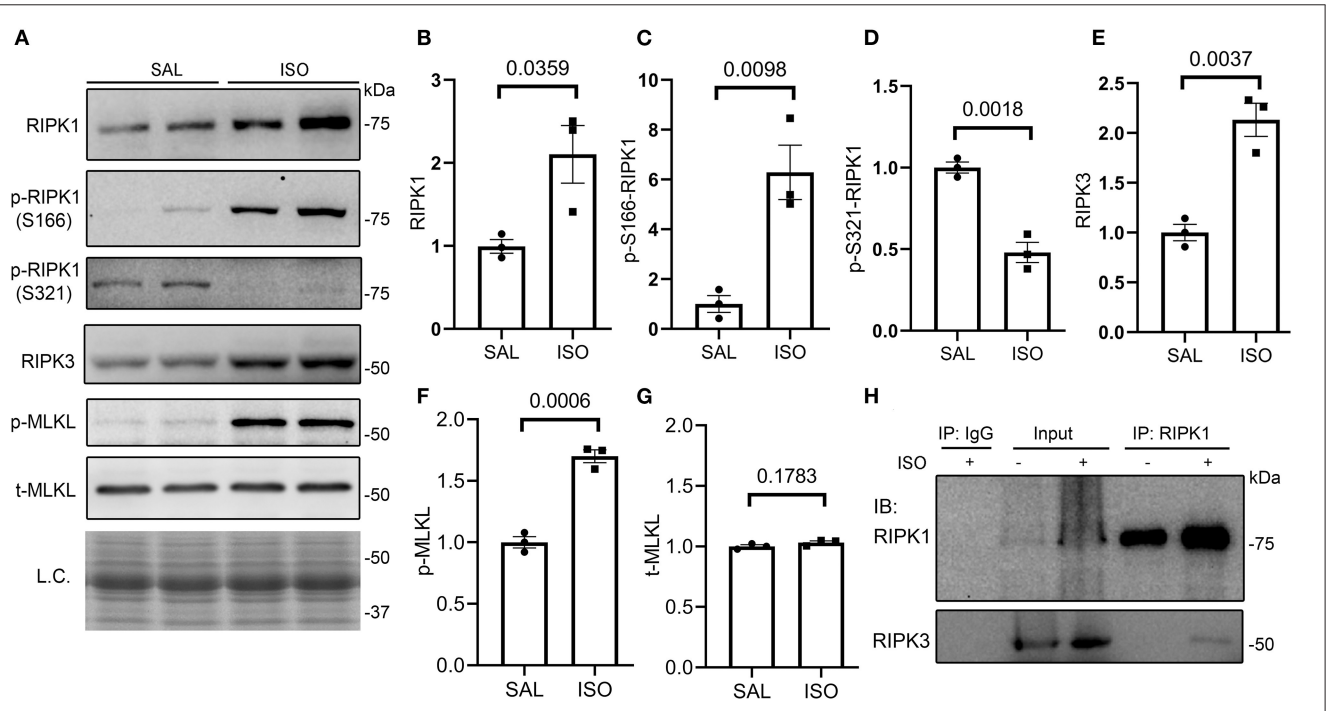

FIGURE 2 | Myocardial RIPK1–RIPK3–MLKL pathway is activated in isoproterenol (ISO)-treated mice. Mice were treated with ISO or saline (SAL) as described in **Figure 1**. Ventricular myocardial samples were collected at 24 h after the second dose of ISO for further analyses, and total proteins were extracted for Western blotting analyses for the indicated proteins. **(A–G)** Representative images **(A)** and pooled densitometry data **(B–G)** of Western blotting analysis for the indicated proteins. p-S166-RIPK1, Ser166-phosphorylated RIPK1; p-S321-RIPK1, Ser321-phosphorylated RIPK1; p-MLKL, Ser345-phosphorylated MLKL; t-MLKL, total MLKL; L.C., loading control that used the stain-free total protein image; mean ± SEM; each dot represents a mouse; $n = 3$ mice (two males and one female) per group; *p*-values shown in this figure are derived from two-sided unpaired *t*-tests with Welch's correction. **(H)** Western blotting analysis (IB) for RIPK1 and RIPK3 that were immunoprecipitated (IP) with IgG or anti-RIPK1 antibodies.

RESULTS

Induction of Massive Cardiomyocyte Necrosis by High Doses of Isoproterenol

The hallmark between necrosis and apoptosis is the loss of membrane integrity of the cell undergoing necrosis, whereas the cell membrane permeability does not increase during *in vivo* apoptosis. As a result, inflammatory responses are triggered by necrosis but not by apoptosis. Hence, we performed the EBD uptake assay to assess cardiomyocyte plasma membrane integrity in mice subjected to ISO or saline treatment. EBD administered *via* a peritoneal injection was not found in the cardiomyocyte compartment of saline treated mice, but a significant proportion of cardiomyocytes in the ISO treated mice contained EBD in their cytoplasm (**Figures 1B,C**; **Supplementary Figure I**), indicative of the loss of plasma membrane integrity in these cardiomyocytes. In response to necrosis, leukocyte infiltration ensues. Our Western blotting analyses showed that myocardial protein levels of CD45, a leukocyte marker, were markedly higher in ISO-treated mice than in the saline-treated group (**Figures 1D,E**, $p = 0.003$), which is further consistent with occurrence of necrosis in ISO-treated mouse hearts.

Activation of the Myocardial RIPK1–RIPK3–MLKL Pathway in Isoproterenol-Treated Mice

To explore the potential pathway leading to necrosis in the ISO-treated hearts, we examined the key features of the canonical necroptotic pathway. At 24 h after the second dose of ISO, myocardial protein levels of RIPK1, Ser166-phosphorylated RIPK1 (p-S166-RIPK1), RIPK3, and Ser345-phosphorylated MLKL (p-MLKL) but not total MLKL were significantly increased, whereas myocardial Ser321-phosphorylated RIPK1 (p-S321-RIPK1) significantly decreased, compared with the saline treated group (**Figures 2A–G**). These changes indicate the activation of the RIPK1–RIPK3–MLKL pathway in the ISO-treated hearts. Another key feature of the activation of the RIPK1–RIPK3 necroptotic pathway is the increased binding of RIPK3 with RIPK1 (44). Our Co-IP experiments revealed a

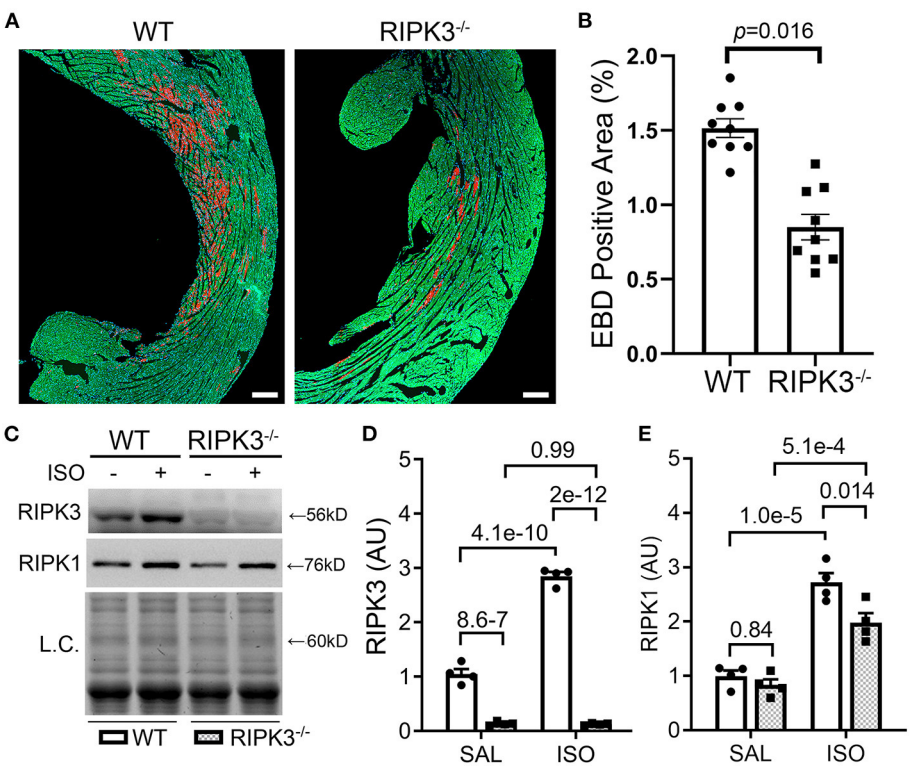

FIGURE 3 | RIPK3 knockout significantly reduced isoproterenol (ISO)-induced cardiomyocyte necrosis. Wild-type and RIPK3 null (RIPK3$^{-/-}$) mice were subjected to the same ISO or saline (SAL) treatment regime and the Evans blue dye (EBD) uptake assays as described in **Figure 1**. **(A,B)** Representative confocal micrographs **(A)** and pooled morphometric data **(B)** of EBD-positive area. Scale bar = 200 μm. For the EBD assays, three mice (one male and two females) per group and three representative sections per heart were used for morphometry. The *p*-value is shown above the bracket and was obtained from nested *t*-test to account for the three technical repeats within each biological repeat. **(C–E)** Western blotting analyses for myocardial levels of the indicated proteins. Shown are representative image **(C)** and pooled densitometry data **(D,E)**. L.C., loading control that used the stain-free total protein image; mean ± SEM; $n = 4$ mice (two males and two females) per group; two-way ANOVA followed by Tukey's test.

significant increase in RIPK1-bound RIPK3 in ISO-treated hearts than in the saline-treated hearts (**Figure 2H**).

Diminishing Isoproterenol-Induced Cardiomyocyte Necrosis by RIPK3 Deficiency in Mice

To test whether the ISO-induced cardiomyocyte necrosis belongs to necroptosis and requires RIPK3, we subjected RIPK3$^{-/-}$ and WT mice to the ISO treatment and compared the severity of necrosis between the two groups. EBD assays showed that the same regime of ISO treatment induced ∼50% less necrosis in RIPK3$^{-/-}$ mice than in WT mice (**Figures 3A,B**, $p = 0.016$). Western blotting analyses detected that ISO treatment significantly reduced the increase of myocardial RIPK1 in RIPK3$^{-/-}$ mice than in WT mice (**Figures 3C,E**). Echocardiograms recorded at 3 h after the second dose of ISO revealed that ISO treatment induced significantly greater increases in left ventricular (LV) ejection fraction (EF) and fractional shortening (FS) and significantly greater decreases in LV chamber diameters at both end-diastole and end-systole in ISO-treated RIPK3$^{-/-}$ mice compared with ISO-treated WT mice (**Supplementary Figures II**, **III**), which is well in line with data where the ISO treatment induced significantly less cardiomyocyte loss in RIPK3$^{-/-}$ mice than in WT mice.

Requirement of RIPK1 Kinase Activity for Isoproterenol to Induce Cardiomyocyte Necrosis

To determine if RIPK1 kinase activity is required for the ISO treatment to induce cardiomyocyte necrosis, we compared the prevalence of ISO-induced cardiomyocyte necrosis in mice pretreated with or without NEC-1, a specific kinase inhibitor of

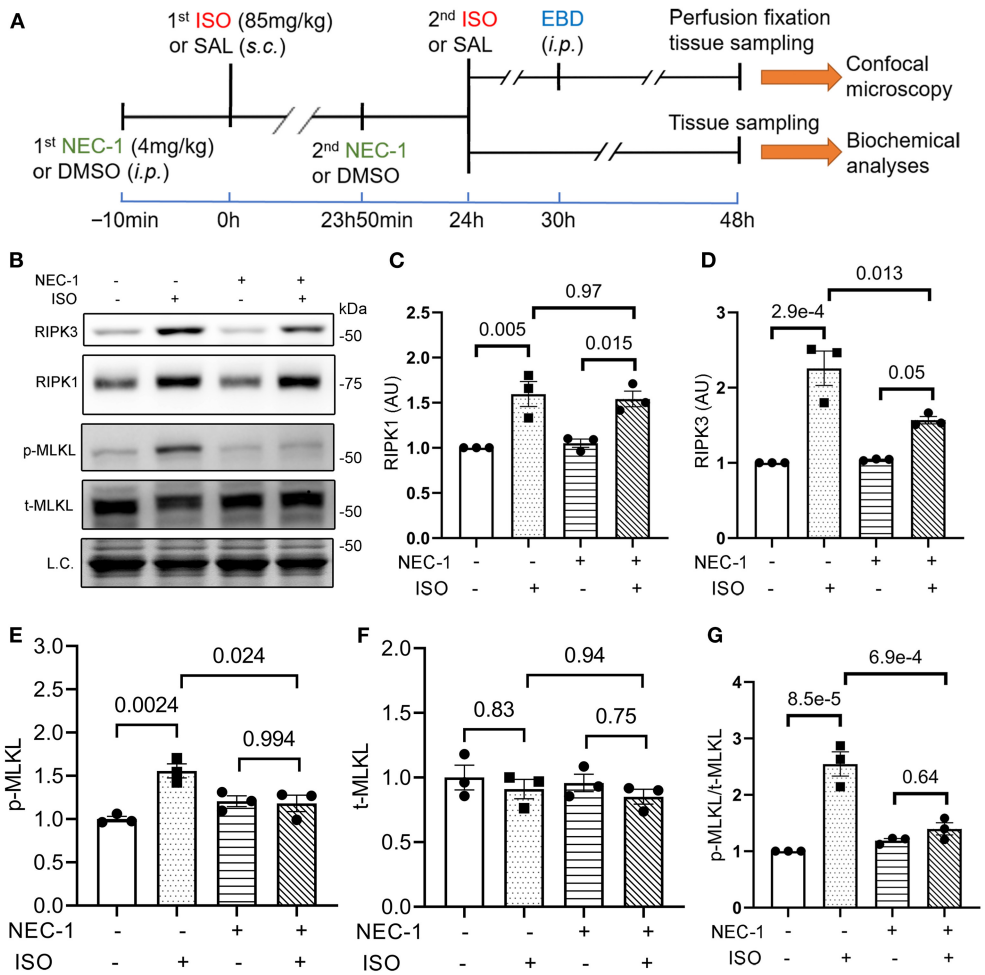

FIGURE 4 | RIPK1 kinase activity is required for the isoproterenol (ISO) treatment to increase RIPK3 and p-MLKL in mouse hearts. **(A)** A schematic for the design of experiments presented in **Figures 4**, **5**. Adult mice were subject to ISO or saline (SAL) treatment as illustrated. Necrostatin-1 (NEC-1; 4 mg/kg, i.p.) or vehicle control (DMSO) was administered 10 min before each ISO or SAL injection. **(B–G)** Western blotting analyses for myocardial levels of the indicated proteins. Ventricular myocardium of wild-type (WT) mice was collected 24 h after the second ISO injection. Shown are representative images **(B)** and pooled quantitative data for the indicated proteins **(C–G)**. Two-way ANOVA followed by Tukey's test was used; mean ± SEM; $n = 3$ mice (either two males + one female or one male + two females) per group. L.C. (loading control) used total protein images obtained with the stain-free total protein imaging technology.

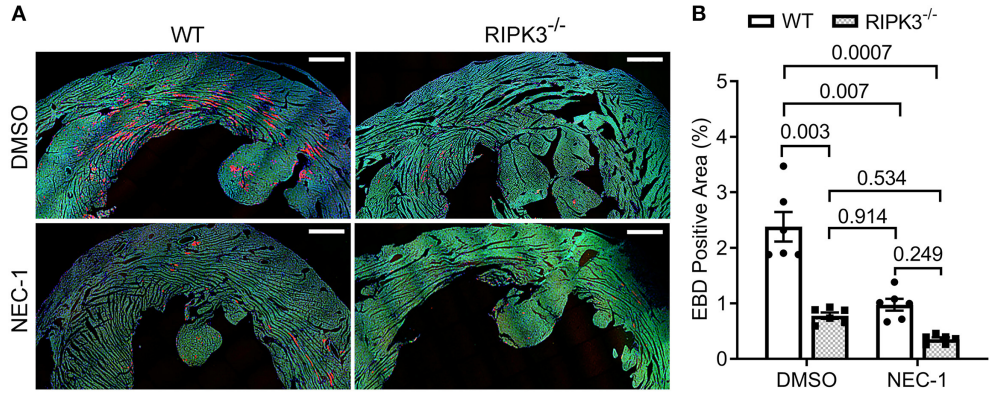

FIGURE 5 | Effect of necrostatin-1 (NEC-1) on isoproterenol (ISO)-induced cardiomyocyte necrosis in wild-type (WT) and RIPK3 knockout mice. WT and RIPK3 null mice were subjected to NEC-1 and ISO treatments as well as the EBD injection as described in **Figure 4A**. Perfusion-fixed myocardial samples were collected 24 h after the second ISO injection for EBD uptake assays. Shown are representative images (**A**; scale bar = 500 μm) and pooled quantitative data **(B)** from the EBD uptake assays. Two representative sections per mouse and three mice (two males and one female) per group were analyzed; mean ± SEM, nested ANOVA followed by Tukey's test. The nested test is used to account for the two technical repeats (two sections per mouse).

RIPK1 (45). ISO-induced increases in RIPK3 and p-MLKL were remarkably attenuated by the NEC-1 pretreatment, although the protein levels of RIPK1 and total MLKL were not affected (**Figure 4**). EBD uptake assays revealed that ISO induced significantly less EBD-positive cardiomyocytes in WT mice pre-treated with NEC-1 than in those pretreated with vehicle control. Again, ISO induced significantly less EBD positivity in RIPK3$^{-/-}$ hearts compared with WT mice, but pre-treatment with NEC-1 did not further reduce ISO-induced EBD-positivity in RIPK3$^{-/-}$ mice (**Figure 5**). These data demonstrate that RIPK1 kinase activity is essential to the induction of cardiomyocyte necrosis by ISO and that RIPK1 and RIPK3 work in the same pathway to mediate ISO-induced cardiomyocyte necroptosis.

DISCUSSION

Catecholamine surges as well as excessive β-adrenergic stimulation are known to induce cardiomyocyte necrosis, but it was not previously known whether the necrosis or a portion of it belongs to regulated necrosis and, if so, which type it would be. The present study unveils for the first time that a large portion (∼50%) of the cardiomyocyte necrosis induced by the ISO regime belongs to necroptosis and is mediated by the RIPK1–RIPK3–MLKL pathway. These are highly significant discoveries because they not only provide a new mechanistic link between many common and rare forms of heart disease and cardiomyocyte necrosis but also identify RIPK1 and RIPK3 as potentially new therapeutic targets for protecting the heart against injury by catecholamine surges or excessive β-adrenergic stimulation.

Cardiomyocyte apoptosis and necrosis are both considered the main modes of cell death in β-adrenergic receptor agonist ISO-induced myocardial injury, but the mechanism underlying necrosis was ill-defined. Here, we confirmed that two consecutive daily doses of ISO (85 mg/kg/day) caused cardiomyocyte necrosis as evidenced by loss of cell membrane integrity in these cells and leukocyte infiltration (**Figure 1**). More importantly, here, we have established that a large proportion of cardiomyocyte necrosis induced by the ISO treatment belongs to necroptosis because blockade of the canonical necroptotic pathway through either ablation of *RIPK3* gene or inhibition of RIPK1 kinase activity remarkably diminished the ability of the ISO treatment to induce cardiac necrosis in mice. At the same time, our discoveries also demonstrate that the necroptosis induced by ISO is mediated by the RIPK1–RIPK3–MLKL pathway. As elaborated below, these discoveries are compellingly supported by multiple lines of evidence.

First, we have collected strong evidence that the ISO treatment can activate the myocardial RIPK1–RIPK3–MLKL pathway. Autophosphorylation of RIPK1 at serine 166 (p-S166-RIPK1) has been extensively used as a biomarker for RIPK1 activation and was recently shown to be essential for RIPK1 to mediate cell death (both apoptosis and necroptosis) and inflammation (46), whereas phosphorylation of RIPK1 at serine 321 inactivates RIPK1 and thereby prevents TNFα from inducing cell death (47). Our experiments detected that ISO treatment led to significant increases in myocardial p-S166-RIPK1 but marked decreases in p-S321-RIPK1 (**Figures 2A–D**); hence, the changes in the phosphorylation of both sites reciprocally indicate that RIPK1 is activated in the heart by the ISO treatment. RIPK1 activation can participate in multiple pathways downstream of TNFR1 stimulation; hence, it is important to define which pathway(s) the activated RIPK1 takes in the ISO-treated mice. To this end, our results clearly show that the canonical necroptotic pathway is the main pathway taken by RIPK1 in the ISO treated hearts. This is because (1) myocardial p-MLKL proteins, the most important component of necrosomes in the canonical necroptotic pathway and an indicator of RIPK3 activation (29, 48), were drastically increased in ISO-treated mice (**Figures 2A,F**); (2) myocardial protein levels of RIPK3, another key component of necrosomes and the central player of the

necroptotic pathway (27), were increased by more than 100% (**Figures 2A,E**); and most importantly, (3) Co-IP revealed that RIPK1-bound RIPK3 was significantly increased in ISO-treated hearts (**Figure 2G**), a requirement for the participation of RIPK1 in the RIPK3-centered necroptotic activation (44, 49, 50).

Second, we have established that RIPK3 is required for a large proportion of cardiomyocyte necrosis induced by the ISO treatment. This is because the amount of necrosis induced by the same regime of ISO treatment was ∼50% less in the RIPK3$^{-/-}$ mice than in WT mice (**Figure 3**). And RIPK3-dependent necrosis represents an important response of the heart to the ISO treatment as echocardiography showed that the ISO-treatment induced greater increases in EF and FS and greater concentric hypertrophy in RIPK$^{-/-}$ mice than in WT mice (**Supplementary Figures II, III**).

Lastly, our experiments showed that RIPK1-selective inhibition with NEC-1 did not discernibly affect the RIPK1 protein levels but significantly attenuated RIPK3 protein increases and nearly completely blocked the upregulation of p-MLKL in the ISO-treated mice (**Figure 4**). Consistent with the biochemical changes, EBD uptake assays revealed that NEC-1 pre-treatment reduced ISO-induced EBD positivity by ∼60% in WT mice and RIPK3 deficiency yielded a similar effect, but NEC-1 failed to further reduce necrosis in RIPK3-deficient mice (**Figure 5**). These new experimental findings demonstrate that RIPK1 kinase activity is required for, and RIPK1 and RIPK3 work in the same pathway in, mediating ISO-induced necroptosis.

Notably, crosstalk among different cell death pathways has been documented. Activation of death receptors usually induces apoptosis *via* the extrinsic pathway, but inhibition of caspase 8 switches it to the canonical necroptotic pathway (RIPK1–RIPK3–MLKL) (22). Oligomerization of p-MLKL at the cell membrane serves as the executioner of necroptosis, which differentiates necroptosis from other types of lytic cell death (51). During innate immune responses, program cell death also can be in another form of regulated necrosis, pyroptosis (52). In pyroptosis, inflammasomes are formed in response to pathogen-associated and damage-associated molecular patterns (PAMPs and DAMPs, respectively), leading to the recruitment of apoptosis-associated speck-like protein containing a CARD (ASC), followed by the recruitment and self-activation of caspase-1; activated caspase 1 processes other molecules including the executioner of pyroptosis, gasdermin D (GSDMD). Similar to the function of p-MLKL in necroptosis, the N-terminal fragment of GSDMD resulting from the caspase 1-mediated proteolytic cleavage undergoes oligomerization to form pores within the cell membrane and thereby cause the cell to swell and burst (52). More recently, the collective activation of all the three programmed cell death pathways (apoptosis, pyroptosis, and necroptosis) in the same population of cultured cells by microbial infection was observed and termed "PANoptosis" (51). The concept of PANoptosis as a form of inflammatory cell death is still in its infancy. Some molecules such as Z-DNA-binding protein (ZBP1) and transforming growth factor β-activated kinase 1 (TAK1) were found to regulate all the three forms of programmed cell death covered by PANoptosis. ZBP1 seemed to be crucial for the activation of all the three pathways by influenza A virus (IAV) infection (53, 54). Inhibition of TAK1 activity by genetic deletion or pathogen-mediated inhibition also activates pyroptosis, apoptosis, and necroptosis (55–58). Physical interactions between molecules known to participate in apoptosis, pyroptosis, and necroptosis have been reported in the cell death induced by the loss of TAK1 (58). A cell death complex composed of key molecules from pyroptosis, extrinsic apoptosis, and necroptosis in the activation of PANoptosis in cultured cells by certain types of bacterial and viral infections was detected by immunoprecipitation and termed the PANoptosome (59). Therefore, there is a possibility that the activation of RIPK1 and RIPK3 and the formation of the RIPK1–RIPK3 complex in the ISO-treated myocardium might be a part of PANoptosis rather than independent necroptosis. However, as evidenced by the marked increases of p-MLKL in ISO-treated hearts (**Figure 2**) and the nearly complete abolishment of the increase in p-MLKL by RIPK1 kinase inhibition (**Figure 4**), increased p-MLKL is intimately involved in the regulated necrosis induced by the ISO treatment. Thus, it is more than likely that necroptosis is a major form of regulated necrosis induced by ISO. It will be very interesting to test in the future whether pyroptosis and PANoptosis are also involved.

Although β-adrenergic activation *per se* should exert vasodilation effects, coronary insufficiency and even myocardial ischemia were observed in the same ISO-induced myocardial injury model as the one used in the present study (21). In fact, this model has been used by many as a non-invasive MI model (21). It is conceivable that myocardial I/R occur in this model; and the cardiac histopathology in this model does resemble MI and I/R injury (21). However, the massive cardiomyocyte necroptosis in this model makes it different from a surgically induced MI model. This is because a prior report shows quite convincingly that RIPK3-mediated necroptosis is not a discernible contributor to the acute infarct size in a mouse model of acute MI induced by coronary artery ligation, although RIPK3 deficiency did attenuate the chronic post-MI maladaptive cardiac remodeling (32). The requirement of RIPK1 kinase activity and the apparent involvement of MLKL in mediating the ISO-induced necroptosis also seem to distinguish this model from a traditional myocardial I/R injury model. This is because a recent high-profile study by Zhang et al. showed that cardiac necroptosis triggered by I/R injury required RIPK3 but not RIPK1 and MLKL. They showed that RIPK3 upregulated by I/R phosphorylates and activates the calcium/calmodulin-dependent protein kinase II (CaMKII) and thereby opened the MPT to induce cardiomyocyte necroptosis (33). However, more recent studies suggest that the RIPK3–MLKL axis may still be important for myocardial necroptosis in I/R injury (34). Moreover, the canonical RIPK1–RIPK3–MLKL pathway has been implicated in cardiomyocyte necroptosis induced by genetic interrogations of key cellular processes in mice; the perturbation of Cullin deneddylation by cardiomyocyte-restricted ablation of *Cops8* gene and the suppression of nuclear DNA-encoded mitochondrial genes required for ATP synthesis due to the knockout of the Hippo signaling effector TEAD1 are among the examples (41, 60, 61). It is well-known that induction of necroptosis by the activation of TNFR1 requires RIPK1 kinase

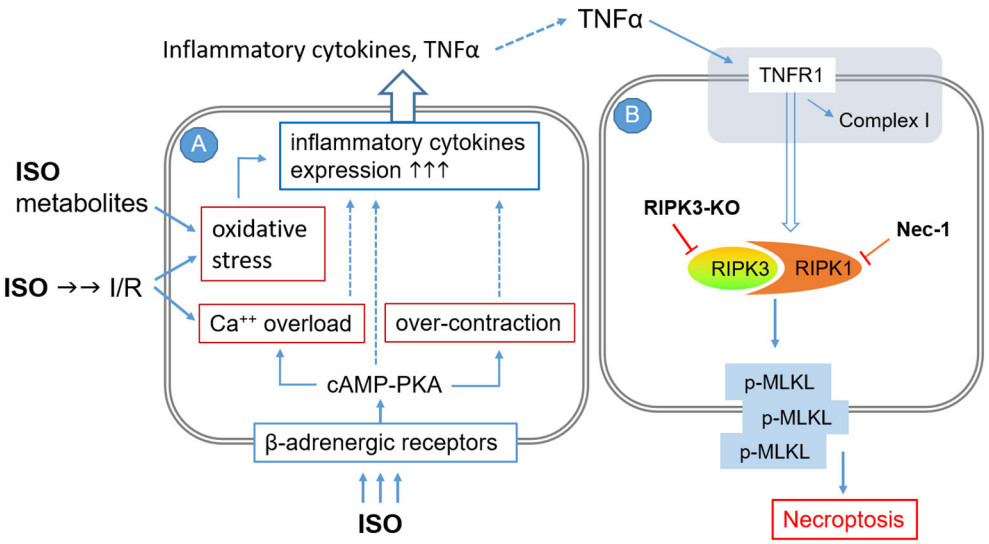

FIGURE 6 | A working model for the potential mechanisms by which high doses of isoproterenol (ISO) induce cardiomyocyte necroptosis. The pathological processes are illustrated to occur sequentially in two adjacent cardiomyocytes (**A** and **B**), but they could potentially take place in the same cell where TNFα and other inflammatory cytokines would be autocrinal. Processes shown in cell **A** are based on previous reports. The pathway modeled in cell **B** is based on the findings of the present study, but the involvement of TNFα and its receptor (shaded area at the top) as well as the requirement of MLKL for the induction of cardiomyocyte necrosis by ISO remain to be fully established. I/R, ischemia/reperfusion; TNFR1, TNFα receptor type 1; RIPK3-KO, RIPK3 knockout; NEC-1, necrostatin-1.

activity (26). Qin et al. reported that myocardial I/R could dysregulate both strands (5p and 3p) of miR-223 in mice, thereby targeting TNFR1 and other regulatory points upstream of RIPK3 to cause cardiac necroptosis (62). By definition, necroptosis and the necrosis driven by the MPT opening are two different types of regulated necrosis (22). Necroptosis can be induced in cells without mitochondria (63). Hence, it will be interesting and important to test in future studies whether CaMKII plays a mediating role in ISO-induced cardiomyocyte necrosis, as CaMKII can be activated by excessive β-adrenergic stimulation.

ISO infusion at a low dose (e.g., 12.5 μg/kg/h) that is capable of inducing cardiac hypertrophy but not fibrosis was shown to rapidly upregulate the gene expression of TNF and other inflammatory cytokines including interleukin (IL)-1β, IL-6, inducible nitric oxide synthase, and monocyte chemotactic protein-1 (MCP-1) in a TNFR1-dependent manner (64). Myocardial TNFα and IL1β protein levels were markedly increased in rats treated with two consecutive daily doses of ISO (100 mg/kg/day, i.p.) (37). Hence, it is very likely that autocrinal or paracrinal TNFα and its activation of TNFR1 mediate the activation of the RIPK1–RIPK3–MLKL pathway by the ISO treatment (**Figure 6**), although no PubMed searchable studies have tested the requirement of TNFR1 in the induction of cardiomyocyte necrosis by catecholamine surges yet. As illustrated in **Figure 6**, several previously reported pathological processes also could serve as the upstream events for the inflammatory responses and cardiac injury. These include, for example, increased oxidative stress resulting from myocardial I/R and catecholamine metabolism, calcium overload and myofibril over-contraction as a result of excessive β-adrenergic receptor activation and coronary insufficiency, and instant cardiomyocyte necrosis caused by myocardial ischemia and other factors (19, 21, 36).

Since pharmacological inhibition of RIPK1 and genetic ablation of RIPK3 prevented a large proportion of ISO-induced cardiomyocyte necrosis, the present study provides a strong argument for targeting RIPK1 or RIPK3 to protect against cardiac injury from catecholamine surges and against maladaptive cardiac remodeling induced by excessive β-adrenergic activation. Given that catecholamine surges play an important role in a broad spectrum of diseases, including stress cardiomyopathy that has been intimately associated with the physical and emotional stress resulting from the current COVID-19 pandemic (10–13), the present study provides a serendipitous and yet strong support for targeting RIPK1 and RIPK3 to treat COVID-19. This is actually very exciting and plausible because both RIPK1 and RIPK3 play critical roles in inflammation (65, 66). And at least two RIPK1 inhibitors have passed through Phase I clinical trials, and many chemical inhibitors of RIPK3 are emerging (67, 68). In fact, several recent reports suggested exploring RIPK1 and RIPK3 as drug targets for COVID-19 (69–71).

Limitation of the Study

The bulk of the experiments of this study was carried out during the COVID-19 pandemic; hence, the experimental design was streamlined. For example, the number of animals per group could have been greater, and the readouts for cardiac injury such as the leakage of cardiac enzymes to the circulation and the effects of RIPK-KO and NEC-1 treatment on myocardial inflammatory responses (e.g., leukocyte infiltration) and other forms of regulated cell death (e.g., apoptosis and pyroptosis) also could have been determined more extensively along with

necroptosis, to get a more complete picture. Nonetheless, we contend that the evidence presented here compellingly supports the main conclusions that unveil a molecular pathway that mediates cardiomyocyte necrosis induced by catecholamine surges, a timely and mechanistic discovery that probably identifies new therapeutic targets for treating cardiac injury induced by catecholamine surges.

DATA AVAILABILITY STATEMENT

The original contributions presented in the study are included in the article/**Supplementary Material**, further inquiries can be directed to the corresponding author/s.

ETHICS STATEMENT

The animal study was reviewed and approved by The Institutional Animal Care and Use Committee (IACUC) of the University of South Dakota.

AUTHOR CONTRIBUTIONS

XW, PW, and JL: conception and experimental design. PW and MC: data collection and interpretation. PW and XW: manuscript preparation. All authors contributed to the article and approved the submitted version.

FUNDING

This study was in part supported by NIH grants HL072166, HL085629, HL131677, and HL153614 (to XW).

ACKNOWLEDGMENTS

We are in debt to Dr. Yibin Wang of the University of California Los Angeles (Los Angeles, CA) for his kind assistance in obtaining the RIPK3 knockout mice for this study. We would like to thank Ms. Megan T. Lewno and Mr. Jack O. Sternburg for their excellent assistance in mouse breeding and genotype determination for the present study and thank Renae L. Sieck, M.S., for her assistance in the manuscript preparation.

SUPPLEMENTARY MATERIAL

The Supplementary Material for this article can be found online at: https://www.frontiersin.org/articles/10.3389/fcvm.2021.740839/full#supplementary-material

REFERENCES

1. Chen Z, Venkat P, Seyfried D, Chopp M, Yan T, Chen J. Brain-heart interaction: cardiac complications after stroke. *Circ Res.* (2017) 121:451–68. doi: 10.1161/CIRCRESAHA.117.311170
2. Pelliccia F, Kaski JC, Crea F, Camici PG. Pathophysiology of takotsubo syndrome. *Circulation.* (2017) 135:2426–41. doi: 10.1161/CIRCULATIONAHA.116.027121
3. Ong GJ, Nguyen TH, Kucia A, Liu SF, Surikow SY, Girolamo O, et al. Takotsubo syndrome: finally emerging from the shadows? *Heart Lung Circ.* (2020) 30:36–44. doi: 10.1016/j.hlc.2020.10.006
4. Shen J, Yu R. Perioperative management of pheochromocytoma: the heart of the issue. *Minerva Endocrinol.* (2013) 38:77–93.
5. Ferreira VM, Marcelino M, Piechnik SK, Marini C, Karamitsos TD, Ntusi NAB, et al. Pheochromocytoma is characterized by catecholamine-mediated myocarditis, focal and diffuse myocardial fibrosis, and myocardial dysfunction. *J Am Coll Cardiol.* (2016) 67:2364–74. doi: 10.1016/j.jacc.2016.03.543
6. Cornu E, Motiejunaite J, Belmihoub I, Vidal-Petiot E, Mirabel M, Amar L. Acute stress cardiomyopathy: heart of pheochromocytoma. *Ann Endocrinol.* (2020) 82:201–5. doi: 10.1016/j.ando.2020.03.011
7. Rathbone J, Franklin R, Gibbs C, Williams D. Review article: role of magnesium sulphate in the management of Irukandji syndrome: a systematic review. *Emerg Med Australas.* (2017) 29:9–17. doi: 10.1111/1742-6723.12694
8. Kido K, Guglin M. Drug-induced takotsubo cardiomyopathy. *J Cardiovasc Pharmacol Ther.* (2017) 22:552–63. doi: 10.1177/1074248417708618
9. Dweck MR, Bularga A, Hahn RT, Bing R, Lee KK, Chapman AR, et al. Global evaluation of echocardiography in patients with COVID-19. *Eur Heart J Cardiovasc Imaging.* (2020) 21:949–58. doi: 10.1093/ehjci/jeaa178
10. Giustino G, Croft LB, Oates CP, Rahman K, Lerakis S, Reddy VY, et al. Takotsubo cardiomyopathy in COVID-19. *J Am Coll Cardiol.* (2020) 76:628–9. doi: 10.1016/j.jacc.2020.05.068
11. Pasqualetto MC, Secco E, Nizzetto M, Scevola M, Altafini L, Cester A, et al. Stress cardiomyopathy in COVID-19 disease. *Eur J Case Rep Intern Med.* (2020) 7:001718. doi: 10.12890/2020_001718
12. Salah HM, Mehta JL. Takotsubo cardiomyopathy and COVID-19 infection. *Eur Heart J Cardiovasc Imaging.* (2020) 21:1299–300. doi: 10.1093/ehjci/jeaa236
13. Jabri A, Kalra A, Kumar A, Alameh A, Adroja S, Bashir H, et al. Incidence of stress cardiomyopathy during the coronavirus disease 2019 pandemic. *JAMA Netw Open.* (2020) 3:e2014780. doi: 10.1001/jamanetworkopen.2020.14780
14. Watkins DB. Pheochromocytoma: a review of the literature. *J Chronic Dis.* (1957) 6:510–27. doi: 10.1016/0021-9681(57)90041-3
15. Pearce RM. Experimental myocarditis; a study of the histological changes following intravenous injections of adrenalin. *J Exp Med.* (1906) 8:400–9. doi: 10.1084/jem.8.3.400
16. Rona G, Chappel CI, Balazs T, Gaudry R. The effect of breed, age, and sex on myocardial necrosis produced by isoproterenol in the rat. *J Gerontol.* (1959) 14:169–73. doi: 10.1093/geronj/14.2.169
17. Rona G, Chappel CI, Balazs T, Gaudry R. An infarct-like myocardial lesion and other toxic manifestations produced by isoproterenol in the rat. *AMA Arch Pathol.* (1959) 67:443–55.
18. Kahn DS, Rona G, Chappel CI. Isoproterenol-induced cardiac necrosis. *Ann N Y Acad Sci.* (1969) 156:285–93. doi: 10.1111/j.1749-6632.1969.tb16735.x
19. Haft JI. Cardiovascular injury induced by sympathetic catecholamines. *Prog Cardiovasc Dis.* (1974) 17:73–86. doi: 10.1016/0033-0620(74)90039-5
20. Wallner M, Duran JM, Mohsin S, Troupes CD, Vanhoutte D, Borghetti G, et al. Acute catecholamine exposure causes reversible myocyte injury without cardiac regeneration. *Circ Res.* (2016) 119:865–79. doi: 10.1161/CIRCRESAHA.116.308687
21. Wong ZW, Thanikachalam PV, Ramamurthy S. Molecular understanding of the protective role of natural products on isoproterenol-induced myocardial infarction: a review. *Biomed Pharmacother.* (2017) 94:1145–66. doi: 10.1016/j.biopha.2017.08.009
22. Del Re DP, Amgalan D, Linkermann A, Liu Q, Kitsis RN. Fundamental mechanisms of regulated cell death and implications for heart disease. *Physiol Rev.* (2019) 99:1765–817. doi: 10.1152/physrev.00022.2018
23. Choi ME, Price DR, Ryter SW, Choi AMK. Necroptosis: a crucial pathogenic mediator of human disease. *JCI Insight.* (2019) 4:e128834. doi: 10.1172/jci.insight.128834

24. Galluzzi L, Vitale I, Aaronson SA, Abrams JM, Adam D, Agostinis P, et al. Molecular mechanisms of cell death: recommendations of the Nomenclature Committee on Cell Death 2018. *Cell Death Differ.* (2018) 25:486–541. doi: 10.1038/s41418-017-0012-4
25. Degterev A, Huang Z, Boyce M, Li Y, Jagtap P, Mizushima N, et al. Chemical inhibitor of nonapoptotic cell death with therapeutic potential for ischemic brain injury. *Nat Chem Biol.* (2005) 1:112–9. doi: 10.1038/nchembio711
26. Hitomi J, Christofferson DE, Ng A, Yao J, Degterev A, Xavier RJ, et al. Identification of a molecular signaling network that regulates a cellular necrotic cell death pathway. *Cell.* (2008) 135:1311–23. doi: 10.1016/j.cell.2008.10.044
27. Newton K, Dugger DL, Wickliffe KE, Kapoor N, de Almagro MC, Vucic D, et al. Activity of protein kinase RIPK3 determines whether cells die by necroptosis or apoptosis. *Science.* (2014) 343:1357–60. doi: 10.1126/science.1249361
28. Wang H, Sun L, Su L, Rizo J, Liu L, Wang LF, et al. Mixed lineage kinase domain-like protein MLKL causes necrotic membrane disruption upon phosphorylation by RIP3. *Mol Cell.* (2014) 54:133–46. doi: 10.1016/j.molcel.2014.03.003
29. Gong YN, Guy C, Olauson H, Becker JU, Yang M, Fitzgerald P, et al. ESCRT-III acts downstream of MLKL to regulate necroptotic cell death and its consequences. *Cell.* (2017) 169:286–300.e216. doi: 10.1016/j.cell.2017.03.020
30. Szobi A, Goncalvesova E, Varga ZV, Leszek P, Kusmierczyk M, Hulman M, et al. Analysis of necroptotic proteins in failing human hearts. *J Transl Med.* (2017) 15:86. doi: 10.1186/s12967-017-1189-5
31. Hu D, Huang J, Hu S, Zhang Y, Li S, Sun Y, et al. A common variant of RIP3 promoter region is associated with poor prognosis in heart failure patients by influencing SOX17 binding. *J Cell Mol Med.* (2019) 23:5317–28. doi: 10.1111/jcmm.14408
32. Luedde M, Lutz M, Carter N, Sosna J, Jacoby C, Vucur M, et al. RIP3, a kinase promoting necroptotic cell death, mediates adverse remodelling after myocardial infarction. *Cardiovasc Res.* (2014) 103:206–16. doi: 10.1093/cvr/cvu146
33. Zhang T, Zhang Y, Cui M, Jin L, Wang Y, Lv F, et al. CaMKII is a RIP3 substrate mediating ischemia- and oxidative stress-induced myocardial necroptosis. *Nat Med.* (2016) 22:175–82. doi: 10.1038/nm.4017
34. Yang Z, Li C, Wang Y, Yang J, Yin Y, Liu M, et al. Melatonin attenuates chronic pain related myocardial ischemic susceptibility through inhibiting RIP3-MLKL/CaMKII dependent necroptosis. *J Mol Cell Cardiol.* (2018) 125:185–94. doi: 10.1016/j.yjmcc.2018.10.018
35. Zhang L, Feng Q, Wang T. Necrostatin-1 protects against paraquat-induced cardiac contractile dysfunction via RIP1-RIP3-MLKL-dependent necroptosis pathway. *Cardiovasc Toxicol.* (2018) 18:346–55. doi: 10.1007/s12012-017-9441-z
36. Rona G. Catecholamine cardiotoxicity. *J Mol Cell Cardiol.* (1985) 17:291–306. doi: 10.1016/S0022-2828(85)80130-9
37. Abdelzaher WY, Ahmed SM, Welson NN, Alsharif KF, Batiha GE, Labib DAA. Dapsone ameliorates isoproterenol-induced myocardial infarction via Nrf2/ HO-1; TLR4/ TNF-alpha signaling pathways and the suppression of oxidative stress, inflammation, and apoptosis in rats. *Front Pharmacol.* (2021) 12:669679. doi: 10.3389/fphar.2021.669679
38. Newton K, Sun X, Dixit VM. Kinase RIP3 is dispensable for normal NF-kappa Bs, signaling by the B-cell and T-cell receptors, tumor necrosis factor receptor 1, and Toll-like receptors 2 and 4. *Mol Cell Biol.* (2004) 24:1464–9. doi: 10.1128/MCB.24.4.1464-1469.2004
39. Grant MKO, Abdelgawad IY, Lewis CA, Seelig D, Zordoky BN. Lack of sexual dimorphism in a mouse model of isoproterenol-induced cardiac dysfunction. *PLoS ONE.* (2020) 15:e0232507. doi: 10.1371/journal.pone.0232507
40. Su H, Li F, Ranek MJ, Wei N, Wang X. COP9 signalosome regulates autophagosome maturation. *Circulation.* (2011) 124:2117–28. doi: 10.1161/CIRCULATIONAHA.111.048934
41. Xiao P, Wang C, Li J, Su H, Yang L, Wu P, et al. COP9 signalosome suppresses RIPK1-RIPK3-mediated cardiomyocyte necroptosis in mice. *Circ Heart Fail.* (2020) 13:e006996. doi: 10.1161/CIRCHEARTFAILURE.120.006996
42. Pan B, Li J, Parajuli N, Tian Z, Wu P, Lewno MT, et al. The calcineurin-TFEB-p62 pathway mediates the activation of cardiac macroautophagy by proteasomal malfunction. *Circ Res.* (2020) 127:502–18. doi: 10.1161/CIRCRESAHA.119.316007
43. Zhang H, Pan B, Wu P, Parajuli N, Rekhter MD, Goldberg AL, et al. PDE1 inhibition facilitates proteasomal degradation of misfolded proteins and protects against cardiac proteinopathy. *Sci Adv.* (2019) 5:eaaw5870. doi: 10.1126/sciadv.aaw5870
44. Zhang DW, Shao J, Lin J, Zhang N, Lu BJ, Lin SC, et al. RIP3, an energy metabolism regulator that switches TNF-induced cell death from apoptosis to necrosis. *Science.* (2009) 325:332–6. doi: 10.1126/science.1172308
45. Degterev A, Hitomi J, Germscheid M, Ch'en IL, Korkina O, Teng X, et al. Identification of RIP1 kinase as a specific cellular target of necrostatins. *Nat Chem Biol.* (2008) 4:313–21. doi: 10.1038/nchembio.83
46. Laurien L, Nagata M, Schunke H, Delanghe T, Wiederstein JL, Kumari S, et al. Autophosphorylation at serine 166 regulates RIP kinase 1-mediated cell death and inflammation. *Nat Commun.* (2020) 11:1747. doi: 10.1038/s41467-020-15466-8
47. Jaco I, Annibaldi A, Lalaoui N, Wilson R, Tenev T, Laurien L, et al. MK2 phosphorylates RIPK1 to prevent TNF-induced cell death. *Mol Cell.* (2017) 66:698–710.e695. doi: 10.1016/j.molcel.2017.05.003
48. Cai Z, Jitkaew S, Zhao J, Chiang HC, Choksi S, Liu J, et al. Plasma membrane translocation of trimerized MLKL protein is required for TNF-induced necroptosis. *Nat Cell Biol.* (2014) 16:55–65. doi: 10.1038/ncb2883
49. Cho YS, Challa S, Moquin D, Genga R, Ray TD, Guildford M, et al. Phosphorylation-driven assembly of the RIP1-RIP3 complex regulates programmed necrosis and virus-induced inflammation. *Cell.* (2009) 137:1112–23. doi: 10.1016/j.cell.2009.05.037
50. He S, Wang L, Miao L, Wang T, Du F, Zhao L, et al. Receptor interacting protein kinase-3 determines cellular necrotic response to TNF-alpha. *Cell.* (2009) 137:1100–11. doi: 10.1016/j.cell.2009.05.021
51. Malireddi RKS, Kesavardhana S, Kanneganti TD. ZBP1 and TAK1: master regulators of NLRP3 inflammasome/pyroptosis, apoptosis, and necroptosis (PAN-optosis). *Front Cell Infect Microbiol.* (2019) 9:406. doi: 10.3389/fcimb.2019.00406
52. Kesavardhana S, Malireddi RKS, Kanneganti TD. Caspases in cell death, inflammation, and pyroptosis. *Annu Rev Immunol.* (2020) 38:567–95. doi: 10.1146/annurev-immunol-073119-095439
53. Kuriakose T, Man SM, Malireddi RK, Karki R, Kesavardhana S, Place DE, et al. ZBP1/DAI is an innate sensor of influenza virus triggering the NLRP3 inflammasome and programmed cell death pathways. *Sci Immunol.* (2016) 1:aag2045. doi: 10.1126/sciimmunol.aag2045
54. Kesavardhana S, Kuriakose T, Guy CS, Samir P, Malireddi RKS, Mishra A, et al. ZBP1/DAI ubiquitination and sensing of influenza vRNPs activate programmed cell death. *J Exp Med.* (2017) 214:2217–29. doi: 10.1084/jem.20170550
55. Malireddi RKS, Gurung P, Mavuluri J, Dasari TK, Klco JM, Chi H, et al. TAK1 restricts spontaneous NLRP3 activation and cell death to control myeloid proliferation. *J Exp Med.* (2018) 215:1023–34. doi: 10.1084/jem.20171922
56. Orning P, Weng D, Starheim K, Ratner D, Best Z, Lee B, et al. Pathogen blockade of TAK1 triggers caspase-8-dependent cleavage of gasdermin D and cell death. *Science.* (2018) 362:1064–9. doi: 10.1126/science.aau2818
57. Sarhan J, Liu BC, Muendlein HI, Li P, Nilson R, Tang AY, et al. Caspase-8 induces cleavage of gasdermin D to elicit pyroptosis during Yersinia infection. *Proc Natl Acad Sci USA.* (2018) 115:E10888–97. doi: 10.1073/pnas.1809548115
58. Malireddi RKS, Gurung P, Kesavardhana S, Samir P, Burton A, Mummareddy H, et al. Innate immune priming in the absence of TAK1 drives RIPK1 kinase activity-independent pyroptosis, apoptosis, necroptosis, and inflammatory disease. *J Exp Med.* (2020) 217:jem.20191644. doi: 10.1084/jem.20191644
59. Christgen S, Zheng M, Kesavardhana S, Karki R, Malireddi RKS, Banoth B, et al. Identification of the PANoptosome: a molecular platform triggering pyroptosis, apoptosis, and necroptosis (PANoptosis). *Front Cell Infect Microbiol.* (2020) 10:237. doi: 10.3389/fcimb.2020.00237
60. Lewno MT, Cui T, Wang X. Cullin deneddylation suppresses the necroptotic pathway in cardiomyocytes. *Front Physiol.* (2021) 12:690423. doi: 10.3389/fphys.2021.690423
61. Liu J, Wen T, Dong K, He X, Zhou H, Shen J, et al. TEAD1 protects against necroptosis in postmitotic cardiomyocytes through regulation of nuclear DNA-encoded mitochondrial genes. *Cell Death Differ.* (2021) 28:2045–59. doi: 10.1038/s41418-020-00732-5

62. Qin D, Wang X, Li Y, Yang L, Wang R, Peng J, et al. MicroRNA-223-5p and−3p cooperatively suppress necroptosis in ischemic/reperfused hearts. *J Biol Chem.* (2016) 291:20247–59. doi: 10.1074/jbc.M116.732735
63. Tait SW, Oberst A, Quarato G, Milasta S, Haller M, Wang R, et al. Widespread mitochondrial depletion via mitophagy does not compromise necroptosis. *Cell Rep.* (2013) 5:878–85. doi: 10.1016/j.celrep.2013.10.034
64. Garlie JB, Hamid T, Gu Y, Ismahil MA, Chandrasekar B, Prabhu SD. Tumor necrosis factor receptor 2 signaling limits beta-adrenergic receptor-mediated cardiac hypertrophy in vivo. *Basic Res Cardiol.* (2011) 106:1193–205. doi: 10.1007/s00395-011-0196-6
65. Speir M, Lawlor KE. RIP-roaring inflammation: RIPK1 and RIPK3 driven NLRP3 inflammasome activation and autoinflammatory disease. *Semin Cell Dev Biol.* (2020) 109:114–24. doi: 10.1016/j.semcdb.2020.07.011
66. Liu L, Lalaoui N. 25 years of research put RIPK1 in the clinic. *Semin Cell Dev Biol.* (2021) 109:86–95. doi: 10.1016/j.semcdb.2020.08.007
67. Degterev A, Ofengeim D, Yuan J. Targeting RIPK1 for the treatment of human diseases. *Proc Natl Acad Sci USA.* (2019) 116:9714–22. doi: 10.1073/pnas.1901179116
68. Cuny GD, Degterev A. RIPK protein kinase family: atypical lives of typical kinases. *Semin Cell Dev Biol.* (2020) 109:96–105. doi: 10.1016/j.semcdb.2020.06.014
69. Feng L, Yin YY, Liu CH, Xu KR, Li QR, Wu JR, et al. Proteome-wide data analysis reveals tissue-specific network associated with SARS-CoV-2 infection. *J Mol Cell Biol.* (2020) 12:946–57. doi: 10.1093/jmcb/mjaa033
70. Karki R, Sharma BR, Tuladhar S, Williams EP, Zalduondo L, Samir P, et al. Synergism of TNF-a and IFN-g triggers inflammatory cell death, tissue damage, and mortality in SARS-CoV-2 infection and cytokine shock syndromes. *Cell.* (2020) 184:149–68. doi: 10.1016/j.cell.2020.11.025
71. Zheng M, Williams EP, Malireddi RKS, Karki R, Banoth B, Burton A, et al. Impaired NLRP3 inflammasome activation/pyroptosis leads to robust inflammatory cell death via caspase-8/RIPK3 during coronavirus infection. *J Biol Chem.* (2020) 295:14040–52. doi: 10.1074/jbc.RA120.015036

Conflict of Interest: The authors declare that the research was conducted in the absence of any commercial or financial relationships that could be construed as a potential conflict of interest.

Publisher's Note: All claims expressed in this article are solely those of the authors and do not necessarily represent those of their affiliated organizations, or those of the publisher, the editors and the reviewers. Any product that may be evaluated in this article, or claim that may be made by its manufacturer, is not guaranteed or endorsed by the publisher.

frontiers in Cardiovascular Medicine

ORIGINAL RESEARCH
published: 08 October 2021
doi: 10.3389/fcvm.2021.751359

Antithrombotic Therapy for Chronic Kidney Disease Patients With Concomitant Atrial Fibrillation and Coronary Artery Disease

Kuo-Hua Lee[1,2,3,4†], Shuo-Ming Ou[1,2,3,4†], Yuan-Chia Chu[5,6], Yao-Ping Lin[1,2,3,4], Ming-Tsun Tsai[1,2,3,4] and Der-Cherng Tarng[1,2,3,4,7] on behalf of Evaluating the Prognosis and Impacts in CKD (EPIC) Taiwan Research Group*

[1] Division of Nephrology, Department of Medicine, Taipei Veterans General Hospital, Taipei City, Taiwan, [2] Faculty of Medicine, School of Medicine, National Yang Ming Chiao Tung University, Taipei, Taiwan, [3] Institute of Clinical Medicine, National Yang Ming Chiao Tung University, Taipei City, Taiwan, [4] Center for Intelligent Drug Systems and Smart Bio-devices (IDS^{2}B), Hsinchu, Taiwan, [5] Information Management Office, Taipei Veterans General Hospital, Taipei City, Taiwan, [6] Big Data Center, Taipei Veterans General Hospital, Taipei City, Taiwan, [7] Department and Institute of Physiology, National Yang-Ming University, Taipei City, Taiwan

OPEN ACCESS

Edited by:
Xiaofeng Yang,
Temple University, United States

Reviewed by:
Mohit Turagam,
Mount Sinai Hospital, United States
Jing-Song Ou,
The First Affiliated Hospital of Sun Yat-sen University, China

***Correspondence:**
Der-Cherng Tarng
dctarng@vghtpe.gov.tw

† These authors have contributed equally to this work and share first authorship

Specialty section:
This article was submitted to Cardiovascular Therapeutics, a section of the journal Frontiers in Cardiovascular Medicine

Received: *01 August 2021*
Accepted: *15 September 2021*
Published: *08 October 2021*

Citation:
Lee K-H, Ou S-M, Chu Y-C, Lin Y-P, Tsai M-T and Tarng D-C (2021) Antithrombotic Therapy for Chronic Kidney Disease Patients With Concomitant Atrial Fibrillation and Coronary Artery Disease. Front. Cardiovasc. Med. 8:751359. doi: 10.3389/fcvm.2021.751359

Background: Oral anticoagulants (OAC) plus antiplatelets is recommended for patients with atrial fibrillation (AF) and coronary artery disease (CAD) to reduce thromboembolism. However, there is limited evidence regarding antithrombotic therapy for patients with concomitant chronic kidney disease (CKD), AF, and CAD, especially those not undergoing percutaneous coronary intervention. We aimed to use real-world data assessing the efficacy and safety of antithrombotic regimens in this population.

Methods: We used a single-center database of 142,624 CKD patients to identify those receiving antithrombotic therapy for AF and CAD between 2010 and 2018. Patients taking warfarin or direct OAC (DOAC) alone were grouped in the OAC monotherapy ($n = 537$), whereas those taking OAC plus antiplatelets were grouped in the combination therapy ($n = 2{,}391$). We conducted propensity score matching to balance baseline covariates. The endpoints were all-cause mortality, major adverse cardiovascular events, and major bleedings.

Results: After 1:4 matching, the number of patients in OAC monotherapy and combination therapy were 413 and 1,652, respectively. Between the two groups, combination therapy was associated with higher risks for ischemic stroke (HR 2.37, CI 1.72–3.27), acute myocardial infarction (HR 6.14, CI 2.51–15.0), and hemorrhagic stroke (HR 3.57, CI 1.35–9.81). The results were consistent across CKD stages. In monotherapy, DOAC users were associated with lower risks for all-cause mortality, AMI, and gastrointestinal bleeding than warfarin, but the stroke risk was similar between the two subgroups.

Conclusions: For patients with concomitant CKD, AF and CAD not undergoing PCI, OAC monotherapy may reduce stroke and AMI risks. DOAC showed more favorable outcomes than warfarin.

Keywords: anticoagulation, acute myocardial infarction, atrial fibrillation, stroke, thromboembolism

INTRODUCTION

Patients with chronic kidney disease (CKD) have a high risk of cardiovascular (CV) comorbidities including atrial fibrillation (AF) and coronary artery disease (CAD). These three disease entities concomitantly affect each other and share common risk factors such as age, smoking, hypertension, dyslipidemia, and diabetes mellitus (DM). Approximately 5–10% of patients with CKD concomitantly have AF and CAD, and the coexistence creates a vicious cycle (1). With CKD progression, the loss of antioxidant capacity enhances the progression of coronary atherosclerosis and vascular calcification that aggravate myocardial ischemia. The increasing severity of CAD and subsequent cardiac remodeling might predispose individuals to AF. In addition, AF can reduce cardiac output, thus accelerating the deterioration of CKD. Consequently, these patients experience rapid deterioration in renal function and develop adverse CV events.

Combined oral anticoagulants (OAC) and antiplatelets have been suggested for antithrombotic therapy in patients with both AF and CAD. However, such a combination may lead to adverse effects such as hemorrhagic stroke and major bleeding, especially in patients with CKD. Accordingly, previous research aimed to investigate modified antithrombotic regimens with better efficacy and safety for these high-risk patients. Previous randomized controlled trials (RCT) have shown that the combination of warfarin plus clopidogrel exerted an antithrombotic effect equal to that exerted by the conventional triple therapy of warfarin, aspirin, and clopidogrel on patients with AF undergoing percutaneous coronary intervention (2, 3). In comparison to triple therapy, the RE-DUAL trial reported that the use of dabigatran plus clopidogrel leads to comparable CV outcomes and causes less bleeding (4). Furthermore, Yasuda et al. demonstrated that rivaroxaban monotherapy was associated with a lower risk of major bleeding and was non-inferior to rivaroxaban combined with a single antiplatelet agent in terms of efficacy in patients with AF and stable CAD undergoing PCI (5). However, because the number of patients with CKD [defined as those with an estimated glomerular filtration rate (eGFR) of <60 mL/min per 1.73 m^2] in these RCTs was low, evidence regarding the safety of antithrombotic therapy in patients with CKD remains limited. Moreover, PCI in the management of CAD among patients with CKD is sometimes limited to the risk of contrast-induced renal failure. Therefore, in this study, we investigated the efficacy and safety of antithrombotic therapy in patients with CKD with concomitant AF and CAD in the Evaluating the Prognosis and Impacts in CKD (EPIC) Research of Taipei Veterans General Hospital (VGH).

METHODS

Data Source

This study was based on a single-center, retrospective, observational design. Our main data source was derived from the Big Data Center (BDC) of Taipei VGH. The database contains data regarding demographic characteristics, diagnostic codes, imaging studies, medical procedures, and laboratory findings for outpatient appointments, emergency department visits, and inpatient admissions from January 2010 through December 2018. We used codes from the International Classification of Diseases, Ninth and Tenth Revision (ICD-9 and ICD-10, respectively) to screen the diagnosis of CKD (ICD-9: 585 and ICD-10: N18), non-valvular AF (ICD-9: 427.31 and ICD-10: I48), and CAD (ICD-9: 410, 411, 412, 413, and 414 and ICD-10: I20, I21, I22, I23, I24, and I25). In addition, we used electronic medical record (EMR) system to collect data that were not included or completely recorded in the Taipei VGH BDC, such as social history, event records, and drug prescriptions. The study protocol was approved by the Institutional Review Board of the Taipei VGH (2017-09-002BC) and fulfilled the ethical guidelines of the Declaration of Helsinki.

Participants

We enrolled patients who had concurrent CKD, CAD, and AF indicated for OAC therapy such as warfarin or direct OACs (DOACs, referred to as apixaban, dabigatran, rivaroxaban, and edoxaban). Patients who met all the following criteria were considered to be eligible for participation: (1) age >20 years, (2) males with a baseline CHA_2DS_2-VASc score of >2 and females with a baseline CHA_2DS_2-VASc score of >3, and (3) use of OACs. Exclusion criteria were as follows: (1) history of PCI before enrollment, (2) use antiplatelets other than aspirin and clopidogrel, (3) use OACs <90 days, (4) no availability of serum creatinine and urine protein measurements at baseline and follow-up. According to the prescriptions, patients receiving warfarin or DOACs alone were grouped into the OAC monotherapy group, whereas patients receiving an OAC plus antiplatelets were grouped into the combination therapy group.

Follow-Up and Endpoints

The index date was defined as the first prescription of OACs. Patients were followed up since the index date until death, loss to follow-up, censoring, or December 31, 2018. We included laboratory tests associated with CV risks such as total and low-density lipoprotein cholesterol, triglyceride, glucose, glycated hemoglobin, and hemoglobin. In addition, the baseline serum creatinine and urine protein-to-creatinine ratio were collected. Data of these measurements closest to the index date within 1 month were defined as the baseline. The eGFR values were calculated for serum creatinine by using the Chronic Kidney Disease Epidemiology Collaboration equation. We identified concomitant medications by using the EMR, and only drug exposure within 90 days before the index date was included. Comorbidity patterns in this study were hypertension, DM, congestive heart failure (CHF), and malignancy. Primary outcomes were all-cause mortality and major adverse cardiac events (MACE) including ischemic stroke, acute myocardial infarction, transient ischemic attack, peripheral artery occlusive disease, and hospitalization for CHF. Secondary endpoints were major bleeding, including hemorrhagic stroke, gastrointestinal (GI) bleeding, and other bleeding events. Renal outcomes included CKD progression characterized by the first occurrence

of eGFR declines of >20, >30, >40, and >50%, end-stage renal disease (ESRD), and initiation of dialysis.

Statistical Analysis

Missing values were imputed using the multiple imputation method by fully conditional specification with five repetitions to establish a complete dataset. The baseline characteristics were compared between the two groups of patients by using the x^2 test for categorical variables and independent *t*-test and Mann–Whitney *U*-test for parametric and non-parametric continuous variables, respectively. Propensity scores were calculated with all baseline covariates by using a logistic regression model, and propensity score matching was conducted through the nearest neighbor approach with a caliper of 0.01. The standardized difference was calculated to assess the balance between the two groups after matching, and a difference of <0.2 in the score was considered to indicate a negligible imbalance.

We used the as-treated approach to account for switching antithrombotic medications in a real-world setting. The treatment effect for the time to the first event was estimated using Cox proportional-hazards models. The strength of the association between the exposure and outcome is presented as the hazard ratio (HR) with the 95% confidence interval (CI). The cumulative incidences of all-cause mortality, adverse CV events, CKD progression, and major bleeding were compared among patients receiving different antithrombotic therapies by using the

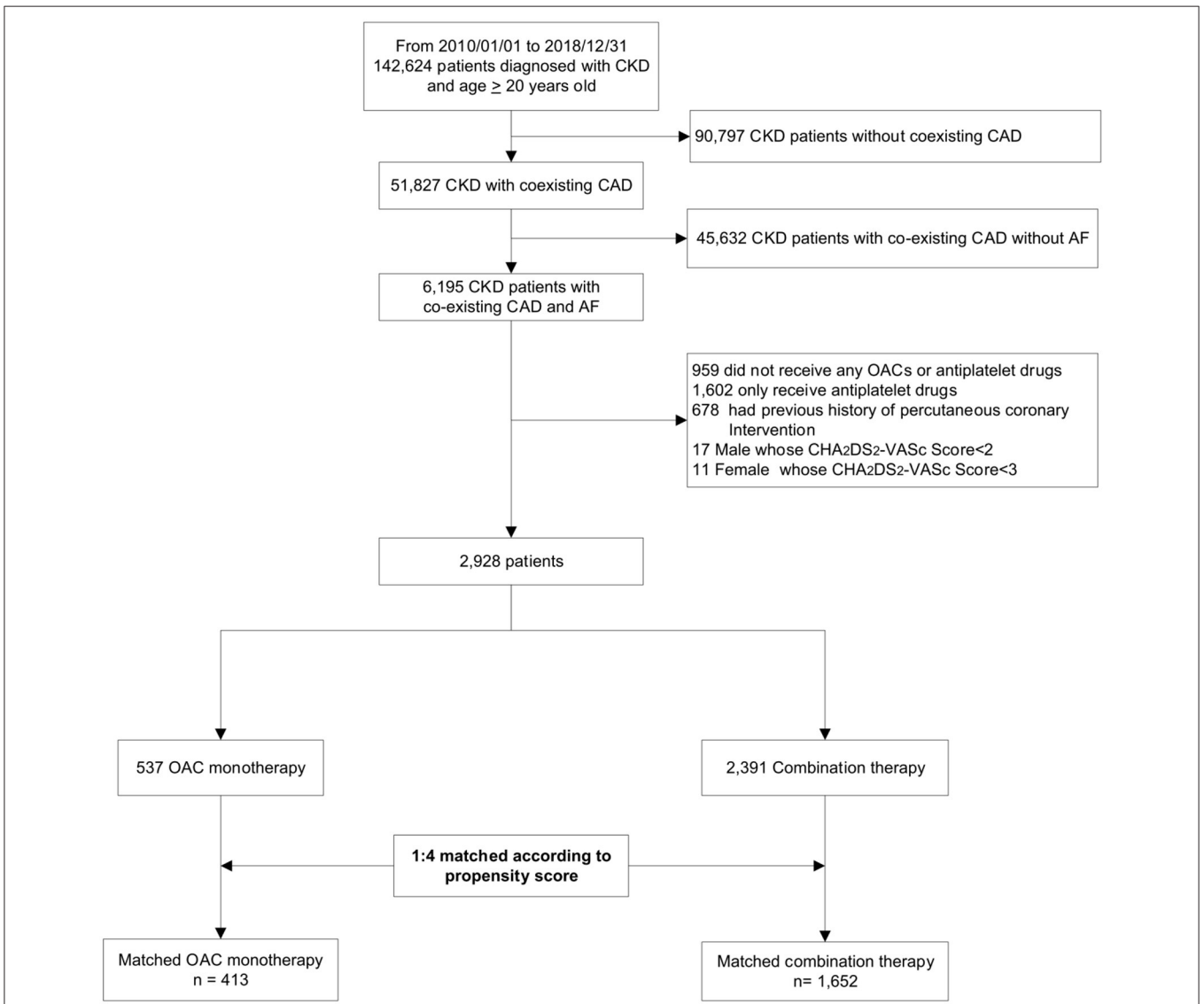

FIGURE 1 | Flowchart of study enrollment. This hospital-based cohort included a total of 142,624 patients with CKD between 2010 and 2018. After excluding ineligible patients, we identified 2,928 patients with concurrent AF and CAD not undergoing percutaneous coronary intervention, and divided them into OAC monotherapy group ($n = 537$) and combination therapy (OAC plus antiplatelets, $n = 2,391$) according to their antithrombotic regimens. Finally, we conducted a 1:4 propensity-score matching to balance baseline covariates. CKD, chronic kidney disease; CAD, coronary artery disease; AF, atrial fibrillation; OAC, oral anticoagulant.

modified Kaplan–Meier method and tested using the log-rank statistic. A $P < 0.05$ was considered statistically significant. All analyses were conducted using SAS 9.4 software (SAS Institute Inc., Cary, NC, USA).

RESULTS

Study Population Characteristics

The patient enrollment process is depicted in **Figure 1**. A total of 142,624 patients were diagnosed of CKD between 2010 and 2018. After excluding patients who did not meet the inclusion criteria, we identified 2,928 patients with concomitant CAD and AF indicated for OAC therapy stratified by the CHA_2DS_2-VASc score. Among eligible participants, 537 were included into the OAC monotherapy group, whereas 2,391 were included into the combination therapy group. The baseline clinical characteristics of these patients are listed in **Table 1**. After 1:4 propensity score matching, the baseline covariates were comparable between the two groups. Furthermore, the distribution balance for the propensity score and the balance plot of absolute standardized effect sizes before and after matching are shown in **Supplementary Table 1**; **Figures 1**, **2**, respectively.

MACE and Bleeding Risks Associated Wih OAC in Combination With Antiplatelets

Figure 2 shows the cumulative event-free probability curve of all-cause mortality, AMI, ischemic stroke, and hemorrhagic stroke between the two groups. During the follow-up period of 88.5 ± 66.4 months, patients receiving OAC monotherapy were found to have more favorable outcomes (all $P < 0.05$; log-rank test). As shown in **Table 2**, compared with the OAC monotherapy group, the combination therapy group had increased risks of all-cause mortality (HR 1.31, 95% CI 1.01–1.71, $P = 0.044$), ischemic stroke (HR 2.37, 95% CI 1.72–3.27, $P < 0.001$), and

TABLE 1 | Baseline characteristics of the study population.

	Before propensity score matching			After propensity score matching		
	OAC monotherapy (*n* = 537)	**Combination therapy* (*n* = 2,391)**	**SMD**	**OAC monotherapy (*n* = 413)**	**Combination therapy* (*n* = 1,652)**	**SMD**
Age, years	78.5 [68.8, 84.2]	80.0 [71.2, 85.8]	0.143	79.8 [71.2, 84.8]	80.4 [72.0, 85.7]	0.041
Male, n (%)	338 (62.9)	1,697 (71.0)	0.171	298 (72.2)	1,171 (70.9)	0.028
Cholesterol, mg/dL	161.0 [139.0, 186.0]	160.0 [137.0, 183.0]	0.085	160.0 [138.0, 184.0]	161.0 [137.0, 183.0]	0.062
LDL, mg/dL	93.0 [77.0, 114.0]	92.0 [74.0, 113.0]	0.068	91.0 [76.0, 113.0]	92.0 [75.0, 113.0]	0.063
TG, mg/dL	92.0 [65.0, 128.0]	91.0 [67.0, 127.5]	0.061	92.0 [65.0, 127.0]	91.0 [67.0, 129.0]	0.065
Glucose, mg/dL	118.0 [101.0, 155.0]	118.0 [100.0, 150.0]	0.021	118.0 [102.0, 155.0]	117.0 [99.0, 150.0]	0.038
HbA1c, %	6.6 [5.9, 7.7]	6.7 [6.0, 8.0]	0.023	6.6 [6.0, 7.7]	6.6 [6.0, 7.8]	0.025
Hemoglobin, g/dL	12.7 [11.2, 13.9]	12.6 [11.2, 14.0]	0.011	12.8 [11.3, 14.0]	12.6 [11.2, 14.0]	0.023
eGFR, mL/min/1.73 m^2			0.121			0.088
>90	37 (6.9)	124 (5.2)		22 (5.3)	90 (5.4)	
60–89	209 (38.9)	849 (35.5)		164 (39.7)	592 (35.8)	
30–59	223 (41.5)	1,050 (43.9)		172 (41.6)	720 (43.6)	
15–29	44 (8.2)	240 (10.0)		37 (9.0)	175 (10.6)	
<15	24 (4.5)	128 (5.4)		18 (4.4)	75 (4.5)	
UPCR, mg/mg	0.2 [0.1, 0.9]	0.2 [0.1, 1.0]	0.050	0.2 [0.1, 1.0]	0.2 [0.1, 0.9]	0.032
Hypertension, *n* (%)	343 (63.9)	1,768 (73.9)	0.219	300 (72.6)	1,218 (73.7)	0.025
DM, *n* (%)	178 (33.1)	921 (38.5)	0.112	149 (36.1)	623 (37.7)	0.034
CHF, *n* (%)	247 (46.0)	1,068 (44.7)	0.027	179 (43.3)	732 (44.3)	0.02
Malignancy, *n* (%)	120 (22.3)	615 (25.7)	0.079	98 (23.7)	425 (25.7)	0.046
ACEIs/ARBs, *n* (%)	339 (63.1)	1,706 (71.4)	0.176	275 (66.6)	1,157 (70.0)	0.074
β-blockers, *n* (%)	305 (56.8)	1,545 (64.6)	0.161	264 (63.9)	1,039 (62.9)	0.021
α-blockers, *n* (%)	144 (26.8)	886 (37.1)	0.221	141 (34.1)	545 (33.0)	0.024
CCBs, *n* (%)	229 (42.6)	1,177 (49.2)	0.132	190 (46.0)	790 (47.8)	0.036
Statins, *n* (%)	126 (23.5)	911 (38.1)	0.321	126 (30.5)	504 (30.5)	<0.001
OHAs, *n* (%)	91 (16.9)	513 (21.5)	0.115	76 (18.4)	339 (20.5)	0.054
Insulins, *n* (%)	113 (21.0)	642 (26.9)	0.136	95 (23.0)	429 (26.0)	0.069

Data are presented as n (%) or median [interquartile range].

**Refers to oral anticoagulants plus antiplatelets.*

OAC, oral anticoagulant; SMD, standardized mean difference; LDL, low-density lipoprotein; TG, triglyceride; HbA1C, glycated hemoglobin; eGFR, estimated glomerular filtration rate; UPCR, urine protein-to-creatinine ratio; DM, diabetes mellitus; CHF, congestive heart failure; ACEI, angiotensin converting enzyme inhibitor; ARB, angiotensin receptor blocker; CCB, calcium channel blockers; OHA, oral hypoglycemic agent.

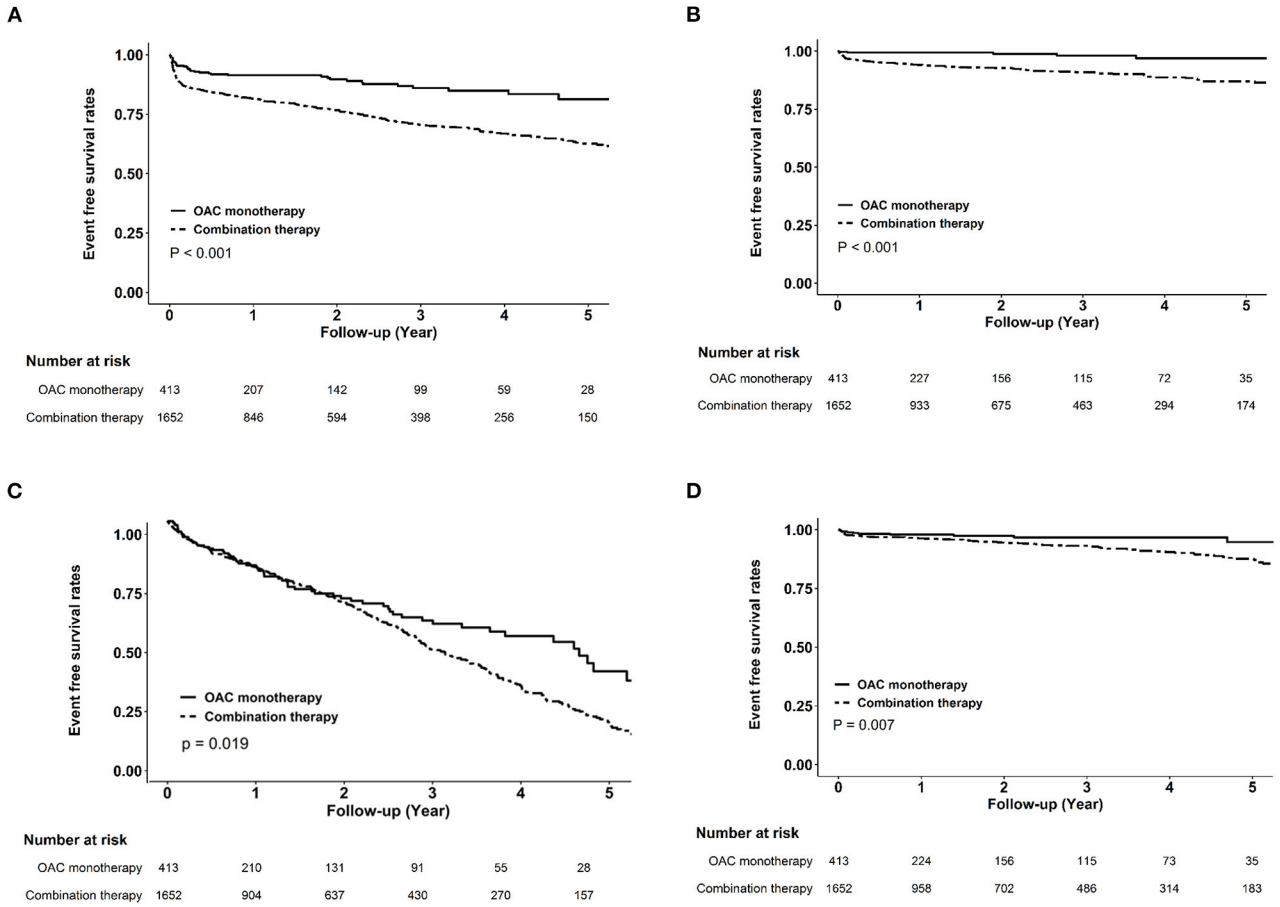

FIGURE 2 | Kaplan–Meier curves of clinical endpoints between oral anticoagulant monotherapy and combination therapy in the matched cohort. Compared with combination therapy, oral anticoagulant monotherapy was associated with higher cumulative event-free probabilities for ischemic stroke **(A)**, myocardial infarction **(B)**, all-cause mortality **(C)**, and hemorrhagic stroke **(D)**.

AMI (HR 6.14, 95% CI 2.51–15.0, $P < 0.001$). Moreover, the combination therapy group had a higher risk of hemorrhagic stroke (HR 3.57, 95% CI 1.3–9.81, $P = 0.014$). The risks of decline in eGFR and ESRD were similar between the two groups.

Subgroup Analyses of MACE and Bleeding Risks Associated With OAC in Combination With Antiplatelets

Supplementary Figures 3–6 compare MACE and bleeding risks among different subgroups of patients receiving OAC monotherapy vs. those receiving combination therapy. Similar to the aforementioned findings, the use of combination therapy was associated with significantly higher risks of ischemic stroke, AMI, all-cause mortality, and hemorrhagic stroke than OAC monotherapy in all subgroups except for age; however, patients aged ≥65 years had higher risks of all-cause mortality (P for interaction $= 0.029$) and hemorrhagic stroke (P for interaction $= 0.011$).

MACE and Bleeding Risks Associated With Warfarin Alone or in Combination With Antiplatelets

As shown in **Table 3**, we divided the matched cohort into four groups in terms with OACs: DOAC monotherapy, DOAC plus antiplatelets, warfarin monotherapy, and warfarin plus antiplatelets. We found that warfarin was associated with higher risks of all-cause mortality (warfarin monotherapy: HR 1.90, 95% CI 1.12–3.22, $P = 0.018$; warfarin plus antiplatelets: HR 2.33, 95% CI 1.47–3.69, $P < 0.001$) compared with DOAC monotherapy. Furthermore, we found that the combination of warfarin with antiplatelets was associated with increased risks of ischemic stroke (HR 2.31, 95% CI 1.47–3.62, $P < 0.001$), AMI (HR 9.4, 95% CI 2.31–38.32, $P = 0.002$), and GI bleeding (HR 2.35, 95% CI 1.38–4.00, $P = 0.002$) among the four subgroups. The risk of CKD progression did not differ between those receiving DOACs and those receiving warfarin, irrespective of whether they were used in combination with antiplatelets.

TABLE 2 | Risks of all-cause mortality, progression of chronic kidney disease, adverse cardiovascular events and bleeding complications between oral anticoagulant monotherapy or combination therapy in patients with chronic kidney disease with atrial fibrillation and coronary artery disease.

Outcomes	OAC monotherapy	Combination therapy*	
	HR (95% CI)	HR (95% CI)	*P*-value
All-cause mortality	Reference	1.31 (1.01–1.71)	0.044
Progression of CKD			
eGFR decline > 20%	Reference	0.88 (0.66–1.17)	0.383
eGFR decline > 30%	Reference	1.15 (0.75–1.77)	0.527
eGFR decline > 40%	Reference	1.08 (0.62–1.89)	0.788
eGFR decline > 50%	Reference	0.86 (0.39–1.89)	0.705
End-stage renal disease†	Reference	1.77 (0.62–5.04)	0.284
Composite renal outcomes‡	Reference	0.75 (0.30–1.88)	0.543
Major adverse cardiac events			
Ischemic stroke	Reference	2.37 (1.72–3.27)	<0.001
AMI	Reference	6.14 (2.51–15.0)	<0.001
Systemic embolism	Reference	1.17 (0.73–1.87)	0.511
TIA	Reference	1.33 (0.7–2.52)	0.386
PAOD	Reference	0.56 (0.22–1.44)	0.229
Hospitalization for CHF	Reference	0.99 (0.86–1.14)	0.906
Bleeding complications			
Hemorrhagic stroke	Reference	3.57 (1.35–9.81)	0.014
GI bleeding	Reference	1.14 (0.84–1.56)	0.405
Other bleeding	Reference	0.99 (0.75–1.31)	0.927

**Refers to an oral anticoagulant plus antiplatelets.*
† eGFR <15 mL/min per 1.73 m^2 necessitating long-term dialysis.
‡ eGFR decline of 50% from baseline or eGFR <15 mL/min per 1.73 m^2 necessitating long-term dialysis.
OAC, oral anticoagulant; HR, hazard ratio; CI, confidence interval; CKD, chronic kidney disease; eGFR, estimated glomerular filtration rates; ESRD, end-stage renal disease; AMI, acute myocardial infarction; TIA, transient ischemic attack; PAOD, peripheral artery occlusive disease; CHF, congestive heart failure; GI, gastrointestinal.

Risks of Thromboembolism and Bleeding Between Warfarin and DOACs

Figure 3 illustrates the risks of thromboembolism and major bleeding associated with warfarin compared with DOACs. In the matched CKD cohort, the risks of all-cause mortality (HR 0.60, 95% CI 0.49–0.74, $P < 0.001$), AMI (HR 0.62, 95% CI 0.43–0.89, $P = 0.013$), and GI bleeding (HR 0.52, 95% CI 0.41–0.68, $P < 0.001$) were significantly lower in patients treated with DOACs compared with those treated with warfarin. Nevertheless, the risks of ischemic and hemorrhage stroke were not different between the two groups. These findings were consistent before and after propensity score matching.

DISCUSSION

This large-scale retrospective cohort study showed that OAC monotherapy appears to a preferable antithrombotic therapy in patients with CKD with concomitant AF and CAD who had not undergone PCI. The findings of propensity score-matched analysis revealed that the additional use of antiplatelets along with OACs did not exert a stronger protective effect on ischemic stroke and AMI but significantly increased the risk of hemorrhagic stroke. The results were consistent across subgroups categorized by sex, history of hypertension or DM, and baseline eGFR. We also found that the use of DOACs in patients with CKD was associated with a lower risk of all-cause mortality, AMI, and GI bleeding than the use of warfarin. Our study indicated that DOAC monotherapy might be feasible for the management of concurrent AF and CAD in high-risk CKD patients.

To the best of our knowledge, this is the first study to show that OAC alone significantly reduced the CV risks and resulted in lower bleeding and mortality risks compared with combination therapy among patients with CKD and concomitant AF and CAD. Antiplatelets have been considered the drug of choice on primary and secondary preventions in patients with CAD and CKD (6), whereas OAC therapy is crucial for lowering the risk for stroke and thromboembolism in patients with concomitant AF and CKD (7). Our finding has clinical relevance since some physicians prefer prescribing antiplatelets instead of OACs for CKD patients at high bleeding risk. However, irrespective of the antiplatelet regimen used, the deletion of OAC from treatment is inadequate for the prevention of thromboembolism in patients with CKD with a CHA_2DS_2-VASc score of 2 or higher (8). On the other hand, we observed that the combined use of antiplatelets with OACs might enhance the risk of AMI among patients with CKD compared to use OACs alone. Although the use of antiplatelets can reduce the risk of ischemic stroke and acute coronary syndrome in patients with normal kidney function, some studies have reported the phenomenon of "antiplatelet resistance" characterized by a poor response to aspirin or clopidogrel in patients with CKD (9, 10). Besides, Jeong et al. have reported that the suboptimal response to antiplatelets is nearly 70% in some of the Asian communities due to genetic polymorphism, and suggested a different therapeutic window of platelet reactivity in East Asians (11, 12). The failure to suppress platelet activity leads to the increased thrombogenicity and may explain the higher risks of ischemic stroke and AMI despite using combination therapy among our participants. Therefore, we suggested that an appropriate OAC use is critical to overcoming the low effectiveness of antiplatelets in patients with CKD with concomitant AF and CAD, especially in those for whom PCI for coronary revascularization is not suitable.

Previous studies and a recent meta-analysis have reached the same conclusion to use OAC monotherapy in patients with AF with stable CAD for 1 year or more after PCI (13, 14). Nevertheless, patients with CKD were often excluded from such clinical trials. By contrast, we included patients with CKD with concomitant CAD who had not yet received PCI. Large-scale prospective CKD trials evaluating the relevance of the proposed treatment strategy are lacking. Our study is the first to illustrate the suitability of OAC prescription in patients with CKD with concomitant AF and CAD.

Although warfarin is the standard treatment for patients with CKD stage 4–5D, we found that DOACs can be a preferred option for the prevention of thromboembolism irrespective of

TABLE 3 | Risks of all-cause mortality, progression of chronic kidney disease, adverse cardiovascular events and bleeding complications between the four groups of antithrombotic treatments in patients with chronic kidney disease with atrial fibrillation and coronary artery disease.

Outcomes	DOAC* monotherapy	Warfarin monotherapy		DOAC* plus antiplatelets		Warfarin plus antiplatelets	
	Crude HR (95% CI)	Crude HR (95% CI)	*P*-value	Crude HR (95% CI)	*P*-value	Crude HR (95% CI)	*P*-value
All-cause mortality	Reference	1.90 (1.12–3.22)	0.018	1.45 (0.9–2.33)	0.123	2.33 (1.47–3.69)	<0.001
Progression of CKD							
eGFR decline > 20%	Reference	1.5 (0.91–2.48)	0.113	1.05 (0.69–1.58)	0.828	1.09 (0.72–1.64)	0.677
eGFR decline > 30%	Reference	1.41 (0.64–3.1)	0.387	1.22 (0.65–2.27)	0.541	1.51 (0.81–2.79)	0.195
eGFR decline > 40%	Reference	0.85 (0.3–2.39)	0.759	0.81 (0.38–1.73)	0.594	1.22 (0.59–2.52)	0.598
eGFR decline > 50%	Reference	1.24 (0.31–4.97)	0.760	0.67 (0.21–2.12)	0.492	1.25 (0.42–3.7)	0.686
End stage renal disease†	Reference	3.53 (0.37–34.01)	0.274	0.79 (0.08–7.59)	0.838	6.93 (0.94–51.11)	0.058
Composite renal outcomes‡	Reference	1.15 (0.23–5.71)	0.864	0.25 (0.05–1.26)	0.093	1.36 (0.4–4.67)	0.626
Major adverse cardiac events							
Ischemic stroke	Reference	1.03 (0.56–1.9)	0.922	2.52 (1.6–3.95)	<0.001	2.31 (1.47–3.62)	<0.001
AMI	Reference	1.54 (0.26–9.23)	0.636	5.96 (1.45–24.58)	0.013	9.4 (2.31–38.32)	0.002
Systemic embolism	Reference	2.45 (0.95–6.35)	0.064	1.94 (0.83–4.55)	0.127	2.11 (0.91–4.91)	0.084
TIA	Reference	0.33 (0.09–1.27)	0.108	1.12 (0.52–2.41)	0.780	0.66 (0.29–1.47)	0.307
PAOD	Reference	0.75 (0.15–3.84)	0.728	0.58 (0.15–2.25)	0.434	0.41 (0.10–1.63)	0.204
Hospitalization for CHF	Reference	1.12 (0.87–1.44)	0.391	0.89 (0.73–1.1)	0.285	1.19 (0.98–1.45)	0.083
Bleeding complications							
Hemorrhagic stroke	Reference	0.79 (0.11–5.63)	0.813	3.31 (0.79–13.91)	0.102	3.03 (0.73–12.68)	0.128
GI bleeding	Reference	2.28 (1.23–4.22)	0.009	1.28 (0.74–2.24)	0.375	2.35 (1.38–4.00)	0.002
Other bleeding	Reference	0.84 (0.50–1.39)	0.489	1.1 (0.74–1.63)	0.631	0.75 (0.5–1.12)	0.161

**Refers to apixaban, dabigatran, rivaroxaban, and edoxaban.*

†Defined as eGFR of <15 mL/min per 1.73 m^2, necessitating long-term dialysis.

‡eGFR decline of 50% from baseline or eGFR < 15 mL/min per 1.73 m^2, necessitating long-term dialysis.

DOAC, direct oral anticoagulant; HR, hazard ratio; CI, confidence interval; CKD, chronic kidney disease; eGFR, estimated glomerular filtration rates; ESRD, end-stage renal disease; TIA, transient ischemic attack; PAOD, peripheral artery occlusive disease; AMI, acute myocardial infarction, CHF, congestive heart failure; GI, gastrointestinal.

the levels of eGFR. Besides, some observational studies have shown that the renal function of warfarin users tends to decline faster than that of DOACs (15, 16). To explain this phenomenon, Brodsky et al. reported that the nephrotoxicity of warfarin were positively correlated with excessive anticoagulation with an international normalized ratio (INR) of >3.0, which may cause clinically relevant bleeding or glomerular hemorrhage termed "anticoagulant-related nephropathy" (17). In this study, we did not find that DOACs were superior to warfarin in terms of renal outcomes; however, DOACs can be an appropriate and safe antithrombotic treatment for patients with CKD, even in the pre-dialysis stages. This finding was parallel to recent studies that suggested DOACs had comparable efficacy and were safer than warfarin in patients with an eGFR of <15 mL/min per 1.73 m^2 and those on hemodialysis (HD) (18–21). Recently the Kidney Disease: Improving Global Outcomes (KDIGO) conference approved the consideration regarding the use of a lower dose of apixaban or rivaroxaban in patients with advanced CKD (22). Accordingly, DOACs potentially have equal effectiveness as warfarin and better safety outcomes in patients with AF with advanced CKD.

A substantial proportion of CKD patients inevitably develop ESRD, leading to high CV risk attributed to anemia, endothelial dysfunction, vascular calcification, and oxidative stress (23). Dialysis therapy *per se* significantly impacts coagulation and thrombosis, and warfarin has also been associated with vascular calcification in HD patients (24–26). Randhawa et al. conducted a meta-analysis with 15 observational studies reporting the outcomes of 47,480 patients with AF and ESRD. They found the use of warfarin had no benefits on lowering risks for ischemic stroke, major bleeding, and mortality, but with a significantly higher risk of hemorrhagic stroke in ESRD patients (27). A recent network meta-analysis also showed no evidence of reducing thromboembolic events with warfarin or DOACs in patients with AF and ESRD (28). Although an increasingly popular approach is to use apixaban for stroke prevention among patients with AF and ESRD, the outcomes derived from previous studies were inconstant (18, 20, 29, 30). Therefore, the lack of robust evidence of an appropriate OAC therapeutic approach for dialysis patients highlights the urgent need for additional research in this population.

This study has some limitations. First, the study population was composed of Taiwanese patients from a single center; thus, the results may not be applicable to other ethnic groups. Second, because of the lack of specific details regarding the

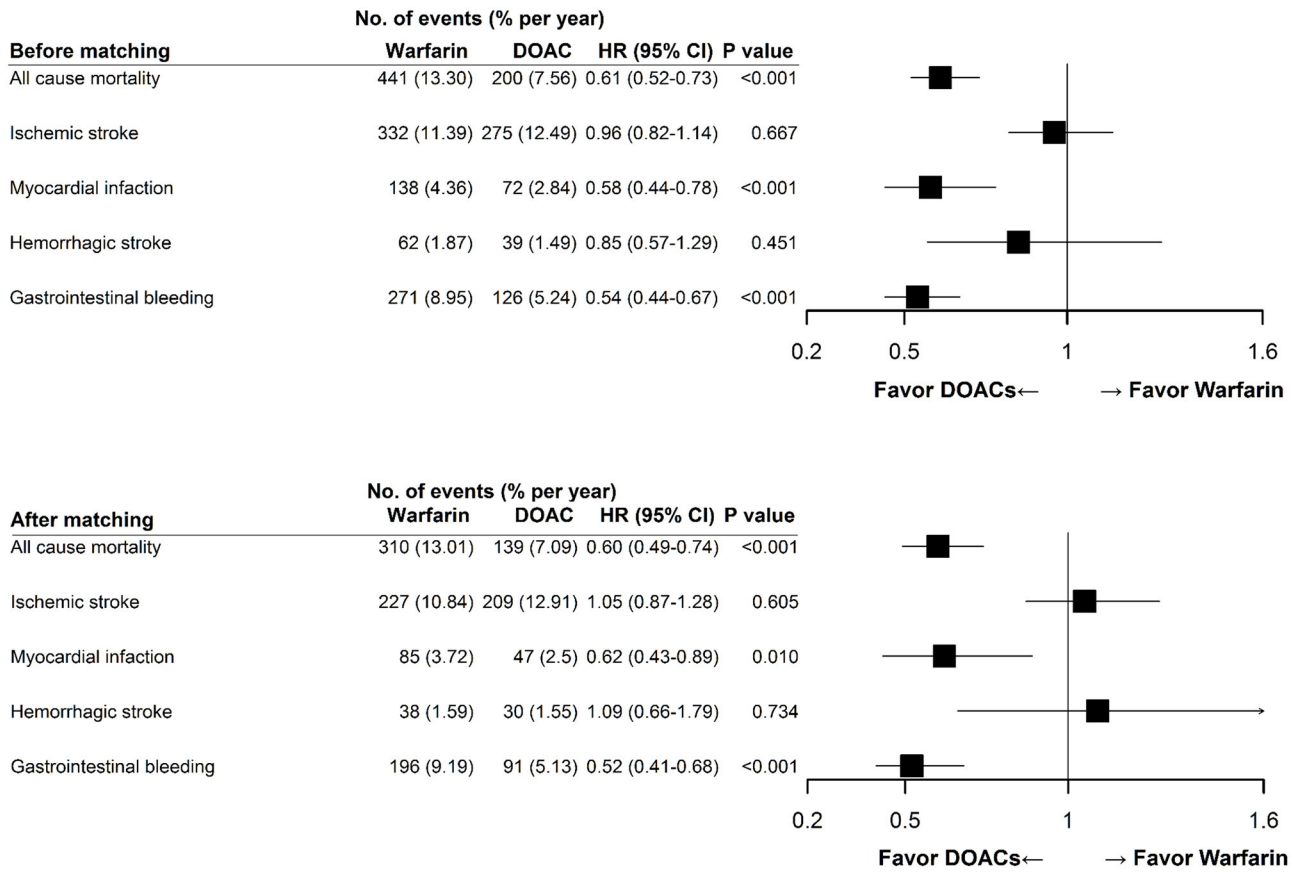

FIGURE 3 | Clinical endpoints of direct oral anticoagulant use compared with warfarin use. Multivariable Cox proportional hazards model showed that DOAC use was associated with lower rates of all-cause mortality, myocardial infarction, and gastrointestinal bleeding, and a similar rate of ischemic and hemorrhagic stroke compared with warfarin use. These findings were consistent before and after propensity score matching. DOAC, direct oral anticoagulant; HR, hazard ratio; CI, confidence interval.

time in the therapeutic range (6) of warfarin, we could not assess the adequacy of OAC therapy in patients treated with warfarin. In consideration of bleeding tendency attributed to uremic toxins, anemia, and platelet dysfunction in patients with advanced CKD and that undergoing dialysis, the INR target of warfarin therapy in patients with ESRD was apparently conservative in clinical practice. We estimated a low TTR in warfarin users, which reflects poor anticoagulation control and might have affected outcomes in this study. Third, selection bias may exist in a retrospective cohort design. However, we adjusted for potential confounders by using propensity score matching. Moreover, we have to acknowledge that the distributions of CKD among our participants were mainly in stages 3 and 4, whereas the number of ESRD patients taking OACs is small; thereby, our findings might not apply to dialysis-dependent CKD patients. Finally, our study is observational in nature; thus, it cannot prove causality. Nevertheless, given the limited evidence from RCTs on antithrombotic therapy exclusively for patients with CKD, our results indicate the effectiveness and safety of using DOACs alone for AF and CAD among patients with CKD in routine clinical practice.

CONCLUSIONS

In patients with CKD with concomitant AF and CAD who had not undergone PCI, OAC in combination with antiplatelets might not provide additional benefits for the prevention of MACE and further be associated with a higher risk of bleeding events. DOACs can be the preferred OAC therapy than warfarin, with a lower risk of all-cause mortality as well as AMI and GI bleeding. Additional prospective clinical studies are needed to reinforce our findings.

DATA AVAILABILITY STATEMENT

The raw data supporting the conclusions of this article will be made available by the authors, without undue reservation.

ETHICS STATEMENT

The studies involving human participants were reviewed and approved by Institutional Review Board of the Taipei Veterans General Hospital. Written informed consent for participation

was not required for this study in accordance with the national legislation and the institutional requirements.

AUTHOR CONTRIBUTIONS

Y-PL and D-CT were involved in planning and supervised the work. K-HL and S-MO processed the experimental data, performed the analysis, drafted the manuscript, and designed the figures. Y-CC designed the model and the computational framework. M-TT aided in interpreting the results and worked on the manuscript. All authors discussed the results and commented on the manuscript.

FUNDING

This work was supported by grants from the Ministry of Science and Technology, ROC (109-2314-B-010-056-MY3 and 109-2314-B-075-066) and Taipei Veterans General Hospital (V108D42-004-MY3-2, V109D50-001-MY3-1, V108C-103, V109C-114, and V109B-016). This work was also financially supported by the Center for Intelligent Drug Systems and Smart Bio-devices (IDS^{2}B) from the Featured Areas Research Center Program within the framework of the Higher Education Sprout Project by the Ministry of Education (MOE) in Taiwan, and Foundation for Poison Control (FPC-110-003).

ACKNOWLEDGMENTS

Members of Evaluating the Prognosis and Impacts in CKD (EPIC) Taiwan Research Group in Taipei Veterans General Hospital include D-CT, S-MO, Y-CC, Y-PL, K-HL, M-TT, Chih-Yu Yang, Wei-Cheng Tseng, and Jia-Sin Liu.

SUPPLEMENTARY MATERIAL

The Supplementary Material for this article can be found online at: https://www.frontiersin.org/articles/10.3389/fcvm.2021.751359/full#supplementary-material

REFERENCES

1. Schmitt J, Duray G, Gersh BJ, Hohnloser SH. Atrial fibrillation in acute myocardial infarction: a systematic review of the incidence, clinical features and prognostic implications. *Eur Heart J.* (2009) 30:1038–45. doi: 10.1093/eurheartj/ehn579
2. Dewilde WJ, Oirbans T, Verheugt FW, Kelder JC, De Smet BJ, Herrman JP, et al. Use of clopidogrel with or without aspirin in patients taking oral anticoagulant therapy and undergoing percutaneous coronary intervention: an open-label, randomised, controlled trial. *Lancet.* (2013) 381:1107–15. doi: 10.1016/S0140-6736(12)62177-1
3. Lamberts M, Gislason GH, Olesen JB, Kristensen SL, Schjerning Olsen AM, Mikkelsen A, et al. Oral anticoagulation and antiplatelets in atrial fibrillation patients after myocardial infarction and coronary intervention. *J Am Coll Cardiol.* (2013) 62:981–9. doi: 10.1016/j.Jacc.2013.05.029
4. Cannon CP, Bhatt DL, Oldgren J, Lip GYH, Ellis SG, Kimura T, et al. Dual antithrombotic therapy with dabigatran after PCI in atrial fibrillation. *N Engl J Med.* (2017) 377:1513–24. doi: 10.1056/NEJMoa1708454
5. Yasuda S, Kaikita K, Akao M, Ako J, Matoba T, Nakamura M, et al. Antithrombotic therapy for atrial fibrillation with stable coronary disease. *N Engl J Med.* (2019) 381:1103–13. doi: 10.1056/NEJMoa1904143
6. Agrawal H, Aggarwal K, Littrell R, Velagapudi P, Turagam MK, Mittal M, et al. Pharmacological and non pharmacological strategies in the management of coronary artery disease and chronic kidney disease. *Curr Cardiol Rev.* (2015) 11:261–9. doi: 10.2174/1573403x1103150514155757
7. Turagam MK, Addepally NS, Velagapudi P. Novel anticoagulants for stroke prevention in atrial fibrillation and chronic kidney disease. *Expert Rev Cardiovasc Ther.* (2013) 11:1297–9. doi: 10.1586/14779072.2013.839188
8. Lip GY, Windecker S, Huber K, Kirchhof P, Marin F, Ten Berg JM, et al. Management of antithrombotic therapy in atrial fibrillation patients presenting with acute coronary syndrome and/or undergoing percutaneous coronary or valve interventions: a joint consensus document of the European Society of Cardiology Working Group on Thrombosis, European Heart Rhythm Association (EHRA), European Association of Percutaneous Cardiovascular Interventions (EAPCI) and European Association of Acute Cardiac Care (ACCA) Endorsed by the Heart Rhythm Society (HRS) and Asia-Pacific Heart Rhythm Society (APHRS). *Eur Heart J.* (2014) 35:3155–79. doi: 10.1093/Eurheartj/Ehu298
9. Morel O, Muller C, Jesel L, Moulin B, Hannedouche T. Impaired platelet P2Y12 inhibition by thienopyridines in chronic kidney disease: mechanisms, clinical relevance and pharmacological options. *Nephrol Dial Transplant.* (2013) 28:1994–2002. doi: 10.1093/ndt/Gft027
10. Polzin A, Dannenberg L, Sansone R, Levkau B, Kelm M, Hohlfeld T, et al. Antiplatelet effects of aspirin in chronic kidney disease patients. *J Thromb Haemost.* (2016) 14:375–80. doi: 10.1111/jth.13211
11. Jeong YH. "East Asian Paradox": Challenge for the current antiplatelet strategy of "one-Guideline-Fits-All Races" in acute coronary syndrome. *Curr Cardiol Rep.* (2014) 16:485. doi: 10.1007/S11886-014-0485-4
12. Kim HK, Tantry US, Smith SC Jr., Jeong MH, Park SJ, Kim MH, et al. The East Asian paradox: an updated position statement on the challenges to the current antithrombotic strategy in patients with cardiovascular disease. Thromb Haemost. (2021) 121:422–32. doi: 10.1055/s-0040-1718729
13. Lee SR, Rhee TM, Kang DY, Choi EK, Oh S, Lip GYH. Meta-analysis of oral anticoagulant monotherapy as an antithrombotic strategy in patients with stable coronary artery disease and nonvalvular atrial fibrillation. *Am J Cardiol.* (2019) 124:879–85. doi: 10.1016/j.Amjcard.2019.05.072
14. Fischer Q, Georges JL, Le Feuvre C, Sharma A, Hammoudi N, Berman E, et al. Optimal long-term antithrombotic treatment of patients with stable coronary artery disease and atrial fibrillation: "OLTAT registry". *Int J Cardiol.* (2018) 264:64–9. doi: 10.1016/j.Ijcard.2018.03.018
15. Chan YH, Yeh YH, Hsieh MY, Chang CY, Tu HT, Chang SH, et al. The risk of acute kidney injury in asians treated with apixaban, rivaroxaban, dabigatran, or warfarin for non-valvular atrial fibrillation: a nationwide cohort study in Taiwan. *Int J Cardiol.* (2018) 265:83–9. doi: 10.1016/j.Ijcard.2018.02.075
16. Yao X, Shah ND, Sangaralingham LR, Gersh BJ, Noseworthy PA. Non-vitamin K antagonist oral anticoagulant dosing in patients with atrial fibrillation and renal dysfunction. *J Am Coll Cardiol.* (2017) 69:2779–90. doi: 10.1016/j.Jacc.2017.03.600
17. Brodsky S, Eikelboom J, Hebert LA. Anticoagulant-related nephropathy. *J Am Soc Nephrol.* (2018) 29:2787–93. doi: 10.1681/ASN.2018070741
18. Siontis KC, Zhang X, Eckard A, Bhave N, Schaubel DE, He K, et al. Outcomes associated with apixaban use in patients with end-stage kidney disease and atrial fibrillation in the United States. *Circulation.* (2018) 138:1519–29. doi: 10.1161/circulationaha.118.035418
19. Coleman CI, Kreutz R, Sood NA, Bunz TJ, Eriksson D, Meinecke AK, et al. Rivaroxaban versus warfarin in patients with nonvalvular atrial fibrillation and severe kidney disease or undergoing hemodialysis. *Am J Med.* (2019) 132:1078–83. doi: 10.1016/j.Amjmed.2019.04.013
20. Reed D, Palkimas S, Hockman R, Abraham S, Le T, Maitland H. Safety and effectiveness of apixaban compared to warfarin in dialysis patients. *Res Pract Thromb Haemost.* (2018) 2:291–98. doi: 10.1002/Rth2.12083
21. Schafer JH, Casey AL, Dupre KA, Staubes BA. Safety and efficacy of apixaban versus warfarin in patients with advanced chronic kidney disease. *Ann Pharmacother.* (2018) 52:1078–84. doi: 10.1177/1060028018781853

22. Turakhia MP, Blankestijn PJ, Carrero JJ, Clase CM, Deo R, Herzog CA, et al. Chronic kidney disease and arrhythmias: conclusions from a kidney disease: improving global outcomes (KDIGO) controversies conference. *Eur Heart J.* (2018) 39:2314–25. doi: 10.1093/Eurheartj/Ehy060
23. Cachofeiro V, Goicochea M, de Vinuesa SG, Oubina P, Lahera V, Luno J. Oxidative stress and inflammation, a link between chronic kidney disease and cardiovascular disease. *Kidney Int Suppl.* (2008) 2008:S4–9. doi: 10.1038/ki.2008.516
24. Lee KH Li SY, Liu JS, Huang CT, Chen YY, Lin YP, et al. Association of warfarin with congestive heart failure and peripheral artery occlusive disease in hemodialysis patients with atrial fibrillation. *J Chin Med Assoc.* (2017) 80:277–82. doi: 10.1016/j.Jcma.2016.10.012
25. Danziger J. Vitamin K-dependent proteins, warfarin, and vascular calcification. *Clin J Am Soc Nephrol.* (2008) 3:1504–10. doi: 10.2215/CJN.00770208
26. Tsai MT, Chen YY, Chang WJ Li SY. Warfarin accelerated vascular calcification and worsened cardiac dysfunction in remnant kidney mice. *J Chin Med Assoc.* (2018) 81:324–30. doi: 10.1016/j.Jcma.2017.08.021
27. Randhawa MS, Vishwanath R, Rai MP, Wang L, Randhawa AK, Abela G, et al. Association between use of warfarin for atrial fibrillation and outcomes among patients with end-stage renal disease: a systematic review and meta-analysis. *JAMA Netw Open.* (2020) 3:e202175. doi: 10.1001/Jamanetworkopen.2020.2175
28. Kuno T, Takagi H, Ando T, Sugiyama T, Miyashita S, Valentin N, et al. Oral anticoagulation for patients with atrial fibrillation on long-term hemodialysis. *J Am Coll Cardiol.* (2020) 75:273–85. doi: 10.1016/j.Jacc.2019.10.059
29. Mavrakanas TA, Garlo K, Charytan DM. Apixaban versus no anticoagulation in patients undergoing long-term dialysis with incident atrial fibrillation. *Clin J Am Soc Nephrol.* (2020) 15:1146–54. doi: 10.2215/CJN.11650919
30. Bowie M, Valencia V, Perez-Alvarez I, Tran MH. Safety analysis of apixaban versus warfarin in patients with advanced kidney disease. *J Thromb Thrombolysis.* (2018) 46:246–52. doi: 10.1007/S11239-018-1683-5

Conflict of Interest: The authors declare that the research was conducted in the absence of any commercial or financial relationships that could be construed as a potential conflict of interest.

Publisher's Note: All claims expressed in this article are solely those of the authors and do not necessarily represent those of their affiliated organizations, or those of the publisher, the editors and the reviewers. Any product that may be evaluated in this article, or claim that may be made by its manufacturer, is not guaranteed or endorsed by the publisher.

frontiers in Cardiovascular Medicine

CLINICAL TRIAL
published: 25 October 2021
doi: 10.3389/fcvm.2021.761112

External Counterpulsation Improves Angiogenesis by Preserving Vascular Endothelial Growth Factor-A and Vascular Endothelial Growth Factor Receptor-2 but Not Regulating MicroRNA-92a Expression in Patients With Refractory Angina

Ade Meidian Ambari[1], Gracia Lilihata[1], Ervan Zuhri[1], Elok Ekawati[2], Shoma Adhi Wijaya[2], Bambang Dwiputra[1], Renan Sukmawan[1], Basuni Radi[1], Sofia Mubarika Haryana[3], Suko Adiarto[1], Dicky A. Hanafy[1], Dian Zamroni[1], Elen Elen[1], Arwin S. Mangkuanom[1] and Anwar Santoso[1]

[1] Department of Cardiology and Vascular Medicine, Faculty of Medicine Universitas Indonesia - National Cardiovascular Center Harapan Kita, Jakarta, Indonesia, [2] Division of Cardiovascular Research and Development, National Cardiovascular Center Harapan Kita, Jakarta, Indonesia, [3] Department of Histology and Cell Biology, Faculty of Medicine, Public Health and Nursing, Universitas Gadjah Mada, Yogyakarta, Indonesia

OPEN ACCESS

Edited by:
Xiaofeng Yang,
Temple University, United States

Reviewed by:
Yu Sun,
Temple University, United States
Owais Bhat,
Virginia Commonwealth University, United States

***Correspondence:**
Anwar Santoso
awscip@gmail.com

Specialty section:
This article was submitted to Cardiovascular Therapeutics, a section of the journal Frontiers in Cardiovascular Medicine

Received: 19 August 2021
Accepted: 22 September 2021
Published: 25 October 2021

Citation:
Ambari AM, Lilihata G, Zuhri E, Ekawati E, Wijaya SA, Dwiputra B, Sukmawan R, Radi B, Haryana SM, Adiarto S, Hanafy DA, Zamroni D, Elen E, Mangkuanom AS and Santoso A (2021) External Counterpulsation Improves Angiogenesis by Preserving Vascular Endothelial Growth Factor-A and Vascular Endothelial Growth Factor Receptor-2 but Not Regulating MicroRNA-92a Expression in Patients With Refractory Angina. Front. Cardiovasc. Med. 8:761112. doi: 10.3389/fcvm.2021.761112

Objective: External counterpulsation (ECP) provides long-term benefits of improved anginal frequency and exercise tolerance in patients with refractory angina (RA). This is postulated as a result of improved angiogenesis and endothelial function through an increase in shear stress. Angiogenesis is mainly represented by vascular endothelial growth factor-A (VEGF-A) and its receptor, vascular endothelial growth factor receptor-2 (VEGFR-2). The microRNA-92a (miR-92a) is a flow-sensitive miRNA that regulates atherosclerosis and angiogenesis in response to shear stress. Thus, ECP beneficial effect might be achieved through interaction between VEGF-A, VEGFR-2, and miR-92a. This study aims to evaluate the ECP effect on VEGF-A, VEGFR-2, and miR-92a in patients with RA in a sham-controlled manner.

Methods: This was a randomized sham-controlled trial, enrolling 50 patients with RA who have coronary artery disease (CAD). Participants were randomized (1:1 ratio) to 35 sessions of either ECP ($n = 25$) or sham ($n = 25$), each session lasting for 1 h. Plasma levels of VEGF-A and VEGFR-2 were assayed by the ELISA technique. The quantitative reverse transcription-polymerase chain reaction (qRT-PCR) was performed to measure miR-92a circulating levels in plasma.

Result: External counterpulsation significantly preserved VEGF-A and VEGFR-2 level compared to sham [ΔVEGF-A: 1 (−139 to 160) vs.−136 (−237 to 67) pg/ml, $p = 0.026$; ΔVEGFR-2: −171(-844 to +1,166) vs. −517(−1,549 to +1,407) pg/ml, $p = 0.021$, respectively]. Circulating miR-92a increased significantly in ECP [5.1 (4.2–6.4) to 5.9 (4.8–6.4), $p < 0.001$] and sham [5.2 (4.1–9.4) to 5.6 (4.8–6.3), $p = 0.008$] post-intervention. The *fold changes* tended to be higher in ECP group, although

was not statistically different from sham [*fold changes* ECP = 4.6 (0.3–36.5) vs. sham 2.8 (0–15), $p = 0.33$)].

Conclusion: External counterpulsation improved angiogenesis by preserving VEGF-A and VEGFR-2 levels. Both ECP and sham increased miR-92a significantly, yet the changes were not different between the two groups. (Study registered on www.clinicaltrials.gov, no: NCT03991871, August 8, 2019, and received a grant from the National Health Research and Development of Ministry of Health of Indonesia, No: HK.02.02/I/27/2020).

Keywords: external counter pulsation (ECP), vascular endothelial growth factor (VEGF), vascular endothelial growth factor-A (VEGF-A), vascular endothelial growth factor receptor-2 (VEGFR-2), micro RNA-92a (miR-92a), angiogenesis

INTRODUCTION

Refractory angina (RA), typically occurring in patients with advanced, often diffuse coronary artery disease (CAD), is described as angina that is still present despite optimal pharmacologic, intervention, or surgery which has been provided for >3 months (1). It is an emergent problem in patients with advanced CAD due to an aging population and improved survival from CAD (2, 3). Management of RA is aimed at toward reducing symptoms, improve quality of life (QoL), and preventing future cardiovascular events. Unfortunately, as many as 15% of the patients fail to respond to the management mentioned above or are ineligible to further intervention (2). Therefore, researchers are always trying to find new alternatives in clinical management.

External counterpulsation (ECP) is a noninvasive therapy employing external compressive cuffs on the calves and lower and upper thighs. It sequentially inflates cuffs from distal to proximal ends synchronized with the cardiac cycle detected by an electrocardiogram (ECG). The cuffs are inflated in early diastole to boost coronary artery perfusion, venous return, and then deflated simultaneously in systole to reduce systemic vascular resistance, cardiac workload, and enhance systemic perfusion (4). The effect of diastolic augmentation and increased coronary perfusion pressure was thought to be the reason for improvement in angina symptoms. However, improvement of symptoms was shown to persist for years after the completion of treatment, which could not be described by the acute hemodynamic effect only (5). Increased shear stress in coronary circulation by ECP treatment is then proposed as a principal underlying mechanism, resulting in multiple downstream favorable mechanisms, including an increase in angiogenesis, collateral circulation, improved endothelial function, and reduced arterial stiffness (4, 6, 7).

Improvement in angiogenesis has been indicated by many studies as one of the main mechanisms (8–12). Angiogenesis is mainly represented by vascular endothelial growth factor-A (VEGF-A) and vascular endovascular growth factor receptor-2 (VEGFR-2). There are several types of VEGF, including VEGF-A, VEGF-B, VEGF-C, VEGF-D, and VEGF-E. Among these types the VEGF-A plays the most important role in controlling angiogenesis (13). VEGF-A signaling goes through the class IV receptor tyrosine kinase group, the VEGF receptors (VEGFR). Although the VEGF-A ligand can bind to two VEGF-R receptors, namely VEGFR-1 and VEGFR-2, VEGF-A will primarily signal endothelial cell proliferation, survival, migration, and vascular permeability *via* VEGFR-2 (14). A previous study stated that ECP has a tendency for increasing VEGF (but not specifically VEGF-A) release in patients with CAD (15). However, there is no study that clearly and specifically evaluated the impact of ECP on VEGF-A and VEGFR-2 levels in a sham-controlled manner. Furthermore, high shear-stress flow has been shown by *in vitro* studies to decrease miRNA-92a (miR-92a), a pro-atherosclerotic and anti-angiogenesis miRNA (16). Due to scientific gaps in the effect of ECP on angiogenesis and miRNA-92a, this study aims to evaluate the effect of ECP therapy on angiogenesis represented by VEGF-A and VEGFR-2 and flow-sensitive miR-92a in patients with RA.

MATERIALS AND METHODS

Study Design and Site of the Study

The HARTEC study was a randomized sham-controlled clinical trial with a parallel assignment to evaluate the effect of ECP therapy on angiogenesis, represented by the concentration of VEGF-A and VEGFR-2. The study also measured the expression of miR-92a since miR-92a is known as a mechano-miRNA that is affected by the high shear stress involved in the regulation of angiogenesis.

The study was conducted at the National Cardiovascular Center, Harapan Kita Hospital, Jakarta, Indonesia. This site was chosen because it is a tertiary hospital for cardiovascular care for most patients with severity levels-III (the highest level) referred from over the country. The study design has been registered on www.clinicaltrials.gov with an identifier number of NCT03991871 on August 8, 2019.

Study Population

The study participants were patients with RA who did not respond to escalating medical treatment, determined by following the stepwise strategy of pharmacological agents based on the 2019 ESC Guidelines to diagnose and manage chronic coronary syndrome (17) after 3 months. Inclusion criteria were defined as the following: patients with angina pectoris aged 21–80 years old, suffering from RA with Canadian Cardiovascular

Society (CCS) II–IV and who were not eligible for percutaneous coronary intervention (PCI) or coronary artery bypass grafting (CABG). The patients had stenosis on the left main (LM) coronary artery; more than 50% of patients had stenosis either on the main right coronary artery (RCA) and left anterior descending (LAD) artery, or more than 70% of them had left circumflex (LCX) artery. They were also not suitable candidates for further revascularization procedures decided in a presurgical conference in our hospital, or they refused any revascularization option. This conference was a regular meeting discussing the best option procedures in our hospital for patients with CAD.

Accordingly, the exclusion criteria were determined as follows: aorta and abdominal aneurysm, acute coronary syndrome within preceding 3 months, acute heart failure, severe aortic regurgitation, stage-III hypertension, peripheral artery disease, deep vein thrombosis, pregnancy, any surgical procedures in the preceding 6-weeks or cardiac catheterization in the preceding 2 weeks, bleeding diathesis, any fracture or burn wound hampered cuff compression, and finally arrhythmia unsynchronized with electrocardiogram (ECG). Our fellow clinicians screened for eligibility and only eligible patients were referred to our ECP clinic.

Basic demography, medical history, physical examination, medicinal use history, ECG, chest-x-ray, echocardiography, abdominal and vascular ultrasound, and Doppler study were conducted before randomization. Patients were to be reviewed for the WHO-5 Well-Being Index on QoL (18) and angina CCS class before and after the ECP and sham procedures. All the available data were stored in the HARTEC-database.

Intervention and Sham-Procedures

A total of 50 patients were randomized and assigned to the ECP and sham groups. The randomization of generating the allocation sequence to the ECP or the sham group was carried out using computer-based random numbers. Furthermore, they were randomized in a 1:1 ratio to ECP or sham groups. The patients, outcome assessors, and data analysts were kept blinded to the assignment.

The patient randomized to the ECP group underwent a 35-hour of ECP sessions, consisting of 1 hour each day and 5-days per week from Monday to Friday, until 7 weeks. Three pairs of pneumatic cuffs were wrapped around the leg of the patient on calves, thighs, and buttocks while lying on a couch. The cuffs were inflated sequentially from distal to proximal ends at the onset of diastole. Then, they were deflated rapidly and simultaneously at the onset of systole. Protocol-specified applied pressure of up to 300 mmHg was provided within 5 min. The ECP device utilized was the Renew^{TM} NCP-5 (Singapore 554910, 2018). Patients assigned to the sham procedure underwent an identical treatment and frequency. The sham procedure was designed to be similar to ECP therapy, however with a pressure of only 75 mmHg to provide a feeling of being pressurized. Hence, patients would not realize which assignment they obtained.

The principal investigator did not know which patient was allocated. The procedures were operated on by another cardiologist registering in the area of cardiovascular disease (CVD) Prevention and Rehabilitation in our hospital. During the procedures, the vital signs and any adverse events were closely monitored and noted.

Outcomes

Primary outcomes were the changes in VEGF-A, VEGFR-2, and miR-92a levels after completion of therapy compared to that in the baseline between ECP and sham groups. Secondary outcomes were CCS class changes, a 6-min walk test (6MWT), and WHO-5 Well Being Index improvement (18).

Laboratory Examination

Patients were asked to come for blood sampling within 1 week before starting the treatment and 1 week after the completion of the treatment. Six milliliters of venous blood were drawn. The venous blood was kept in EDTA-tube; subsequently, plasma and peripheral blood mononuclear cells (PBMC) were separated by centrifuge within 30 min. Samples were centrifuged at 2,100 g for 10 min and then stored in multiple aliquots at -80°C and then assayed for VEGFR-2, VEGF-A, and miR-92a.

Vascular endothelial growth factor receptor-**2** analysis was performed on plasma samples using Human VEGFR2/KDR Quantikine ELISA Kit (Code: DVR 200, R&D Systems, Inc., MN, USA) according to the instructions of the manufacturer. The VEGF-A analysis was also carried out on the plasma sample using Human VEGF-A Elisa (Code: ELH-VEGF-1, RayBiotech, Inc, GA, USA) based on the instructions of the manufacturer. All the ELISA measurements were performed by individuals blinded to the clinical data of the patients.

According to the instructions of the manufacturer, total RNA was extracted using the miRNeasy Serum/Plasma kit (Qiagen, cat No 217184). The *cel-miR*-39 (Qiagen, cat. No 219610) was added as a control to correct for sample-to-sample variation (19). Then on 2 ng/ul of the sample, we performed reverse transcription using the TaqMan^{TM}-MicroRNA Reverse Transcription Kit (ABI, Carslbard, CA, USA). Subsequently, a 2 μl complementary DNA (cDNA) sample (duplo) was used to detect miR-92a (ID 000431) with the corresponding TaqMan^{TM} microRNA assay kit by quantitative PCR (ABI 7500 Fast). The quantitative reverse transcription-polymerase chain reaction (qRT-PCR) was performed according to the recommendation of the manufacturer and in accordance with the previous study (19). The ΔCT of miR-92a was obtained after normalization to control as ΔCT = mean CT miR92a - mean CT *cel*-miR-39, and expressed as $2^{-\Delta CT.}$ *Fold changes* of miR-92a after the procedure were expressed as $2^{-\Delta\Delta CT}$ (20, 21). Data were presented after transformation which was multiplied by 10^6 and then log-transformed (22).

Statistical Analysis

We performed an intention-to-treat analysis. All statistical analyses were performed using SPSS (version 25.0; SPSS Inc, Chicago, IL, 2017). Categorical variables were presented as numbers and percentages, while numerical variables were provided as mean and SD or median and minimum-maximum

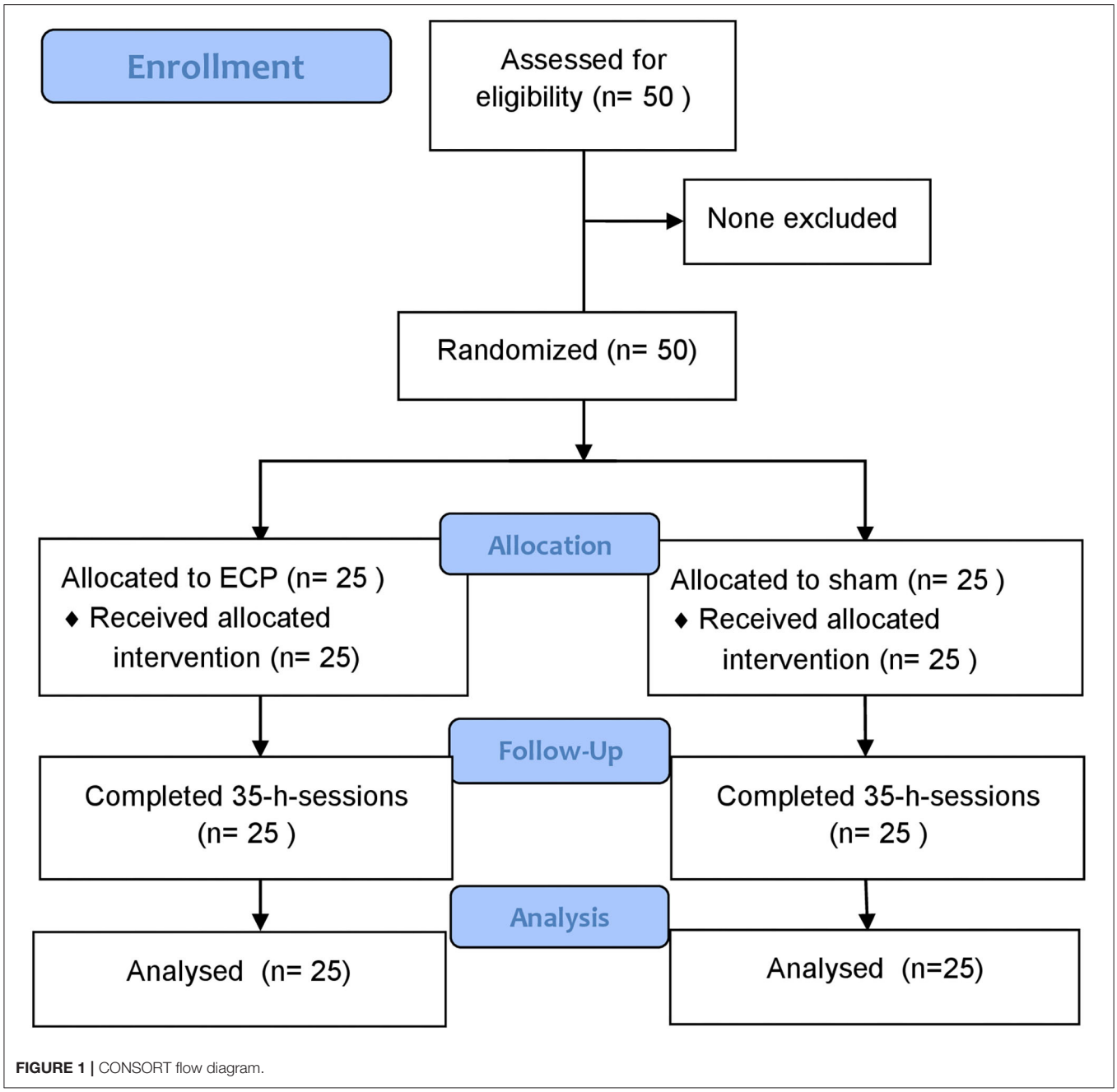

FIGURE 1 | CONSORT flow diagram.

values if they were not normally distributed. Normality test was performed by Shapiro–Wilk test due to the small sample size.

A paired *t*-test compared the value of the change (before-after procedures), and the independent *t*-test was used to compare variables between the groups, if appropriate. Otherwise, a nonparametric test was used. Similarly, $\chi 2$ was used for binary and categorical variables. Multivariate analysis of covariance (MANCOVA) was performed applying the changes of VEGF-A, VEGFR-2, and miR-92a as dependent variables. The independent variable for the model was the ECP vs. sham procedures. If there is a variable imbalance between the groups, it should be constructed as a covariate model. The MANCOVA provides an overall test of significance, which gives an exact probability of the effect of the independent variable on the dependent variables. Wilk's Lambda test was used to assess the statistical significance between the groups.

Since no previous study investigating the effect of ECP on the changes of the above biomarkers are available, the study was deemed as a pilot study. We decided to have at least 25 sample sizes for each arm. This sample size determination was calculated to have a power of 90% and with an expected small standardized

difference of 0.1–0.3 (23). All hypothesis tests were two-sided with a significance level set at $P < 0.05$.

Ethical Clearance

This study had been reviewed and received ethical approval by the Research Ethics Committee/Independent Review Board (REC/IRB) of National Cardiovascular Center—Harapan Kita Hospital, Jakarta—Indonesia, No: 02.01/VII/226/KEP 059/2017, on Dec 21, 2017. All participants have provided their written consent.

TABLE 1 | Baseline characteristics.

Variables	ECP ($n = 25$)	Sham ($n = 25$)	*P* value
Age, n (%)			0.57
≥60 years	11 (44)	13 (52)	
<60 years	14 (56)	12 (48)	
[a]Gender, *n* (%)			
Male	23 (92)	21 (84)	0.67
Female	2 (8)	4 (16)	
SBP (mmHg)	124.1 ± 9.4	117.1 ± 7.5	0.19
DBP (mmHg)	67.1 ± 3.4	66.1 ± 0.3	0.70
BMI (kg/m^2)	26.7(22 to 31.8)	24(21 to 29)	0.02
LVEF (%)	52.1 ± 6	49.1 ± 8	0.52
[a]Previous CABG, *n* (%)	1 (4)	7 (28)	0.05
Previous PCI, *n* (%)	15 (60)	9 (36)	0.09
Diabetes mellitus, *n* (%)	15 (60)	11 (44)	0.26
Smoking, *n* (%)	19 (76)	17 (68)	0.53
Alcohol, *n* (%)	8 (32)	6 (24)	0.53
Hypertension, *n* (%)	15 (60)	10 (40)	0.16
Dyslipidemia, (%)	19 (76)	14 (56)	0.14
Stroke, *n* (%)	6 (24)	5 (20)	0.73
Familial history of CAD, *n* (%)	14 (56)	10 (40)	0.26
Physically active, *n* (%)	19 (76)	15 (60)	0.23
[a]Aspirin, *n* (%)	22 (88)	19 (76)	0.46
Clopidogrel, *n* (%)	16 (64)	18 (72)	0.54
[a]Ticagrelor, *n* (%)	3 (12)	1 (4)	0.61
[a]Nitrat, *n* (%)	20 (80)	23 (92)	0.42
ACE inhibitor, *n* (%)	7 (28)	6 (24)	0.75
ARB, *n* (%)	13 (52)	16 (64)	0.39
[a]Beta blocker, *n* (%)	24 (96)	22 (88)	0.61
[a]Statin, *n* (%)	25 (100)	22 (88)	0.24
[a]Trimetazidine, *n* (%)	4 (16)	4 (16)	1.00
Diuretic, *n* (%)	16 (64)	14 (56)	0.56
CCB, *n* (%)	14 (56)	8 (32)	0.09
6MWT (m)	341.2 (±80)	322.8 (±85)	0.42
CCS class	2 (1 to 4)	2 (1 to 3)	0.25
QoL WHO-5 Well-Being Index	68.5 (±14.5)	68.2 (±14)	0.95
Diastolic/Systolic Ratio	1.2(±0.25)	0.8 (±0.15)	<0.0001

n, absolute number; ECP, external counterpulsation; SBP, systolic blood pressure; DBP, diastolic blood pressure; BMI, body mass index; LVEF, left ventricle ejection fraction); CABG, coronary artery bypass graft; PCI, percutaneous coronary intervention; CAD, coronary artery disease; ACE, angiotensin converting enzyme; ARB, angiotensin receptor blocker; CCB, calcium channel blocker; 6MWT, six-min walking test; CCS, Canadian Cardiovascular Scoring; NYHA, New York Heart Association; QoL WHO-5, Quality of Life measured by WHO-5 Well-Being Index.

[a]Analysis by Fisher's test (do not qualify for chi-square test).

Normally distributed value is presented as mean (± SD) if not normally distributed is presented as median (mininum–maximum).

Normality test by Shapiro–Wilk, homogeneity test by Levene's test.

Numeric variables were analyzed by independent-t-test or Mann–Whitney test.

RESULTS

Patient Characteristics

Our study population consisted of 50 patients with RA who have been documented as having CAD, 25 patients in the ECP group, and 25 patients in the sham group. All patients completed the full course of treatment and blood sampling and were included in the final analysis (**Figure 1**). The baseline characteristics of these patients are shown in **Table 1**. Effective hemodynamic augmentation was reached in the ECP group with a mean diastolic-to-systolic ratio of 1.2 compared to only 0.8 in the sham group (**Table 1**).

All patients assigned to the ECP group completed their 35-hour sessions, so did the sham group. There were no significant differences in the baseline characteristics between the groups, except for body mass index (BMI); male sex was predominantly observed than those of the female sex. The patients in the ECP group were significantly more overweight [26.7 (22–31.8) vs. 24 (21–29), $P = 0.02$] than those in the sham group. The cardiovascular risk factors were comparable between the groups. Diabetes mellitus, hypertension, dyslipidemia, and family history of CAD proportions were more than half encountered in patients. About one-fifth of them have suffered from a stroke. All patients in both groups similarly received the optimal treatment for chronic coronary syndrome, as presented in **Table 1**. No major adverse cardiovascular events were observed during the study period.

ECP Preserved VEGF-A and VEGFR-2 Levels

The level of VEGF-A in the ECP group was significantly preserved compared to the sham group [ΔVEGF-A 1 pg/ml (−139 to +160) vs. −136 pg/ml (−237 to +67); consecutively, $P = 0.026$] (**Table 2**). As shown in **Figure 2**, VEGFR-2 level was also preserved in the ECP group (**Figure 2A**) but decreased significantly in the sham group (**Figure 2B**). The reduction of VEGFR-2 was larger in the sham group compared to the

TABLE 2 | ΔVEGF-A and ΔVEGFR-2 after-before intervention in ECP and sham group.

[a,b]Variables	ECP ($n = 25$)	Sham ($n = 25$)	*P*-value
ΔVEGF-A level (pg/ml)	1 (−139 to160)	−136 (−237 to 67)	0.026
ΔVEGFR-2 level (pg/ml)	−171 (−844 to +1,166)	−517 (−1,549 to +1,407)	0.021

Δ, delta or change; n, absolute number; ECP, external counter pulsation; VEGF-A, vascular endothelial growth factor-A; VEGFR-2, vascular endothelial growth factor receptor-2; pg/ml, picogram/milliliter.

[a]Normality test by Shapiro–Wilk. [b]Analysis by Mann–Whitney test.

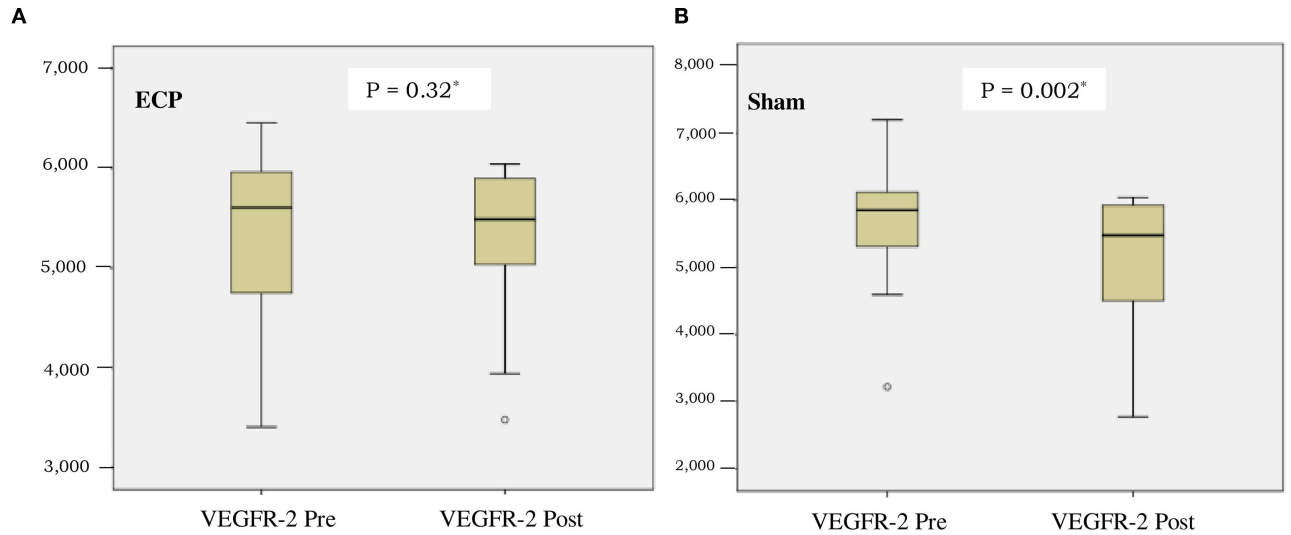

FIGURE 2 | Boxplot of vascular endothelial growth factor receptor-2 (VEGFR-2) concentration before and after intervention in external counter pulsation (ECP) group **(A)** and sham group **(B)**. *Analysis by Wilcoxon test.

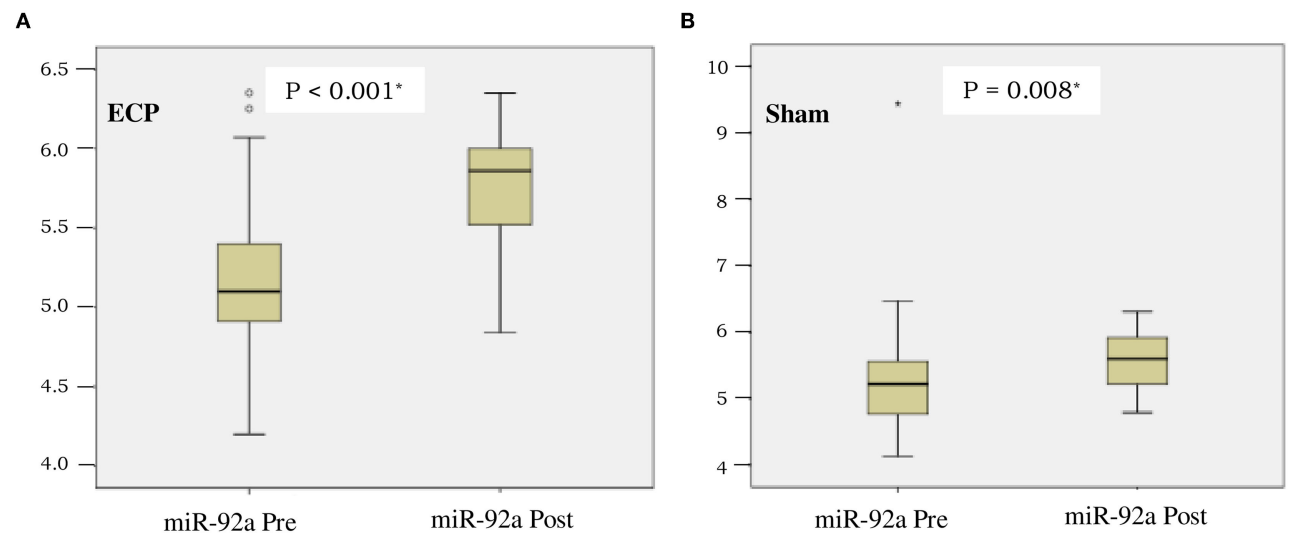

FIGURE 3 | Boxplot of microRNA-92a (miR-92A) expression before and after intervention in ECP group **(A)** and sham group **(B)**. *Analysis by Wilcoxon test.

ECP group [-517 pg/ml (−1,549 to +1,407) vs.−171 (−844 to +1,166); consecutively, $P = 0.021$]. A negative mark denoted that the levels of VEGF-A and VEGFR-2 decreased in the post-ECP and sham procedures (**Table 2**; **Figure 2**).

Levels of miR-92 Increased After the Procedures

The concentration of miR-92a was comparable between the groups before the procedures were conducted ($P = 0.68$). After completion of the procedures, the miR-92a level in plasma increased significantly in ECP [as shown in **Figure 3A**, from 5.1 (4.2–6.4) to 5.9 (4.8–6.4), $p < 0.001$] and sham group (as shown in **Figure 3B**, from 5.2 (4.1–9.4) to 5.6 (4.8–6.3), $p = 0.008$]. Delta changes and *fold changes* tended to be larger in ECP group although not reaching statistically significant differences in sham group [delta ECP 0.7(−0.5 to +1.6) vs. delta sham 0.5 (−4.2 to +1.2), $p = 0.33$; *fold changes* ECP = 4.6 (0.3–36.5) vs. sham 2.8 (0–15), $p = 0.33$)] (**Table 3**).

Effect of ECP on Dependent Variables

Although there was an imbalance of BMI between the groups, the effect of ECP on angiogenesis remained significant after adjustment for BMI (**Table 4**). MANCOVA test was used to distinguish the two groups with multiple dependent variables.

TABLE 3 | MicroRNA-92a expression in ECP group and sham group, before and after intervention.

Variables	ECP ($n = 25$)	Sham ($n = 25$)	*P* value[a]
*miR-92a expression, before	5.1 (+4.2 to +6.4)	5.2 (+4.1 to +9.4)	0.68
*miR-92a expression, after	5.9 (+4.8 to +6.4)	5.6 (+4.8 to +6.3)	0.09
Delta mir-92a, after-before	0.7 (-0.5 to +1.6)	0.5 (−4.2 to +1.2)	0.33
$^{+}$*Fold-changes* mir-92a, after: before	4.6 (0.3 to 36.5)	2.8 (0 to 15)	0.33

n, absolute number; ECP, external counter pulsatio); miR-92a, microRNA-92a.
[a]*Analysis by Mann–Whitney test, presented as median (min-max).*
**miR-92a expression was the result of formula* $2^{-\Delta ct}$ *transformed by multiplying with* 10^6 *then log 10.*
$^{+}$*Fold changes of miR-92a expression were the result of formula* $2^{-\Delta\Delta ct}$.

TABLE 4 | Multivariate analysis the effect of ECP on dependent variables.

Risk Factors	Delta VEGF-A			Delta VEGFR-2			Delta miR-92a		
	Partial Eta Square	B coefficient	*P*-value[a]	Partial Eta Square	B coefficient	*P*-value[a]	Partial Eta Square	B coefficient	*P*-value[a]
BMI	0.006	2.853	0.597	0.005	−17.223	0.636	0.036	0.042	0.195
ECP	0.083	56.664	0.047	0.094	409.625	0.034	0.006	0.089	0.593

ECP, external counter pulsation; VEGF-A, vascular endothelial growth factor-A; VEGFR-2, vascular endothelial growth factor receptor-2, miR-92a: microRNA-92a.
[a]*Analysis by MANCOVA and Wilk–Lambda test.*

TABLE 5 | Differences in CCS class, 6MWT and QoL WHO-5 in ECP and sham group, before and after intervention.

Variable	ECP ($n = 25$)	Sham ($n = 25$)	*P* Value
[a,b]Δ CCS Class	−1 (−2 to 0)	−1 (−2 to −1)	NS
[a,b]Δ 6MWT (m)	41 (−58 to +330)	19 (−55 to +190)	NS
[a,b]Δ QoL WHO-5	8 (0 to +32)	4 (−6 to +28)	NS
[a,c]Δ EF (%)	1.3 (±14)	−0.32 (±11)	NS

Δ, delta or change; ECP, external counter pulsation; CCS, Canadian Cardiovascular Society; 6MWT, 6-min walk test; QoL, quality of life; WHO, World Health Organization.
[a]*Normality test by Shapiro-Wilk test.*
[b]*Mean difference analysis was performed by Mann-Whitney test.*
[c]*Mean difference analysis was performed by Independent-t-test.*
**NS: Not Significant.*

ECP and Clinical Effect

Although there were no significant differences observed between the groups, the ECP group tended to show an improved aerobic capacity detected by 6MWT, QoL measured by the WHO-5 Well Being Index, and ejection fraction (EF) (**Table 5**).

DISCUSSION

There is a growing prevalence of refractory ischemia due to residual CAD even after revascularization procedures, such as PCI and/or CABG. As a matter of fact, as shown in **Table 1**, 16 of the 25 patients in each group have had previous revascularizations with PCI + CABG. Thus, 64% of the patients with RA in each group had residual CAD with recurrent ischemia.

This study has demonstrated that in patients with RA, ECP maintains angiogenesis, as measured by the data showing that VEGF-A level in the ECP group remains stable. On the contrary, VEGF-A significantly decreases in the sham group. Similarly, the significant preservation of angiogenesis in the ECP group is also demonstrated by a more significant reduction of VEGFR-2 in the sham group than in the ECP group (**Table 2**; **Figure 2**). An imbalance of BMI between the groups might be due to chance. Furthermore, after being adjusted using MANCOVA analysis, the ECP still reveals a significant effect on the changes in angiogenesis (**Table 4**). This evidence might be pointed out by the data proved by Ebos et al. (24), which confirmed that VEGF-A binding to and activation of VEGFR-2 leads to downregulation and a decrease in VEGFR-2 production in angiogenesis. A previous study also demonstrated that increased VEGF-A production might induce angiogenesis by initiating reactive oxygen species-endoplasmic reticulum (ER) stress-autophagy axis in endothelial cells (25).

The acute effect of the ECP is to increase the coronary blood flow and improve endothelial function (26) during diastole while reducing the cardiac workload at the onset of systole. Although the long-term mechanism is yet unknown, it is thought to result from an increase in endothelial shear stress (ESS), wherein it stimulates collateralization and angiogenesis to the ischemic region, among other mechanisms (27, 28). The high-shear stress of ECP, which comprises radial, circumferential, and longitudinal forces, will inhibit atherosclerosis (29, 30). Increased ESS would increase nitric oxide (NO) production (31) and VEGF-A (32).

The complex process of mechano-reception and mechano-transduction, leading to pro-atherosclerosis or anti-atherosclerosis state, is regulated by micro-RNA (miR). The miR is a small noncoding RNA that post-transcriptionally

controls gene expression and regulates a wide range of physiological and pathophysiological processes (33). Among them, miR-92a has been shown as one valuable therapeutic target in the setting of ischemic disease. The miR-92a was highly expressed in human endothelial cells, and it controlled the growth of new angiogenesis. Forced overexpression of miR-92a in human endothelial cells blocked sprout formation in angiogenesis, inhibited vascular network formation, and reduced endothelial cell migration (34). Meanwhile, inhibition of miR-92a increased angiogenesis in mice after ischemia and also enhances ischemic tissue repair, improves endothelial dysfunction, reduces inflammation, and stabilizes atherosclerotic plaques (34–36).

Previous studies have shown that miR-92a is a flow-sensitive miRNA, whose expression was increased in low ESS exposure, while decreased in a high laminar or pulsatile ESS (37). In contrast, our study showed that miR-92a was increased in patients with RA after ECP intervention. However, it should be pointed out that in the aforementioned studies, the reduction of miR-92a was observed from *in vitro* studies conducted in a 24-hour continuous exposure of laminar and a high-ESS in cell culture medium, then intracellular miR-92a was measured (36, 38). Meanwhile, our study measured circulating miR-92a in plasma. Whether the circulating level of miRNA could affect intracellular gene expression or if the circulating miRNA level correlates with the intracellular level needs to be confirmed. The increase in circulating miR-92a level might indicate the release from cell and significantly decreased the uptake by target cell, which might mitigate its intracellular proatherosclerotic level (39). Alternatively, other miRNAs might have played a more important role in this regulation.

Whether the increase in circulating miR-92a is a favorable regulation or a counterregulatory effect is still unknown. However, a study by Marfella et al. (20) has shown that the level of miR-92a in circulation increased in patients with heart failure who experienced an improvement in EF and left ventricle dimension after cardiac resynchronization therapy (CRT). Studies in cancer tissues have also shown that miR-92a regulates PTEN/AKT signaling pathway by inhibiting PTEN, thus, activates AKT signaling (40, 41). Activation of AKT signaling results in cell cycle progression, survival, metabolism, and migration. The AKT pathway also plays an important role in angiogenesis stimulation through the effect on endothelial cell and other cells that produce angiogenesis signals, such as tumor cells (42).

Our subjects were all patients with RA having severe long-standing CAD and endothelial dysfunction. Thus, the ischemic myocardium and dysfunctional endothelial cell may produce distinct responses compared to normal endothelial cell in the culture medium. Accordingly, a study by Song et al. (43) showed that cardiomyocyte exposed to 48 h of hypoxia expressed higher miR-92a compared to those in normoxia condition. Thus, a comparison with a normal subject might be needed to evaluate the response to ECP. Alternatively, increased expression of miR-92a is possibly due to homeostasis counter-regulatory phenomenon in the ischemic myocardium of patients with RA as a result of enhanced angiogenesis in the ECP group by high-ESS. The previous study has shown that vascular endothelial growth factor (VEGF) overexpression could increase vascular permeability and tissue oedema, pericardial effusion, and angioma formation (44).

Interestingly, circulating miR-92a also significantly increases in the sham group so that the difference between the two groups becomes not significant. Generally, *in vitro* studies of miR-92a utilizes a perfusion system to generate shear stress of about 12 dynes/ cm^2 (16, 36). This value is lower than the shear stress generated by ECP in the human and animal study, which ranges from 20 to 40 dynes/cm^2 (29, 45). Thus, sham treatment with 75 mmHg pressure given might also result in increased ***shear stress*** to some level that might also regulate miR-92a.

Although not statistically significant, ECP tended to increase the QoL and aerobic capacity compared to sham. However, this study was underpowered to evaluate these clinical endpoints. The previous randomized sham-controlled trial has shown that ECP significantly reduced anginal frequency and increased exercise-induced ischemia time (46). A registry-based study also showed an improvement in angina class and frequency, as well as an improvement in the QoL, which persisted up until 3 years after therapy in patients with or without heart failure (5, 47). A meta-analysis by Zhang et al. (48) which included 18 studies with a total of 1,768 patients confirmed that ECP resulted in the improvement of at least one angina class in 85% of patients. Biomarker studies have shown an increase in NO synthesis and a decrease in endothelin-1 following ECP indicating an improvement in endothelial function (31, 49) which is in accordance with our study that shows better angiogenesis marker after ECP treatment. However, further studies are needed to evaluate whether improvement in angiogenesis marker will be sustained in the long term after completion of ECP and its relation to the clinical outcome. A sub-analysis study from Pravian et al. (50) has shown that although ECP did not improve left ventricular (LV) longitudinal strain globally or segmentally, there was an improvement in segments with post-systolic shortening (PSS) which indicates improvement in myocardial perfusion.

No serious adverse effect occurred during the treatment in both groups. However, we acknowledge that there are some limitations to the study. First, there was an imbalance of BMI variables between the groups, although it does not affect the conclusion. Second, ECP has the drawbacks of its high cost and is not covered by our national health insurance, thus limiting its availability and accessibility. Its cumbersome technique also requires a specialized technician and long-term commitment from the patient to complete the whole treatment session. Third, we did not include normal healthy subjects to compare the response to shear stress by ECP on VEGF-A, VEGFR-2, or miR-92a level because of ethical considerations and our hospital standard care restriction. Fourth, we did not provide a comparison of circulating miR-92a with its intracellular expression. Fifth, we only used the ELISA method to

measure the levels of VEGF-A and VEGFR-2 protein in plasma. Future studies incorporating several measurement techniques are needed to achieve a more solid conclusion. Furthermore, larger studies are needed to ascertain the benefit of ECP on angiogenesis marker, miR-92a, CCS, 6MWT, and QoL. Interestingly, several other invasive options to reduce angina symptoms in patients with RA, such as cell-based therapies, gene therapy, spinal cord stimulation (SCS), trans-myocardial laser revascularization (TMLR), and coronary sinus reduction can also serve as a promising option and necessitate further investigation (4, 17).

CONCLUSIONS

In summary, the present study demonstrates that ECP may improve angiogenesis by preserving the expression of VEGF-A and VEGFR-2. However, both ECP and sham increase miR-92a circulating level significantly, and the number of changes was not different between the two groups.

DATA AVAILABILITY STATEMENT

The original contributions presented in the study are included in the article/**Supplementary Material**, further inquiries can be directed to the corresponding author/s.

ETHICS STATEMENT

The studies involving human participants were reviewed and approved by Research Ethics Committee/Independent Review Board (REC/IRB) of National Cardiovascular Center – Harapan Kita Hospital, Jakarta – Indonesia. The patients/participants provided their written informed consent to participate in this study.

AUTHOR CONTRIBUTIONS

AA, AS, GL, EZ, BD, RS, BR, SH, SA, DH, DZ, EEl, and AM contributed to the conception and design of the study. GL and EZ organized the database. EEk and SW designed, performed laboratory examinations, and analyzed the result. GL and EZ performed the statistical analysis. AA, AS, EZ, and GL wrote the first draft of the manuscript. BD, RS, BR, SH, EEk, SW, SA, DH, DZ, EEl, and AM wrote sections of the manuscript. All authors contributed to manuscript revision and read and approved the submitted version.

FUNDING

This study was funded by the National Health Research and Development of the Ministry of Health of Indonesia (No: HK.02.02/I/27/2020). Support for the laboratory and data analysis was provided by the National Cardiovascular Center, Harapan Kita Hospital, Jakarta. Open access publication fees payable by authors will be partially reimbursed by a Grant from the National Health Research and Development of the Ministry of Health of Indonesia as part of the agreement.

ACKNOWLEDGMENTS

We extend our gratitude to Nunung Nusyarofah SKM, MKM, and Onetusfifsi Putra SKM, MKM for supporting the analysis of the data in the study, and to Dwi Pratami Septiara MBiomed for the diligent laboratory support.

SUPPLEMENTARY MATERIAL

The Supplementary Material for this article can be found online at: https://www.frontiersin.org/articles/10.3389/fcvm.2021.761112/full#supplementary-material

REFERENCES

1. Waltenberger J. Chronic refractory angina pectoris: Recent progress and remaining challenges. *Eur Heart J.* (2017) 38:2556–8. doi: 10.1093/eurheartj/ehx421
2. Mannheimer C, Camici P, Chester MR, Collins A, DeJongste M, Eliasson T, et al. The problem of chronic refractory angina; report from the ESC Joint Study Group on the Treatment of Refractory Angina. *Eur Heart J.* (2002) 23:355–70. doi: 10.1053/euhj.2001.2706
3. McGillion M, Arthur HM, Cook A, Carroll SL, Victor JC, L'allier PL, et al. Canadian Cardiovascular Society; Canadian Pain Society. Management of patients with refractory angina: Canadian Cardiovascular Society/Canadian Pain Society joint guidelines. *Can J Cardiol.* (2012) 28:S20–41. doi: 10.1016/j.cjca.2011.07.007
4. Cheng K, de Silva R. New Advances in the management of refractory angina pectoris. *Eur Cardiol.* (2018) 13:70–9. doi: 10.15420/ecr.2018:1:2
5. Loh PH, Cleland JG, Louis AA, Kennard ED, Cook JF, Caplin JL, et al. Enhanced external counterpulsation in the treatment of chronic refractory angina: a long-term follow-up outcome from the International Enhanced External Counterpulsation Patient Registry. *Clin Cardiol.* (2008) 31:159–64. doi: 10.1002/clc.20117
6. Kim MC, Kini A, Sharma SK. Refractory angina pectoris: Mechanism and therapeutic options. *J Am Coll Cardiol.* (2002) 39:923–34. doi: 10.1016/s0735-1097(02)01716-3
7. Nichols WW, Estrada JC, Braith RW, Owens K, Conti CR. Enhanced external counterpulsation treatment improves arterial wall properties and wave reflection characteristics in patients with refractory angina. *J Am Coll Cardiol.* (2006) 48:1208–14. doi: 10.1016/j.jacc.2006.04.094
8. Lawson WE, Hui JC, Cohn PF. Long-term prognosis of patients with angina treated with enhanced external counterpulsation: five-year follow-up study. *Clin Cardiol.* (2000) 23:254–8. doi: 10.1002/clc.4960230406
9. Buschmann EE, Utz W, Pagonas N, Schulz-Menger J, Busjahn A, Monti J, et al. Arteriogenesis Network (Art. Net) Improvement of fractional flow reserve and collateral flow by treatment with external counterpulsation (ArtNet-2 Trial). *Eur J Clin Invest.* (2009) 39:866–75. doi: 10.1111/j.1365-2362.2009.02192.x
10. Eslamian F, Aslanabadi N, Mahmoudian B. Shakouri SK.Therapeutic effects of enhanced external counterpulsation on clinical sumptoms, echocardiographic measurements, perfusion scan parameters and exercise tolerance test in coronary artery disease patients with refractory angina. *Int J Med Sci Public Health.* (2013) 2:179–87. doi: 10.5455/ijmsph.2013.2.179-187
11. Wu G, Du Z, Hu C, Zheng Z, Zhan C, Ma H, et al. Angiogenic effects of long-term enchanced external counterpulsation in a dog model of

myocardial infarction. *Am J Physiol Heart Circ Physiol*. (2006) 290: H248-5. doi: 10.1152/ajpheart.01225.2004
12. Barsheshet A, Hod H, Shechter M, Sharabani-Yosef O, Rosenthal E, Barbash IM, et al. The effects of external counter pulsation therapy on circulating endothelial progenitor cells in patients with angina pectoris. *Cardiology*. (2008) 110:160–6. doi: 10.1159/000111925
13. Shibuya M. Vascular endothelial growth factor (VEGF) and its receptor (VEGFR) signaling in angiogenesis: a crucial target for anti- and pro-angiogenic therapies. *Genes Cancer*. (2011) 2:1097–105. doi: 10.1177/1947601911423031
14. Peach CJ, Mignone VW, Arruda MA, Alcobia DC, Hill SJ, Kilpatrick LE, et al. Molecular pharmacology of VEGF-A isoforms: binding and signalling at VEGFR2. *Int J Mol Sci*. (2018) 19:1264. doi: 10.3390/ijms19041264
15. Arora R, Chen HJ, Rabbani L. Effects of enhanced counterpulsation on vascular cell release of coagulation factors. *Heart Lung*. (2005) 34:252–6. doi: 10.1016/j.hrtlng.2005.03.005
16. Wu W, Xiao H, Laguna-Fernandez A, Villarreal G Jr, Wang KC, Geary GG, et al. Flow-Dependent Regulation of Kruppel-Like Factor 2 Is Mediated by MicroRNA-92a. *Circulation*. (2011) 124:633–41. doi: 10.1161/CIRCULATIONAHA.110.005108
17. Knuuti J, Wijns W, Saraste A, Capodanno D, Barbato E, Funck-Brentano C, et al. ESC Scientific document group. 2019 ESC Guidelines for the diagnosis and management of chronic coronary syndromes. *Eur Heart J*. (2020) 41:407–477. doi: 10.1093/eurheartj/ehz425
18. Topp CW, Ostergaard SD, SØndergaard S, Bech P. The WHO-5 well-being index: A systematic review of the literature. *PsychotherPsychosom*. (2015) 84:167–76. doi: 10.1159/000376585
19. Kroh EM, Parkin RK, Mitchell PS, Tewari M. Analysis of circulating microRNA biomarkers in plasma and serum using quantitative reverse transcription-PCR (qRT-PCR). *Methods*. (2010) 50:298–301. doi: 10.1016/j.ymeth.2010.01.032
20. Marfella R, Di Filippo C, Potenza N, Sardu C, Rizzo MR, Siniscalchi M, et al. Circulating microRNA changes in heart failure patients treated with cardiac resynchronization therapy: responders vs. non-responders. *Eur J Heart Fail*. (2013) 15:1277–88. doi: 10.1093/eurjhf/hft088
21. Livak KJ, Schmittgen TD. Analysis of relative gene expression data using real-time quantitative PCR and the $2^{-\Delta\Delta CT}$ method. *Methods*. (2001) 25:402–8. doi: 10.1006/meth.2001.1262
22. Simionescu N, Niculescu LS, Carnuta MG, Sanda GM, Stancu CS, Popescu AC, et al. Hyperglycemia determines increased specific microRNAs levels in sera and HDL of acute coronary syndrome patients and stimulates microRNAs production in human macrophages. *PLoS ONE*. (2016) 11:e0161201. doi: 10.1371/journal.pone.0161201
23. Whitehead AL, Julious SA, Cooper CL, Campbell MJ. Estimating the sample size for a pilot randomised trial to minimise the overall trial sample size for the external pilot and main trial for a continuous outcome variable. *Stat Methods Med Res*. (2016) 25:1057–73. doi: 10.1177/0962280215588241
24. Ebos JM, Lee CR, Bogdanovic E, Alami J, Van Slyke P, Francia G, et al. Vascular endothelial growth factor-mediated decrease in plasma soluble vascular endothelial growth factor receptor-2 levels as a surrogate biomarker for tumor growth. *Cancer Res*. (2008) 68:521–9. doi: 10.1158/0008-5472.CAN-07-3217
25. Zou J, Fei Q, Xiao H, Wang H, Liu K, Liu M, et al. VEGF-A promotes angiogenesis after acute myocardial infarction through increasing ROS production and enhancing ER stress-mediated autophagy. *J Cell Physiol*. (2019) 234:17690–703. doi: 10.1002/jcp.28395
26. Bonetti PO, Barsness GW, Keelan PC, Schnell TI, Pumper GM, Kuvin JT, et al. Enhanced external counterpulsation improves endothelial function in patients with symptomatic coronary artery disease. *J Am Coll Cardiol*. (2003) 41:1761–68. doi: 10.1016/s0735-1097(03)00329-2
27. Michaels AD, Kennard ED, Kelsey SF, Holubkov R, Soran O, Spence S, et al. Does higher diastolic augmentation predict clinical benefit from enhanced external counterpulsation? Data from the International EECP Patient Registry (IEPR). *Clin Cardiol*. (2001) 24:453–58. doi: 10.1002/clc.4960240607
28. Yang DY, Wu GF. Vasculoprotective properties of enhanced external counterpulsation for coronary artery disease: Beyond the hemodynamics. *Int J Cardiol*. (2013) 166:38–43. doi: 10.1016/j.ijcard.2012.04.003
29. Zhang Y, He X, Chen X, Ma H, Liu D, Luo J, et al. Enhanced external counterpulsation inhibits intimal hyperplasia by modifying shear stress responsive gene expression in hypercholesterolemic pigs. *Circulation*. (2007) 116:526–34. doi: 10.1161/CIRCULATIONAHA.106.647248
30. Kwak BR, Bäck M, Bochaton-Piallat ML, Caligiuri G, Daemen MJ, Davies PF, et al. Biomechanical factors in atherosclerosis: mechanisms and clinical implications. *Eur Heart J*. (2014) 35:3013–20. doi: 10.1093/eurheartj/ehu353
31. Akhtar M, Wu GF, Du ZM, Zheng ZS, Michaels AD. Effect of external counterpulsation on plasma nitric oxide and endothelin-1 levels. *Am J Cardiol*. (2006) 98:28–30. doi: 10.1016/j.amjcard.2006.01.053
32. Pourmoghadas M, Nourmohamamadi H, Tabesh F, Haghjoo S, Tabesh E. Effect of enhanced external counter pulsation on plasma level of nitric oxide and vascular endothelial growth factor. *ARYA Atheroscler J*. (2009) 5:59–63. doi: 10.1016/j.ijcard.2010.08.020
33. Van Rooij E, Olson EN. MicroRNAs: powerful new regulators of heart disease and provocative therapeutic targets. *J Clin Invest*. (2007) 117:2369–76. doi: 10.1172/JCI33099
34. Bonauer A, Carmona G, Iwasaki M, Mione M, Koyanagi M, Fischer A, et al. MicroRNA-92a controls angiogenesis and functional recovery of ischemic tissues in mice. *Science*. (2009) 324:1710–3. doi: 10.1126/science.1174381
35. Hinkel R, Penzkofer D, Zühlke S, Fischer A, Husada W, Xu QF, et al. Inhibition of microRNA-92a protects against ischemia/reperfusion injury in a large-animal model. *Circulation*. (2013) 128:1066–75. doi: 10.1161/CIRCULATIONAHA.113.001904
36. Loyer X, Potteaux S, Vion AC, Guérin CL, Boulkroun S, Rautou PE, et al. Inhibition of microRNA-92a prevents endothelial dysfunction and atherosclerosis in mice. *Circ Res*. (2014) 114:434–43. doi: 10.1161/CIRCRESAHA.114.302213
37. Kumar S, Kim CW, Simmons RD, Jo H. Role of flow-sensitive microRNAs in endothelial dysfunction and atherosclerosis: mechanosensitive athero-miRs. *Arterioscler Thromb Vasc Biol*. (2014) 34:2206–16. doi: 10.1161/ATVBAHA.114.303425
38. Wang KC, Garmire LX, Young A, Nguyen P, Trinh A, Subramaniam S, et al. Role of microRNA-23b in flow-regulation of Rb phosphorylation and endothelial cell growth. *Proc Natl Acad Sci U S A*. (2010) 107:3234–9. doi: 10.1073/pnas.0914825107
39. Fichtlscherer S, De Rosa S, Fox H, Schwietz T, Fischer A, Liebetrau C, et al. Circulating microRNAs in patients with coronary artery disease. *Circ Res*. (2010) 107:677–84. doi: 10.1161/CIRCRESAHA.109.215566
40. Lu C, Shan Z, Hong J, Yang L. MicroRNA-92a promotes epithelial-mesenchymal transition through activation of PTEN/PI3K/AKT signaling pathway in non-small cell lung cancer metastasis. *Int J Oncol*. (2017) 51:235–44. doi: 10.3892/ijo.2017.3999
41. Ke TW, Wei PL, Yeh KT, Chen WT, Cheng YW. MiR-92a promotes cell metastasis of colorectal cancer through PTEN-mediated PI3K/AKT pathway. *Ann Surg Oncol*. (2015) 22:2649–55. doi: 10.1245/s10434-014-4305-2
42. Carnero A, Paramio JM. The PTEN/PI3K/AKT Pathway *in vivo*, cancer mouse models. *Front Oncol*. (2014) 4:252. doi: 10.3389/fonc.2014.00252
43. Song YS, Joo HW, Park IH, Shen GY, Lee Y, Shin JH, et al. Bone marrow mesenchymal stem cell-derived vascular endothelial growth factor attenuates cardiac apoptosis via regulation of cardiac miRNA-23a and miRNA-92a in a rat model of myocardial infarction. *PLoS ONE*. (2017) 12:e0179972. doi: 10.1371/journal.pone.0179972
44. Roy H, Bhardwaj S, Ylä-Herttuala S. Biology of vascular endothelial growth factors. *FEBS Lett*. (2006) 580:2879–87. doi: 10.1016/j.febslet.2006.03.087
45. Braith RW, Casey DP, Beck DT. Enhanced external counterpulsation for ischemic heart disease: a look behind the curtain. *Exerc Sport Sci Rev*. (2012) 40:145–152. doi: 10.1097/JES.0b013e318253de5e
46. Arora RR, Chou TM, Jain D, Fleishman B, Crawford L, McKiernan T, et al. Effects of enhanced external counterpulsation on Health-Related Quality of Life continue 12 months after treatment: a substudy of the Multicenter Study of Enhanced External Counterpulsation. *J Investig Med*. (2002) 50:25–32. doi: 10.2310/6650.2002.33514
47. Soran O, Kennard ED, Kfoury AG, Kelsey SF; IEPR Investigators. Two-year clinical outcomes after enhanced external counterpulsation (EECP) therapy in patients with refractory angina pectoris and left ventricular dysfunction (report from The International EECP Patient Registry). *Am J Cardiol*. (2006) 97:17–20. doi: 10.1016/j.amjcard.2005.07.122
48. Zhang C, Liu X, Wang X, Wang Q, Zhang Y, Ge Z. Efficacy of enhanced external counterpulsation in patients with chronic refractory angina on

canadian cardiovascular society (CCS) angina class: an updated meta-analysis. *Medicine (Baltimore).* (2015) 94:e2002. doi: 10.1097/MD.0000000000002002
49. Braith RW, Conti CR, Nichols WW, Choi CY, Khuddus MA, Beck DT, et al. Enhanced external counterpulsation improves peripheral artery flow-mediated dilation in patients with chronic angina: a randomized sham-controlled study. *Circulation.* (2010) 122:1612–20. doi: 10.1161/CIRCULATIONAHA.109.923482
50. Pravian D, Soesanto AM, Ambari AM, Kuncoro BRMAS, Dwiputra B, Muliawan HS, et al. The effect of external counterpulsation on intrinsic myocardial function evaluated by speckle tracking echocardiography in refractory angina patients: a randomized controlled trial. *Int J Cardiovasc Imaging.* (2021) 37:2483–90. doi: 10.1007/s10554-021-02289-x

Conflict of Interest: The authors declare that the research was conducted in the absence of any commercial or financial relationships that could be construed as a potential conflict of interest.

Publisher's Note: All claims expressed in this article are solely those of the authors and do not necessarily represent those of their affiliated organizations, or those of the publisher, the editors and the reviewers. Any product that may be evaluated in this article, or claim that may be made by its manufacturer, is not guaranteed or endorsed by the publisher.

frontiers in Cardiovascular Medicine

ORIGINAL RESEARCH
published: 29 October 2021
doi: 10.3389/fcvm.2021.750381

Cost-Effectiveness Evaluation of Add-on Empagliflozin in Patients With Heart Failure and a Reduced Ejection Fraction From the Healthcare System's Perspective in the Asia-Pacific Region

Chia-Te Liao[1,2,3†], Chun-Ting Yang[4†], Fang-Hsiu Kuo[2], Mei-Chuan Lee[1,5], Wei-Ting Chang[2,6,7], Hsin-Ju Tang[8], Yi-Ming Hua[5], Hung-Yu Chang[9,10], Zhih-Cherng Chen[2], Carol Strong[1], Huang-Tz Ou[4,11] and Han Siong Toh[6,12,13*]*

[1] Department of Public Health, College of Medicine, National Cheng Kung University, Tainan, Taiwan, [2] Division of Cardiology, Department of Internal Medicine, Chi Mei Medical Center, Tainan, Taiwan, [3] Department of Electrical Engineer, Southern Taiwan University of Science and Technology, Tainan, Taiwan, [4] Institute of Clinical Pharmacy and Pharmaceutical Sciences, College of Medicine, National Cheng Kung University, Tainan, Taiwan, [5] Department of Pharmacy, Chi Mei Medical Center, Tainan, Taiwan, [6] Institute of Clinical Medicine, College of Medicine, National Cheng Kung University, Tainan, Taiwan, [7] Department of Biotechnology, Southern Taiwan University of Science and Technology, Tainan, Taiwan, [8] Department of Nursing, Chang Gung University of Science and Technology, Chiayi, Taiwan, [9] Faculty of Medicine, School of Medicine, National Yang Ming Chiao Tung University, Taipei, Taiwan, [10] Heart Center, Cheng Hsin General Hospital, Taipei, Taiwan, [11] Department of Pharmacy, College of Medicine, National Cheng Kung University, Tainan, Taiwan, [12] Department of Intensive Care Medicine, Chi Mei Medical Center, Tainan, Taiwan, [13] Department of Health and Nutrition, Chia Nan University of Pharmacy & Science, Tainan, Taiwan

OPEN ACCESS

Edited by:
Xiaofeng Yang,
Temple University, United States

Reviewed by:
Unchalee Permsuwan,
Chiang Mai University, Thailand
Hankil Lee,
Ajou University, South Korea

***Correspondence:**
Chia-Te Liao
drctliao@gmail.com
Han Siong Toh
kampungths@gmail.com

†These authors have contributed equally to this work

Specialty section:
This article was submitted to Cardiovascular Therapeutics, a section of the journal Frontiers in Cardiovascular Medicine

Received: 30 July 2021
Accepted: 05 October 2021
Published: 29 October 2021

Citation:
Liao C-T, Yang C-T, Kuo F-H, Lee M-C, Chang W-T, Tang H-J, Hua Y-M, Chang H-Y, Chen Z-C, Strong C, Ou H-T and Toh HS (2021) Cost-Effectiveness Evaluation of Add-on Empagliflozin in Patients With Heart Failure and a Reduced Ejection Fraction From the Healthcare System's Perspective in the Asia-Pacific Region. Front. Cardiovasc. Med. 8:750381. doi: 10.3389/fcvm.2021.750381

Background: EMPEROR-Reduced trial provides promising evidence on the efficacy of empagliflozin adding to the standard treatment in patients with heart failure and reduced ejection fraction (HFrEF). This study aimed to investigate the cost-effectiveness of add-on empagliflozin vs. standard therapy alone in HFrEF from the perspective of the Asia-Pacific healthcare systems.

Methods: A Markov model was constructed to simulate HFrEF patients and to project the lifetime direct medical costs and quality-adjusted life years (QALY) of both therapies. Transitional probabilities were derived from the EMPEROR-Reduced trial. Country-specific costs and utilities were extracted from published resources. Incremental cost-effectiveness ratio (ICER) against willingness to pay (WTP) threshold was used to examine the cost-effectiveness. A series of sensitivity analyses was performed to ensure the robustness of the results.

Results: The ICERs of add-on empagliflozin vs. standard therapy alone in HFrEF were US$20,508, US$24,046, US$8,846, US$53,791, US$21,543, and US$20,982 per QALY gained in Taiwan, Japan, South Korea, Singapore, Thailand, and Australia, respectively. Across these countries, the probabilities of being cost-effective for using add-on empagliflozin under the WTP threshold of 3-times country-specific gross domestic product per capita were 93.7% in Taiwan, 95.6% in Japan, 96.3% in South Korea, 94.2%

Singapore, 51.9% in Thailand, and 95.9% in Australia. The probabilities were reduced when shortening the time horizon, assuming the same cardiovascular mortality for both treatments, and setting lower WTP thresholds.

Conclusion: Adding empagliflozin to HFrEF treatment is expected to be a cost-effective option among the Asia-Pacific countries. The cost-effectiveness is influenced by the WTP thresholds of different countries.

Keywords: cost-effectiveness, empagliflozin, SGLT2 inhibitor, heart failure with a reduced ejection fraction (HFrEF), systolic heart failure, Asia-Pacific

BACKGROUND

Heart failure (HF) is a clinical syndrome manifesting the final status of most cardiovascular diseases (1). Globally, an estimated HF prevalence is between 1 and 2% of the adult population, and the prevalence is estimated to be 1.3–6.7% in East Asia (2, 3). During the last few decades, the prevalence continues to grow with the rapidly aging population and improving healthcare for critical cardiovascular diseases (4, 5). Particularly, the prevalence soars up to more than 10% in populations aged 70 years or older in developed countries (6). Thus, the worldwide financial burden of HF care is projected to increase substantially in the following decades (7).

At present, several sodium-glucose cotransporter 2 (SGLT2) inhibitors, which were initially developed as glucose-lowering agents for type 2 diabetes, have been shown promising benefits to reduce the risk of hospitalization for HF (HHF) and cardiovascular death regardless of the presence or absence of diabetes (8, 9). The Cardiovascular and Renal Outcomes with Empagliflozin in Heart Failure (EMPEROR-Reduced) trial is a large-scale, multinational, multicenter, double-blind, randomized controlled trial to investigate the effects of SLGT2 inhibitors on cardiovascular outcomes among patients with heart failure and a reduced ejection fraction (HFrEF). In 3,730 HFrEF patients with or without type 2 diabetes mellitus, the addition of empagliflozin (10 mg once daily) reduces cardiovascular mortality by 31% and hospitalization for progression of HF by 8%, when compared to the standard guideline-directed medical therapy alone (9).

However, in addition to clinical effectiveness, the economic benefits also play an essential role in healthcare decision making. Although another SGLT2 inhibitor, dapagliflozin, has been shown to be a cost-effective add-on therapy for HFrEF in some countries (10–12), the cost-effectiveness data of empagliflozin in HFrEF treatment remains sparse. Besides, cost-effectiveness may be altered due to the diversity of healthcare systems across different countries. Until now, health economic evaluation of adding empagliflozin to standard care for HFrEF populations in the Asia-Pacific countries remains lacking. Thus, to fill this gap, the objective of this study is to assess the cost-effectiveness of add-on empagliflozin to standard therapy vs. standard therapy alone in HFrEF patients from a healthcare system's perspective in Taiwan and other Asia-Pacific countries.

METHODS

Rationale and Structure of Model

This study constructed a decision model and Markov model to assess the pharmacoeconomic benefit of empagliflozin (10 mg once daily) added to standard therapy vs. standard therapy alone in patients with HFrEF in Taiwan and other Asia-Pacific countries. The model followed the standard structure of the HF model (13, 14), wherein each month, all patients with HF have a risk of either stable HF without further adverse effects, hospitalization for acute decompensated HF, or death (**Figure 1**, **Supplementary Figure 1**). This two-state Markov model simulated HF patients for the Taiwanese and other Asia-Pacific populations, and data on efficacy and safety were adopted from the EMPEROR-Reduced trial (9). We simulated subjects with equivalent characteristics as the trial population. Additionally, we modeled the costs and health utilities for the time horizon of 15 years.

The decision analysis estimated the economic outcomes, including lifetime medical costs, life years, quality-adjusted life years (QALYs), and incremental cost-effectiveness ratio (ICER) (15). The model used 1 month as each cycle duration because the acute stage usually lasts 1 month. In the base-case analysis, the starting age for the simulated subjects was 67 years old according to the EMPEROR-Reduced trial, and all subjects progressed from stable HFrEF without acute events through the Markov model until death or until a 15-year horizon, which is close to the life expectancy of the Asia-Pacific countries (16, 17). Cost and utility data were discounted by an annual rate of 3% according to the Taiwan Guidelines of Methodological Standards for Pharmacoeconomic Evaluation. All the analyses were conducted on Microsoft Excel, SAS software V9.4 and TreeAge 2020. This study was granted exemption from review by the Ethics Committee of Chi Mei Medical Center (Ref.11005-E02).

Model Population, Model Assumption, and Transitional Probability

The study modeled a population that was similar to the EMPEROR-Reduced trial. Briefly, the eligibility criteria of patients enrolled in the trial included age $\geq$ 18 years, left ventricular ejection fraction of $\leq$ 40%, New York Heart Association functional class (NYHA Fc) II-IV and N-terminal pro-brain natriuretic peptide $>$ 600 pg/mL (1,200 pg/mL for patients with atrial fibrillation). All patients were required

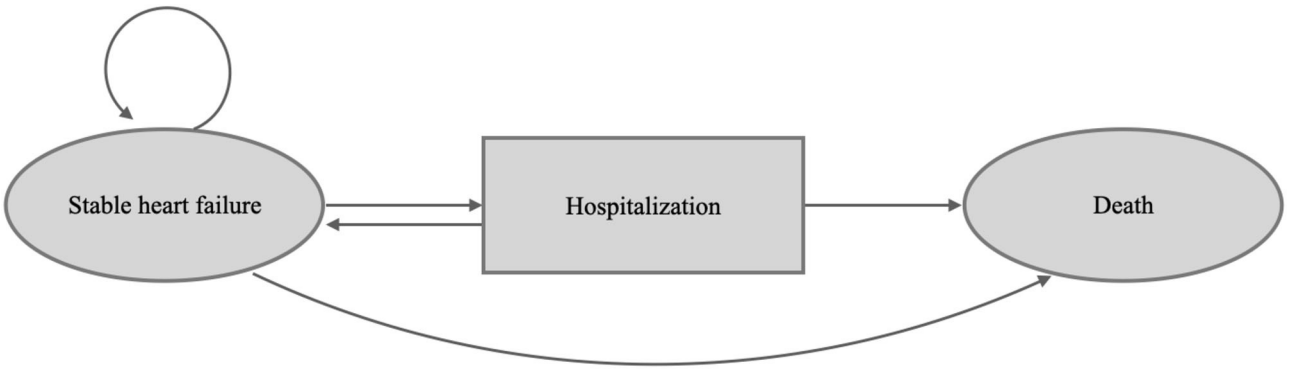

FIGURE 1 | Patients occupy health states, shown in the ovals. Patients transition from different health states represented as arrows based on transition probabilities.

to receive standard HF care, including diuretics, inhibitors of the renin-angiotensin system and neprilysin, beta-blockers, mineralocorticoid receptor antagonists, and, when indicated, cardiac devices. The detailed inclusion and exclusion criteria of the EMPEROR-Reduced trial and the baseline characteristics of the patients have been presented elsewhere (9). The patients were followed up for a median of 16 months, and the primary endpoints were hospitalization due to worsening heart failure or death from cardiovascular causes.

In this model, the populations using standard therapy with or without empagliflozin (10 mg once daily) were assumed to have stable HF status at the beginning, with no clinical events occurring in the first cycle. Then, the modeled patients moved onto the next status, i.e., hospitalization or death, based on the corresponding transitional probability. Monthly transitional probabilities were converted from annual transitional probabilities, which were derived from the proportion of given events occurring over a median follow-up period of 16 months from the EMPEROR-Reduced trial (9, 18) (**Table 1**, **Supplementary Table 1**).

Patients in the model who underwent hospitalization due to HF decompensation either moved back to stable HF status or death after the acute stage. The different statuses were assumed to be independent without interaction and were not allowed to occur simultaneously. The transitional probability of each status was constant over time. One-off treatment costs were only obtained for acute stages of HHF and cardiovascular death. Furthermore, the treatment effect was assumed to be consistent throughout.

Utilities and Costs

Utility scores were applied for each cycle for patients in the HF state based on EQ-5D scores or the Kansas City Cardiomyopathy Questionnaire (KCCQ) scores obtained from the published studies (10, 19). Utilities were assumed to be the same across both treatment regimens. Since HHF and aging are not chronic conditions, disutility was used in the model (19, 20). Input annual utility scores are presented in **Table 1**.

Costs for HF management were estimated among populations with chronic HF, identified from Taiwan's National Health Insurance Research Database (NHIRD). People who met both the following criteria were defined as patients with chronic HF: (1) $\geq$2 diagnoses of HF in the outpatient care department within 180 days in 2015, and (2) without any admission or emergency visits for HF in the previous 180 days of the first HF diagnosis in 2015.

To measure the cost of chronic HF care, chronic HF patients were followed up until the development of an acute HF event (i.e., hospitalization or emergency visit for HF), death, or the end of December 2018, whichever came first. Chronic HF costs were calculated as the sum of medical expenditure divided by the total number of followed person-months. For the cost estimation of HF hospitalization, patients with HF events were identified first, and the medical costs in the first and the following months were measured separately as model inputs. Regarding death, death cases and death causes were identified through the Cause of Death files in the NHIRD, and the medical costs within 1 month before cardiovascular and non-cardiovascular death were estimated. In the analysis, the cost was updated for inflation to 2020 using the medical consumer price index and are presented in US dollars (US$).

Base-Case Cost-effectiveness Analysis

The model was run with a time horizon of 15 years (180 cycles). We projected the discounted lifetime healthcare costs by multiplying the number of subjects with the sum of the costs in every health status. QALY was estimated using the utility values associated with each health status multiplied by the proportion of subjects living in that status. Total QALYs and life years were accumulated from the QALY and life year values in each cycle. ICER, including costs per QALY and life year gained, was calculated by dividing the incremental costs by the incremental QALYs and life years. We applied the willingness to pay (WTP) threshold of US$25,000 and 75,000, which was close to the one-time (1x) and three-times (3x) gross domestic product (GDP) per capita of Taiwan in 2020, to determine if add-on empagliflozin vs. standard care alone in HFrEF was a very cost-effective (i.e., ICER $\leq$ US$25,000) or only a cost-effective (i.e., ICER $\leq$ US$75,000) option (21, 22).

TABLE 1 | Input parameters for base-case analysis in the model in Taiwan setting.

Variables	Estimates	Standard error/Range	Distribution	References
Transitional probabilities				
Hospitalization for heart failure			Beta	EMPEROR-Reduced trial (9)
Add-on empagliflozin	0.008811915	0.002165244		
Standard therapy alone	0.012566527	0.002578038		
Cardiovascular death				
Add-on empagliflozin	0.006589325	0.00187447		
Standard therapy alone	0.007131185	0.001947398		
All-cause death				
Add-on empagliflozin	0.002113141	0.001063894		
Standard therapy alone	0.002177683	0.001078827		
Utility score				
Stable heart failure	0.770	0.016	Beta	(10, 19)
Decrement for age	−0.0016	0.0001		
Hospital for heart failure	−0.321	0.02		
Monthly costs (US$)				
Monthly costs of empagliflozin (10 mg once per day)	35	17.5	Gamma	NHIRD
Monthly costs of stable heart failure	450	225		
Mean costs of hospitalization for heart failure	2,887	1,443.5		
Costs before cardiovascular death	3,430	1,715		
Costs before all-cause death	3,390	1,695		

NHIRD, National Health Insurance Research Database.
The monthly transition probabilities were transformed by the following process.
(1) Probability (obtained from the EMPEROR-Reduced trial) to a rate = [-ln (1-p)] ÷ t.
(2) Rate to a probability (monthly transition probability applied in the analyses) = 1- exp(-rt).
Where r = rate, p = probability, and t = time.
Example: the probability of hospitalization for heart failure is 13.2% over the follow-up period in the EMEPROR-Reduced trial.
16-month probability was transformed to one-month rate and then one-month rate was transformed to one-month probability.
one-month rate = (-ln (1-0.132)/16 = 0.00885.
one-month possibility = 1-exp (−0.00885) = 0.008811915.

One-Way Sensitivity Analyses

We performed one-way sensitivity analysis with varying values for all input parameters through plausible ranges (± 10%) or alternative values to evaluate the robustness of our cost-effectiveness analysis results. The results are presented as a tornado diagram in **Figure 2**.

Probabilistic Sensitivity Analyses

To assess the intra-individual and parameter uncertainties, we conducted a probabilistic sensitivity analysis (PSA) by the Monte Carlo Simulation (23), in which subjects were randomly sampled and simulations were repeated 1,000 times to obtain the outcomes. As for the input variable ranges in the simulation, beta distribution was used for transitional probabilities, beta distribution for utilities (utility value ranged between 0 and 1), and gamma distribution for costs (costs could not be <0) (24). The PSA results are presented in the cost-effectiveness acceptability curve (**Supplementary Figures 3, 4**).

Scenario Analyses in the Asia-Pacific Countries

Since the results of cost-effectiveness evaluation are likely to be country- or ethnicity-specific, we reiterated the analyses under the settings of other countries with universal healthcare coverage in the Asia-Pacific region, including Japan, South Korea, Singapore, Thailand, and Australia, to evaluate the cost-effectiveness in the individual countries. We modeled the different costs and utilities from the included countries to compare the pharmacoeconomic benefits from the healthcare system's perspective. The values of the input parameters were extracted from the published sources (**Supplementary Table 2**) (25–29). Base-case analysis and PSA were both performed for each country. WTP thresholds with 1x and 3x GDP per capita of each country were also used to determine if add-on empagliflozin is a very cost-effective or only a cost-effective option, respectively (21). The cost-effectiveness results are presented in **Table 3**, **Figure 3**.

Scenario Analyses in Consideration of Adverse Events and Other Variables

Moreover, we constructed the Model 2 (**Supplementary Figure 2**) to account for the impact of adverse events on our results. The state of hospitalization not only included worsened HF, but also adverse events including hypoglycemia, urinal tract infection, genital infection, bone fracture, and amputation (9). The input variable values are reported in **Table 1**, **Supplementary Tables 1, 2**. The

Input parameter	Lower limit	ICER difference	Upper limit	ICER difference
Transitional probability for CV death (Empagliflozin)	0.005930393	-6362	0.007248258	-198552
Transitional probability for CV death (Placebo)	0.006418067	-64458	0.007844304	-6459
Transitional probability for non-CV death (Placebo)	0.001959915	-3344	0.002395451	6971
Transitional probability for non-CV death (Empagliflozin)	0.001901827	-3349	0.002324455	6814
Utility for stable heart failure	0.693	-1875	0.847	2294
Cost for stable heart failure	405	-2031	495	2030
Empagliflozin price	31.5	-1507	38.5	1506
Transitional probability for HHF (Placebo)	0.011309874	-773	0.01382318	783
Transitional probability for HHF (Empagliflozin)	0.007930724	-585	0.009693107	589
Cost for HHF	2598.3	-205	3175.7	205

CV, cardiovascular; HHF, hospitalization for heart failure; ICER, incremental cost-effectiveness ratio

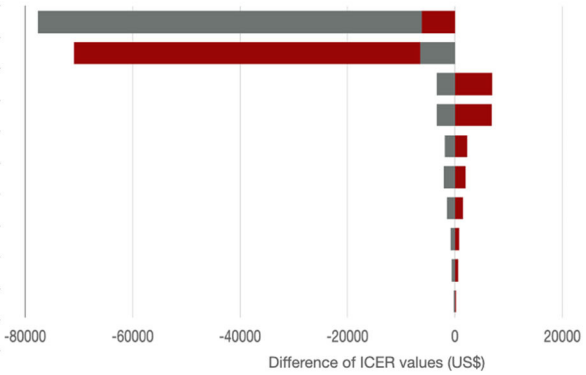

FIGURE 2 | The tornado diagram presents the results of one-way sensitivity analysis. The red and gray bar represent the corresponding incremental cost-effective ratio values when the lower and upper limits of the parameters were used. ICER, incremental cost-effectiveness ratio; CV, cardiovascular; HHF, Hospitalization for heart failure.

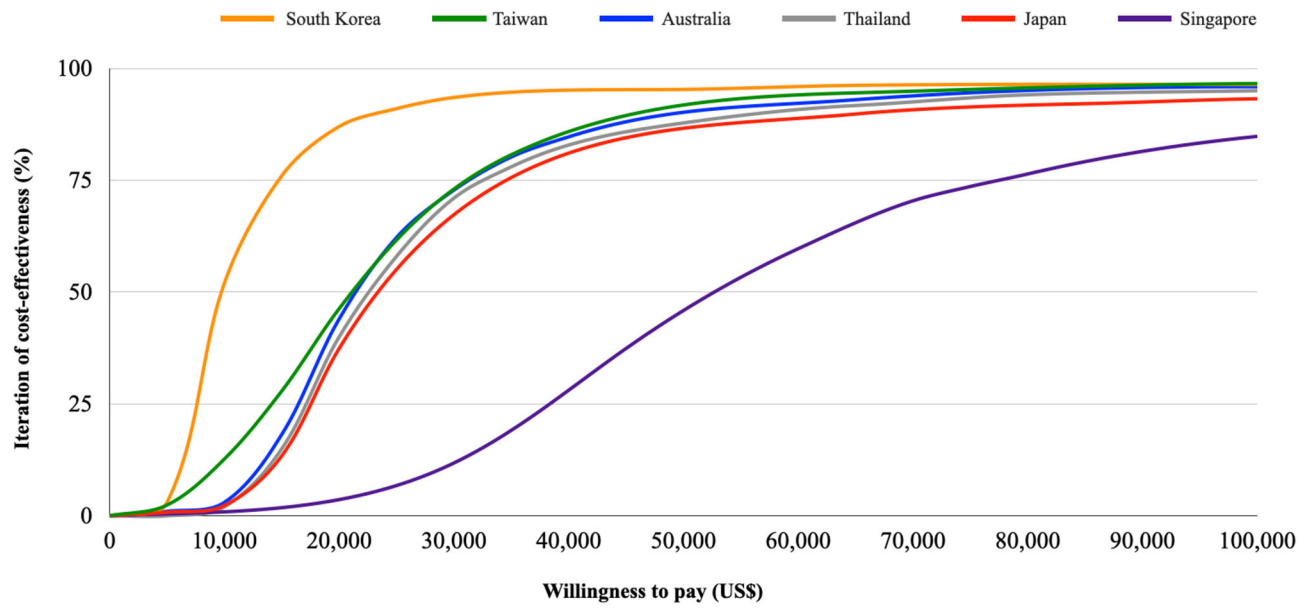

FIGURE 3 | Cost-effectiveness acceptability curve. Iterations of the cost-effectiveness of empagliflozin vs. placebo under different willingness to pay thresholds in Taiwan, Japan, South Korea, Singapore, Thailand, and Australia.

cost-effectiveness results are presented in **Table 2**, and the depicted cost-effectiveness acceptance curve compared to the original model is shown in **Supplementary Figure 5**.

Other scenario sensitivity analyses were performed to account for more considerable influences on ICER among the variables, i.e., time horizon, discount rate, risk of cardiovascular and non-cardiovascular death, risk of HHF, and the costs of drugs and HHF. Half costs of empagliflozin and HHF US$17.5 and US$ 1,443.5 were tested. To provide more information, we also calculated the costs of empagliflozin so that the regimen would be cost-effective at the different WTP thresholds of US$20,000, US$17,500, US$15,000, US$12,500, and US$10,000. Discount rates of 0 and 10% were input to assess the different economic conditions. We used the time horizons of 30 years and 16 months (the follow-up duration in the EMPEROR-Reduced trial) to assess the pharmacoeconomic incentive in the different periods.

Subgroup Analyses

We further performed subgroup cost-effectiveness analyses according to the EMPEROR-Reduced trial, i.e., aged $\geq$ 65 or $<$ 65 years, varied ethnicities Black, Asian, White), different renal functions (estimated glomerular filtration rate, eGFR $\geq$ 60 or $<$ 60 ml/min/1.73 m^2), with or without diabetes, ischemic cause for HF, and concomitant use with sacubitril/valsartan (9).

TABLE 2 | The results of base-case cost-effectiveness analysis, probabilistic sensitivity analysis, scenario sensitivity analyses, and subgroup analyses in Taiwan setting.

In Taiwan setting	Costs (US$)			QALYs			ICERs	Result from PSA	
	Empagliflozin	Placebo	Incremental costs	Empagliflozin	Placebo	Incremental QALYs		Iteration of WTP threshold at US$ 25,000	Iteration of WTP threshold at US$ 75,000
Base-case analysis	79,141	71,739	7,402	9.66	9.30	0.36	20,508	63.4%	93.7%
Per LY gained instead of QALY gained	79,141	71,739	7,402	12.89	12.42	0.47	15,693	77.9%	95.8%
Scenario sensitivity analysis	79,542	71,987	7,555	9.56	9.23	0.33	22,581	55.4%	91.1%
Account for adverse events									
Time horizon (30 years)	89,576	80,189	9,387	10.93	10.40	0.54	17,492	77.4%	98.6%
Time horizon (16 months)	15,184	14,232	952	1.86	1.85	0.01	91,617	36.8%	47.1%
Discounting rate at 0%	92,829	83,839	8,990	11.33	10.87	0.46	19,469	68.2%	95.8%
Discounting rate at 10%	57,477	52,479	4,997	7.02	6.80	0.21	23,305	53.8%	90.8%
Risk of cardiovascular mortality of empagliflozin equal to placebo	76,671	71,717	4,954	9.34	9.30	0.04	112,186	20%	45.3%
Risk of non-cardiovascular death for empagliflozin equal to placebo	78,822	71,717	7,105	9.62	9.30	0.32	22,039	57.9%	91.2%
Risk of HHF for empagliflozin equal to placebo	79,385	71,717	7,667	9.66	930	0.36	21,412	59.8%	94.2%
Half the monthly costs of empagliflozin (US$17.5)	76,401	71,717	4,684	9.66	9.30	0.36	12,976	83.6%	96.5%
Half the costs of treatment of hospitalization for heart failure	78,133	70,359	7,774	9.66	9.30	0.36	21,532	59%	93.5%
Different drug prices of empagliflozin at different WTP thresholds to meet the cost-effectiveness in Taiwan setting									
WTP (US$)	**10,000**	**12,500**	**15,000**	**17,500**	**20,000**				
Monthly costs (US$)	8.2	14	19.5	25.6	31.5				

QALY, quality-adjusted life year; ICER, incremental cost-effectiveness ratio; PSA, probabilistic sensitivity analyses; WTP, willingness to pay; LY, life years; HHF, hospitalization for heart failure.

RESULTS

At the end of the 15-year simulation, the mortality rates were 79.3% in the empagliflozin group and 81.4% in the standard therapy group. For every 1,000 patients with HFrEF treated with empagliflozin, ∼296 HHF (803 vs. 1,099) were averted over the 15-year horizon.

Table 2 shows the results of the base-case analysis in which 10 mg of empagliflozin once daily added to standard therapy in patients with HFrEF produced better effectiveness than standard therapy alone (9.66 vs. 9.30 QALYs, and 12.89 vs. 12.42 life years) in the model. Simultaneously, add-on empagliflozin spent more lifetime medical costs (US$79,141 vs. US$71,739). The ICERs in the model were US$20,508 per QALY gained, and US$15,693 per life year gained.

Figure 2 shows the tornado diagram presenting the impact of the different ranges of variables on the ICERs. The probability of cardiovascular death influenced ICER the most, followed by the probability of non-cardiovascular death, monthly costs and utility of stable HF. ICER values were also sensitive to the drug price of empagliflozin, and the probability and costs of HHF.

PSA results are shown in **Table 2**, **Supplementary Figures 3, 4**. The likelihood iteration of cost-effectiveness for the empagliflozin regimen vs. standard therapy alone was 63.4 vs. 36.6% at US$25,000, and 93.7 vs. 6.3% at US$75,000 in the Taiwan setting.

Table 2 demonstrates the results of the scenario analyses. With 30 years and 16 months as the time horizon, the ICER became US$17,492 and US$91,617. At discount rates of 0 and 10%, the ICER changed to US$19,469 and US$23,305, respectively. Since cardiovascular death had the strongest influence in the model, we performed a scenario test by assuming the same risk of cardiovascular death in both regimens. Then, the ICER soared up to US$112,186. However, assuming equivalent values of risk for non-cardiovascular death and HHF, the ICER did not change noticeably (US$ 22,039 and US$21,412). At the half costs of empagliflozin and HHF, the ICER changed to US$12,976 and US$21,532. Notably, if the monthly cost of empagliflozin became <US$31.5, US$25.6, US$19.5, US$14.0, and US$8.2, the corresponding ICERs decrease to below the WTP thresholds at US$20,000, US$17,500, US$15,000, US$12,500, and US$10,000. Taking into account the scenario with adverse events, the Model 2 showed that both therapies produced more medical costs and fewer QALYs, and the ICER value increased from US$20,508 to US$22,581, compared to the original model (**Supplementary Figure 5**).

Table 3, **Figure 3** show the results of base-case analysis and PSA for add-on empagliflozin in HFrEF treatment in different Asia-Pacific countries. The Singapore setting resulted in the most costs from the regimen (US$148,751), while the South Korean setting produced the least (US$15,934). The QALYs gained between both therapies did not show much difference across the countries, but all had higher QALYs gained with add-on empagliflozin. The ICER value in the Singapore setting was the highest at US$53,791, followed by Japan (US$24,046), Thailand (US$21,543), Australia (US$20,982), Taiwan (US$20,508), and South Korea (US$8,846). Given the WTP thresholds at 1x and 3x

TABLE 3 | Base-case analysis and probabilistic sensitivity analysis of cost-effectiveness for add-on empagliflozin vs. standard therapy alone among patients with heart failure and a reduced ejection fraction in the included Asia-Pacific countries.

Asia-Pacific countries	Costs (US$)			QALYs			ICERs	Result from PSA	
	Empagliflozin	Placebo	Incremental costs	Empagliflozin	Placebo	Incremental QALYs		Iteration of WTP threshold at one-time GDP per capita*	Iteration of WTP threshold at three-times GDP per capita*
Taiwan setting	79,141	71,739	7,402	9.66	9.30	0.36	20,508	63.4%	93.7%
Japan setting	45,210	37,664	7,546	8.37	8.06	0.31	24,046	77.9%	95.6%
South Korea setting	15,934	13,158	2,776	8.37	8.06	0.31	8,846	93.6%	96.3%
Singapore setting	148,751	130,602	188,149	9.02	8.68	0.34	53,791	58.1%	94.2%
Thailand setting	21,805	15,247	6,558	8.11	7.81	0.30	21,543	0%	51.9%
Australia setting	56,356	49,573	6,783	8.63	8.31	0.32	20,982	89%	95.9%

QALY, quality-adjusted life year; ICER, incremental cost-effectiveness ratio; PSA, probabilistic sensitivity analyses; WTP, willingness to pay; GDP, gross domestic product.

**GDP per capita (2020): US$25,000 for Taiwan; US$39,000 for Japan; US$30,000 for South Korea; US$58,000 for Singapore; US$7,300 for Thailand; US$52,000 for Australia.*

GDP per capita in each country, the likelihood iterations of being a very cost-effective and only a cost-effective option for add-on empagliflozin vs. standard therapy alone were 63.4 and 93.7% for Taiwan, 77.9 and 95.6% for Japan, 93.6 and 96.3% for South Korea, 58.1 and 94.2% for Singapore, 0 and 51.9% for Thailand, and 89 and 95.9% for Australia.

In the subgroup analyses, at a WTP threshold of US$25,000, the probabilities of cost-effectiveness of add-on empagliflozin therapy were similar irrespective of the subjects being older or younger than 65 years. The regimen had the highest probability of being cost-effective for Black people, followed by Asians and White people. In the subpopulation with diabetes, eGFR $\geq$ 60 ml/min/1.73m^2, non-ischemic HF, NYHA Fc II, or concomitant sacubitril/valsartan use, add-on empagliflozin therapy was more cost-effective at the WTP threshold of US$25,000, compared to those without diabetes or sacubitril/valsartan use and those with eGFR $<$ 60 ml/min/1.73 m^2, ischemic HF, or NYHA Fc III-IV (**Supplementary Table 4**, **Supplementary Figure 6**).

DISCUSSION

From our results, the incremental costs per QALY and life year gained in the base-case analysis and PSA were lower than 1x and 3x the GDP per capita in Taiwan, Japan, Singapore, South Korea, and Australia. Namely, adding empagliflozin to standard therapy was likely to be a very cost-effective add-on therapy from a national payer's perspective in these countries. Regarding Thailand, ICER is only lower than 3x the GDP per capita, and thus, adding empagliflozin is only a cost-effective option. Although the incremental cost per life year gained was lower than the incremental cost per QALY gained, using this ICER value may lead to an underestimation. Mainly, chronic clinical events severely influence the quality of life. For example, the utility of heart failure is only 0.77 of one perfectly healthy year. In comparison to life years, QALY provides a more appropriate evaluation of the cost-effectiveness of new treatments for chronic diseases (30).

In the one-way sensitivity analysis, the risk of cardiovascular death had the most significant impact on the ICERs. To assess the impact of the parameters, we used the hypothetical scenario to evaluate the ICERs. In the EMPEROR-Reduced trial, the add-on empagliflozin regimen had a lower risk of cardiovascular death than in the placebo group (hazard ratio 0.92, 95% confidence interval 0.75–1.12), despite the difference being statistically insignificant (9). If the cardiovascular death risk was the same in both therapies, the add-on empagliflozin regimen would not have pharmacoeconomic incentives (ICER of US$112,186), meaning that the pharmacoeconomic benefits may need to be carefully re-assessed with real-world data after the initial use of empagliflozin in HFrEF patients. However, given the same risks of non-cardiovascular death and HHF for both therapies, empagliflozin remained a very cost-effective therapy in HFrEF treatment. On the other hand, costs of empagliflozin substantially influenced the pharmacoeconomic benefits, while HHF costs had less influence. For example, at the half-cost of empagliflozin and HHF, ICER values became US$12,976 and US$21,532 per QALY gained, respectively. This hypothetic scenario may provide reference to support that negotiating the drug price may result in more pharmacoeconomic benefits than adjusting the healthcare costs for HHF. In addition, the current study also estimated the appropriate drug price to meet the cost-effectiveness of empagliflozin given the different WTP thresholds from US$10,000 to US$25,000. The results also provide scientific references for policymaking or bargaining drug costs for the target population.

In another scenario analysis, ICER values remained $<$ US$25,000 regardless of the different discount rates (0–10%), which may strengthen the robustness of the cost-effectiveness of empagliflozin when accounting for the time factor. Different time horizons of 30 years and 16 months were applied to take into consideration the super-aged society and the follow-up period of the EMPEROR-Reduced trial. We observed that the longer the time horizon, the smaller the ICER values, indicating that the regimen has more pharmacoeconomic incentives in long-term use. In addition, we constructed the Model 2 to simulate the complexity accounting for the impact of adverse events. Although the ICER increased from US$20,508 to US$22,581, the pharmacoeconomic benefit was still attractive. This may be consistent with the condition that except for uncomplicated genital tract infections, most adverse events did not show significant differences between the two therapies (9). In the subgroup analysis, we found that using add-on empagliflozin in the Black and Asian population with HFrEF was likely to yield more pharmacoeconomic benefits, compared to Caucasians. Furthermore, the populations with diabetes, eGFR $\geq$ 60 ml/min/1.73 m^2, non-ischemic HF, NYHA Fc II, or concomitant sacubitril/valsartan use were likely to show more benefits in terms of cost-effectiveness. Policymakers may prioritize specific patient groups for the add-on therapy in HFrEF under the financial constraints of the healthcare system (**Supplementary Table 4**, **Supplementary Figure 6**).

In our study, the pharmacoeconomic attraction differs across the different country settings. South Korea had the lowest ICER value (US$8,846) mainly due to the lowest drug cost of empagliflozin. Conversely, Singapore had the highest ICER value (US$53,791), which may be due to the expensive medical spending. However, despite the higher medical expenditure, empagliflozin is still highly possible to be a very cost-effective treatment in the Singapore setting due to the higher WTP threshold. Likewise, although medical costs were lower in Thailand with a median ICER value in the Asia-Pacific region, the regimen would be only cost-effective due to the lower WTP threshold.

To the best of our knowledge, the current analysis is the first to assess the cost-effectiveness of empagliflozin added to standard therapy in patients with HFrEF. Dapagliflozin has been shown to be cost-effective add-on therapy for patients with HFrEF in the U.K. (ICER £5822/QALY gained), Germany (ICER €5379/QALY gained), Spain (ICER €9406/QALY gained), and Australia (ICER A$12,482/QALY gained) (10, 11) Comparing the two SGLT2 inhibitors in HFrEF treatment, the ICER yielded by empagliflozin

was likely to be greater than that yielded by dapagliflozin in spite of the different settings, e.g., A$12,482/QALY gained for dapagliflozin vs. US$20,982/QALY gained for empagliflozin in the Australia setting. The disparity in the clinical efficacy of cardiovascular and non-cardiovascular death might be the major influence (31).

There are some limitations of the current study. First, the study parameters were collected from several sources, which may contribute to the uncertainty. However, we derived the clinical transitional probabilities from only the EMPEROR-Reduced trial. The design of double-blinded randomized controlled trial may help to mitigate the uncertainty and provide convincing evidence (32). Besides, we tested all input parameters in various sensitivity analyses, and the pharmacoeconomic conclusion did not change. Second, using parameters from different races might lead to uncertainty because Asians composed only 13–14% of all subjects in the trial. Nevertheless, the PSA using Monte Carlo Model considered a different and wide range of the transitional probabilities, which may cover the probabilities in different races. Besides, the hazard ratio of primary outcomes for Asians was 0.57 (0.41–0.78), which was better than the entire enrolled population [0.75, (0.65–0.68)] (14). If we only used the variables from Asian populations, the pharmacoeconomic benefit would become more positive in our analyses (**Supplementary Table 4**, **Supplementary Figure 6**). Third, Taiwan and some Asia-Pacific countries have not reached a public consensus on the WTP threshold, and the pharmacoeconomic incentives may differ according to the different thresholds. Thus, the study provided the iteration of the cost-effectiveness using different WTP thresholds in Asia-Pacific countries (from US$0 to US$100,000) to ameliorate the concern (**Figure 3**). Fourth, the model might simplify the real-world conditions. For example, the current study assumed that the influence of adverse events was neglected, and the transitional probabilities were constant irrespective of the comorbidities, recurrent diseases, and aging. The assumption may not be sufficient to reflect the possible changes in the risks of disease progression or death over time with the aging of patients in a chronic disease course of HF. To ameliorate the concerns, we performed a series of sensitivity analyses, including PSA with a varied range of transitional probabilities and scenario analyses with different time horizons. Besides, we took account of the adverse events in the Model 2 for base-case analysis and PSA. In these analyses, the positive conclusions did not change. The abovementioned consistent findings between these base-case analyses and further analyses strengthened the robustness of the pharmacoeconomic benefits.

Finally, the current analysis was performed from the perspective of a national healthcare system, and the costs only included direct medical costs. Although the different level of cost resources, treatment context, and WTP thresholds across different countries would influence the cost-effectiveness results (national-level medical costs database in Taiwan, South Korea, Singapore, Australia, and hospital-level data in Japan and Thailand) (22–26), the current study extracted the data all from the healthcare system's perspective and further performed PSA with gamma distribution covering a wide and varied range of costs to strengthen the robustness of findings. Also, the study provided the different probabilities of cost-effectiveness for add-on empagliflozin vs. standard care alone in HFrEF treatment under various WTP thresholds. Nevertheless, the health technique assessment of add-on empagliflozin in HFrEF treatment may still require a more comprehensive evaluation by considering the financial strains of the healthcare system, reimbursement policy, societal costs, opportunity costs, equity, and equality. Further studies are also needed to consider the costs from a societal perspective, such as indirect medical costs, productivity loss, and social services.

CONCLUSIONS

In conclusion, our results showed that add-on empagliflozin in patients with HFrEF produced improved effectiveness accompanied with acceptable costs. Although empagliflozin is likely to be a cost-effective treatment for HFrEF, the pharmacoeconomic benefits are influenced by the WTP thresholds across different healthcare systems in the Asia-Pacific region.

DATA AVAILABILITY STATEMENT

Publicly available datasets were analyzed in this study. This data can be found at: Taiwan National Health Insurance Database.

AUTHOR CONTRIBUTIONS

C-TL and C-TY contributed to this study, including the conception and design of the work, and drafting of the manuscript. F-HK, M-CL, and W-TC contributed to the acquisition, analysis, and interpretation of data for this work. H-TO, H-JT, and Y-MH contributed to modifying the model structure. Z-CC, H-YC, CS, and HST critically revised the manuscript. All authors gave final approval and agreed to be accountable for all aspects of work ensuring integrity and accuracy.

SUPPLEMENTARY MATERIAL

The Supplementary Material for this article can be found online at: https://www.frontiersin.org/articles/10.3389/fcvm.2021.750381/full#supplementary-material

REFERENCES

1. Kemp CD, Conte JV. The pathophysiology of heart failure. *Cardiovasc Pathol.* (2012) 21:365–71. doi: 10.1016/j.carpath.2011.11.007
2. Guo Y, Lip GY, Banerjee A. Heart failure in East Asia. *Curr Cardiol Rev.* (2013) 9:112–22. doi: 10.2174/1573403X11309020004
3. Savarese G, Lund LH. Global public health burden of heart failure. *Cardiac Failure Rev.* (2017) 3:7. doi: 10.15420/cfr.2016:25:2

4. Huang CH, Chien KL, Chen WJ, Sung FC, Hsu HC, Su TC, et al. Impact of heart failure and left ventricular function on long-term survival—report of a community-based cohort study in Taiwan. *Eur J Heart Fail.* (2007) 9:587–93. doi: 10.1016/j.ejheart.2007.02.008
5. Tseng CH. Clinical features of heart failure hospitalization in younger and elderly patients in Taiwan. *Eur J Clin Invest.* (2011) 41:597–604. doi: 10.1111/j.1365-2362.2010.02447.x
6. Ponikowski P, Voors AA, Anker SD, Bueno H, Cleland JGF, Coats AJS, et al. 2016 ESC Guidelines for the diagnosis treatment of acute chronic heart failure: The Task Force for the diagnosis treatment of acute chronic heart failure of the European Society of Cardiology (ESC) Developed with the special contribution of the Heart Failure Association (HFA) of the ESC. *Europ Heart J.* (2016). 37:2129–200. doi: 10.1093/eurheartj/ehw128
7. Heidenreich PA, Albert NM, Allen LA, Bluemke DA, Butler J, Fonarow GC, et al. Forecasting the impact of heart failure in the United States: a policy statement from the American Heart Association. *Circulation.* (2013) 6:606–19. doi: 10.1161/HHF.0b013e318291329a
8. McMurray JJ, Solomon SD, Inzucchi SE, Køber L, Kosiborod MN, Martinez FA, et al. Dapagliflozin in patients with heart failure and reduced ejection fraction. *N Engl J Med.* (2019) 381:1995–2008. doi: 10.1056/NEJMoa1911303
9. Packer M, Anker SD, Butler J, Filippatos G, Pocock SJ, Carson P, et al. Cardiovascular and renal outcomes with empagliflozin in heart failure. *N Engl J Med.* (2020) 383:1413–24. doi: 10.1056/NEJMoa2022190
10. McEwan P, Darlington O, McMurray JJ, Jhund PS, Docherty KF, Böhm M, et al. Cost-effectiveness of dapagliflozin as a treatment for heart failure with reduced ejection fraction: a multinational health-economic analysis of DAPA-HF. *Eur J Heart Fail.* (2020) 22:2147–56. doi: 10.1002/ejhf.1978
11. Savira F, Wang BH, Kompa AR, Ademi Z, Owen AJ, Zoungas S, et al. Cost-effectiveness of dapagliflozin in chronic heart failure: an analysis from the Australian healthcare perspective. *Eur J Prev Cardiol.* (2020) 28:975–82.
12. Krittayaphong R, Permsuwan U. Cost-utility analysis of add-on dapagliflozin treatment in heart failure with reduced ejection fraction. *Int J Cardiol.* (2021) 322:183–90. doi: 10.1016/j.ijcard.2020.08.017
13. Chan DC, Heidenreich PA, Weinstein MC, Fonarow GC. Heart failure disease management programs: a cost-effectiveness analysis. *Am Heart J.* (2008) 155:332–8. doi: 10.1016/j.ahj.2007.10.001
14. Gaziano TA, Fonarow GC, Claggett B, **Chan WW**, Deschaseaux-Voinet C, Turner SJ, et al. Cost-effectiveness analysis of sacubitril/valsartan vs enalapril in patients with heart failure and reduced ejection fraction. *JAMA Cardiol.* (2016) 1:666–72. doi: 10.1001/jamacardio.2016.1747
15. Briggs A, Sculpher M, Claxton K. *Decision Modelling for Health Economic Evaluation*. Oxford, United Kingdom: Oup Oxford (2006).
16. World Health Organization. "*Life Expectancy and Healthy Life Expectancy, Data by Country*". World Health Organization (2020). Available online at: https://apps.who.int/gho/data/node.main.688 (accessed September 10, 2021)
17. Ministry of the Interior, Taiwan. *Annual Report of Life Table in Taiwan Area*. Available online at: https://ws.moi.gov.tw/001/Upload/400/relfile/0/4405/48349492-6f8c-453b-a9d1-4a8f0593b979/year/year.html (accessed September 3, 2021)
18. Sonnenberg FA, Beck JR. Markov models in medical decision making: a practical guide. *Med Decision Making.* (1993) 13:322–38. doi: 10.1177/0272989X9301300409
19. Sullivan PW, Ghushchyan V. Preference-based EQ-5D index scores for chronic conditions in the United States. *Med Decision Making.* (2006) 26:410–20. doi: 10.1177/0272989X06290495
20. Lee MC, Liao CT, Toh HS, Chou CC, Chang WT, Chen ZC, et al. Cost-effectiveness analysis of rivaroxaban plus aspirin versus aspirin alone in secondary prevention among patients with chronic cardiovascular diseases. *Cardiovasc Drugs Ther.* (2020) 35:539–47. doi: 10.1007/s10557-020-07059-w
21. "World Economic Outlook Database, October 2020". *World Economic Outlook*. Washington, DC, United States: International Monetary Fund (2020).
22. Bertram MY, Lauer JA, De Joncheere K, Edejer T, Hutubessy R, Kieny MP, et al. Cost–effectiveness thresholds: pros and cons. *Bull World Health Organ.* (2016) 94:925. doi: 10.2471/BLT.15.164418
23. Briggs AH, Ades A, Price MJ. Probabilistic sensitivity analysis for decision trees with multiple branches: use of the Dirichlet distribution in a Bayesian framework. *Med Decision Making.* (2003) 23:341–50. doi: 10.1177/0272989X03255922
24. Briggs AH. Handling uncertainty in cost-effectiveness models. *Pharmacoeconomics.* (2000) 17:479–500. doi: 10.2165/00019053-200017050-00006
25. Inomata T, Izumi T, Kobayashi M. Cost-effectiveness analysis of carvedilol for the treatment of chronic heart failure in Japan. *Circ J.* (2004) 68:35–40. doi: 10.1253/circj.68.35
26. Park SK, Hong SH, Kim H, Kim S, Lee EK. Cost-utility analysis of sacubitril/valsartan use compared with standard care in chronic heart failure patients with reduced ejection fraction in South Korea. *Clin Ther.* (2019) 41:1066–79. doi: 10.1016/j.clinthera.2019.04.031
27. Liang L, Wu D. BC, Aziz MIA, Wong R, Sim D, Leong KTG, et al. Cost-effectiveness of sacubitril/valsartan versus enalapril in patients with heart failure and reduced ejection fraction. *J Med Econ.* (2018) 21:174–81. doi: 10.1080/13696998.2017.1387119
28. Permsuwan U, Phrommintikul A, Silavanich V. Cost-effectiveness of cardiac resynchronization therapy in patients with heart failure in Thailand. *Clinicoecon Outcomes Res.* (2020) 12:579. doi: 10.2147/CEOR.S268553
29. Chin KL, Zomer E, Wang BH, Liew D. Cost-effectiveness of switching patients with heart failure and reduced ejection fraction to sacubitril/valsartan: the Australian perspective. *Heart Lung Circul.* (2020) 29:1310–7. doi: 10.1016/j.hlc.2019.03.007
30. Chapman RH, Berger M, Weinstein MC, Weeks JC, Goldie S, Neumann PJ. When does quality-adjusting life-years matter in cost-effectiveness analysis? *Health Econ.* (2004) 13:429–36. doi: 10.1002/hec.853
31. Zannad F, Ferreira JP, Pocock SJ, Anker SD, Butler J, Filippatos G, et al. SGLT2 inhibitors in patients with heart failure with reduced ejection fraction: a meta-analysis of the EMPEROR-Reduced and DAPA-HF trials. *Lancet.* (2020) 396:819–29. doi: 10.1016/S0140-6736(20)31824-9
32. Sibbald B, Roland M. Understanding controlled trials. Why are randomised controlled trials important? *BMJ.* (1998) 316:201. doi: 10.1136/bmj.316.7126.201

Conflict of Interest: The authors declare that the research was conducted in the absence of any commercial or financial relationships that could be construed as a potential conflict of interest.

Publisher's Note: All claims expressed in this article are solely those of the authors and do not necessarily represent those of their affiliated organizations, or those of the publisher, the editors and the reviewers. Any product that may be evaluated in this article, or claim that may be made by its manufacturer, is not guaranteed or endorsed by the publisher.

frontiers in Cardiovascular Medicine

REVIEW
published: 26 November 2021
doi: 10.3389/fcvm.2021.771298

Mitochondrial Transfer in Cardiovascular Disease: From Mechanisms to Therapeutic Implications

Jun Chen[1], *Jinjie Zhong*[1], *Lin-lin Wang*[2]* *and Ying-ying Chen*[1]*

[1] Department of Basic Medicine Sciences, and Department of Obstetrics of the Second Affiliated Hospital, Zhejiang University School of Medicine, Hangzhou, China, [2] Department of Basic Medicine Sciences, and Department of Orthopaedics of Sir Run Run Shaw Hospital, Zhejiang University School of Medicine, Hangzhou, China

Mitochondrial dysfunction has been proven to play a critical role in the pathogenesis of cardiovascular diseases. The phenomenon of intercellular mitochondrial transfer has been discovered in the cardiovascular system. Studies have shown that cell-to-cell mitochondrial transfer plays an essential role in regulating cardiovascular system development and maintaining normal tissue homeostasis under physiological conditions. In pathological conditions, damaged cells transfer dysfunctional mitochondria toward recipient cells to ask for help and take up exogenous functional mitochondria to alleviate injury. In this review, we summarized the mechanism of mitochondrial transfer in the cardiovascular system and outlined the fate and functional role of donor mitochondria. We also discussed the advantage and challenges of mitochondrial transfer strategies, including cell-based mitochondrial transplantation, extracellular vesicle-based mitochondrial transplantation, and naked mitochondrial transplantation, for the treatment of cardiovascular disorders. We hope this review will provide perspectives on mitochondrial-targeted therapeutics in cardiovascular diseases.

Keywords: cardiovascular disease, mitochondria, mitochondrial transfer, mitochondrial transplantation, tunneling nanotubes, extracellular vesicles

OPEN ACCESS

Edited by:
Xiaofeng Yang,
Temple University, United States

Reviewed by:
Sandra Anjo,
University of Coimbra, Portugal
Ruijing Zhang,
Second Hospital of Shanxi Medical University, China

***Correspondence:**
Lin-lin Wang
wanglinlin@zju.edu.cn
Ying-ying Chen
bchenyy@zju.edu.cn

Specialty section:
This article was submitted to Cardiovascular Therapeutics, a section of the journal Frontiers in Cardiovascular Medicine

Received: *06 September 2021*
Accepted: *08 November 2021*
Published: *26 November 2021*

Citation:
Chen J, Zhong J, Wang L-l and Chen Y-y (2021) Mitochondrial Transfer in Cardiovascular Disease: From Mechanisms to Therapeutic Implications. Front. Cardiovasc. Med. 8:771298. doi: 10.3389/fcvm.2021.771298

INTRODUCTION

Cardiovascular diseases refer to a group of disorders affecting the heart and blood vessels, including coronary artery disease (such as myocardial infarction), arrhythmia, hypertensive heart disease, valvular heart disease, cardiomyopathy, et al. (1, 2). Mitochondria not only serve as power plants in cells but also act as crucial regulators in many biological processes, including reactive oxygen species (ROS) signaling, redox balance, calcium homeostasis, protein quality control, and programmed cell death (3, 4). The abnormal morphology and dysfunction of mitochondria have been proven as the principal mechanisms in the pathogenesis of cardiovascular diseases, such as heart failure, myocardial infarction, atherosclerosis, and hypertension (4–6). So mitochondria-targeted therapy is suggested to be a potential treatment strategy for cardiovascular diseases. In recent years, a large number of pharmaceutical compounds and nutritional supplements that can boost mitochondrial bioenergetics efficiency have been developed. However, clinical trials of these agents for cardiovascular diseases were hardly approved to carry out, even less to evaluate their clinical effectiveness and safety. The main obstacle is because many protein

components of mitochondria are the network hubs of multiple biological pathways. If a chemical compound targeting one of these hubs is used, it can not only modify the anticipated biological pathways but also change other unexpected mitochondrial processes (5). Therefore, patients with cardiovascular diseases would fail to achieve the desired outcomes by using these mitochondrial-targeted drugs (5). Given the complexity of the biological function of mitochondria, researchers have begun to consider rescuing the injured cells through mitochondrial transfer, that is, replacing damaged mitochondria with healthy mitochondria from donor cells.

The intercellular mitochondrial transfer was reported for the first time by Spees and colleagues in 2006. They demonstrated that transferring functional mitochondria of bone marrow-derived stem cells to defective parenchymal cells increases the aerobic respiration capacity of recipient mitochondria (7). Nowadays, more and more studies have revealed that cells in the cardiovascular system (such as cardiomyocytes, vascular smooth muscle cells, endothelial cells, et al.) can act as donors or recipients during mitochondrial transfer under physiological conditions (8–12). However, harmful stimuli (such as ischemia-reperfusion, oxidative stress, and toxic chemicals) can change the direction and efficiency of intercellular mitochondrial transfer. Studies have shown that cells can eliminate defective mitochondria by delivering them to recipient cells (such as macrophages) to maintain homeostasis. And the released mitochondria can also act as a distress signal to activate the rescue properties of recipient cells (12, 13). Meanwhile, damaged cells can take up exogenous functional mitochondria and integrate them into endogenous mitochondria networks, which improve their biological process and enhance their repairability (14, 15). In this review, we summarized the mechanism and function of mitochondrial transfer in the cardiovascular system. We also discussed the advantages and challenges of mitochondrial transfer strategies in the treatment of cardiovascular disorders. We hope this review will provide perspectives on mitochondrial-targeted therapeutics in cardiovascular diseases.

MECHANISMS OF INTERCELLULAR MITOCHONDRIAL TRANSFER

Intercellular transfer of mitochondria in the cardiovascular system is through several pathways, including tunneling nanotubes (TNTs), extracellular vesicles (EVs), naked mitochondria extrusion, and others.

Mitochondrial Transfer *via* Tunneling Nanotubes

TNTs, also called membrane nanotubes, are long tubular membrane structures (**Figure 1**). TNTs were discovered as unique structures for intercellular communication for the first time by Rustom and coworkers in 2004 (16). Recent studies have shown that cells in cardiovascular systems (such as cardiomyocytes, cardiac fibroblasts, endothelial cells, and vascular smooth muscle cells) can exchange mitochondria with their neighboring cells *via* TNTs (**Table 1**) (8–12, 15, 17–24). The intercellular transfer of mitochondria through TNTs could be unidirectional or bidirectional. The diameter of TNTs ranges from 50 to 1,000 nm (8, 17, 21, 22, 24). The length of TNTs, which differs in various types of cells, is usually 5–120 μm (8, 9, 17). Actin is the principal component of TNTs, and filamentous actin (F-actin) polymerization is necessary for the assembly of TNTs (15, 18, 23). Besides actin, another cytoskeleton component, microtubule, is also found in some TNTs (23). Both F-actin and microtubules could act as cytoskeletal tracks for the movement of mitochondria. TNTs containing both microtubules and F-actin are large in diameter (>0.7 μm) and responsible for the long-distance delivery of mitochondria. TNTs containing only actin are small in diameter (<0.7 μm) and in charge of the short-distance transport of mitochondria (19, 21, 25–28).

There are two different mechanisms involved in the formation of TNTs. **(1) Cell dislodgment mechanism**. Cells contact each other, then quickly migrate in opposite directions, retaining a thread of membrane between these two detached cells which finally develop into TNTs (9, 18). **(2) Actin-driven protrusion mechanism**. Filopodia-like membrane protrusions extend beyond the cell and elongate in an F-actin polymerization-dependent manner. Then the elongated protrusions connect with the target cells or other protrusions to form the TNTs (9, 12, 29). Unlike other cellular protrusions, these filopodia-like protrusions do not anchor to the substratum but suspend in the culture medium, which makes it possible for long-distance communication between cells (30).

M-Sec, also known as tumor necrosis factor α-inducible protein 2 (TNFαIP2), is reported as a key trigger of TNTs formation. Studies have shown that interaction of M-Sec with RalA can induce the assemble of exocyst complex and then initiate F-actin polymerization, while Cdc42 may be required for the extension process of TNTs (31). The expression of M-sec expression is regulated by many stimuli. Oxidative stress can activate p53, which in turn upregulates M-Sec expression by enhancing epidermal growth factor receptor expression or activating Akt/PI3K/mTOR pathway (32). Treatment of mesenchymal stem cells (MSCs) with TNF-α can increase M-Sec expression and trigger TNTs formation with cardiomyocytes *via* the NF-κB signaling pathway (15).

Some studies have demonstrated that gap junction protein connexin 43 (CX43) is necessary for TNTs formation and TNT-mediated intercellular mitochondrial transfer in non-cardiovascular systems (33–35). However, new evidence has shown that there is no Cx43 exists in the TNTs between cardiomyocytes and cardiac fibroblasts (9). Wang and coworkers have found that Cx43 only anchors at one end of TNT between two human umbilical vein endothelial cells (36). Since gap junctions do not allow the passage of large molecules (>1.2 kDa), Cx43 in the TNTs might only mediate intercellular electrical coupling but not cell-to-cell mitochondrial delivery (36). The role of Cx43 in the formation of TNTs and TNT-mediated mitochondrial transfer in the cardiovascular system still needs to be further explored.

Recently, mitochondrial Rho GTPase 1 (Miro1) has been reported to play a critical role in mediating mitochondrial movement along the TNTs (14, 15). Miro1 is a tail-anchored

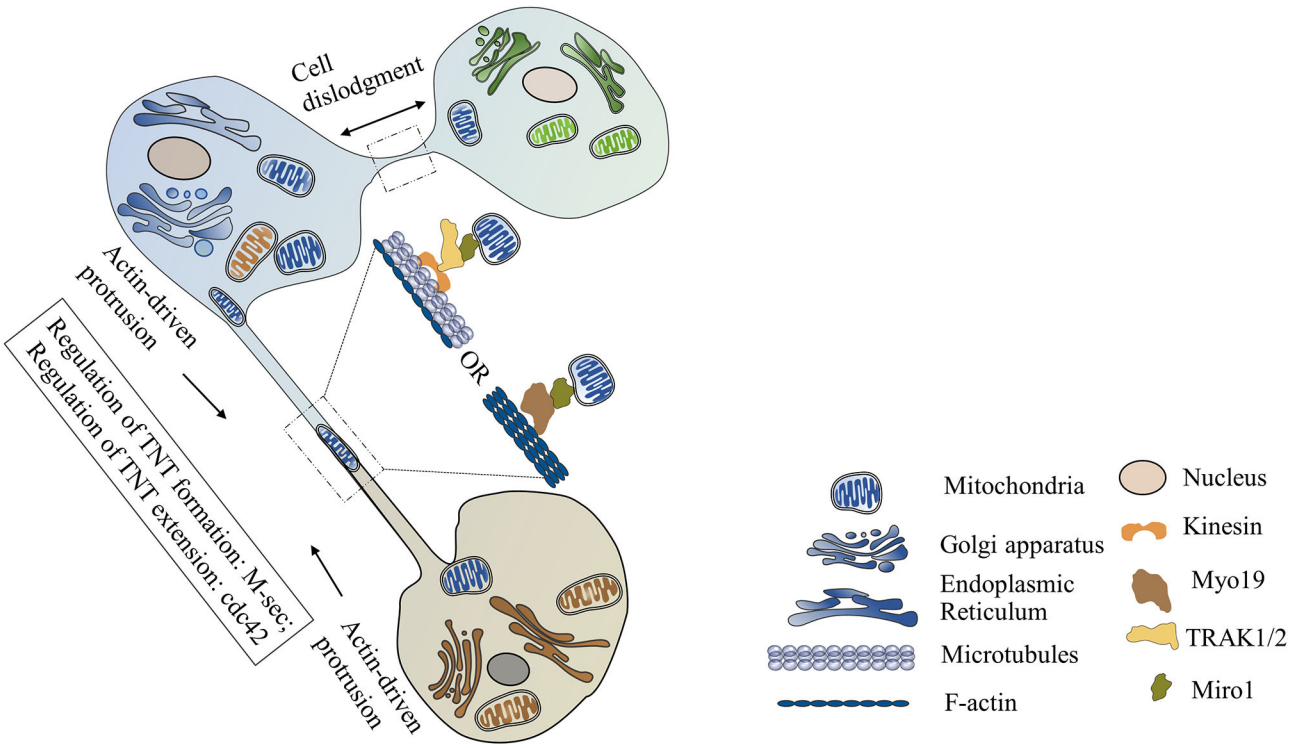

FIGURE 1 | Mitochondrial transfer *via* tunneling nanotubes (TNTs). TNTs are formed *via* cell dislodgment mechanism or actin-driven protrusion mechanism. TNTs containing only actin are small in diameter. TNTs containing both F-actin and microtubules are large in diameter. M-Sec is necessary for the formation of TNTs, while Cdc42 is required for the extension of TNTs. Mitochondrial Rho GTPase 1 (Miro1), a tail-anchored mitochondrial outer membrane protein, plays a critical role in mediating mitochondrial movement along the TNTs. After combing with the adaptor protein TRAK1/2, Miro1 can recruit motor protein kinesin and initiate microtubule-based mitochondrial movement. Miro1 can also mediate actin-based mitochondrial transport *via* binding with motor protein Myo19.

mitochondrial outer membrane protein. After combing with the adaptor protein TRAK1/2, Miro1 can recruit motor proteins (such as kinesin) and initiate microtubule-based mitochondrial movement (37). In a cardiomyocytes and cardiac myofibroblasts co-culture system, mitochondrial transport along microtubules in TNTs is mediated by KIF5B, which is a membrane of the kinesin superfamily (23). Recent studies have shown that Miro1 can also mediate actin-based mitochondrial transport *via* binding with motor protein Myo19 within individual mouse fibroblasts (38). However, whether Miro1 and Myo19 are involved in the mitochondrial movement along F-actin in TNTs still needs to be further investigated.

Mitochondrial Transfer *via* Extracellular Vesicles

Another pathway for cell-to-cell mitochondrial transfer is through EVs (**Figure 2**). The properties of EVs that transfer intact mitochondria or mitochondrial components in the cardiovascular system are listed in **Table 2**.

EVs are phospholipid membrane-bound microparticles released by cells. Exosomes and microvesicles are two major forms of EVs. Exosomes are small EVs (30–150 nm in diameter) that originated from the endosomal networks and are considered to deliver lipids, RNAs, and mitochondrial components (such as mtDNA). Microvesicles derived from cellular plasma membranes are larger than exosomes (100–1,000 nm in diameter) (43). Since mitochondria are elongated organelles with a diameter of 500–1,000 nm, the intact mitochondria more likely exist in the microvesicles but not in the exosomes (44). Many harmful stimuli, such as lipopolysaccharide, can induce endothelial cells to release EVs. Then the EVs are taken up by the recipient cells and cause inflammatory responses. The inflammatory responses might be due to the pro-inflammatory effect of mtDNA in the EVs (39, 41). On the contrary, hypoxia-injured cardiomyocytes can uptake the EVs containing respiratory-competent mitochondria to increase their rescue ability (40).

Recent studies have suggested that selective packaging of mitochondrial content into EVs depends on optic atrophy 1 (OPA1) and sorting nexin 9 (Snx9) proteins (45), but the exact mechanism is unclear. The formation of exosomes is initiated *via* membrane invagination to generate multivesicular late endosomes. Then the multivesicular late endosomes fuse with the plasma membrane, leading to the release of exosomes into the extracellular space. The biogenesis and release process of microvesicles is different from exosomes. Microvesicles are generated *via* membrane blebbing and then released into the extracellular environment by separating from the plasma

TABLE 1 | Properties of mitochondrial transfer-related TNTs in cardiovascular system.

Donor cells	Recipient cells	Cytoskeleton compounds	Diameter	Length	Stimulus	References
Bidirectional mitochondrial transfer						
MSCs	Cardiomyocytes or cardiac myoblasts	F-actin	200–500 nm	–	Physiological condition, hypoxia, doxorubicin, tumor necrosis factor-α	(15, 17)
MSCs	Vascular smooth muscle cells	F-actin	–	–	Physiological condition	(10)
MSCs	HUVECs	F-actin, or both F-actin and microtubules	–	–	Bidirectional (physiological condition), unidirectional (hypoxia, cytarabine)	(12, 18)
Cardiomyocytes	Cardiac fibroblasts	F-actin and microtubules	–	13.9 ± 10.4 μm	Physiological condition	(9)
Microvascular endothelial cells	Microvascular endothelial cells	F-actin or microtubules or both	180–400 nm	10–100 μm	Physiological condition	(19)
Unidirectional mitochondrial transfer						
Cardiomyocytes	MSCs	F-actin, or both F-actin and microtubules	760 ± 30 nm; or ∼100 nm	31.66 ± 1.43 μm	Physiological condition; hypoxia	(11, 20–22)
Cardiomyocytes	Cardiac myofibroblasts	F-actin and microtubules	–		Hypoxia	(23)
Cardiomyocytes	Endothelial progenitor cells	–	50–800 nm	5–120 μm	Physiological condition	(8)
Stem cell	Neonatal cardiomyocytes	F-actin and microtubules	500–1,000 nm	80–100 μm	Physiological condition, lipopolysaccharide	(24)

TNTs, tunneling nanotubes; HUVECs, umbilical vein endothelial cells; MSCs, mesenchymal stem cells.

membrane in Ca^{2+}-dependent enzymatic machinery (46). Integrins on the surface of EVs have been widely reported as major regulators of anchoring EVs on recipient cells (47, 48). Once attaching the recipient cells, EVs can directly fuse with the recipient cell membrane or be engulfed by recipient cells through multiple pathways, including clathrin-dependent endocytosis, caveolin-mediated endocytosis, lipid raft-mediated endocytosis, phagocytosis, and micropinocytosis (49–51).

In 2020, a new type of mitochondria-containing EVs called exophers was discovered in hearts by Nicolas et al. (42). The structure of exophers from cardiac tissues is similar to that of neural exophers of *C. elegans*, which mainly contain misfolded proteins and damaged mitochondria (52). Different from the traditional EVs, cardiac exophers are large membrane-surrounded microparticles with an average diameter of 3.5 μm, which allows intact mitochondria to be packed in (42). The formation of cardiac exophers is motivated by the cardiac-specific autophagy mechanism. A large number of exophers extruded by cardiomyocytes can be engulfed by cardiac-resident macrophages *via* Mertk-mediated endocytosis. Such kind of crosstalk between cardiomyocytes and immune cells is required for the maintenance of mitochondrial fitness and cardiovascular health (42).

Mitochondrial Transfer *via* Naked Mitochondria Extrusion

Many studies have shown that the intact respiratory competent mitochondria exist in healthy human and animal blood which might be released by resting or activated platelets (53, 54). Likewise, mitochondria can also be released into the environment in the form of naked organelles by many normal or abnormal cells beyond platelets (54). For example, extracellular mitochondria are found in the endothelial progenitor cells culture system under physiological conditions (55). Monocytic cells can extrude naked mitochondria after being attacked by lipopolysaccharide (41). It has been proven that intact cell-free mitochondria are released from platelets through an actin-dependent but microtubule-independent mechanism (56).

However, the uptake mechanism of cell-free mitochondria by recipient cells has not been fully clarified. A few previous reports have shown that MSCs engulf platelet-derived functional mitochondria through clathrin-mediated endocytosis and enhance their pro-angiogenic activity (49). Some evidence has demonstrated that autologous mitochondria can be internalized into cardiomyocytes through actin-dependent endocytosis. Neither caveola-mediated nor clathrin-mediated endocytosis is involved in the mitochondrial internalization into cardiomyocytes (57). It has been reported that H9C2 rat cardiomyocytes can recognize and engulf exogenous mitochondria released from human uterine endometrial gland-derived MSCs in a co-incubation system. The uptake of mitochondria by cardiomyocytes is mainly *via* micropinocytosis (58). During the mitochondrial internalization process, cells can discriminate intact mitochondria from other similar microparticles and only engulf mitochondria (59). So the internalization mechanism of naked mitochondria might be different according to the types of recipient cells and the origin of naked mitochondria.

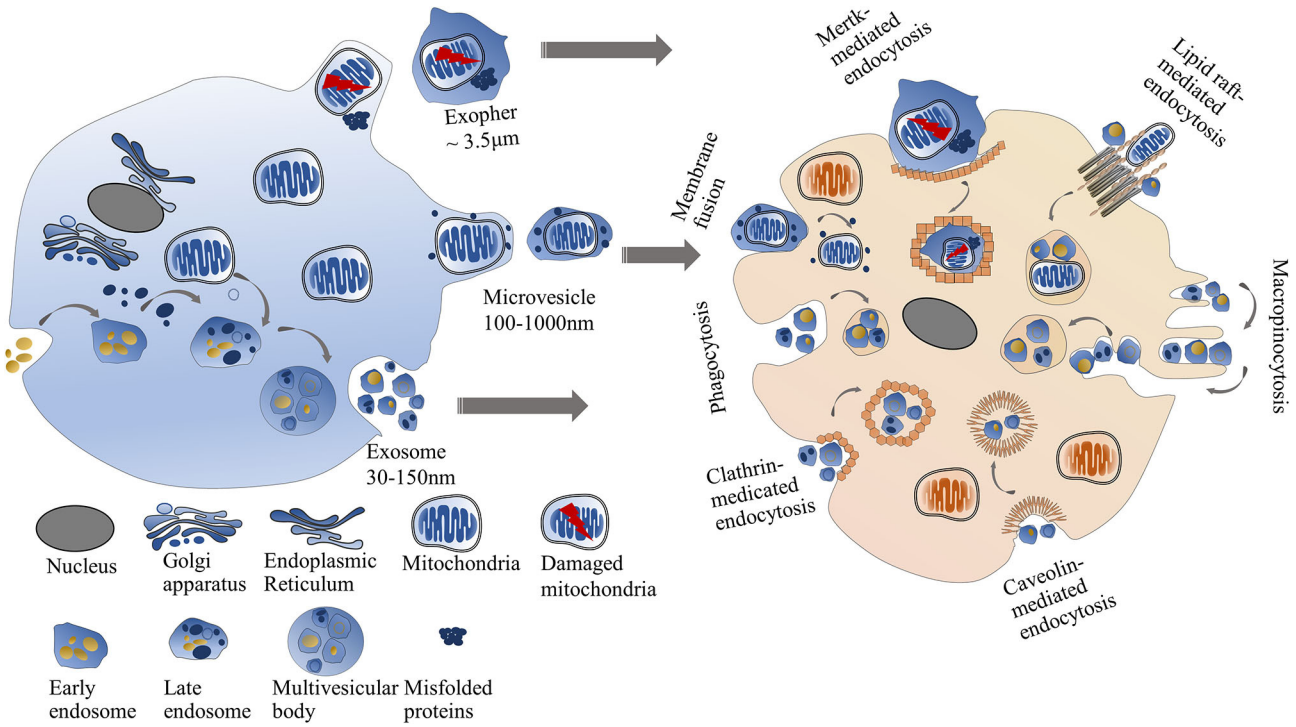

FIGURE 2 | Mitochondrial transfer *via* EVs. The intercellular mitochondrial transfer can be mediated through EVs including exosomes, microvesicles, and exophers. Exosomes are smaller than microvesicles. Exophers are large membrane-surrounded microparticles usually containing damaged mitochondria and misfolded proteins. Exosomes or microvesicles can directly fuse with the recipient cell membrane or be engulfed by recipient cells through multiple pathways, including clathrin-dependent endocytosis, caveolin-mediated endocytosis, lipid raft-mediated endocytosis, phagocytosis, and micropinocytosis. Cardiac exophers can internalized into recipient cells *via* Mertk-mediated endocytosis.

TABLE 2 | Characteristics of mitochondrial transfer-related EVs in cardiovascular system.

EVs	Donor cells	Recipient cells	Size	Compounds	Effect on recipient cells	References
Exosomes	KSHV-infected HUVECs	Uninfected HUVECs	30–40 nm	mtDNA	Antiviral effect	(39)
Microvesicles	Healthy iCMs	Hypoxia-injured iCMs	98–677 nm	intact mitochondria	Improvement of intracellular energetics	(40)
Microvesicles	Lipopolysaccharide stimulated THP-1 monocytic cells	HUVECs	206.6 ± 89.8 nm	Intact mitochondria, and some mitochondrial components	Activation of inflammatory response	(41)
Exophers	Cardiomyocytes	Cardiac-resident macrophages	3.5 ± 0.1μm	Mitochondria	Preservation of metabolic stability	(42)

EVs, extracellular vesicles; KSHV, Kaposi's sarcoma-associated herpesvirus; HUVECs, human umbilical vein endothelial cells; mtDNA, mitochondrial DNA; iCMs, induced pluripotent stem cell–derived cardiomyocytes.

Mitochondrial Transfer *via* Other Pathways

Other pathways, such as cell fusion, are also found to be involved in intercellular mitochondrial transfer. In 2003, bone marrow-derived MSCs was reported to donate their mitochondria to cardiomyocytes through cell fusion. The cell fusion between MSCs and skeletal muscles is at a very low rate, suggesting that cell fusion is a kind of cell-specific machinery for cell-to-cell mitochondrial transfer (60).

FATE OF DONOR MITOCHONDRIA IN RECIPIENT CELLS

Studies have shown that most healthy donor mitochondria can successfully escape from the endo-lysosomal system after being transferred into damaged cardiomyocytes and quickly integrate into the host mitochondrial network (61, 62). The combination of donor and recipient mitochondria within cardiomyocytes is a transient event that lasts about 4 h (62).

The mechanism of mitochondrial integration might involve dynamic movements of mitochondrial fusion and fission. Many studies have demonstrated that mitofusin 1 (Mfn1) and Mfn2 are necessary for the fusion of mitochondrial outer membrane, optic atrophy 1 (Opa1) is responsible for the fusion of mitochondrial inner membrane (63), and dynamin-related protein 1 (Drp1) is required for mitochondrial fission (64, 65). In non-cardiomyocytes, mitochondrial transplantation can enhance the expression of Mfn2 and Opa1 and decrease the level of Drp1, which results in mitochondrial fusion (66). In the co-culture system of iPS-derived cardiomyocytes and cardiac fibroblasts, the mitochondrial fusion of donor and recipient mitochondria might be more likely due to the high Mfn1 and Opa1 protein levels in mitochondria (62). A minority of donor mitochondria that cannot flee from lysosomes undergo degradation through autophagy (62). This phenomenon has been confirmed by Louwagie and coworkers, whose studies have shown that the number of lysosomes in the recipient cells elevates after 4 h of mitochondrial transfer, accompanied by a higher mitophagy of donor mitochondria and a lower mitophagy of host mitochondria (61).

On the contrary, the main function of transferring defective mitochondria from damaged cells to healthy cells is to ask for help. After that, these foreign mitochondria in recipient cells will eventually be trapped in the LC3B-labeled phagosomes and eliminated *via* mitophagy, which ensures the normal functions of recipient mitochondria (14).

Besides mitochondrial fusion, a structure called mitochondrial nanotunnels also allows the exchange of matrix between two individual mitochondria. The mitochondrial nanotunnels in cardiomyocytes are a thin double-membrane tunneling structure with 40–200 nm in diameter and 0.7–14 μm in length (67, 68). Mitochondrial components like mitochondrial DNA, proteins, lipids can freely diffuse through the mitochondrial nanotunnels. Although the rate of mitochondrial matrix exchange *via* mitochondrial nanotunnels is slower than that of mitochondrial fusion mode, it provides the possibility for long-range communication between two individual mitochondria (67, 68). Whether the mitochondrial nanotunnels participate in the communication of donor and recipient mitochondria still needs to be further explored.

ROLE OF MITOCHONDRIAL TRANSFER

Role of Mitochondrial Transfer Under Physiological Conditions

The cell-to-cell mitochondrial transfer has been detected in the cardiovascular system under physiological conditions (**Table 3**). In 2005, the unidirectional mitochondrial transfer from neonatal cardiomyocytes to endothelial progenitor cells was observed for the first time by Koyanagi et al. (8). After receiving donor mitochondria, endothelial progenitor cells acquire a cardiomyocyte-like phenotype through reprogramming (8). Meanwhile, a bidirectional mitochondrial transfer has been detected between cardiac myocytes and MSCs in a co-culture system (22). Migration of mitochondria from MSCs into fully differentiated cardiomyocytes can reprogram the adult cardiomyocytes and regress them to a progenitor-like state (20). Likewise, the mitochondrial transfer from embryonic cardiomyocytes to MSCs initiates stem cells differentiation toward cardiac cells, which might be an essential mechanism of stem cell-based therapies for cardiovascular disorders (22). Studies have also shown that mitochondrial transfer between vascular smooth muscle cells and MSCs is required to promote stem cells proliferation (10). These results suggest that intercellular mitochondrial transfer might play an important role in the regulation of cardiovascular system development.

Although cardiomyocytes account for about 70–85% of the adult myocardial tissue volume (72), non-myocytes in cardiac tissues are essential for heart health. Cardiomyocytes and cardiac fibroblasts are the two most abundant cell types in mammalian hearts. Recent studies have demonstrated that mitochondrial exchange between cardiomyocytes and fibroblasts is a distinct intercellular communication pattern, which might be indispensable for normal cardiac function (9). But the exact molecular mechanism remains unclear. In 2020, Nicolas-Avila and colleagues found that cardiomyocytes can eliminate their abnormal mitochondria by delivering them to heart-resident macrophages under physiological conditions. Harmful stimuli, such as ischemia or isoproterenol challenge, can enhance the efficiency of mitochondrial transfer and accelerate the clearance of dysfunctional mitochondria (42). The mitochondrial transfer from cardiomyocytes to macrophages is beneficial to maintain the mitochondrial fitness of cardiomyocytes, reduce the accumulation of pro-inflammatory material, and prevent the activation of inflammasome (42). Studies have also demonstrated a low mitochondrial transfer between heart-resident macrophages and other non-myocytes (such as endothelial cells), suggesting intercellular mitochondrial transfer within the heart has a highly cell-specific feature. These studies demonstrated that cell-to-cell mitochondrial transfer might be essential for maintaining normal cardiac homeostasis.

Role of Mitochondrial Transfer Under Pathophysiological Conditions

Under pathophysiology conditions such as ischemic cardiomyopathy, damaged cells can not only release dysfunctional mitochondria to ask for help but also take up exogenous functional mitochondria to rescue their own mitochondria network (**Table 3**). The transfer of healthy mitochondria toward injured cells has multiple protective mechanisms include the following. **(1) Improvement of mitochondrial biogenesis**. The perturbation of mitochondrial biogenesis is known as the fundamental mechanism of cardiovascular diseases (6). Transfer of healthy mitochondria to the injured cardiomyocytes or endothelial cells can increase cellular ATP levels through elevating oxidative phosphorylation and tricarboxylic acid (TCA) cycle and reducing glycolysis (12, 15, 57, 61, 69). The improvement of mitochondrial biogenesis is due to the renewal of damaged mitochondrial DNA and increased expression of mitochondrial respiration-related protein through activation of peroxisome proliferator-activated

TABLE 3 | Role of mitochondrial transfer under physiological and pathophysiological conditions.

Role of mitochondrial transfer	Mechanism	References
Physiological condition		
(1) Regulation of cardiovascular system development	• Reprograming the adult cardiomyocytes and endothelial progenitor cells	(8, 22)
	• Promoting stem cells proliferation and differentiation toward cardiac cells	(10, 22)
(2) Maintaining normal cardiac homeostasis	• Clearance of dysfunctional mitochondria of cardiomyocytes by macrophages	(42)
Pathophysiological condition		
(1) Release of dysfunctional mitochondria to ask for help	• Mitochondria from damaged cardiomyocytes or endothelial cells acted as a danger signaling for stem cells	(14)
(2) Rescuing damaged cells by taking up functional mitochondria	• Improvement of mitochondrial biogenesis (elevating oxidative phosphorylation, reducing glycolysis, and increasing cellular ATP levels)	(12, 15, 40, 57, 61, 69–71)
	• Enhancement of antioxidant capacity (overexpression of heme oxygenase-1)	(14, 15, 70)
	• Reduction of apoptosis (decrease of Bax/Bcl-2 ratio and the inhibition of caspase-3 activity)	(11, 61)

receptor-gamma coactivator 1-alpha (PGC-1α)-mediated pathway (40, 57, 70, 71). It has been reported that this beneficial effect of the mitochondrial transfer can last for a long time (at least 28 days) in ischemic cardiomyocytes (73), which is in contrast to the short-term improvement of energy metabolism found in normal cardiomyocytes (74). **(2) Enhancement of antioxidant capacity.** Mitochondria are vital organelles that regulate redox balance *via* their pro-oxidant and antioxidant functions. Oxidative stress-induced injury is involved in the pathogenesis of many cardiovascular diseases, including atherosclerosis, myocardial ischemia-reperfusion injury, and hypertension (75–77). Inflammatory response, triggered by excessive ROS level, is also associated with vascular dysfunction in many pathophysiology conditions (78, 79). Recent studies have shown that the delivery of healthy mitochondria to cardiac cells or endothelial cells can protect them against oxidative damage (14, 70). Transplantation of MSCs to a doxorubicin-induced animal cardiomyopathy model also alleviates cardiac inflammation *via* mitochondrial transfer (15). The protective mechanism might be due to the overexpression of heme oxygenase-1, which has well-known properties of anti-oxidative and anti-inflammatory activities (14). **(3) Reduction of apoptosis.** Apoptosis is one of the most common patterns of programmed cell death in the cardiovascular system (80). Cardiomyocytes and endothelial cells are prone to apoptosis under various cellular stress (such as hypoxia, chemicals, and metabolic stress). Many studies have shown that transfer of healthy mitochondria to these injury cells can reduce apoptosis (11, 15, 18, 23, 69). The anti-apoptotic effect of mitochondrial transfer has been shown to have a gender-specific characteristic in pregestational diabetes mellitus-exposed offspring (61). The mechanism of mitochondrial transfer-induced anti-apoptosis might involve the decrease of Bax/Bcl-2 ratio and the inhibition of caspase-3 activity (11, 61).

In short, a series of studies implied the significance of mitochondrial transfer in the cardiovascular system. In physiological conditions, cardiac fibroblasts and cardiomyocytes show frequent intercellular communication through bidirectional mitochondrial transfer, which is critical in maintaining normal cardiac function (9). Although this phenomenon is observed in an *in vitro* model, whether it exists i*n vivo* has not been confirmed. Meanwhile, transferring distressed mitochondria to macrophages is also critical to the fitness of cardiomyocytes (42). It is undoubted that mitochondria containing the information of donor cells once internalized into recipient cells can trigger a cascade of response, which in turn acts on donor cells. For instance, cardiomyocytes and endothelium suffered ischemia/reperfusion injury deliver mitochondria as signals to MSCs to ask for help. After receiving mitochondria, MSCs enhance the biogenesis of mitochondria and promote the capacity of anti-apoptosis, then generously donate functional mitochondria to distressed cells (14).

THERAPEUTIC STRATEGIES OF MITOCHONDRIAL TRANSFER FOR CARDIOVASCULAR DISEASES

Since transferring healthy mitochondria to damaged cells can alleviate injury and enhance the repairability of the target cells. Mitochondrial transplantation has been suggested as a promising therapeutic strategy for cardiovascular diseases. The most common methods of mitochondrial transplantation used for the treatment of cardiovascular diseases are cell-mediated therapy and cell-free therapy (including naked mitochondria transplantation and EV-based transplantation) (**Figure 3** and **Table 4**).

Cell-Based Mitochondrial Transplantation

MSCs and progenitor cells have been recognized as the preferred mitochondria donors for the treatment of cardiovascular diseases due to their abundant sources and high mitochondrial respiratory activity. Animal experiments and clinical trials have shown that transplantation of MSCs can successfully repair injured myocardium in ischemic cardiomyopathy (81–84). The

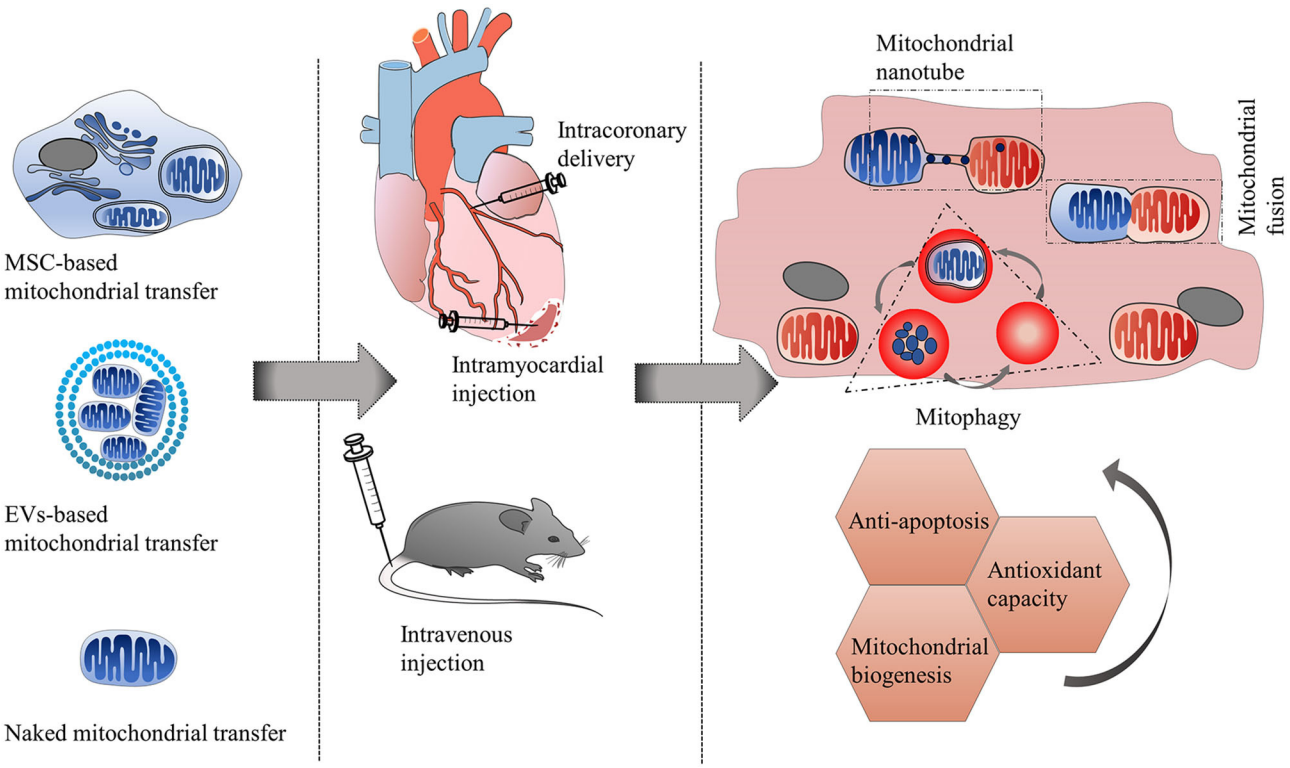

FIGURE 3 | Therapeutic strategies of mitochondrial transfer for cardiovascular diseases. The most common methods of mitochondrial transplantation used for the treatment of cardiovascular diseases (such as ischemic cardiomyopathy, anthracycline-induced cardiomyopathy) are cell-mediated therapy and cell-free therapy (including naked mitochondria transplantation and EV-based transplantation). Routes of administration can be intramyocardial injection, intracoronary delivery, and intravenous injection. After approaching the recipient cells, exogenous mitochondria can integrate with recipient mitochondria through mitochondrial fusion and fission machinery, or be trapped by lysosomes and be autophagy degraded. Some donor mitochondria might only communicate with recipient mitochondria *via* mitochondrial nanotunnels, without undergoing mitochondrial fusion. The transfer of healthy mitochondria toward injured cells has multiple protective mechanisms including improvement of mitochondrial biogenesis, enhancement of antioxidant capacity and reduction of apoptosis.

protective mechanism of MSCs therapy has been proven mainly *via* mitochondrial transfer in *vitro* or in *vivo* studies. For example, MSCs can prevent vascular endothelial cells injury in an ischemia-reperfusion model by enhancing aerobic respiration and reducing apoptosis through transferring mitochondria to endothelial cells (12). Mitochondria transferring from MSCs can protect cardiomyocytes against oxidative stress-induced injury by improving mitochondrial respiration function (11, 14, 15, 17, 70). MSCs transplantation has also been reported to reduce myocardial fibrosis, alleviate left ventricular dilatation, and improve cardiac function in an animal model of anthracycline-induced cardiomyopathy through mitochondrial transfer (15).

MSCs used in clinical trials can be originated from widely various tissues. Paliwal and coworkers have reported that the MSCs derived from pulp and Wharton's jelly have lower mitochondrial transfer abilities but higher mitochondrial respiration capacities than those of MSCs from bone marrow and adipose (70). Compared with bone marrow-derived MSCs, human-induced pluripotent stem cell-derived MSCs have higher efficiency of mitochondrial transfer due to their higher expression of Miro1 and TNFαIP2 (15). So the difference in mitochondrial transfer capacity and effectiveness of these tissue-specific MSCs need to be considered in cell-based therapy for cardiovascular diseases.

Whether the beneficial effect of MSCs transplantation is mainly due to mitochondrial transfer remains controversial. A few previous studies have reported that MSCs can rescue damaged cells through paracrine mechanisms (96). However, many in *vitro* studies have proven that the cardiovascular protective effect of stem cell-based therapy is mainly dependent on the transfer of functional mitochondria rather than the secretion of paracrine factors (12, 15). Since MSCs have limited trans-differentiation abilities into cardiomyocytes or other vascular components *in vivo*, it seems that the protective effect of MSCs transplantation is also unlikely due to their differentiation capacity (97). However, recent studies have shown that the emergence of many safety issues such as undesired differentiation, pro-arrhythmia, and microcirculation occlusion limit the clinical use of stem cell-based therapy (98–100).

Naked Mitochondria Transplantation

Naked mitochondrial transplantation refers to the transplantation of isolated and uncoated mitochondria to

TABLE 4 | Summary of mitochondrial transfer strategies for cardiovascular diseases.

	Cell-based mitochondrial transplantation	EV-based mitochondrial transplantation	Naked mitochondrial transplantation
Origins	MSCs and progenitor cells	MSCs-derived EVs	Mitochondria isolated from healthy cardiac or skeletal muscle
Application	Ischemia-reperfusion injury, and anthracycline-induced cardiomyopathy	Ischemia-reperfusion injury	Right heart failure, ischemia-reperfusion injury, and ischemia/reperfusion injury of diabetic heart
Route of administration	Intramyocardial injection	Intracoronary or intravenous injection	Intramyocardial, intracoronary, or intravenous injection
Major outcome	Improving cardiac function Alleviating left ventricular dilatation Reducing myocardial fibrosis	Improving myocardial contractility Preventing left ventricular remodeling	Decreasing infarct size Improving ventricular function Enhancing coronary blood flow Delaying the progression of right heart failure
Advantages	Abundant sources Good quality and integrity of mitochondria	High stability of mitochondria No risk of microvascular obstruction No risk of cardiac arrhythmia	No risk of autoimmune response No risk of microvascular obstruction No risk of cardiac arrhythmia Without intramyocardial hematoma
Disadvantages	Undesired differentiation Cardiac arrhythmia Microcirculation occlusion Difference in mitochondrial transfer capacity and effectiveness due to origins of MSCs	Heterogeneity of EVs' cargo content due to different cellular origins and isolation methods	Lower stability than EV-coated mitochondia Low yields of good-quality mitochondria Limited viability of transferred mitochondria For intramyocardial injection: (1) multiple injections are required; (2) The need for thoracotomy prior to the intramyocardial injection; (3) lower mitochondrial internalization (3∼7%) than that of intracoronary injection; (4) clusters found in intramyocardial injection site For intravenous injection: lack of tissue-specific delivery
Reference	(15, 81–84)	(40)	(62, 71, 73, 85–95)

EV, extracellular vesicle; MSCs, mesenchymal stem cells.

the injured tissues through circulation delivery or local injection (85, 86). The transplantation of naked mitochondria for the treatment of cardiovascular diseases can be traced back to 2009 when McCully's laboratory at Harvard demonstrated for the first time that intramyocardial injection of respiration-competent mitochondria could reduce infarct size and promote postischemic functional recovery in an animal model of heart ischemia-reperfusion injury (85). The optimal dose of mitochondria needed for efficiently protecting against ischemia-reperfusion injury ranges from 2×10^5 to 2×10^8 per gram wet weight (62, 71, 73, 87). Autologous mitochondria isolated from healthy cardiac or skeletal muscle are the dominant sources of donor mitochondria (85, 87, 101). The uptake of autologous mitochondria by cardiomyocytes is usually within minutes *via* internalization (62, 73). Exogenous mitochondria can also enter into cardiomyocytes without being cleared by lysosomes or autophagosomes. However, it takes more than 8 h for cardiomyocytes to engulf the xenogeneic mitochondria (73). In 2017, the first clinical use of mitochondrial transplantation was performed in five pediatric patients who suffered from cardiac ischemia-reperfusion injury. Four in five patients who accepted intramyocardial injection of autologous mitochondria have shown an improvement in ventricular function without any short-term side effects (such as arrhythmia, mitochondrial autoimmune response, and intramyocardial hematoma) (101).

Although intramyocardial injection of mitochondria has been proven efficient and safe in the treatment of myocardial ischemic disease, there are still a few limitations. For example, only a small number of donor mitochondria is allowed to inject within the myocardium per shot, and the percentage of mitochondrial internalization at each injection site is also pretty low (about 3–7%) (71, 73, 87). So multiple injections are required to ensure the extensive distribution of donor mitochondria throughout the ischemic heart, which increases the difficulty of operation. In addition, the need for thoracotomy prior to the intramyocardial injection may also be a huge obstacle limiting the clinical application of mitochondrial transplantation for potential patients (101).

Since 2016, researchers have begun to test the feasibility of intracoronary delivery as an alternative mitochondrial transplantation method (88). Both autologous and exogenous mitochondria can rapidly spread throughout the whole heart within 10 min of coronary perfusion rather than occur in clusters as found in intramyocardial injection. Furthermore, intracoronary delivery also results in a higher mitochondrial internalization into cardiomyocytes (∼23%) than intramyocardial injection (88). In animal models of regional ischemia-reperfusion injury, both preischemic or postischemic intracoronary injection of autologous mitochondria can decrease infarct size, enhance coronary blood flow, and

increase cardiac function (88–91). Intracoronary injection of healthy mitochondria also has powerful cardiac protection against globally ischemic injury of donor hearts and global ischemia/reperfusion injury of diabetic heart (88, 92–94). No signs of microvascular obstruction and cardiac arrhythmia are observed after intracoronary injection of mitochondria (91). The safety and efficacy of intracoronary delivery of mitochondria make it a promising treatment for myocardial infarction through percutaneous coronary intervention.

Considering the clinical use of mitochondrial transplantation, intravenous injection of mitochondria might be more feasible than intramyocardial and intracoronary administration. Intravenous delivery of mitochondria has been used as a promising therapeutic method for fatty liver and Parkinson's disease (102, 103). Recent studies have shown that intravenous injection of viable exogenous mitochondria for 3 weeks can improve right ventricular function in an animal model of pulmonary hypertension (86). After systemic administration, the mitochondria are observed in various tissues, including heart (102, 103). The stability of naked mitochondria in the bloodstream and tissue-specific delivery may be the key factors for successful therapy in ischemic or non-ischemic cardiovascular disorders.

Besides ischemic heart injury, recent studies have also found that mitochondrial transplantation can delay the progression of right heart failure (86, 95) and improve myocardium metabolism of offspring born to diabetic mothers (61). Although studies have confirmed the efficiency of naked mitochondrial transplantation, how to obtain high yields of good-quality mitochondria is still a challenge. Enhancing the efficiency of mitochondrial internalization into target cells and maintaining the viability of transferred mitochondria are also crucial problems to assure the efficient clinical application of naked mitochondria transplantation.

EV-Based Mitochondrial Transplantation

Another method of cell-free therapy is mitochondria-rich EVs transplantation. EVs have been recognized as a powerful platform for mitochondrial delivery (40, 104, 105). MSCs from different tissues are the main sources of EVs (106). Although many studies have proven that MSCs-derived EVs can serve as a potential therapy for the treatment of cardiovascular disease, whether the protective effect is mainly dependent on their mitochondria cargo is unclear (107). In 2021, Ikeda's laboratory at Stanford isolated some mitochondria-rich EVs from human-induced pluripotent stem cell-derived cardiomyocytes. The diameter of these EVs ranges from 98 to 677 nm (40). The outer lipid bilayer of EVs usually serves as a security guard that keeps the mitochondria maintaining their morphological and functional integrity. The mitochondria encapsulated within EVs are found more stable than naked mitochondria under extracellular environmental stress, such as calcium overload and oxidative stress (40). In *vitro* and in *vivo* studies have demonstrated that transplantation of mitochondria-rich EVs can restore intracellular bioenergetics, prevent post-ischemic left ventricular remodeling, and improve myocardial contractility (40). Since the diameters of MSC-derived EVs are usually $<10\,\mu m$ (108), intravenous or intracoronary injection of EVs has no risk of microvascular obstruction. The intramyocardial injection of mitochondria-rich EVs into the peri-infarct region does not induce cardiac arrhythmia (40), which supports the opinion of Adamiak and coworkers that MSC-derived EVs are safer than MSCs (109). The cargo content of EVs mainly includes mitochondria and their components, nucleic acids, lipids, and proteins, which can be altered according to their cellular origins and isolation methods (107). The complex composition of different EVs makes them have distinctive mechanisms and effects on various diseases. Ikeda and coworkers have found that the beneficial effect of mitochondria-rich EVs transplantation on myocardial ischemia-reperfusion injury was not only due to mitochondria cargo but also due to non-mitochondrial cargo (40). In order to reduce the heterogeneity of EVs and guarantee the therapeutic effect, it is necessary to set up a standardized EV isolation protocol. Meanwhile, how to improve the targeting specificity of EVs is also an issue needed to be further investigated (110).

In conclusion, many in *vivo* studies have proven the effectiveness of mitochondrial transplantation in the treatment of different cardiovascular diseases. Ischemia/reperfusion injury is one of the most common diseases in the cardiovascular system. Researchers delivered mitochondria to rescue damaged cardiac tissue through different administrational routes in various species (14, 40, 69, 73). Comfortingly, all of these studies have confirmed the significant improvement of cardiac function after mitochondrial transplantation. In a clinical trial, autologous mitochondria from skeletal muscle were injected into the damaged cardiomyocytes of pediatric patients suffering ischemia/reperfusion injury, which effectively promote the recovery of postischemic myocardium without adverse short-term complications (101). Functional mitochondrial delivery has been used for some other cardiovascular diseases (including heart failure, anthracycline-induced cardiomyopathy, pregestational diabetes-induced cardiac malfunction, heart transplantation) and to some extent improve the prognosis (15, 61, 70, 94).

ETHICAL ISSUES

In 2015, the United Kingdom became the first country in the world to legislate and permit the clinical use of mitochondrial donation technology (111). However, there are still controversies about the ethical issues of the mitochondrial transfer strategy. **(1) Mitochondrial-nuclear incompatibility.** Studies have shown that the efficiency of cellular energy metabolism depends on about 2000 mitochondrial proteins. Most of these proteins are encoded by the nuclear genome, and only 13 proteins are encoded by the mitochondrial genome (112). So the compatibility of donor mitochondria and recipient cell nuclei is critical for the normal mitochondrial respiratory function of recipient cells (113–115). Many researchers have suggested

that mitochondria originated only from the same cells or species are the ideal donors for reducing mitochondria-nuclear incompatibility and ensuring successful mitochondrial transfer (116, 117). **(2) Transmission of detrimental mutation.** The mutation rate of mtDNA is significantly higher than that of nuclear DNA due to a lack of histone protection and less efficient repairability (118). Meanwhile, studies have shown that mitochondrial fragmentation of donor mitochondria increases when using the standard mitochondrial isolation methods. And elevated mitochondrial fission is closely related to mtDNA abnormalities (119, 120). The mutated mtDNA of donor mitochondria can be transmitted to the recipient cells during intercellular mitochondrial transfer. When the accumulation of mutated mtDNA exceeds the threshold, cellular dysfunction, and abnormal morphology will occur (121). Such detrimental effects on recipient cells might be unpredictable due to intra- and inter-cellular mitochondrial heterogeneity (122). Therefore, the establishment of ethical guidelines is a prerequisite for ensuring the safe application of mitochondrial transfer strategies in the treatment of cardiovascular diseases.

DISCUSSION AND FUTURE PERSPECTIVES

Mitochondrial dysfunction plays a crucial role in the development and progression of cardiovascular disorders, which provides the possibility for mitochondrial transfer as an effective therapeutic strategy in the treatment of cardiovascular diseases. With the emergence of new technologies, trends in mitochondrial transplantation therapeutics are changing from cell-based to cell-free therapy. EVs-based mitochondrial delivery is considered more promising than naked mitochondria transplantation in the treatment of cardiovascular diseases, but it still has some limitations. Recently, some researchers developed a new delivery system by artificially encapsulating isolated mitochondria with some biocompatible polymers (such as dextran triphenylphosphonium complexes, transactivator of transcription dextran complexes) (69, 123). The polymer-coated delivery system, which almost exclusively contains mitochondria, is considered better than the EV-based delivery system. Meanwhile, the polymer-coated mitochondria have a higher transfer efficiency and a more powerful rescue capability than those of naked mitochondria, suggesting that they might become a more feasible and promising strategic alternative for mitochondrial transplantation in the future (69, 123). Although many preclinical experiments have proven the advantages of mitochondrial delivery in treating cardiovascular diseases, there are still a few technical challenges and ethical issues that need to be resolved (124). The efficiency and safety of mitochondrial transplantation in treating cardiovascular diseases still need to be further evaluated before conducting clinical trials.

AUTHOR CONTRIBUTIONS

JC wrote the manuscript and prepared the tables. JZ wrote the manuscript and made the figures. L-lW and Y-yC edited the manuscript. All authors contributed to the article and approved the submitted version.

FUNDING

This work was supported by the National Natural Science Foundation of China (Grant Numbers: 81871541 and 81471837).

REFERENCES

1. Zhang Y, Murugesan P, Huang K, Cai H. NADPH oxidases and oxidase crosstalk in cardiovascular diseases: novel therapeutic targets. *Nat Rev Cardiol.* (2020) 17:170–94. doi: 10.1038/s41569-019-0260-8
2. Sun HJ, Wu ZY, Nie XW, Bian JS. Role of endothelial dysfunction in cardiovascular diseases: the link between inflammation and hydrogen sulfide. *Front Pharmacol.* (2019) 10:1568. doi: 10.3389/fphar.2019.01568
3. Dey S, DeMazumder D, Sidor A, Foster DB, O'Rourke B. Mitochondrial ROS drive sudden cardiac death and chronic proteome remodeling in heart failure. *Circ Res.* (2018) 123:356–71. doi: 10.1161/CIRCRESAHA.118.312708
4. Zhou B, Tian R. Mitochondrial dysfunction in pathophysiology of heart failure. *J Clin Invest.* (2018) 128:3716–26. doi: 10.1172/JCI120849
5. Bonora M, Wieckowski MR, Sinclair DA, Kroemer G, Pinton P, Galluzzi L. Targeting mitochondria for cardiovascular disorders: therapeutic potential and obstacles. *Nat Rev Cardiol.* (2019) 16:33–55. doi: 10.1038/s41569-018-0074-0
6. Poznyak AV, Ivanova EA, Sobenin IA, Yet SF, Orekhov AN. The role of mitochondria in cardiovascular diseases. *Biology.* (2020) 9:137. doi: 10.3390/biology9060137
7. Spees JL, Olson SD, Whitney MJ, Prockop DJ. Mitochondrial transfer between cells can rescue aerobic respiration. *Proc Natl Acad Sci USA.* (2006) 103:1283–8. doi: 10.1073/pnas.0510511103
8. Koyanagi M, Brandes RP, Haendeler J, Zeiher AM, Dimmeler S. Cell-to-cell connection of endothelial progenitor cells with cardiac myocytes by nanotubes: a novel mechanism for cell fate changes? *Circ Res.* (2005) 96:1039–41. doi: 10.1161/01.RES.0000168650.23479.0c
9. He K, Shi X, Zhang X, Dang S, Ma X, Liu F, et al. Long-distance intercellular connectivity between cardiomyocytes and cardiofibroblasts mediated by membrane nanotubes. *Cardiovasc Res.* (2011) 92:39–47. doi: 10.1093/cvr/cvr189
10. Vallabhaneni KC, Haller H, Dumler I. Vascular smooth muscle cells initiate proliferation of mesenchymal stem cells by mitochondrial transfer via tunneling nanotubes. *Stem Cells Dev.* (2012) 21:3104–13. doi: 10.1089/scd.2011.0691
11. Han H, Hu J, Yan Q, Zhu J, Zhu Z, Chen Y, et al. Bone marrow-derived mesenchymal stem cells rescue injured H9c2 cells via transferring intact mitochondria through tunneling nanotubes in an *in vitro* simulated ischemia/reperfusion model. *Mol Med Rep.* (2016) 13:1517–24. doi: 10.3892/mmr.2015.4726
12. Liu K, Ji K, Guo L, Wu W, Lu H, Shan P, et al. Mesenchymal stem cells rescue injured endothelial cells in an *in vitro* ischemia-reperfusion model via tunneling nanotube like structure-mediated mitochondrial transfer. *Microvasc Res.* (2014) 92:10–8. doi: 10.1016/j.mvr.2014.01.008
13. Davis CH, Kim KY, Bushong EA, Mills EA, Boassa D, Shih T, et al. Transcellular degradation of axonal mitochondria. *Proc Natl Acad Sci USA.* (2014) 111:9633–8. doi: 10.1073/pnas.1404651111
14. Mahrouf-Yorgov M, Augeul L, Da Silva CC, Jourdan M, Rigolet M, Manin S, et al. Mesenchymal stem cells sense mitochondria released from damaged cells as danger signals to activate their rescue properties. *Cell Death Differ.* (2017) 24:1224–38. doi: 10.1038/cdd.2017.51

15. Zhang Y, Yu Z, Jiang D, Liang X, Liao S, Zhang Z, et al. iPSC-MSCs with high intrinsic MIRO1 and sensitivity to TNF-alpha yield efficacious mitochondrial transfer to rescue anthracycline-induced cardiomyopathy. *Stem Cell Rep.* (2016) 7:749–63. doi: 10.1016/j.stemcr.2016.08.009
16. Rustom A, Saffrich R, Markovic I, Walther P, Gerdes HH. Nanotubular highways for intercellular organelle transport. *Science.* (2004) 303:1007–10. doi: 10.1126/science.1093133
17. Cselenyak A, Pankotai E, Horvath EM, Kiss L, Lacza Z. Mesenchymal stem cells rescue cardiomyoblasts from cell death in an *in vitro* ischemia model via direct cell-to-cell connections. *BMC Cell Biol.* (2010) 11:29. doi: 10.1186/1471-2121-11-29
18. Feng Y, Zhu R, Shen J, Wu J, Lu W, Zhang J, et al. Human bone marrow mesenchymal stem cells rescue endothelial cells experiencing chemotherapy stress by mitochondrial transfer via tunneling nanotubes. *Stem Cells Dev.* (2019) 28:674–82. doi: 10.1089/scd.2018.0248
19. Astanina K, Koch M, Jungst C, Zumbusch A, Kiemer AK. Lipid droplets as a novel cargo of tunnelling nanotubes in endothelial cells. *Sci Rep.* (2015) 5:11453. doi: 10.1038/srep11453
20. Acquistapace A, Bru T, Lesault PF, Figeac F, Coudert AE, le Coz O, et al. Human mesenchymal stem cells reprogram adult cardiomyocytes toward a progenitor-like state through partial cell fusion and mitochondria transfer. *Stem Cells.* (2011) 29:812–24. doi: 10.1002/stem.632
21. Zhang J, Zhang J, Zhao L, Xin Y, Liu S, Cui W. Differential roles of microtubules in the two formation stages of membrane nanotubes between human mesenchymal stem cells and neonatal mouse cardiomyocytes. *Biochem Biophys Res Commun.* (2019) 512:441–7. doi: 10.1016/j.bbrc.2019.03.075
22. Plotnikov EY, Khryapenkova TG, Vasileva AK, Marey MV, Galkina SI, Isaev NK, et al. Cell-to-cell cross-talk between mesenchymal stem cells and cardiomyocytes in co-culture. *J Cell Mol Med.* (2008) 12:1622–31. doi: 10.1111/j.1582-4934.2007.00205.x
23. Shen J, Zhang JH, Xiao H, Wu JM, He KM, Lv ZZ, et al. Mitochondria are transported along microtubules in membrane nanotubes to rescue distressed cardiomyocytes from apoptosis. *Cell Death Dis.* (2018) 9:81. doi: 10.1038/s41419-017-0145-x
24. Yang H, Borg TK, Ma Z, Xu M, Wetzel G, Saraf LV, et al. Biochip-based study of unidirectional mitochondrial transfer from stem cells to myocytes via tunneling nanotubes. *Biofabrication.* (2016) 8:015012. doi: 10.1088/1758-5090/8/1/015012
25. MacAskill AF, Kittler JT. Control of mitochondrial transport and localization in neurons. *Trends Cell Biol.* (2010) 20:102–12. doi: 10.1016/j.tcb.2009.11.002
26. Dupont M, Souriant S, Lugo-Villarino G, Maridonneau-Parini I, Verollet C. Tunneling nanotubes: intimate communication between myeloid cells. *Front Immunol.* (2018) 9:43. doi: 10.3389/fimmu.2018.00043
27. Li RF, Zhang W, Man QW, Zhao YF, Zhao Y. Tunneling nanotubes mediate intercellular communication between endothelial progenitor cells and osteoclast precursors. *J Mol Histol.* (2019) 50:483–91. doi: 10.1007/s10735-019-09842-y
28. Panasiuk M, Rychlowski M, Derewonko N, Bienkowska-Szewczyk K. Tunneling nanotubes as a novel route of cell-to-cell spread of herpesviruses. *J Virol.* (2018) 92:e00090–18. doi: 10.1128/JVI.00090-18
29. Qin Y, Jiang X, Yang Q, Zhao J, Zhou Q, Zhou Y. The functions, methods, and mobility of mitochondrial transfer between cells. *Front Oncol.* (2021) 11:672781. doi: 10.3389/fonc.2021.672781
30. Gerdes HH, Bukoreshtliev NV, Barroso JF. Tunneling nanotubes: a new route for the exchange of components between animal cells. *FEBS Lett.* (2007) 581:2194–201. doi: 10.1016/j.febslet.2007.03.071
31. Hase K, Kimura S, Takatsu H, Ohmae M, Kawano S, Kitamura H, et al. M-Sec promotes membrane nanotube formation by interacting with Ral and the exocyst complex. *Nat Cell Biol.* (2009) 11:1427–32. doi: 10.1038/ncb1990
32. Wang Y, Cui J, Sun X, Zhang Y. Tunneling-nanotube development in astrocytes depends on p53 activation. *Cell Death Differ.* (2011) 18:732–42. doi: 10.1038/cdd.2010.147
33. Osswald M, Jung E, Sahm F, Solecki G, Venkataramani V, Blaes J, et al. Brain tumour cells interconnect to a functional and resistant network. *Nature.* (2015) 528:93–8. doi: 10.1038/nature16071
34. Yao Y, Fan XL, Jiang D, Zhang Y, Li X, Xu ZB, et al. Connexin 43-mediated mitochondrial transfer of iPSC-MSCs alleviates asthma inflammation. *Stem Cell Reports.* (2018) 11:1120–35. doi: 10.1016/j.stemcr.2018.09.012
35. Tishchenko A, Azorin DD, Vidal-Brime L, Munoz MJ, Arenas PJ, Pearce C, et al. Cx43 and associated cell signaling pathways regulate tunneling nanotubes in breast cancer cells. *Cancers.* (2020) 12:2798. doi: 10.3390/cancers12102798
36. Wang X, Veruki ML, Bukoreshtliev NV, Hartveit E, Gerdes HH. Animal cells connected by nanotubes can be electrically coupled through interposed gap-junction channels. *Proc Natl Acad Sci USA.* (2010) 107:17194–9. doi: 10.1073/pnas.1006785107
37. Kassab S, Albalawi Z, Daghistani H, Kitmitto A. Mitochondrial arrest on the microtubule highway-a feature of heart failure and diabetic cardiomyopathy? *Front Cardiovasc Med.* (2021) 8:689101. doi: 10.3389/fcvm.2021.689101
38. Lopez-Domenech G, Covill-Cooke C, Ivankovic D, Halff EF, Sheehan DF, Norkett R, et al. Miro proteins coordinate microtubule- and actin-dependent mitochondrial transport and distribution. *EMBO J.* (2018) 37:321–36. doi: 10.15252/embj.201696380
39. Jeon H, Lee J, Lee S, Kang SK, Park SJ, Yoo SM, et al. Extracellular vesicles from KSHV-infected cells stimulate antiviral immune response through mitochondrial DNA. *Front Immunol.* (2019) 10:876. doi: 10.3389/fimmu.2019.00876
40. Ikeda G, Santoso MR, Tada Y, Li AM, Vaskova E, Jung JH, et al. Mitochondria-rich extracellular vesicles from autologous stem cell-derived cardiomyocytes restore energetics of ischemic myocardium. *J Am Coll Cardiol.* (2021) 77:1073–88. doi: 10.1016/j.jacc.2020.12.060
41. Puhm F, Afonyushkin T, Resch U, Obermayer G, Rohde M, Penz T, et al. Mitochondria are a subset of extracellular vesicles released by activated monocytes and induce type I IFN and TNF responses in endothelial cells. *Circ Res.* (2019) 125:43–52. doi: 10.1161/CIRCRESAHA.118.314601
42. Nicolas-Avila JA, Lechuga-Vieco AV, Esteban-Martinez L, Sanchez-Diaz M, Diaz-Garcia E, Santiago DJ, et al. A network of macrophages supports mitochondrial homeostasis in the heart. *Cell.* (2020) 183:94–109 e23. doi: 10.1016/j.cell.2020.08.031
43. French KC, Antonyak MA, Cerione RA. Extracellular vesicle docking at the cellular port: extracellular vesicle binding and uptake. *Semin Cell Dev Biol.* (2017) 67:48–55. doi: 10.1016/j.semcdb.2017.01.002
44. Ratajczak MZ, Ratajczak J. Horizontal transfer of RNA and proteins between cells by extracellular microvesicles: 14 years later. *Clin Transl Med.* (2016) 5:7. doi: 10.1186/s40169-016-0087-4
45. Todkar K, Chikhi L, Desjardins V, El-Mortada F, Pepin G, Germain M. Selective packaging of mitochondrial proteins into extracellular vesicles prevents the release of mitochondrial DAMPs. *Nat Commun.* (2021) 12:1971. doi: 10.1038/s41467-021-21984-w
46. Guse AH. Second messenger function and the structure-activity relationship of cyclic adenosine diphosphoribose (cADPR). *FEBS J.* (2005) 272:4590–7. doi: 10.1111/j.1742-4658.2005.04863.x
47. Pang A, Cui Y, Chen Y, Cheng N, Delaney MK, Gu M, et al. Shear-induced integrin signaling in platelet phosphatidylserine exposure, microvesicle release, and coagulation. *Blood.* (2018) 132:533–43. doi: 10.1182/blood-2017-05-785253
48. Tang TT, Lv LL, Wang B, Cao JY, Feng Y, Li ZL, et al. Employing macrophage-derived microvesicle for kidney-targeted delivery of dexamethasone: an efficient therapeutic strategy against renal inflammation and fibrosis. *Theranostics.* (2019) 9:4740–55. doi: 10.7150/thno.33520
49. Levoux J, Prola A, Lafuste P, Gervais M, Chevallier N, Koumaiha Z, et al. Platelets facilitate the wound-healing capability of mesenchymal stem cells by mitochondrial transfer and metabolic reprogramming. *Cell Metab.* (2021) 33:283–99 e9. doi: 10.1016/j.cmet.2020.12.006
50. van Niel G, D'Angelo G, Raposo G. Shedding light on the cell biology of extracellular vesicles. *Nat Rev Mol Cell Biol.* (2018) 19:213–28. doi: 10.1038/nrm.2017.125
51. Zhang Y, Tan J, Miao Y, Zhang Q. The effect of extracellular vesicles on the regulation of mitochondria under hypoxia. *Cell Death Dis.* (2021) 12:358. doi: 10.1038/s41419-021-03640-9
52. Melentijevic I, Toth ML, Arnold ML, Guasp RJ, Harinath G, Nguyen KC, et al. *C. elegans* neurons jettison protein aggregates and mitochondria under neurotoxic stress. *Nature.* (2017) 542:367–71. doi: 10.1038/nature21362

53. Stephens OR, Grant D, Frimel M, Wanner N, Yin M, Willard B, et al. Characterization and origins of cell-free mitochondria in healthy murine and human blood. *Mitochondrion.* (2020) 54:102–12. doi: 10.1016/j.mito.2020.08.002
54. Al Amir Dache Z, Otandault A, Tanos R, Pastor B, Meddeb R, Sanchez C, et al. Blood contains circulating cell-free respiratory competent mitochondria. *Faseb J.* (2020) 34:3616–30. doi: 10.1096/fj.201901917RR
55. Hayakawa K, Chan SJ, Mandeville ET, Park JH, Bruzzese M, Montaner J, et al. Protective effects of endothelial progenitor cell-derived extracellular mitochondria in brain endothelium. *Stem Cells.* (2018) 36:1404–10. doi: 10.1002/stem.2856
56. Boudreau LH, Duchez AC, Cloutier N, Soulet D, Martin N, Bollinger J, et al. Platelets release mitochondria serving as substrate for bactericidal group IIA-secreted phospholipase A2 to promote inflammation. *Blood.* (2014) 124:2173–83. doi: 10.1182/blood-2014-05-573543
57. Pacak CA, Preble JM, Kondo H, Seibel P, Levitsky S, Del Nido PJ, et al. Actin-dependent mitochondrial internalization in cardiomyocytes: evidence for rescue of mitochondrial function. *Biol Open.* (2015) 4:622–6. doi: 10.1242/bio.201511478
58. Kitani T, Kami D, Matoba S, Gojo S. Internalization of isolated functional mitochondria: involvement of macropinocytosis. *J Cell Mol Med.* (2014) 18:1694–703. doi: 10.1111/jcmm.12316
59. Kesner EE, Saada-Reich A, Lorberboum-Galski H. Characteristics of mitochondrial transformation into human cells. *Sci Rep.* (2016) 6:26057. doi: 10.1038/srep26057
60. Alvarez-Dolado M, Pardal R, Garcia-Verdugo JM, Fike JR, Lee HO, Pfeffer K, et al. Fusion of bone-marrow-derived cells with Purkinje neurons, cardiomyocytes and hepatocytes. *Nature.* (2003) 425:968–73. doi: 10.1038/nature02069
61. Louwagie EJ, Larsen TD, Wachal AL, Gandy TCT, Baack ML. Mitochondrial transfer improves cardiomyocyte bioenergetics and viability in male rats exposed to pregestational diabetes. *Int J Mol Sci.* (2021) 22:2382. doi: 10.3390/ijms22052382
62. Cowan DB, Yao R, Thedsanamoorthy JK, Zurakowski D, Del Nido PJ, McCully JD. Transit and integration of extracellular mitochondria in human heart cells. *Sci Rep.* (2017) 7:17450. doi: 10.1038/s41598-017-17813-0
63. Tian R, Colucci WS, Arany Z, Bachschmid MM, Ballinger SW, Boudina S, et al. Unlocking the secrets of mitochondria in the cardiovascular system: path to a cure in heart failure-a report from the 2018 National Heart, Lung, and Blood Institute Workshop. *Circulation.* (2019) 140:1205–16. doi: 10.1161/CIRCULATIONAHA.119.040551
64. Zhou XL, Wu X, Xu QR, Zhu RR, Xu H, Li YY, et al. Notch1 provides myocardial protection by improving mitochondrial quality control. *J Cell Physiol.* (2019) 234:11835–41. doi: 10.1002/jcp.27892
65. Zhou H, Wang S, Zhu P, Hu S, Chen Y, Ren J. Empagliflozin rescues diabetic myocardial microvascular injury via AMPK-mediated inhibition of mitochondrial fission. *Redox Biol.* (2018) 15:335–46. doi: 10.1016/j.redox.2017.12.019
66. Chang JC, Chang HS, Wu YC, Cheng WL, Lin TT, Chang HJ, et al. Mitochondrial transplantation regulates antitumour activity, chemoresistance and mitochondrial dynamics in breast cancer. *J Exp Clin Cancer Res.* (2019) 38:30. doi: 10.1186/s13046-019-1028-z
67. Lavorato M, Iyer VR, Dewight W, Cupo RR, Debattisti V, Gomez L, et al. Increased mitochondrial nanotunneling activity, induced by calcium imbalance, affects intermitochondrial matrix exchanges. *Proc Natl Acad Sci USA.* (2017) 114:E849–58. doi: 10.1073/pnas.1617788113
68. Huang X, Sun L, Ji S, Zhao T, Zhang W, Xu J, et al. Kissing and nanotunneling mediate intermitochondrial communication in the heart. *Proc Natl Acad Sci USA.* (2013) 110:2846–51. doi: 10.1073/pnas.1300741110
69. Maeda H, Kami D, Maeda R, Murata Y, Jo JI, Kitani T, et al. TAT-dextran-mediated mitochondrial transfer enhances recovery from models of reperfusion injury in cultured cardiomyocytes. *J Cell Mol Med.* (2020) 24:5007–20. doi: 10.1111/jcmm.15120
70. Paliwal S, Chaudhuri R, Agrawal A, Mohanty S. Human tissue-specific MSCs demonstrate differential mitochondria transfer abilities that may determine their regenerative abilities. *Stem Cell Res Ther.* (2018) 9:298. doi: 10.1186/s13287-018-1012-0
71. McCully JD, Levitsky S, Del Nido PJ, Cowan DB. Mitochondrial transplantation for therapeutic use. *Clin Transl Med.* (2016) 5:16. doi: 10.1186/s40169-016-0095-4
72. Zhou P, Pu WT. Recounting cardiac cellular composition. *Circ Res.* (2016) 118:368–70. doi: 10.1161/CIRCRESAHA.116.308139
73. Masuzawa A, Black KM, Pacak CA, Ericsson M, Barnett RJ, Drumm C, et al. Transplantation of autologously derived mitochondria protects the heart from ischemia-reperfusion injury. *Am J Physiol Heart Circ Physiol.* (2013) 304:H966–82. doi: 10.1152/ajpheart.00883.2012
74. Ali Pour P, Kenney MC, Kheradvar A. Bioenergetics consequences of mitochondrial transplantation in cardiomyocytes. *J Am Heart Assoc.* (2020) 9:e014501. doi: 10.1161/JAHA.119.014501
75. Suen J, Thomas J, Kranz A, Vun S, Miller M. Effect of flavonoids on oxidative stress and inflammation in adults at risk of cardiovascular disease: a systematic review. *Healthcare.* (2016) 4:69. doi: 10.3390/healthcare4030069
76. Al-Rawi NH, Shahid AM. Oxidative stress, antioxidants, and lipid profile in the serum and saliva of individuals with coronary heart disease: is there a link with periodontal health? *Minerva Stomatol.* (2017) 66:212–25. doi: 10.23736/S0026-4970.17.04062-6
77. Doroszko A, Dobrowolski P, Radziwon-Balicka A, Skomro R. New insights into the role of oxidative stress in onset of cardiovascular disease. *Oxid Med Cell Longev.* (2018) 2018:9563831. doi: 10.1155/2018/9563831
78. Steven S, Frenis K, Oelze M, Kalinovic S, Kuntic M, Bayo Jimenez MT, et al. Vascular inflammation and oxidative stress: major triggers for cardiovascular disease. *Oxid Med Cell Longev.* (2019) 2019:7092151. doi: 10.1155/2019/7092151
79. Karbach S, Wenzel P, Waisman A, Munzel T, Daiber A. eNOS uncoupling in cardiovascular diseases–the role of oxidative stress and inflammation. *Curr Pharm Des.* (2014) 20:3579–94. doi: 10.2174/13816128113196660748
80. Del Re DP, Amgalan D, Linkermann A, Liu Q, Kitsis RN. Fundamental mechanisms of regulated cell death and implications for heart disease. *Physiol Rev.* (2019) 99:1765–817. doi: 10.1152/physrev.00022.2018
81. Heldman AW, DiFede DL, Fishman JE, Zambrano JP, Trachtenberg BH, Karantalis V, et al. Transendocardial mesenchymal stem cells and mononuclear bone marrow cells for ischemic cardiomyopathy: the TAC-HFT randomized trial. *JAMA.* (2014) 311:62–73. doi: 10.1001/jama.2013.282909
82. Trachtenberg B, Velazquez DL, Williams AR, McNiece I, Fishman J, Nguyen K, et al. Rationale and design of the transendocardial injection of autologous human cells (bone marrow or mesenchymal) in chronic ischemic left ventricular dysfunction and heart failure secondary to myocardial infarction (TAC-HFT) trial: a randomized, double-blind, placebo-controlled study of safety and efficacy. *Am Heart J.* (2011) 161:487–93. doi: 10.1016/j.ahj.2010.11.024
83. Williams AR, Trachtenberg B, Velazquez DL, McNiece I, Altman P, Rouy D, et al. Intramyocardial stem cell injection in patients with ischemic cardiomyopathy: functional recovery and reverse remodeling. *Circ Res.* (2011) 108:792–6. doi: 10.1161/CIRCRESAHA.111.242610
84. Malliaras K, Li TS, Luthringer D, Terrovitis J, Cheng K, Chakravarty T, et al. Safety and efficacy of allogeneic cell therapy in infarcted rats transplanted with mismatched cardiosphere-derived cells. *Circulation.* (2012) 125:100–12. doi: 10.1161/CIRCULATIONAHA.111.042598
85. McCully JD, Cowan DB, Pacak CA, Toumpoulis IK, Dayalan H, Levitsky S. Injection of isolated mitochondria during early reperfusion for cardioprotection. *Am J Physiol Heart Circ Physiol.* (2009) 296:H94–H105. doi: 10.1152/ajpheart.00567.2008
86. Hsu CH, Roan JN, Fang SY, Chiu MH, Cheng TT, Huang CC, et al. Transplantation of viable mitochondria improves right ventricular performance and pulmonary artery remodeling in rats with pulmonary arterial hypertension. *J Thorac Cardiovasc Surg.* (2020) S0022-5223:32372-2. doi: 10.1016/j.jtcvs.2020.08.014
87. Kaza AK, Wamala I, Friehs I, Kuebler JD, Rathod RH, Berra I, et al. Myocardial rescue with autologous mitochondrial transplantation in a porcine model of ischemia/reperfusion. *J Thorac Cardiovasc Surg.* (2017) 153:934–43. doi: 10.1016/j.jtcvs.2016.10.077
88. Cowan DB, Yao R, Akurathi V, Snay ER, Thedsanamoorthy JK, Zurakowski D, et al. Intracoronary delivery of mitochondria

to the ischemic heart for cardioprotection. *Plos One.* (2016) 11:e0160889. doi: 10.1371/journal.pone.0160889
89. Blitzer D, Guariento A, Doulamis IP, Shin B, Moskowitzova K, Barbieri GR, et al. Delayed transplantation of autologous mitochondria for cardioprotection in a porcine model. *Ann Thorac Surg.* (2020) 109:711–9. doi: 10.1016/j.athoracsur.2019.06.075
90. Guariento A, Blitzer D, Doulamis I, Shin B, Moskowitzova K, Orfany A, et al. Preischemic autologous mitochondrial transplantation by intracoronary injection for myocardial protection. *J Thorac Cardiovasc Surg.* (2020) 160:e15–e29. doi: 10.1016/j.jtcvs.2019.06.111
91. Shin B, Saeed MY, Esch JJ, Guariento A, Blitzer D, Moskowitzova K, et al. A novel biological strategy for myocardial protection by intracoronary delivery of mitochondria: safety and efficacy. *JACC Basic Transl Sci.* (2019) 4:871–88. doi: 10.1016/j.jacbts.2019.08.007
92. Guariento A, Doulamis IP, Duignan T, Kido T, Regan WL, Saeed MY, et al. Mitochondrial transplantation for myocardial protection in ex-situperfused hearts donated after circulatory death. *J Heart Lung Transplant.* (2020) S1053-2498:31625-9. doi: 10.1016/j.healun.2020.01.1319
93. Doulamis IP, Guariento A, Duignan T, Orfany A, Kido T, Zurakowski D, et al. Mitochondrial transplantation for myocardial protection in diabetic hearts. *Eur J Cardiothorac Surg.* (2020) 57:836–45. doi: 10.1093/ejcts/ezz326
94. Moskowitzova K, Shin B, Liu K, Ramirez-Barbieri G, Guariento A, Blitzer D, et al. Mitochondrial transplantation prolongs cold ischemia time in murine heart transplantation. *J Heart Lung Transplant.* (2019) 38:92–9. doi: 10.1016/j.healun.2018.09.025
95. Weixler V, Lapusca R, Grangl G, Guariento A, Saeed MY, Cowan DB, et al. Autogenous mitochondria transplantation for treatment of right heart failure. *J Thorac Cardiovasc Surg.* (2021) 162:e111–21. doi: 10.1016/j.jtcvs.2020.08.011
96. Sid-Otmane C, Perrault LP, Ly HQ. Mesenchymal stem cell mediates cardiac repair through autocrine, paracrine and endocrine axes. *J Transl Med.* (2020) 18:336. doi: 10.1186/s12967-020-02504-8
97. Bagno L, Hatzistergos KE, Balkan W, Hare JM. Mesenchymal stem cell-based therapy for cardiovascular disease: progress and challenges. *Mol Ther.* (2018) 26:1610–23. doi: 10.1016/j.ymthe.2018.05.009
98. Macia E, Boyden PA. Stem cell therapy is proarrhythmic. *Circulation.* (2009) 119:1814–23. doi: 10.1161/CIRCULATIONAHA.108.779900
99. Saei Arezoumand K, Alizadeh E, Pilehvar-Soltanahmadi Y, Esmaeillou M, Zarghami N. An overview on different strategies for the stemness maintenance of MSCs. *Artif Cells Nanomed Biotechnol.* (2017) 45:1255–71. doi: 10.1080/21691401.2016.1246452
100. Furlani D, Ugurlucan M, Ong L, Bieback K, Pittermann E, Westien I, et al. Is the intravascular administration of mesenchymal stem cells safe? Mesenchymal stem cells and intravital microscopy. *Microvasc Res.* (2009) 77:370–6. doi: 10.1016/j.mvr.2009.02.001
101. Emani SM, Piekarski BL, Harrild D, Del Nido PJ, McCully JD. Autologous mitochondrial transplantation for dysfunction after ischemia-reperfusion injury. *J Thorac Cardiovasc Surg.* (2017) 154:286–9. doi: 10.1016/j.jtcvs.2017.02.018
102. Fu A, Shi X, Zhang H, Fu B. Mitotherapy for fatty liver by intravenous administration of exogenous mitochondria in male mice. *Front Pharmacol.* (2017) 8:241. doi: 10.3389/fphar.2017.00241
103. Shi X, Zhao M, Fu C, Fu A. Intravenous administration of mitochondria for treating experimental Parkinson's disease. *Mitochondrion.* (2017) 34:91–100. doi: 10.1016/j.mito.2017.02.005
104. Mobarrez F, Fuzzi E, Gunnarsson I, Larsson A, Eketjall S, Pisetsky DS, et al. Microparticles in the blood of patients with SLE: size, content of mitochondria and role in circulating immune complexes. *J Autoimmun.* (2019) 102:142–9. doi: 10.1016/j.jaut.2019.05.003
105. Herrmann IK, Wood MJA, Fuhrmann G. Extracellular vesicles as a next-generation drug delivery platform. *Nat Nanotechnol.* (2021) 16:748–59. doi: 10.1038/s41565-021-00931-2
106. Cai J, Wu J, Wang J, Li Y, Hu X, Luo S, et al. Extracellular vesicles derived from different sources of mesenchymal stem cells: therapeutic effects and translational potential. *Cell Biosci.* (2020) 10:69. doi: 10.1186/s13578-020-00427-x
107. Sherman CD, Lodha S, Sahoo S. EV cargo sorting in therapeutic development for cardiovascular disease. *Cells.* (2021) 10:1500. doi: 10.3390/cells10061500
108. Bolli R, Tang XL, Sanganalmath SK, Rimoldi O, Mosna F, Abdel-Latif A, et al. Intracoronary delivery of autologous cardiac stem cells improves cardiac function in a porcine model of chronic ischemic cardiomyopathy. *Circulation.* (2013) 128:122–31. doi: 10.1161/CIRCULATIONAHA.112.001075
109. Adamiak M, Cheng G, Bobis-Wozowicz S, Zhao L, Kedracka-Krok S, Samanta A, et al. Induced pluripotent stem cell (iPSC)-derived extracellular vesicles are safer and more effective for cardiac repair than iPSCs. *Circ Res.* (2018) 122:296–309. doi: 10.1161/CIRCRESAHA.117.311769
110. Wang X, Chen Y, Zhao Z, Meng Q, Yu Y, Sun J, et al. Engineered exosomes with ischemic myocardium-targeting peptide for targeted therapy in myocardial infarction. *J Am Heart Assoc.* (2018) 7:e008737. doi: 10.1161/JAHA.118.008737
111. Falk MJ, Decherney A, Kahn JP. Mitochondrial replacement techniques–implications for the clinical community. *N Engl J Med.* (2016) 374:1103–6. doi: 10.1056/NEJMp1600893
112. Dorji J, Vander Jagt CJ, Garner JB, Marett LC, Mason BA, Reich CM, et al. Expression of mitochondrial protein genes encoded by nuclear and mitochondrial genomes correlate with energy metabolism in dairy cattle. *BMC Genomics.* (2020) 21:720. doi: 10.1186/s12864-020-07018-7
113. Meiklejohn CD, Holmbeck MA, Siddiq MA, Abt DN, Rand DM, Montooth KL. An incompatibility between a mitochondrial tRNA and its nuclear-encoded tRNA synthetase compromises development and fitness in Drosophila. *PLoS Genet.* (2013) 9:e1003238. doi: 10.1371/journal.pgen.1003238
114. Trier CN, Hermansen JS, Saetre GP, Bailey RI. Evidence for mito-nuclear and sex-linked reproductive barriers between the hybrid Italian sparrow and its parent species. *PLoS Genet.* (2014) 10:e1004075. doi: 10.1371/journal.pgen.1004075
115. Ma H, Marti Gutierrez N, Morey R, Van Dyken C, Kang E, Hayama T, et al. Incompatibility between nuclear and mitochondrial genomes contributes to an interspecies reproductive barrier. *Cell Metab.* (2016) 24:283–94. doi: 10.1016/j.cmet.2016.06.012
116. Caicedo A, Aponte PM, Cabrera F, Hidalgo C, Khoury M. Artificial mitochondria transfer: current challenges, advances, and future applications. *Stem Cells Int.* (2017) 2017:7610414. doi: 10.1155/2017/7610414
117. Mitalipov S, Wolf DP. Clinical and ethical implications of mitochondrial gene transfer. *Trends Endocrinol Metab.* (2014) 25:5–7. doi: 10.1016/j.tem.2013.09.001
118. Xu S, Schaack S, Seyfert A, Choi E, Lynch M, Cristescu ME. High mutation rates in the mitochondrial genomes of Daphnia pulex. *Mol Biol Evol.* (2012) 29:763–9. doi: 10.1093/molbev/msr243
119. Picard M, Taivassalo T, Ritchie D, Wright KJ, Thomas MM, Romestaing C, et al. Mitochondrial structure and function are disrupted by standard isolation methods. *PLoS ONE.* (2011) 6:e18317. doi: 10.1371/journal.pone.0018317
120. Busch KB, Kowald A, Spelbrink JN. Quality matters: how does mitochondrial network dynamics and quality control impact on mtDNA integrity? *Philos Trans R Soc Lond B Biol Sci.* (2014) 369:20130442. doi: 10.1098/rstb.2013.0442
121. Mustafa MF, Fakurazi S, Abdullah MA, Maniam S. Pathogenic mitochondria DNA mutations: current detection tools and interventions. *Genes.* (2020) 11:192. doi: 10.3390/genes11020192
122. Aryaman J, Johnston IG, Jones NS. Mitochondrial heterogeneity. *Front Genet.* (2018) 9:718. doi: 10.3389/fgene.2018.00718
123. Wu S, Zhang A, Li S, Chatterjee S, Qi R, Segura-Ibarra V, et al. Polymer functionalization of isolated mitochondria for cellular transplantation and metabolic phenotype alteration. *Adv Sci.* (2018) 5:1700530. doi: 10.1002/advs.201700530

124. Newson AJ, Wilkinson S, Wrigley A. Ethical and legal issues in mitochondrial transfer. *EMBO Mol Med.* (2016) 8:589–91. doi: 10.15252/emmm.201606281

Conflict of Interest: The authors declare that the research was conducted in the absence of any commercial or financial relationships that could be construed as a potential conflict of interest.

Publisher's Note: All claims expressed in this article are solely those of the authors and do not necessarily represent those of their affiliated organizations, or those of the publisher, the editors and the reviewers. Any product that may be evaluated in this article, or claim that may be made by its manufacturer, is not guaranteed or endorsed by the publisher.

frontiers in Cardiovascular Medicine

ORIGINAL RESEARCH
published: 01 December 2021
doi: 10.3389/fcvm.2021.777355

Atrial Fibrillation Ablation Using Robotic Magnetic Navigation Reduces the Incidence of Silent Cerebral Embolism

Jie Zheng[1†], Meng Wang[2†], Qun-feng Tang[3†], Feng Xue[4†], Ku-lin Li[1], Shi-peng Dang[1], Xiao-yu Liu[1], Xiao-xi Zhao[1], Chang-ying Zhang[1], Zhi-ming Yu[1], Bing Han[2], Ting-bo Jiang[4*], Yan Yao[5*] and Ru-Xing Wang[1*]*

[1] Department of Cardiology, Wuxi People's Hospital Affiliated to Nanjing Medical University, Wuxi, China, [2] Department of Cardiology, Xuzhou Central Hospital, Xuzhou, China, [3] Department of Radiology, Wuxi People's Hospital Affiliated to Nanjing Medical University, Wuxi, China, [4] Department of Cardiology, The First Hospital Affiliated to Soochow University, Suzhou, China, [5] Department of Cardiology, Fuwai Hospital, Chinese Academy of Medical Sciences - Peking Union Medical College, Beijing, China

OPEN ACCESS

Edited by:
Xiaofeng Yang,
Temple University, United States

Reviewed by:
Kimberly R. Rebello,
Baylor College of Medicine, United States
Masashi Kanemoto,
Saiseikai Yamaguchi General Hospital, Japan

***Correspondence:**
Ru-Xing Wang
ruxingw@aliyun.com
Bing Han
hbing777@hotmail.com
Ting-bo Jiang
18906201122@189.cn
Yan Yao
ianyao@263.net.cn

[†] These authors have contributed equally to this work

Specialty section:
This article was submitted to Cardiovascular Therapeutics, a section of the journal Frontiers in Cardiovascular Medicine

Received: 15 September 2021
Accepted: 02 November 2021
Published: 01 December 2021

Citation:
Zheng J, Wang M, Tang QF, Xue F, Li KL, Dang SP, Liu XY, Zhao XX, Zhang CY, Yu ZM, Han B, Jiang TB, Yao Y and Wang RX (2021) Atrial Fibrillation Ablation Using Robotic Magnetic Navigation Reduces the Incidence of Silent Cerebral Embolism. Front. Cardiovasc. Med. 8:777355. doi: 10.3389/fcvm.2021.777355

Background: The incidence of silent cerebral embolisms (SCEs) has been documented after pulmonary vein isolation using different ablation technologies; however, it is unreported in patients undergoing with atrial fibrillation (AF) ablation using Robotic Magnetic Navigation (RMN). The purpose of this prospective study was to investigate the incidence, risk predictors and probable mechanisms of SCEs in patients with AF ablation and the potential impact of RMN on SCE rates.

Methods and Results: We performed a prospective study of 166 patients with paroxysmal or persistent AF who underwent pulmonary vein isolation. Patients were divided into RMN group ($n = 104$) and manual control (MC) group ($n = 62$), and analyzed for their demographic, medical, echocardiographic, and risk predictors of SCEs. All patients underwent cerebral magnetic resonance imaging within 48 h before and after the ablation procedure to assess cerebral embolism. The incidence and potential risk factors of SCEs were compared between the two groups. There were 26 total cases of SCEs in this study, including 6 cases in the RMN group and 20 cases in the MC group. The incidences of SCEs in the RMN group and the MC group were 5.77 and 32.26%, respectively ($X^2 = 20.63$ $P < 0.05$). Univariate logistic regression analysis demonstrated that ablation technology, CHA_2DS_2-VASc score, history of cerebrovascular accident/transient ischemic attack, and low ejection fraction were significantly associated with SCEs, and multivariate logistic regression analysis showed that MC ablation was the only independent risk factor of SCEs after an AF ablation procedure.

Conclusions: Ablation technology, CHA_2DS_2-VASc score, history of cerebrovascular accident/transient ischemic attack, and low ejection fraction are associated with SCEs. However, ablation technology is the only independent risk factor of SCEs and RMN can significantly reduce the incidence of SCEs resulting from AF ablation.

Clinical Trial Registration: ChiCTR2100046505.

Keywords: silent cerebral embolism, atrial fibrillation, ablation technology, robotic magnetic navigation, catheter ablation

WHAT'S NEW?

- This is the first study comparing AF ablation using robotic magnetic navigation with manual control, showing significant reduction in the incidence of silent cerebral embolisms after ablation procedure.
- Ablation technology, CHA_2DS_2-VASc score, CVA/TIA history, and low ejection fraction are associated with silent cerebral embolisms in AF ablation patients, and among these factors, ablation technology is the only independent risk factor of silent cerebral embolisms.
- The mechanisms of decreased incidence of silent cerebral embolisms in AF ablation using robotic magnetic navigation may be due to the reduction of gaseous microbubbles, clot formation and char formation.

INTRODUCTION

Atrial fibrillation (AF) is the most common sustained cardiac arrhythmia with an increasing prevalence that affects at least 1% of the population worldwide and is associated with increased morbidity and mortality (1). AF catheter ablation with the goal of pulmonary vein isolation (PVI) has been established as an important therapeutic option for the treatment of AF. However, the complexity of the procedure may expose patients to a considerable number of complications. Stroke and thromboembolism are among the most harmful periprocedural complications following AF ablation procedures (2). Although symptomatic cerebral embolisms are rare (<1%) during PVI procedures (3, 4), new silent cerebral embolisms (SCEs) detected by cerebral magnetic resonance imaging (MRI) scans have a reported incidence of >10%, with some publications reporting SCEs in up to 30% of patients (5, 6). The long-term clinical significance of SCEs remains unclear, however they may correlate with neurologic deficits, including an increased risk of dementia. Therefore, it is imperative to take measures to reduce the risk of SCEs.

The issue of SCEs developing perioperatively in AF patients undergoing catheter ablation was first brought to general attention by Lickfett et al. (7) in 2006. Several mechanisms have been suggested as being potentially responsible for SCEs after AF catheter ablation, including macrobubble development within stationary sheaths, radiofrequency- and heat- related denaturation of fibrinogen to fibrin, and catheter manipulation in the left atrium (8). In the last decade, the exploration of SCE mechanisms has been focused on the risk of different AF ablation technologies and new ablation tools, which have various effects on the incidence of SCEs (9, 10). A high incidence of SCEs has been reported recently using the duty-cycled phased-radiofrequency ablation tool (6).

Robotic navigation technology has emerged as an important new tool to facilitate catheter ablation of arrhythmias (11). Mechanical robotic navigation has previously been shown to have a similar rate of SCEs compared to manual control (MC) ablation which we hypothesize is due to the similar manual pull-wire catheter technology employed (12). Robotic magnetic navigation (RMN) employs a fundamentally different mechanism of action. Direct manipulation of the catheter tip using magnetic fields allows for the elimination of pull-wires and braided shafts making the catheter body extremely soft and flexible providing a gentle interface with tissue. The enhanced steerability enables reaching targets without extensive sheath manipulation (13–15).

Numerous studies have shown RMN to be as effective as MC ablation (16–18), while reducing periprocedural complications and fluoroscopy exposure (19), but incidence of SCEs has not been reported. The purpose of this prospective pilot study was to examine the incidence of SCEs and investigate the potential risk predictors and possible mechanisms of SCEs in AF patients undergoing RMN-assisted PVI.

METHODS

Patient Population

In this multi-center prospective pilot study (Registered Clinical Trial Number: ChiCTR2100046505), a total of 166 AF patients, including 110 paroxysmal and 56 persistent AF patients, 100 males and 66 females, with mean age of 61.03 ± 9.58 (25-79) years, were enrolled for AF ablation at Wuxi People's Hospital affiliated to Nanjing Medical University (Wuxi, China), Xuzhou Central Hospital (Xuzhou, China), and the First Hospital affiliated to Soochow University (Suzhou, China). In these three centers, 104 AF patients were ablated using RMN at Wuxi People's Hospital affiliated to Nanjing Medical University (RMN group), and 62 AF patients were ablated using MC ablation at Xuzhou Central Hospital and the First Hospital affiliated to Soochow University (MC group). All patients were undergoing their first AF ablation procedure and no redo cases were included in this study.

The criteria of inclusion and exclusion, and the definitions of paroxysmal AF and persistent AF were the same as we previously reported (14). In brief, paroxysmal AF was defined as self-terminating within 7 days or terminated with electrical or pharmacological cardioversion. Persistent AF was defined as lasting >7 days, requiring cardioversion or other intervention or failed cardioversion, or cardioversion was no longer attempted. All patients provided written informed consent prior to study enrollment. The study protocol was reviewed and approved by the ethics committees of all three centers.

Electrophysiological Study and Catheter Ablation

AF ablation using RMN in 104 patients was performed as we previously reported (14). Procedures in the RMN group were performed using the Niobe Magnetic Navigation System (Stereotaxis, Inc., St Louis, MO, USA) paired with a Siemens Axiom Artis fluoroscopy system (Siemens, Erlangen, Germany). Atrial septum puncture was performed only once and one Swartz SL1 sheath was placed into the left atrium. The third-generation irrigated magnetic catheters (Navistar RMT Thermocool; Biosense Webster, Inc. Diamond Bar, California)

were steered omni-directionally by a magnet field-controlled system which follows the direction of applied vectors, and were advanced or retracted in 1 to 9 mm steps by a mechanical device (QuikCAS^{TM} automated catheter advancement system, Stereotaxis, St. Louis, MO, USA). Ablation was performed remotely from the control room, away from radiation exposure, utilizing the computer mouse and keyboard of the RMN.

The AF ablation procedures in 62 AF patients with MC technology were performed using the commonly used technologies and methods described by Haissaguerre and colleagues previously. In brief, after placing a diagnostic catheter into the coronary sinus, the atrial septum was punctured twice and two Swartz SL1 sheaths were placed into the left atrium. An irrigated-tip contact force ablation catheter (Thermocool SmartTouch, Biosense Webster, Diamond Bar, CA, USA) was used to perform the ablation. Radiofrequency energy was applied in a power-controlled mode with a power limit of 30–35 W and a maximum temperature of 43°C, which is the same as AF ablation procedure using RMN. In the process of the entire AF ablation procedure, the two sheaths were constantly being moved backward and forward, especially the sheath for ablation. Catheter exchanges from one sheath to the other sheath were often performed to facilitate the catheter ablation of pulmonary vein isolation.

Only circumferential PVI was performed in patients with paroxysmal AF. In patients with persistent AF, linear ablation of the left atrial roof and mitral isthmus was performed in addition to circumferential PVI. Electrical cardioversion was carried out for persistent AF patients with failure to maintain sinus rhythm after AF ablation procedures. During the entire AF ablation procedure, the sheath was fixed to the mechanical device (QuikCAS^{TM}) and almost no catheter exchanges were needed.

Left atrial thrombi in all enrolled patents were ruled out by transesophageal echocardiography 24 h before the ablation procedure. All procedures were performed under deep sedation using boluses of midazolam, fentanyl and a continuous infusion of propofol.

Periprocedural Anticoagulation

Warfarin or new oral anticoagulants (Dabigatran or Rivaroxaban) were taken orally no <3 weeks prior to the ablation procedure and taken for 2 months after ablation in all patients. If the patients chose warfarin as an oral anticoagulation, an international normalized ratio (INR) ≥2.0 was achieved and initiated ≥3 weeks before the procedures. If the patients chose Dabigatran or Rivaroxaban, we did not perform the routine monitoring of INR. After atrial septal puncture, heparin was immediately injected as a bolus of 70–100 I.U. per kg body weight from a peripheral vein. Heparin was administered later through the cooling fluid of the ablation catheter as well as via intermittent venous injections. The activated clotting time (ACT) was measured every 20–30 min to maintain 250 to 300 s during the ablation procedures. Oral anticoagulation was maintained throughout the ablation procedures without interruption or bridging and for the duration of follow-up.

Diffusion-Weighted MRI

A cerebral MRI was performed within 48 h before and after each PVI procedure using GE Sigma Excite 1.5 or 3.0 T scanners (Magnetom Aera, Siemens Healthcare, Erlangen, Germany or Magnetom Trio, Siemens Medical Solution, Erlangen, Germany) as previously reported (20). Diffusion-weighted MRI (DW-MRI) images from before and after the AF ablation procedure were analyzed and compared to identify any procedure-related acute cerebral lesions. Acute cerebral lesions were defined as the presence of focal diffusion abnormalities (bright hyper-intense lesions) in either a cortical or subcortical location, or in the vascular territory of the perforating arteries. The location and sizes of focal diffusion abnormalities were analyzed. Locations were categorized as: (1) left or right hemisphere and (2) locations within the (a) the frontal lobe, (b) parietal lobe, (c) temporal lobe, (d) precentral gyrus, (e) occipital lobe, (f) postcentral gyrus, or (g) cerebellum. The sizes of SCEs were defined as small (≤3 mm maximum diameter), medium (3 to 10 mm) and large (≥10 mm). In the case of differing DW-MRI readings, a consensus was obtained. All DW-MRI data, including number, location, and size of embolic lesions, were analyzed independently by two experienced radiologists who were blinded to the study data. No differences in evaluation, classification, or quantitative results were noted between the two experts.

Statistical Analysis

All continuous data were checked for normality with the Kolmogorov-Smirnov test and the Levene test was used for homogeneity of variance. Normally distributed continuous variables are described as mean ± standard deviations ($\overline{X} \pm$ SD). Categorical variables are described as median with inter-quartile range. The data distribution was compared using either the Student *t*-test or Mann-Whitney U test. For categorical data, the count and percentages were provided and compared by using a Chi-square test or Fisher exact test for low expected count. A logistic regression analysis was performed to investigate the relationship between SCEs and the baseline or procedural characteristics. The variables with either $P < 0.05$ or important clinical variables, such as diabetes and high score in the univariate analysis were selected for testing in the multivariate analysis. All tests were 2-sided, and statistical significance was set at a value of $P < 0.05$. Statistical analysis was carried out using SPSS 22.0 (IBM Corporation, Armonk, New York, USA).

RESULTS

Patient Characteristics

One hundred and sixty six patients including 104 in the RMN group and 62 in MC group were enrolled and ablated in the study. Differences were noted with respect to several baseline characteristics, including age, CHA_2DS_2-VASc score, cardioversion, left atrial diameter, ejection fraction, heart function class, and history of cerebrovascular accident/transient ischemic attack (CVA/TIA). No remarkable distinction was found in sex, body mass index, AF type, AF duration, ACT during procedure, or comorbidities such as hypertension, coronary artery disease, diabetes mellitus,

TABLE 1 | Baseline clinical and demographic characteristics of the study population.

Variables	All population (n = 166)	RMN group (n = 104)	MC group (n = 62)	P-value
Sex (M/F)	100/66	65/39	35/27	0.441
Age (y)	61.03 ± 9.58	59.06 ± 10.10	64.34 ± 7.65	0.000
BMI (kg/m^2)	24.64 ± 2.57	24.50 ± 2.34	24.88 ± 2.96	0.404
AF type				
Paroxysmal AF/Persistent AF	110/56	70/34	40/22	0.713
AF duration (m)	24	24	30	0.445
CHA_2DS_2-VASc score	2.48 ± 1.58	2.12 ± 1.36	3.08 ± 1.74	0.000
Cardioversion (Y/N)	56/110	29/75	27/35	0.039
ACT during procedure (s)	285.90 ± 14.94	285.12 ± 14.57	287.23 ± 15.58	0.380
LA diameter (mm)	37.93 ± 5.76	38.97 ± 5.16	36.19 ± 6.31	0.002
EF (%)	60.67 ± 5.68	62.50 ± 4.73	57.60 ± 5.84	0.000
Heart Function Class (NYHA)	1.16 ± 0.38	1.23 ± 0.45	1.03 ± 0.18	0.001
Comorbidity (n)				
HTN	76	43	33	0.137
CAD	34	26	8	0.062
DM	19	10	9	0.337
Dyslipidemia	4	4	0	0.298
Hyperthyroidism	5	1	4	0.065
CVA/TIA history	8	1	7	0.005
Others	13	5	8	0.076
Absence of underlying diseases (n)	44	26	18	0.569
Lab examinations				
BUN (mmol/L)	5.35 ± 1.52	5.09 ± 1.53	5.79 ± 1.41	0.004
Cr (mmol/L)	72.53 ± 18.76	80.72 ± 17.19	58.80 ± 12.14	0.000
FBG (mmol/L)	5.29 ± 1.44	5.15 ± 1.49	5.51 ± 1.34	0.117
TC (mmol/L)	4.24 ± 0.93	4.25 ± 0.88	4.23 ± 1.00	0.897
LDL (mmol/L)	2.41 ± 0.81	2.27 ± 0.78	2.64 ± 0.83	0.004
TG (mmol/L)	1.89 ± 1.36	2.08 ± 1.57	1.56 ± 0.81	0.046

The data are presented as the mean ± SD or n (%). RMN, robotic magnetic navigation; MC, manual control; BMI, body mass index; AF, atrial fibrillation; ACT, activated clotting time; LA diameter, left atrial diameter; Y, yes; N, no; HTN, hypertension; CAD, coronary artery disease; DM, diabetes mellitus; CVA, cerebrovascular accident; TIA, transient ischemic attack; BUN, blood urea nitrogen; Cr, creatinine; FBG, fasting blood glucose; TC, total cholesterol; LDL, low density lipoprotein; TG, triglyceride; Absence of underlying diseases, refers to patients with no other cardiovascular co-morbidity or no other co-morbidities at all.

and dislipidemia. The baseline clinical and demographic characteristics of the study population are detailed in **Table 1**.

Patients With or Without Silent Cerebral Embolism

Additionally, we compared the characteristics of patients with SCE and without SCE. We found that there were significant differences in CHA_2DS_2-VASc score, ejection fraction, CVA/TIA history, and creatinine between two groups. There were no differences in sex, age, body mass index, AF type and other variables. The detailed characteristics of patients with SCE and without SCE are demonstrated in **Table 2**.

Incidence, Localization, Number, and Size of Silent Cerebral Embolism

There were 26 total cases of SCE observed in this study, including 6 in the RMN group and 20 in the MC group. The incidences of SCE in the RMN group and MC group were 5.77 and 32.26%, respectively ($X^2 = 20.63$ $P < 0.001$). The cerebral MRIs of SCEs in the 6 cases observed in the RMN group are shown in **Figure 1**, and the cerebral MRIs for the 20 cases of SCE in the MC group are provided in the **Supplementary Data file**.

Localization, number and size of SCEs in all 26 patients are annotated in **Table 3**. There were 32 total SCEs including 1 (3.13%) patient with multiple cerebral embolisms in the RMN group and 4 (12.50%) patients with multiple cerebral embolisms in the MC group ($X^2 = 0.012$, $P > 0.99$). Among the 32 cerebral embolisms, 9 (28.13%) were located in frontal lobes (4 in right frontal lobes and 5 in left frontal lobes), 8 (25.00%) in occipital lobes (4 each in left and right occipital lobes respectively), 5 (15.63%) in the parietal lobes (3 in left parietal lobes and 2 in right parietal lobes), 2 (6.25%) in right corona radiata and one (3.13%) each in the left thalamus, right insular lobe, and left basal ganglia. No SCEs

TABLE 2 | Characteristics of patients with SCE and without SCE.

Variables	All population (n = 166)	SCE group (n = 26)	No SCE group (n = 140)	P-value
Sex (M/F)	100/66	12/14	88/52	0.110
Age (years)	61.03 ± 9.58	61.96 ± 8.92	60.86 ± 9.72	0.591
BMI (kg/m^2)	24.64 ± 2.57	25.52 ± 2.79	24.44 ± 2.49	0.057
AF type				
Paroxysmal AF/Persistent AF	110/56	017/9	93/47	0.918
AF duration time (month)	24	24	24	0.365
CHA_2DS_2-VASc score	2.48 ± 1.58	3.31 ± 1.64	2.32 ± 1.52	0.003
Cardioversion (Y/N)	56/110	10/16	46/94	0.579
ACT during procedure (seconds)	285.90 ± 14.94	289.96 ± 15.73	285.15 ± 14.73	0.132
LAD (mm)	37.93 ± 5.76	36.08 ± 6.49	38.28 ± 5.57	0.073
EF (%)	60.67 ± 5.68	58.62 ± 5.75	61.05 ± 5.60	0.044
Heart Function Class (NYHA)	1.16 ± 0.38	1.08 ± 0.27	1.17 ± 0.40	0.251
Comorbidity (*n*)				
HTN	76	14	62	0.369
CAD	34	4	30	0.603
DM	19	3	16	1.000
Dyslipidemia	4	0	4	1.000
Hyperthyroidism	5	2	3	0.128
CVA/TIA history	8	4	4	0.022
Others	13	2	11	0.977
Absence of underlying diseases (n)	44	7	37	1.000
Lab examinations				
BUN (mmol/L)	5.35 ± 1.52	5.47 ± 1.48	5.33 ± 1.53	0.669
Cr (mmol/L)	72.53 ± 18.76	64.59 ± 17.75	74.01 ± 18.63	0.018
FBG (mmol/L)	5.29 ± 1.44	5.58 ± 1.01	5.23 ± 1.50	0.254
TC (mmol/L)	4.24 ± 0.93	4.14 ± 0.95	4.26 ± 0.92	0.541
LDL (mmol/L)	2.41 ± 0.81	2.43 ± 0.75	2.40 ± 0.83	0.866
TG (mmol/L)	1.89 ± 1.36	1.85 ± 0.95	1.89 ± 1.42	0.893

The data are presented as the mean ± SD or n (%). LAD, left atrial diameter; EF, ejection fraction; HTN, hypertension; CAD, coronary artery disease; DM, diabetes mellitus; BUN, blood urea nitrogen; Cr, creatinine; FBG, fasting blood glucose; TC, total cholesterol; LDL, low density lipoprotein; TG, triglyceride; CVA, cerebrovascular accident; TIA, transient ischemic attack; Y, yes; N, no; Absence of underlying diseases, refers to patients with no other cardiovascular co-morbidity or no other co-morbidities at all.

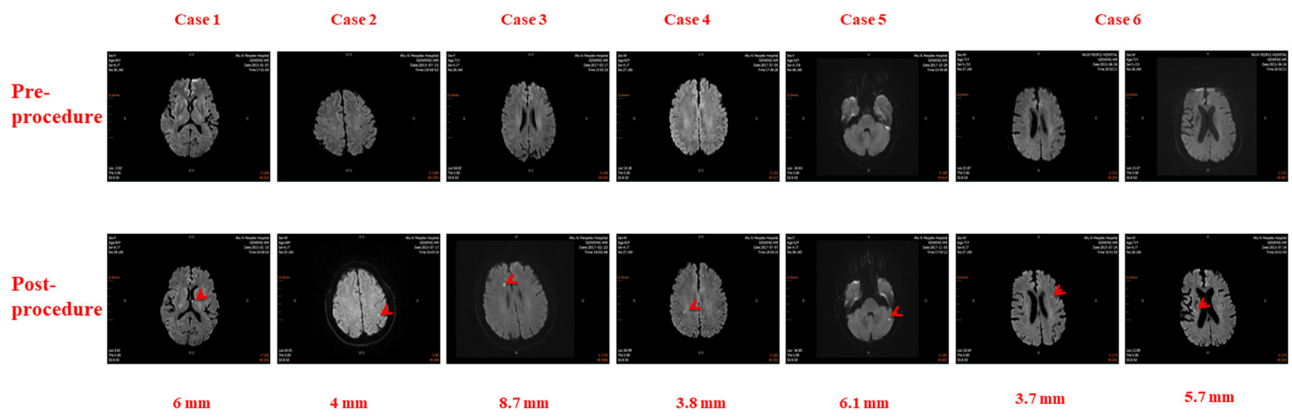

FIGURE 1 | Cerebral Magnetic Resonance Images in six patients before and after Atrial Fibrillation Ablation using Magnetic Navigation System: Case 1: Left thalamus (6 mm), Case 2: Left parietal lobe (4 mm), Case 3: Right frontal lobe (8.7 mm), Case 4: Right parietal lobe (3.8 mm), Case 5: Left cerebellum (6.1 mm), Case 6: Left frontal lobe (3.7 mm) and Right corona radiata (5.7 mm).

TABLE 3 | Localization, number and size of SCE in 26 patients.

Case	Group	Location	Size (mm)
1	RMN	Left thalamus	6
2	RMN	Left parietal lobe	4
3	RMN	Right frontal lobe	8.7
4	RMN	Right parietal lobe	3.8
5	RMN	Left cerebellum	6.1
6	RMN	Left frontal lobe/Right corona radiata	3.7/5.7
7	MC	Left occipital lobe	13
8	MC	Left frontal lobe	3.5
9	MC	Right parietal lobe	8.6
10	MC	Left cerebellum	7.3
11	MC	Right occipital lobe	3.6
12	MC	Right frontal lobe	1.9
13	MC	Right frontal lobe	3.6
14	MC	Left occipital lobe	9.3
15	MC	Left frontal lobe	6.5
16	MC	Right cerebellum	4.2
17	MC	Left frontal lobe/Right occipital lobe/Left occipital lobe	2.9/2.9/2.6
18	MC	Right insular lobe/Left frontal lobe	2.8/9.6
19	MC	Right frontal lobe	4.5
20	MC	Left occipital lobe	3
21	MC	Bilateral cerebellum	4.2/2.4
22	MC	Right occipital lobe	9.3
23	MC	Right parietal lobe/Left basal ganglia	5.2/10.8
24	MC	Right corona radiata	5
25	MC	Right occipital lobe	3
26	MC	Left parietal lobe	4

RMN, robotic magnetic navigation; MC, manual control.

were found in the temporal lobe, precentral/postcentral gyrus, or left/right hemisphere.

The sizes of cerebral embolisms were 5.37±2.81 (1.90–13.00) mm. Of the 32 SCEs, 8 (25.00%) were of small size (≤3 mm), 22 SCEs (68.75%) were medium size (3–10 mm), and 2 (6.25%) were large size (≥10 mm). There was no difference in sizes between the RMN and MC groups [5.43 ± 1.79 (3.70–8.70) mm and 5.35 ± 3.07 (1.90–13.00) mm, respectively ($t = 0.090$, $P > 0.05$)].

Risk Predictors of Silent Cerebral Embolism

Univariate logistic analysis demonstrated that ablation technology, CHA_2DS_2-VASc score, CVA/TIA history, and low ejection fraction were associated with SCEs ($P < 0.05$), however, multivariate logistic regression analysis demonstrated that ablation technology was the only independent risk factor for SCEs (odds ratio [OR] 7.78, 95% confidence interval [CI] 2.92-20.75, $P < 0.001$) (**Table 4**). Compared with MC ablation, AF ablation using RMN significantly reduced the incidence of SCE ($X^2 = 20.63$ $P < 0.001$).

DISCUSSION

Main Findings

AF ablation carries a low risk of symptomatic cerebral ischemia but is associated with a substantial risk of SCEs detectable with MRI. The incidence of SCEs after AF ablation is affected by different ablation technologies; however, it has not been previously reported for patients undergoing AF ablation using RMN. To the best of our knowledge this is the first prospective study of this kind. The main findings are that: (1) AF ablation using RMN significantly reduced the incidence of SCEs after AF ablation procedures; (2) Ablation technology, CHA_2DS_2-VASc score, CVA/TIA history, and low ejection fraction were associated with SCEs in AF ablation patients; (3) SCEs were mainly located in the frontal lobe, occipital lobe, and parietal lobe; and the sizes of SCEs were not observed to differ significantly between RMN ablation and MC ablation groups.

Definition and Incidence of Silent Cerebral Embolism

Since the first description of SCEs in patients after AF ablation in 2006 (7), SCEs have been widely reported (5, 21, 22). SCE is now defined as ≥1 cerebral infarctions of hypointense lesions on T1-weighted images and hyperintense lesions on T2-weighted images of cerebral MRI, without a history of corresponding stroke or TIA (21). Incidence of SCEs after AF ablation ranges from 1 to ∼40% depending on the different risk factors (23, 24). Gaita et al. (25) assessed the thromboembolic risk with preprocedural and postprocedural cerebral MRI, either silent or clinically manifest, in the context of AF ablation, and found AF ablation carried a low risk of symptomatic cerebral ischemia (0.4%) but was associated with a substantial risk of SCEs (14%) as detected on cerebral MRI. Ichiki et al. (26) investigated the incidence of cerebral thromboembolism after complex fractionated atrial electrogram ablation with or without PVI and found the incidence of cerebral thromboembolism after PVI ranges from 2 to 14%. The prevalence has been reported from 6.8 to 38.4% for patients ablated with irrigated-tip radiofrequency catheters (21, 27). Cerebral thromboembolism can be found using high-resolution DW-MRI after AF ablation (28, 29). In this study, we explored the incidence of SCEs in AF ablation using RMN and found that the incidence of SCEs in the RMN group was only 5.77% as compared to 32.26% in the MC group, suggesting that AF ablation using RMN can significantly reduce the incidence of SCEs after procedures.

Localization, Number and Size of Silent Cerebral Embolism

FLAIR-MRI usually reveals pre-existing cerebral lesions, while DW-MRI demonstrates new SCEs (28, 29). Therefore, we used DW-MRI to evaluate SCEs in this study, and found SCEs were generally distributed throughout the brain, and often involved in the cerebral cortex and cerebellum (20, 22). In our study, we

TABLE 4 | Risk factors of silent cerebral embolism after pulmonary vein isolation in atrial fibrillation ablation.

Variable	Univariate analysis	Multivariate analysis			
	P-value	Wald	Odds ratio	95% CI	*P-value*
Sex	0.110				
Age	0.588				
BMI	0.120				
AF type	0.918				
AF duration	0.419				
CHA_2DS_2-VASc score	0.003				
Cardioversion	0.579				
ACT	0.130				
LA diameter	0.072				
Heart functional class	0.244				
EF	0.044				
Ablation technology	0.000	16.785	7.778	2.915–20.751	0.000
Underlying diseases					
HTN	0.369				
CAD	0.483				
DM	0.987				
Dislipidemia	0.383				
Hyperthyroidism	0.128				
CVA/TIA history	0.006				

BMI, body mass index; AF, atrial fibrillation; ACT, activated clotting time; LA diameter, left atrial diameter; EF, ejection fraction; HTN, hypertension; CAD, coronary artery disease; DM, diabetes mellitus; CVA, cerebrovascular accident; TIA, transient ischemic attack.

also found most SCEs were located in the lobes of the cortex, but that SCEs were also observed in the left thalamus, right insular lobe and left basal ganglia. Previous studies have demonstrated that SCEs were generally small in size, and most SCEs observed acutely after AF ablation procedures were ≤10 mm in diameter (20, 30). In Deneke et al. (30) 52% of the lesions were small (≤3 mm), 42% were medium (4 to 10 mm) and 6% were of large diameter >10 mm. However, in our study, 68.75% of lesions were medium (3 to 10 mm), 25.00% were small (≤3 mm), and 6.25% were large (≥10 mm). Furthermore, the sizes of SCEs were almost the same between the two groups. We compared our patients' data and ablation procedure with Deneke et al. and found that CHA2DS2-VASc scores in our population were much higher than those in the Deneke et al. population. Additionally, ACTs in our study were shorter than those in the Deneke et al. study, which may be two important causes for the difference in SCE sizes.

Potential Risk Factors for Silent Cerebral Embolism

SCE is a potential serious complication during AF ablation and 10 times more common than clinical stroke (31). Though patients with SCEs often experience no immediate neurological symptoms, many studies have demonstrated that incurring cerebral acute lesions as a result of PVI may be associated with longer-term adverse neuropsychological outcomes such as an increased risk of stroke and cognitive impairment (32). Therefore, it is of great clinical importance to investigate the risk factors of SCEs associated with AF ablation in an attempt to reduce SCEs (23).

Schrickel et al. (33) showed that coronary artery disease, left ventricular dilation, and hypertrophy were potential risk predictors of SCEs. Martinek et al. (34) found that a variety of different clinical and procedural factors seemed to contribute to the risk of SCEs. Clinical parameters showing a significant correlation with SCEs in univariate analysis were age, persistent AF, and spontaneous echo contrast in transesophageal echocardiography. Significant procedural parameters were electric cardioversion, PVI only, and ablation of complex atrial electrograms. Independent risk factors in multivariate analysis were age, spontaneous echo contrast and ablation of complex atrial electrograms.

Previous studies also confirmed that procedural ACT and performing cardioversion during the procedures were the risk predictors of post-AF ablation SCEs (26, 35). ACT levels of >300 s have been recommended to better reduce thromboembolic risk (36, 37). A 2.75-fold increase in the risk of subclinical cerebral embolism was related to periprocedural cardioversion (26). Pianelli et al. (38) suggested that delaying electrical cardioversion until after a 4-week anticoagulation period could reduce the risk of SCEs and is a viable and safer option in patients for which the ablation procedure does not result in acute termination of AF. However, the association between brain lesions and periprocedural cardioversion is not fully resolved as evident in other studies (20, 39, 40). In our study, ACT was maintained at >250 s and one-half of patients underwent cardioversion in the RMN group.

Although the percentage of patients requiring cardioversion was much higher in the MC group, our finding is that ACT

and cardioversion are not major contributors to SCEs in this study.

Another important risk factor of SCEs is AF ablation technology. Different technologies can have varying effects on the incidence of SCEs. The incidence of SCEs after AF ablation may change according to the technology used (25). Herrera Siklódy et al. (9) compared the safety of different devices by screening for SCEs after AF ablation with either conventional irrigated radiofrequency, cryoballoon, or multielectrode phased radiofrequency pulmonary vein ablation catheter (PVAC). The incidence of SCEs in the irrigated radiofrequency group, cryoballoon group and PVAC group were 7.4, 4.3, and 37.5%, respectively. In another study, the incidence of SCEs after AF ablation differed depending on the technology used: PVAC increased the risk of SCEs 1.48 times compared to irrigated radiofrequency and cryoballoon ablation (25). It is currently clear that the prevalence of SCEs after AF ablation is related to ablation technologies (9, 22, 35, 41, 42), and therefore in this study, we investigated the incidence of SCEs in AF patients using RMN.

Analyzing the baseline clinical characteristics of the study population, we found that there were significant differences in age, CHA_2DS_2-VASc score, cardioversion, left atrial diameter, ejection fraction, NYHA heart function class and CVA/TIA history between two groups (**Table 1**), but when we compared the characteristics of patients with and without SCEs, we found that there were only statistical differences in CHA_2DS_2-VASc score, ejection fraction and CVA/TIA history between the two groups, though the range of ejection fraction in both groups was approximately 55–65%, which is normal, the clinical significance of this value is questionable (**Table 2**). To investigate the potential risk factors of SCEs, we first performed univariate logistic regression which indicated that ablation technology, CHA_2DS_2-VASc score, CVA/TIA history and low ejection fraction were significantly associated with SCEs. In a multivariate logistic regression analysis model, when ablation technology, CHA_2DS_2-VASc score, ejection fraction and CVA/TIA history were included as the controlling variables, we found that ablation technology (MC ablation) was the only independent risk factor of SCEs, with an odds ratio of 7.778.

Mechanisms of Silent Cerebral Embolism

In 2003, SCE was first reported in patients with valvular aortic stenosis who underwent retrograde catheterization of the aortic valve and had 22% silent ischemic brain lesions (43). In 2006, SCE was first reported in patients undergoing AF ablation (7). In the years that have passed, the mechanisms of SCE associated with AF ablation are not yet fully understood (27, 44). The genesis of SCE appears to be multifactorial (24), and in recent years, several probable embolic sources have been considered such as: (1) gaseous emboli entrapped within the sheath during catheter insertion or extraction; (2) particulate emboli (so-called char) as a result of denaturation of tissue; (3) regional micro-thrombi formed at the ablation site; (4) micro-thrombi inside the sheath or other artificial instruments; and (5) gaseous emboli formed during heating of blood.

In 2011, Boersma (45) commented "no bubbles, no troubles" when reflecting on the mechanism of SCEs after AF ablation, suggesting that if no bubbles appeared during an AF ablation procedure, then there would be no SCEs (troubles). Nagy-Balón et al. (46) compared the occurrence of bubble formation seen on intracardiac echocardiography and the microembolic signals detected by transcranial Doppler on the use of different ablation technologies and found that most of these microemboli are gaseous in nature. Previous animal studies also have demonstrated that direct arterial injection of gaseous material similar to that generated by AF ablation can recreate SCEs seen in patients post-procedure (44). The second largest source of gaseous emboli in the animal model was found to be introduction of air into the left atrium via the sheaths during catheter insertion and removal (40). Air microemboli may be introduced into the blood stream through sheaths and catheters or may develop during ablation as a result of blood boiling during AF ablation (42).

Thrombus formation during and after AF ablation might result from platelet and coagulation system activation either directly at the catheter surface or at the site of endothelial application (42). The exact mechanisms of SCEs after AF ablation are unknown, as is the precise composition of the microemboli which generate microembolic signals. The possibilities include thrombus, coagulum/char, air, or steam (47). Risk factors associated with increased incidence of SCEs involve patient-specific, technology-associated and procedural determinants (25). It is currently clear that the prevalence of SCEs following AF ablation is related to ablation technology (9, 22, 38, 39).

Possible Mechanisms of Decreased Incidence of SCE in AF Ablation Using RMN

The exact mechanisms of SCEs after AF ablation are still unknown, and we do not yet know the precise composition of the microembolic signals (47). However, it is commonly accepted that the increased thrombotic risk is due to intraprocedural introduction of gaseous microbubbles into the left atrium, thrombus formation within the lumens of long sheaths, char formation on the ablation catheter tip, and the potential for thrombus formation on the ablated atrial endocardium (48). Furthermore, the technology used for ablation does seem important as demonstrated by phased radiofrequency ablation more often resulting in observing abnormalities on cerebral MRI (25, 26), however, AF ablation using a novel gold tip resulted in SCEs in approximately only one out of 10 patients (49). The mechanisms of decreased incidence of SCEs in AF ablation using RMN may be as follows:

AF Ablation Using RMN Reduces Gaseous Microbubbles

The study of Nagy-Baló indicated that 80% of the microemboli are gaseous, suggesting that gaseous microbubbles may be more prevalent during AF ablation procedures (47). More aggressive anticoagulation reduced but did not eliminate the occurrence of microembolic signals, supporting the hypothesis that thrombus only accounts for a minority of the particulate embolic burden (46). Air embolisms are the main mechanism

of SCEs, which has also been confirmed after second-generation cryoballoon ablation procedures (50). Air embolisms may be related to the introduction of ablation devices (51, 52). Multiple intraprocedural exchanges of catheters have a major impact on the risk for SCEs. When exchanging catheters in transseptal sheaths, gaseous emboli can be entrapped within the sheath during catheter insertion or removal.

Regarding AF ablation using RMN, when an AF ablation procedure is performed, only one Swartz sheath is inserted into the right femoral vein, and fixed on a computer-controlled catheter advancing system (QuikCAS, Niobe Stereotaxis, St. Louis, MO, USA). There is no relative movement between the sheath and the femoral vein, and no exchange of catheter during the entire AF ablation procedure. However, a double transseptal puncture is needed and two Swartz sheaths are placed in the left atrium when MC ablation is performed. Multiple catheter exchanges to facilitate the catheter ablation of pulmonary vein isolation during a MC ablation procedure may introduce gaseous microbubbles to the left atrium, which could lead to greater SCE formation.

Single Sheath in Left Atrium Reduces Clot Formation

In addition to air/gas embolism, clot formation is one of the main causes of SCE origin during AF ablation (53). Many studies have confirmed that the more sheaths or other artificial instruments in the left atrium, the more micro-thrombi will appear, leading to more SCE formation. When AF ablation using RMN is performed, only one Swartz sheath and one ablation catheter enter the left atrium (14). However, when MC ablation is performed, a double transseptal puncture is utilized, and two Swartz sheaths and other mapping catheters like a Lasso or Pentaray catheter (Biosense Webster, Inc., Diamond Bar, CA) are placed in the left atrium. Micro-thrombi may be formed inside the sheaths or other artificial instruments.

Uniquely Flexible RMN Catheter Reduces Char Formation and Complications

Microparticles, so-called char resulting from tissue denaturation, are also one of the main causes of SCE origin during AF ablation (27, 40, 53). Char formation may be induced by the energy source and / or catheter tip pressure on the tissue (53). Techniques and technologies to reduce excess char embolism have helped to reduce SCE prevalence, suggesting that char formation is a common perpetrator (47).

The RMN catheter's uniquely flexible shaft provides increased safety as well as equivalent or superior efficacy (54, 55). These results are achieved due to the catheter's atraumatic design, superior reach, and tip stability on the myocardium.

Bhaskaran et al. (55) performed an experimental study to compare lesion dimensions and evaluate the effect of heart wall motion in a myocardial phantom using RMN vs. MC. They found that similar lesion dimensions were observed in the stationary model; however, the lesion dimensions were more focal and deeper with RMN compared to MC in the presence of simulated wall motion, demonstrating greater catheter stability in the RMN group. During motion, the manual catheter slid across the surface 5.5 mm while the magnetic catheter maintained stable focal contact. A sliding catheter requires more total energy delivery to achieve an effective lesion at the target site. Therefore, the RMN catheter's stability may be a factor in reducing tip char formation during AF ablation procedure.

Study Limitations

There are at least three limitations in this study. First, this study is a prospective but non-randomized trial. However, between the two groups there were few significant differences in either the baseline characteristics or the characteristics of patients with SCEs and without SCEs. Second, this novel research was designed to be a pilot study analyzing the incidence of SCEs using RMN and thus contributing important information regarding the effect of ablation technologies and techniques on SCEs. The incidence of SCEs in the RMN group is significantly lower than in the MC group, however, the results must be interpreted acknowledging that the sample size was smaller in the MC group, and therefore a larger, multi-center, prospective study may be warranted. Finally, the exact mechanisms of decreased SCEs using RMN ablation remain elusive. The three main mechanisms we provided in the discussion are the probable mechanisms, and the use of intracardiac ultrasound in further studies may help us to delineate more exact mechanisms.

CONCLUSIONS

AF ablation carries a low risk of symptomatic cerebral ischemia but is associated with a substantial risk of SCEs. Ablation technology, CHA_2DS_2-VASc score, CVA/TIA history, and low ejection fraction are associated with SCEs after AF ablation procedure. However, ablation technology is the only independent risk factor of SCEs and RMN can significantly reduce the incidence of SCEs resulting from AF ablation.

DATA AVAILABILITY STATEMENT

The original contributions presented in the study are included in the article/**Supplementary Material**, further inquiries can be directed to the corresponding author/s.

ETHICS STATEMENT

The studies involving human participants were reviewed and approved by 1. Wuxi People's Hospital Affiliated to Nanjing Medical University; 2. Xuzhou Central Hospital; 3. First Hospital Affiliated to Soochow University. The patients/participants provided their written informed consent to participate in this study.

AUTHOR CONTRIBUTIONS

RXW, YY, BH, and TBJ contributed to the design of study, analysis, and interpretation of data for the publication, writing of the manuscript, and the final approval of the manuscript. KLL, XYL, and XXZ contributed to performing the procedures of atrial fibrillation. QFT, CYZ, and ZMY performed the analysis of MRI images. MW and SPD contributed to the acquisition and statistical analysis of data for the study. All authors contributed

to the manuscript revision and reading and approved the submitted version.

FUNDING

This study was supported in part by grants from the National Natural Science Foundation of China (81770331), Natural Science Foundation of Jiangsu Province (BK20151110), and Chinese Cardiovascular Association V.G foundation (grant number: 2017-CCA-VG-040).

SUPPLEMENTARY MATERIAL

The Supplementary Material for this article can be found online at: https://www.frontiersin.org/articles/10.3389/fcvm.2021.777355/full#supplementary-material

REFERENCES

1. Camm AJ, Kirchhof P, Lip GY, Schotten U, Savelieva I, Ernst S, et al. ESC Committee for Practice Guidelines. Guidelines for the management of atrial fibrillation: the Task Force for the Management of Atrial Fibrillation of the European Society of Cardiology (ESC). *Europace.* (2010) 12:1360–420. doi: 10.1093/europace/euq350
2. Madhavan M, Graff-Radford J, Piccini JP, Gersh BJ. Cognitive dysfunction in atrial fibrillation. *Nat Rev Cardiol.* (2018) 15:744–56. doi: 10.1038/s41569-018-0075-z
3. Cappato R, Calkins H, Chen SA, Davies W, Iesaka Y, Kalman J, et al. Updated worldwide survey on the methods, efficacy, and safety of catheter ablation for human atrial fibrillation. *Circ Arrhythm Electrophysiol.* (2010) 3:32–8. doi: 10.1161/CIRCEP.109.859116
4. Gautam S, John RM, Stevenson WG, Jain R, Epstein LM, Tedrow U, et al. Effect of therapeutic INR on activated clotting times, heparin dosage, and bleeding risk during ablation of atrial fibrillation. *J Cardiovasc Electrophysiol.* (2011) 22:248–54. doi: 10.1111/j.1540-8167.2010.01894.x
5. Sugioka K, Takagi M, Sakamoto S, Fujita S, Ito A, Iwata S, et al. Predictors of silent brain infarction on magnetic resonance imaging in patients with nonvalvular atrial fibrillation: a transesophageal echocardiographic study. *Am Heart J.* (2015) 169:783–90. doi: 10.1016/j.ahj.2015.03.016
6. Keçe F, Bruggemans EF, de Riva M, Alizadeh Dehnavi R, Wijnmaalen AP, Meulman TJ, et al. Incidence and clinical significance of cerebral embolism during atrial fibrillation ablation with duty-cycled phased-radiofrequency versus cooled-radiofrequency: a randomized controlled trial. *JACC Clin Electrophysiol.* (2019) 5:318–26. doi: 10.1016/j.jacep.2018.11.008
7. Lickfett L, Hackenbroch M, Lewalter T, Selbach S, Schwab JO, Yang A, et al. Cerebral diffusion-weighted magnetic resonance imaging: a tool to monitor the thrombogenicity of left atrial catheter ablation. *J Cardiovasc Electrophysiol.* (2006) 17:1–7. doi: 10.1111/j.1540-8167.2005.00279.x
8. Sorgente A, Ceccarelli A, Cappato R. Silent cerebral embolism and new technologies for catheter ablation of atrial fibrillation: time to take a deep breath. *J Cardiovasc Electrophysiol.* (2013) 24:22–3. doi: 10.1111/jce.12016
9. Herrera Siklódy C, Deneke T, Hocini M, Lehrmann H, Shin DI, Miyazaki S, et al. Incidence of asymptomatic intracranial embolic events after pulmonary vein isolation: comparison of different atrial fibrillation ablation technologies in a multicenter study. *J Am Coll Cardiol.* (2011) 58:681–8. doi: 10.1016/j.jacc.2011.04.010
10. Nakamura K, Sasaki T, Take Y, Minami K, Inoue M, Asahina C, et al. Incidence and characteristics of silent cerebral embolisms after radiofrequency-based atrial fibrillation ablation: a propensity score-matched analysis between different mapping catheters and indices for guiding ablation. *J Cardiovasc Electrophysiol.* (2021) 32:16–26. doi: 10.1111/jce.14800
11. Bassil G, Markowitz SM, Liu CF, Thomas G, Ip JE, Lerman BB, et al. Robotics for catheter ablation of cardiac arrhythmias: current technologies and practical approaches. *J Cardiovasc Electrophysiol.* (2020) 31:739–52. doi: 10.1111/jce.14380
12. Rillig A, Meyerfeldt U, Tilz RR, Talazko J, Arya A, Zvereva V, et al. Incidence and long-term follow-up of silent cerebral lesions after pulmonary vein isolation using a remote robotic navigation system as compared with manual ablation. *Circ Arrhythm Electrophysiol.* (2012) 5:15–21. doi: 10.1161/CIRCEP.111.967497
13. Lin C, Pehrson S, Jacobsen PK, Chen X. Initial experience of a novel mapping system combined with remote magnetic navigation in the catheter ablation of atrial fibrillation. *J Cardiovasc Electrophysiol.* (2017) 28:1387–92. doi: 10.1111/jce.13332
14. Zhao XX, Li KL, Wang RX, Zheng J, Liu XY, Dang SP, et al. Comparisons of efficacy, safety, and recurrence risk factors of paroxysmal and persistent atrial fibrillation catheter ablation using robotic magnetic navigation system. *Clin Cardiol.* (2019) 42:418–24. doi: 10.1002/clc.23156
15. Kataria V, Berte B, Vandekerckhove Y, Tavernier R, Duytschaever M. Remote magnetic versus manual navigation for radiofrequency ablation of paroxysmal atrial fibrillation: long-term, controlled data in a large cohort. *Biomed Res Int.* (2017) 2017:6323729. doi: 10.1155/2017/6323729
16. Jia K, Jin Q, Liu A, Wu L. Remote magnetic navigation versus manual control navigation for atrial fibrillation ablation: a systematic review and meta-analysis. *J Electrocardiol.* (2019) 55:78–86. doi: 10.1016/j.jelectrocard.2019.05.001
17. Ghadban R, Gifft K, Luebbering Z, Sodhi S, Cooper D, Enezate T. Radiofrequency atrial fibrillation ablation with irrigated tip catheter using remote magnetic navigation compared with conventional manual method. *J Interv Card Electrophysiol.* (2020) 62:95–102. doi: 10.1007/s10840-020-00879-8
18. Elisabeth Noten AM, Kis Z, Akca F, Bhagwandien R, Wijchers S, Yap SC, et al. Robotic navigation shows superior improvement in efficiency for atrial fibrillation ablation. *J Atr Fibrillation.* (2019) 11:2108. doi: 10.4022/jafib.2108
19. Virk SA, Kumar S. Remote magnetic versus manual catheter navigation for atrial fibrillation ablation: a meta-analysis. *Circ Arrhythm Electrophysiol.* (2019) 12:e007517. doi: 10.1161/CIRCEP.119.007517
20. Haeusler KG, Koch L, Herm J, Kopp UA, Heuschmann PU, Endres M, et al. 3 Tesla MRI-detected brain lesions after pulmonary vein isolation for atrial fibrillation: results of the MACPAF study. *J Cardiovasc Electrophysiol.* (2013) 24:14–21. doi: 10.1111/j.1540-8167.2012.02420.x
21. Gaita F, Anselmino M. Silent cerebral events during catheter ablation for atrial fibrillation: not yet to be forgotten. *JACC Clin Electrophysiol.* (2018) 4:1610–2. doi: 10.1016/j.jacep.2018.08.023
22. Miki K, Nakano M, Aizawa K, Hasebe Y, Kimura Y, Morosawa S, et al. Risk factors and localization of silent cerebral infarction in patients with atrial fibrillation. *Heart Rhythm.* (2019) 16:1305–13. doi: 10.1016/j.hrthm.2019.03.013
23. Deneke T, Nentwich K, Krug J, Müller P, Grewe PH, Mügge A, et al. Silent cerebral events after atrial fibrillation ablation - overview and current data. *J Atr Fibrillation.* (2014) 6:996. doi: 10.4022/jafib.996
24. Gaita F, Leclercq JF, Schumacher B, Scaglione M, Toso E, Halimi F, et al. Incidence of silent cerebral thromboembolic lesions after atrial fibrillation ablation may change according to technology used: comparison of irrigated radiofrequency, multipolar nonirrigated catheter and cryoballoon. *J Cardiovasc Electrophysiol.* (2011) 22:961–8. doi: 10.1111/j.1540-8167.2011.02050.x
25. Gaita F, Caponi D, Pianelli M, Scaglione M, Toso E, Cesarani F, et al. Radiofrequency catheter ablation of atrial fibrillation: a cause of silent thromboembolism? Magnetic resonance imaging assessment of cerebral thromboembolism in patients undergoing ablation of atrial fibrillation. *Circulation.* (2010) 122:1667–73. doi: 10.1161/CIRCULATIONAHA.110.937953
26. Ichiki H, Oketani N, Ishida S, Iriki Y, Okui H, Maenosono R, et al. Incidence of asymptomatic cerebral microthromboembolism after atrial fibrillation ablation guided by complex fractionated atrial electrogram. *J Cardiovasc Electrophysiol.* (2012) 23:567–73. doi: 10.1111/j.1540-8167.2011.02259.x
27. Nakamura T, Okishige K, Kanazawa T, Yamashita M, Kawaguchi N, Kato N, et al. Incidence of silent cerebral infarctions after catheter ablation of atrial fibrillation utilizing the second-generation cryoballoon. *Europace.* (2017) 19:1681–8. doi: 10.1093/europace/euw191

28. von Bary C, Deneke T, Arentz T, Schade A, Lehrmann H, Eissnert C, et al. Silent cerebral events as a result of left atrial catheter ablation do not cause neuropsychological sequelae–a MRI-controlled multicenter study. *J Interv Card Electrophysiol.* (2015) 43:217–26. doi: 10.1007/s10840-015-0004-6
29. Yu Y, Wang X, Li X, Zhou X, Liao S, Yang W, et al. Higher incidence of asymptomatic cerebral emboli after atrial fibrillation ablation found with high-resolution diffusion-weighted magnetic resonance imaging. *Circ Arrhythm Electrophysiol.* (2020) 13:e007548. doi: 10.1161/CIRCEP.119.007548
30. Deneke T, Shin DI, Balta O, Bünz K, Fassbender F, Mügge A, et al. Postablation asymptomatic cerebral lesions: long-term follow-up using magnetic resonance imaging. *Heart Rhythm.* (2011) 8:1705–11. doi: 10.1016/j.hrthm.2011.06.030
31. Healey JS, Nair GM. Does catheter ablation for atrial fibrillation increase or reduce neurological insult? *Curr Opin Cardiol.* (2012) 27:36–40. doi: 10.1097/HCO.0b013e32834d846a
32. Neumann T, Kuniss M, Conradi G, Janin S, Berkowitsch A, Wojcik M, et al. MEDAFI-Trial (Micro-embolization during ablation of atrial fibrillation): comparison of pulmonary vein isolation using cryoballoon technique vs. radiofrequency energy. *Europace.* (2011) 13:37–44. doi: 10.1093/europace/euq303
33. Schrickel JW, Lickfett L, Lewalter T, Mittman-Braun E, Selbach S, Strach K, et al. Incidence and predictors of silent cerebral embolism during pulmonary vein catheter ablation for atrial fibrillation. *Europace.* (2010) 12:52–7. doi: 10.1093/europace/eup350
34. Martinek M, Sigmund E, Lemes C, Derndorfer M, Aichinger J, Winter S, et al. Asymptomatic cerebral lesions during pulmonary vein isolation under uninterrupted oral anticoagulation. *Europace.* (2013) 15:325–31. doi: 10.1093/europace/eus329
35. Verma A, Debruyne P, Nardi S, Deneke T, DeGreef Y, Spitzer S, et al. Evaluation and reduction of asymptomatic cerebral embolism in ablation of atrial fibrillation, but high prevalence of chronic silent infarction: results of the evaluation of reduction of asymptomatic cerebral embolism trial. *Circ Arrhythm Electrophysiol.* (2013) 6:835–42. doi: 10.1161/CIRCEP.113.000612
36. Calkins H, Kuck KH, Cappato R, Brugada J, Camm AJ, Chen SA, et al. 2012 HRS/EHRA/ECAS expert consensus statement on catheter and surgical ablation of atrial fibrillation: recommendations for patient selection, procedural techniques, patient management and follow-up, definitions, endpoints, and research trial design. *Heart Rhythm.* (2012) 9:632–96. doi: 10.1016/j.hrthm.2011.12.016
37. Forleo GB, Della Rocca DG, Lavalle C, Mantica M, Papavasileiou LP, Ribatti V, et al. A patient with asymptomatic cerebral lesions during AF ablation: how much should we worry? *J Atr Fibrillation.* (2016) 8:1323. doi: 10.4022/jafib.1323
38. Pianelli M, Scaglione M, Anselmino M, Caponi D, Garcia P, Cesarani F, et al. Delaying cardioversion following 4-week anticoagulation in case of persistent atrial fibrillation after a transcatheter ablation procedure to reduce silent cerebral thromboembolism: a single-center pilot study. *J Cardiovasc Med.* (2011) 12:785–9. doi: 10.2459/JCM.0b013e32834ba0eb
39. Wissner E, Metzner A, Neuzil P, Petru J, Skoda J, Sediva L, et al. Asymptomatic brain lesions following laserballoon-based pulmonary vein isolation. *Europace.* (2014) 16:214–9. doi: 10.1093/europace/eut250
40. Di Biase L, Gaita F, Toso E, Santangeli P, Mohanty P, Rutledge N, et al. Does periprocedural anticoagulation management of atrial fibrillation affect the prevalence of silent thromboembolic lesion detected by diffusion cerebral magnetic resonance imaging in patients undergoing radiofrequency atrial fibrillation ablation with open irrigated catheters? Results from a prospective multicenter study. *Heart Rhythm.* (2014) 11:791–8. doi: 10.1016/j.hrthm.2014.03.003
41. Scaglione M, Blandino A, Raimondo C, Caponi D, Di Donna P, Toso E, et al. Impact of ablation catheter irrigation design on silent cerebral embolism after radiofrequency catheter ablation of atrial fibrillation: results from a pilot study. *J Cardiovasc Electrophysiol.* (2012) 23:801–5. doi: 10.1111/j.1540-8167.2012.02298.x
42. Scaglione M, Caponi D, Anselmino M, Di Clemente F, Blandino A, Ferraris F, et al. Pulmonary vein isolation with a new multipolar irrigated radiofrequency ablation catheter (nMARQ^{TM}): feasibility, acute and short-term efficacy, safety, and impact on postablation silent cerebral ischemia. *J Cardiovasc Electrophysiol.* (2014) 25:1299–305. doi: 10.1111/jce.12500
43. Omran H, Schmidt H, Hackenbroch M, Illien S, Bernhardt P, von der Recke G, et al. Silent and apparent cerebral embolism after retrograde catheterisation of the aortic valve in valvular stenosis: a prospective, randomised study. *Lancet.* (2003) 361:1241–6. doi: 10.1016/S0140-6736(03)12978-9
44. Haines DE, Stewart MT, Barka ND, Kirchhof N, Lentz LR, Reinking NM, et al. Microembolism and catheter ablation II: effects of cerebral microemboli injection in a canine model. *Circ Arrhythm Electrophysiol.* (2013) 6:23–30. doi: 10.1161/CIRCEP.112.973461
45. Boersma LV. Silent cerebral ischemia after AF ablation: no bubbles, no troubles? *Heart Rhythm.* (2011) 8:1712–3. doi: 10.1016/j.hrthm.2011.07.009
46. Nagy-Baló E, Tint D, Clemens M, Beke I, Kovács KR, Csiba L, et al. Transcranial measurement of cerebral microembolic signals during pulmonary vein isolation: a comparison of two ablation techniques. *Circ Arrhythm Electrophysiol.* (2013) 6:473–80. doi: 10.1161/CIRCEP.112.971747
47. Haines DE. Asymptomatic cerebral embolism and atrial fibrillation ablation: what price victory? *Circ Arrhythm Electrophysiol.* (2013) 6:455–7. doi: 10.1161/CIRCEP.113.000539
48. Friedman DJ, Granger CB. Uninterrupted apixaban for atrial fibrillation ablation is a reasonable alternative, but what is the significance of silent cerebral infarctions? *Eur Heart J.* (2018) 39:2956–58. doi: 10.1093/eurheartj/ehy274
49. Schmidt B, Széplaki G, Merkely B, Kautzner J, van Driel V, Bourier F, et al. Silent cerebral lesions and cognitive function after pulmonary vein isolation with an irrigated gold-tip catheter: REDUCE-TE Pilot study. *J Cardiovasc Electrophysiol.* (2019) 30:877–85. doi: 10.1111/jce.13902
50. Boulding W, Glickman SW, Manary MP, Schulman KA, Staelin R. Relationship between patient satisfaction with inpatient care and hospital readmission within 30 days. *Am J Manag Care.* (2011) 17:41–8.
51. Kuwahara T, Takahashi A, Takahashi Y, Kobori A, Miyazaki S, Takei A, et al. Clinical characteristics of massive air embolism complicating left atrial ablation of atrial fibrillation: lessons from five cases. *Europace.* (2012) 14:204–8. doi: 10.1093/europace/eur314
52. Hinkle DA, Raizen DM, McGarvey ML, Liu GT. Cerebral air embolism complicating cardiac ablation procedures. *Neurology.* (2001) 56:792–4. doi: 10.1212/WNL.56.6.792
53. Anselmino M, Matta M, Toso E, Ferraris F, Castagno D, Scaglione M, et al. Silent cerebral embolism during atrial fibrillation ablation:Pathophysiology, prevention and management. *J Atr Fibrillation.* (2013) 6:796. doi: 10.4022/jafib.796
54. Bauernfeind T, Akca F, Schwagten B, de Groot N, Van Belle Y, Valk S, et al. The magnetic navigation system allows safety and high efficacy for ablation of arrhythmias. *Europace.* (2011) 13:1015–21. doi: 10.1093/europace/eur073
55. Bhaskaran A, Barry MA, Al Raisi SI, Chik W, Nguyen DT, Pouliopoulos J, et al. Magnetic guidance versus manual control: comparison of radiofrequency lesion dimensions and evaluation of the effect of heart wall motion in a myocardial phantom. *J Interv Card Electrophysiol.* (2015) 44:1–8. doi: 10.1007/s10840-015-0023-3

Conflict of Interest: The authors declare that the research was conducted in the absence of any commercial or financial relationships that could be construed as a potential conflict of interest.

frontiers in Cardiovascular Medicine

SYSTEMATIC REVIEW
published: 01 December 2021
doi: 10.3389/fcvm.2021.766088

Comparison of Drug-Coated Balloon Angioplasty vs. Drug-Eluting Stent Implantation for Drug-Eluting Stent Restenosis in the Routine Clinical Practice: A Meta-Analysis of Randomized Controlled Trials

Yong Zhu[1], Kesen Liu[1], Xiangyun Kong[2], Jing Nan[3], Ang Gao[1], Yan Liu[1], Hongya Han[1†], Hong Li[1], Huagang Zhu[1], Jianwei Zhang[1] and Yingxin Zhao[1*†]*

[1] Department of Cardiology, Beijing Anzhen Hospital, Capital Medical University, Beijing, China, [2] Department of Cardiology, Beijing Luhe Hospital, Capital Medical University, Beijing, China, [3] Department of Cardiology, Beijing Tiantan Hospital, Capital Medical University, Beijing, China

Introduction: In-stent restenosis (ISR) remains a challenging issue despite the great advance of drug-eluting stents (DES). In addition, the consensus was lacking regarding the optimal strategy for DES-ISR. Therefore, we aimed to evaluate angiographic and clinical outcomes of the two most effective treatments DES vs. drug-eluting balloon (DCB) for patients with DES-ISR.

Methods: This meta-analysis used the data from the randomized controlled trials (RCTs), which were identified by a systematic search in the databases of PubMed, Embase, and Cochrane Library. Target lesion revascularization (TLR) was regarded as the primary endpoint. In addition, the late angiographic outcomes and other clinical outcomes, namely, cardiac death, myocardial infarction (MI), target vessel revascularization, stent thrombosis, and major adverse cardiac events, were also included for analysis.

Results: Five RCTs with about 1,193 patients were included in this meta-analysis for the analysis. For the primary endpoint, the overall pooled outcomes suggested repeat DES implantation was associated with a significant reduction in the term of TLR compared with DCB angioplasty (risk ratio = 1.53, 95% CI 1.15–2.04, $p = 0.003$). But no significant difference in angiographic outcomes and other clinical endpoints were observed between DES and DCB. In the subgroup analysis, DCB was inferior to new-generation DES (NG-DES)/everolimus-eluting stent (EES) in the term of TLR. In addition, this non-significant trend was also noted in the subgroup of the paclitaxel-eluting stent (PES) vs. DCB. For the angiographic endpoints, EES, not PES, was associated with larger minimum lumen diameter [mean difference (MD) = −0.25, 95% CI −0.38 to −0.11, $p = 0.0003$], lower percent diameter stenosis (MD = 7.29%, 95% CI 2.86–11.71%, $p = 0.001$), and less binary restenosis (OR = 2.20, 95% CI 1.18–4.11, $p = 0.01$). But NG-DES/EES was comparable to DCB in cardiac death, MI, and stent thrombosis.

OPEN ACCESS

Edited by:
Xiaofeng Yang,
Temple University, United States

Reviewed by:
Emily Spangler,
University of Alabama at Birmingham, United States
Elisabetta Moscarella,
Universityof Campania Luigi Vanvitelli, Italy

***Correspondence:**
Hongya Han
hhy123100@163.com
Yingxin Zhao
zyingxinmi@163.com

† These authors have contributed equally to this work

Specialty section:
This article was submitted to Cardiovascular Therapeutics, a section of the journal Frontiers in Cardiovascular Medicine

Received: 28 August 2021
Accepted: 31 October 2021
Published: 01 December 2021

Citation:
Zhu Y, Liu K, Kong X, Nan J, Gao A, Liu Y, Han H, Li H, Zhu H, Zhang J and Zhao Y (2021) Comparison of Drug-Coated Balloon Angioplasty vs. Drug-Eluting Stent Implantation for Drug-Eluting Stent Restenosis in the Routine Clinical Practice: A Meta-Analysis of Randomized Controlled Trials. Front. Cardiovasc. Med. 8:766088. doi: 10.3389/fcvm.2021.766088

Conclusions: For the patients with DES-ISR, treatment with DES, especially NG-DES/EES could reduce the risk of TLR significantly compared to DCB at long-term follow-up.

Keywords: in-stent restenosis, drug-eluting stent, drug-eluting balloon, randomized controlled trial, target lesion revascularization

INTRODUCTION

Drug-eluting stents (DES) were widely used to treat ischemic coronary artery disease (CAD) and it has been recommended as the default choice in patients undergoing percutaneous coronary intervention (PCI) (1–3). Although the antirestenotic performance of DES improves significantly compared to bare-metal stents (BMS), 5–10% of patients treated with DES still suffer from restenosis, especially in complex clinical and anatomic settings (4, 5). Several previous studies also demonstrated patients treated for DES-in-stent restenosis (ISR) may have a worse long-term prognosis compared to these patients with BMS-ISR (6, 7). Therefore, DES restenosis after PCI has become an important and challenging issue in routine clinical practice.

With consistent improvement in the technique, various treatment strategies were performed and tested in those patients with DES-ISR, such as balloon angioplasty, cutting balloon, vascular brachytherapy, rotablation, DES implantation, drug-coated balloon (DCB) angioplasty, and excimer laser (8, 9). Among those strategies, repeat DES implantation and DCB angioplasty have been regarded as the most effective therapeutic options and recommended by current guidelines (Class I, Level A) (3). Although several randomized controlled trials (RCTs) have been designed to compare outcomes of DES vs. DCB in patients presenting with DES-ISR (10–14), few of them were powered for clinical endpoints indeed. In addition, the conclusions obtained from the RCTs were controversial and considerable heterogeneity existed in various aspects of those RCTs such as characteristic of participants, type of restenotic stent, and generation of DES used in the repeat stenting arm (10–14). Furthermore, recent strong pieces of evidence suggested the risk of death increased significantly beyond the 1st year in patients treated with paclitaxel-coated devices for peripheral artery disease (15), which raised concerns on DCB in the field of coronary intervention because almost all DCB used in the routine clinical practice were coated with paclitaxel.

Against this background, a comprehensive meta-analysis of RCTs was performed by us to investigate the angiographic and clinical outcomes of repeat DES vs. DCB angioplasty in patients presenting with DES-ISR.

Abbreviations: DES, drug-eluting stents; CAD, coronary artery disease; PCI, percutaneous coronary intervention; BMS, bare-metal stents; DCB, drug-coated balloon; RCTs, randomized controlled trials; TLR, target lesion revascularization; MI, myocardial infarction; TVR, target vessel revascularization; MACEs, major adverse cardiac events; MLD, minimum lumen diameter; DS%, percent diameter stenosis; LLL, late lumen loss; RR, risk ratio; MD, mean difference; CI, confidence interval; EES, everolimus-eluting stents; PES, paclitaxel-eluting stents; NG-DES, new-generation DES; SCB, sirolimus-coated balloon; BVS, bioresorbable vascular scaffolds.

METHODS

This meta-analysis was performed according to the preferred reporting items for systematic reviews and meta-analyses.

Literature Search

A systematic literature search was performed by us in the databases of PubMed, Embase, and Cochrane Library to identify all relevant articles published from inception to June 19, 2021. The three types of search terms (and their similar terms) used in this study were listed as follows: in-stent restenosis OR coronary stent restenosis OR stent restenosis OR restenosis OR ISR; drug-eluting stent OR drug eluting stent OR drug-coated stent OR drug coated stent OR everolimus-eluting stent OR everolimus eluting stent OR everolimus-coated stent OR everolimus coated stent OR zotarolimus-eluting stent OR zotarolimus eluting stent OR zotarolimus-coated stent OR zotarolimus coated stent OR sirolimus-eluting stent OR sirolimus eluting stent OR sirolimus-coated stent OR sirolimus coated stent OR paclitaxel-eluting stent OR paclitaxel eluting stent OR paclitaxel-coated stent OR paclitaxel coated stent OR DES OR EES OR ZES OR SES OR PES; drug-coated balloon OR drug coated balloon OR drug-eluting balloon OR drug eluting balloon OR paclitaxel-coated balloon OR paclitaxel coated balloon OR paclitaxel-eluting balloon OR paclitaxel eluting balloon OR sirolimus-coated balloon OR sirolimus coated balloon OR sirolimus-eluting balloon OR sirolimus eluting balloon OR DCB OR PCB OR SCB. In addition, the reference list of eligible studies and review articles were reviewed by us to identify additional publications as well.

Study Selection

Eligible studies were identified independently by two researchers (YZ and KSL) with the assistance of EndNote software according to the pre-specified PICOS criteria. The PICOS criteria were as follows: (1) patients: patients presenting with DES-ISR; (2) intervention: treatment with DCB; (3) comparison: repeat DES implantation; (4) outcomes: long-term ($\geq$1 year) clinical endpoints and/or follow-up angiographic endpoints; and (5) study design: RCTs.

Study Endpoints and Definitions

The primary endpoint was target lesion revascularization (TLR), which was defined as any revascularization procedure involving the target lesion. Other clinical outcomes, namely, cardiac death, myocardial infarction (MI), target vessel revascularization (TVR), stent thrombosis (definite or probable), and major

adverse cardiac events (MACEs), which was a composite of death, MI, and TLR, were considered as secondary endpoints. Notably, a composite of cardiac death, target vessel MI, and clinically driven TLR reported in the RCT BIOLUX was regarded as MACEs for final analysis.

For the angiographic endpoints, in-segment measurements (the treated area plus its 5 mm proximal/distal edges), namely, minimum lumen diameter (MLD), percent diameter stenosis (DS%), and late lumen loss (LLL) were adopted for the analysis. In addition, binary restenosis, which was defined as >50% diameter stenosis in the segment, was also determined for the analysis.

Data Extraction and Quality Assessment

The data extraction was performed by one author (YZ) with the standardized form recording the key items and verified by another researcher (XYK). For the included studies, the basic characteristics such as lead authors, publication years, period of recruitment, sample size, type of DCB/DES used, follow-up time, and reported outcomes were all collected. In addition to those, the clinical, lesion, procedural characteristics, and dual antiplatelet therapy (DAPT) protocol of the study population were also recorded by us.

Two independent researchers (YL and AG) were responsible for quality assessment. In addition, the quality of RCTs was assessed using revised Jadad's score, which is reliable and convenient. Notably, the discrepancies encountered in processes of study selection, data extraction, and quality assessment were resolved by discussion with the senior researcher (YXZ).

Statistical Analysis

The heterogeneity between included studies was assessed by the Cochrane Q test ($p < 0.1$ indicates significance) and I^2 statistic. When there was no significant heterogeneity across the studies ($p > 0.1$ and $I^2 < 50\%$), the principal measures risk ratio (RR) and mean difference (MD) with the corresponding 95% CI were calculated with the Mantel-Haenszel/inverse variance fixed-effects model. If significant heterogeneity was detected, the random-effects model was performed. In addition, sensitivity analysis or subgroup analysis was also performed approximately to further confirm the conclusions obtained. But the publication bias was not examined in this study because the eligible studies were limited (<10). All the statistical analyses included in this meta-analysis were performed using Review Manager version 5.3 (The Nordic Cochrane Center, Copenhagen, Denmark). In addition, $p < 0.05$ was considered as statistical significance.

RESULTS

Study Selection

As demonstrated in **Figure 1**, the search strategy used in this meta-analysis yielded 1,827 records, of which 1,501 records were left for screening after removing duplicates. After title and abstract screening, a total of 167 full-text articles were assessed for eligibility. In the end, eight articles from five RCTs were included for the final analysis after excluding 159 additional records by reviewing full-text articles (5, 10–14, 16, 17).

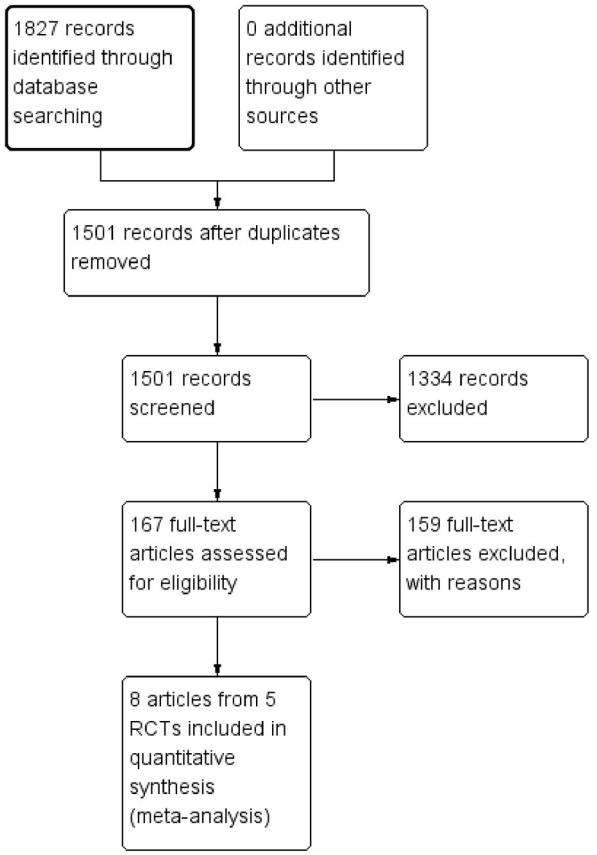

FIGURE 1 | The flow chart of study selection.

General Characteristics of Included Studies and Patients

As present in **Tables 1**, **2**, five multicenter RCTs (eight articles) with about 1,193 patients enrolled from 2009 to 2016 were finally included in this meta-analysis (5, 10–14, 16, 17). In addition, the included RCTs were published from 2013 to 2018. In those included studies, the angiographic follow-up period was 6–9 months, and the follow-up period for clinical outcomes ranges from 12 to 36 months. In addition to these contents, the primary endpoints/objective, inclusion criteria, and exclusion criteria of the eligible studies were also summarized and presented in **Table 2**.

According to data obtained from the included studies (**Table 3**), baseline demographics, lesion, procedure characteristics, and DAPT protocol (except RIBS IV) between the DCB and DES groups were similar. In addition, from **Table 3**, we should realize that almost no patients with target lesions located in the left main artery were included in those eligible RCTs.

DCB vs. DES for Angiographic Endpoints

In this meta-analysis, a total of 816 target lesions treated successfully by either DCB or DES were followed by angiography range from 6 to 9 months. Overall, no significant differences in

TABLE 1 | Main characteristics of the included studies.

References	Data source	Study design	Multicenter	Region	Investigation time	Total patient (lesion)		DCB type	DES type
		Study quality				DCB	DES		
Byrne et al. (10)	ISAR-DESIRE 3	RCT	Yes	Germany	2009–2011	268 (340)		PCB	PES
Kufner et al. (16)		5				137 (172)	131 (168)	(SeQuent please)	(Taxus Liberté)
Xu et al. (11)	PEPCAD China ISR Trial	RCT	Yes	China	2011–2012	215 (221)		PCB	PES
Xu et al. (17)		4				109 (113)	106 (108)	(SeQuent please)	(Taxus Liberté)
Alfonso et al. (12)	RIBS IV	RCT	Yes	Spain	2010–2013	309 (309)		PCB	EES
Alfonso et al. (5)		4				154 (154)	155 (155)	(SeQuent please)	(Xience Prime)
Jensen et al. (14)	BIOLUX	RCT	Yes	Germany	2012–2015	BMS-ISR and DES-ISR:		BTHC based PCB	BP-SES
		4		Latvia		229 (243)		(Pantera LUX)	(Orsiro)
						157 (163)	72 (80)		
Wong et al. (13)	RESTORE	RCT	Yes	South	2013–2016	172 (172)		PCB	EES
		4		Korea		86 (86)	86 (86)	(SeQuent please)	(Xience)

RCT, randomized controlled trial; DCB, drug-coated balloon; DES, drug-eluting stents; PCB, paclitaxel-coated balloon; PES, paclitaxel-eluting stents; everolimus-eluting stents; BP-SES, biodegradable polymer sirolimus-eluting stents.

MLD, DS%, LLL, and binary restenosis were detected between the DES and DCB groups. However, subsequent subgroup analysis demonstrated a significant trend toward an increment in MLD (MD = −0.25 mm, 95 CI −0.38 to −0.11 mm, $p = 0.0003$; $I^2 = 0\%$, $p = 0.70$, **Figure 2A**) was observed in the everolimus-eluting stents (EES) group. In addition, patients receiving EES were associated with significantly lower DS% (MD = 7.29, 95% CI 2.86–11.71, $p = 0.001$; $I^2 = 0\%$, $p = 0.84$, **Figure 2B**) and the risk of binary restenosis (OR = 2.20, 95% CI 1.18–4.11, $p = 0.01$; $I^2 = 0\%$, $p = 0.33$, **Figure 2D**) compared to the patients treated with DCB. However,no significant difference in LLL was noted between DES and DCB (**Figure 2C**).

DCB vs. DES for the Primary Endpoint TLR

In this section, the longest available clinical follow-up periods were considered for the analysis and the primary endpoint TLR was reported in the five RCTs including 1,092 patients. After pooling the data of 573 patients receiving DCB vs. 519 patients receiving DES, this meta-analysis revealed repeat DES implantation was associated with reduced TLR compared to DCB angioplasty in patients presenting with DES-ISR (RR = 1.53, 95% CI 1.15–2.04, $p = 0.003$, **Figure 3**), with low heterogeneity across the trials ($I^2 = 0\%$, $p = 0.50$). In the subgroup analysis, a strong trend toward a decrease in TLR (RR = 1.36, 95% CI 0.96–1.91, $p = 0.08$; $I^2 = 0\%$, $p = 0.56$, **Figure 4**) was even noted in paclitaxel-eluting stent (PES) group, although this difference was not statistically significant compared to DCB.

DCB vs. DES for Secondary Outcomes

For the secondary outcomes, as demonstrated in **Figure 5**, no significant differences in MACEs, cardiac death, MI, and stent thrombosis were noted between the DCB group and the DES group in this meta-analysis. However, repeat DES implantation may be superior to DCB angioplasty in reducing the risk of TVR (RR = 1.50, 95% CI 1.11–2.04, $p = 0.009$; $I^2 = 28\%$, $p = 0.24$, **Figure 5**). In the subgroup analysis (**Table 4**), we also found repeat revascularization with EES, compared with DCB angioplasty, could reduce the risk of MACEs (RR = 1.58, 95% CI 1.03–2.43, $p = 0.04$). However, in terms of cardiac death, DES especially PES may be inferior to DCB.

Publication Bias and Sensitivity Analysis

In this meta-analysis, the publication bias was not assessed by funnel plot because of the limited number of included studies. The sensitivity analysis, which was performed by sequentially omitting one trial at a time, also confirmed that DES outperformed DEB in terms of the primary endpoints TLR. However, after excluding the study from Alfonso et al. the difference in TVR loses significance (RR = 1.34, 95% CI 0.93–1.94, $p = 0.12$).

DISCUSSION

This meta-analysis comprehensively compared the angiographic and clinical endpoints of the two different strategies (DCB vs. DES) for patients presenting with DES-ISR in routine clinical practice. In addition, the major findings were listed as follows: (1) EES, not PES, was superior to DCB in angiographic endpoints, with larger MLD, lower DS%, and less binary restenosis. (2) For the clinical endpoints, the overall pooled outcomes demonstrated revascularization with DES significantly reduced the risk of TLR and TVR compared to DCB angioplasty. (3) In addition to TLR and TVR, EES was also associated with lower MACEs than DCB in the subgroup analysis.

Despite the great advance in primary and secondary prevention, CAD remains the leading cause of mortality worldwide (18, 19). PCI based on DES is the most commonly used strategy for myocardial revascularization in patients with CAD at present (1, 3). Although the efficacy of DES in the prevention of restenosis improves significantly compared to BMS, DES-ISR still develops in 5–10% of patients after DES

TABLE 2 | Reported outcomes and follow-up time.

References	Data source	Follow-up time (month)	The primary endpoint/objective	Major inclusion/exclusion criteria
Byrne et al. (10)	ISAR-DESIRE 3	Angiography: 6–8 months Clinical outcomes: 12 months	DS% in the segment	**Inclusion:** Age > 18 years; DES-ISR (DS% > 50%) with ischemic symptom or objective evidence of myocardial ischemia. **Exclusion:** Target lesion located in LM/coronary bypass graft; STEMI (within 48 h); cardiogenic shock; eGFR < 30 ml/min; life expectancies < 12 months; contraindication/allergy to antiplatelet therapy, paclitaxel, or stainless steel.
Kufner et al. (16)		Clinical outcomes: 36 months	The primary efficacy endpoint: TLR The primary safety endpoint: the composite of death or MI	
Xu et al. (11)	PEPCAD China ISR Trial	Angiography: 9 months Clinical outcomes: 12 months	In segment LLL	**Inclusion:** Age (18–80 years); DES-ISR (Mehran type I to III); DS% > 70 or 50% with documented myocardial ischemia. **Exclusion:** MI (within 1 week); bifurcation with SB > 2.5 mm; lesion with extensive thrombus; severe chronic HF or NYHA IV; severe VHD; stroke within 6 months; eGFR < 30 ml/min.
Xu et al. (17)		Clinical outcomes: 24 months	2-year outcomes and additional subgroup analysis	
Alfonso et al. (12)	RIBS IV	Angiography:6-9 months Clinical outcomes:12 months	In-segment MLD	**Inclusion:** DES-ISR (DS% > 50%) with symptom or objective evidence of ischemia. **Exclusion:** Small vessels (<2.0 mm in diameter); long lesion (>30 mm); total occlusion; DES-ISR within 1 months; DES-ISR presenting acute MI; target lesion with obvious thrombus.
Alfonso et al. (5)		Angiography: 6-9 months Clinical outcomes: 36 months	The main objective: comparison of 3-year clinical outcome The primary endpoint: In-segment MLD	
Jensen et al. (14)	BIOLUX	Angiography: 6 months Clinical outcomes: 18 months	The primary efficacy endpoint: in-stent LLL The primary safety endpoint: TLF at 12 months	**Inclusion:** patients presenting with clinical evidence of IHD and/or a positive functional study, SAP/UAP/silent ischemia and ISR (DS% > 50%) in BMS or DES; number of ISR lesion ≤2; in case of 2 target lesion, both ISR lesions were treated by the same device. **Exclusion:** STEMI (within 72 h); acute cardiac decompensation or cardiogenic shock; LVEF < 30%; target lesion located in LM; target vessel with thrombus; allergies to antiplatelet drugs, heparin, or similar drugs; dialysis or creatinine > 2.5 mg/dl; life expectancy < 18 months; small (diameter < 2 mm) or large (diameter > 4 mm) vessel; short (<6 mm) or diffuse (>28 mm) lesion.
Wong et al. (13)	RESTORE	Angiography: 9 months Clinical outcomes: 12 months	In-segment LLL	**Inclusion:** patients with DES-ISR (DS% > 50%). **Exclusion:** life expectancy < 12 months; contraindication to paclitaxel, everolimus, and antiplatelet drugs.

DS%, percent diameter stenosis; TLR, target lesion revascularization; MI, myocardial infarction; DES, drug-eluting stents; ISR, in-stent restenosis; LM, left main artery; STEMI, ST-segment elevation myocardial infarction; eGFR, estimated glomerular filtration rate; LLL, late lumen loss; SB, side branch; HF, heart failure; NYHA, New York Heart Association; VHD, valvular heart disease; MLD, minimum lumen disease; TLF, target lesion failure; IHD, ischemic heart disease; SAP, stable angina pectoris; UAP, unstable angina pectoris; BMS, bare metal stents; LVEF, left ventricular ejection fraction.

TABLE 3 | Baseline demographics, lesion, and procedure characteristics.

	ISAR-DESIRE 3		PEPCAD China ISR		RIBS IV		BIOLUX		RESTORE	
Variables	**DCB**	**DES**	**DCB**	**DES**	**DCB**	**DES**	**DCB**	**DES**	**DCB**	**DES**
Demographics										
Age, years	67.7 ± 10.4	68.8 ± 10.0	61.8 ± 9.3	62.1 ± 9.3	66 ± 10	66 ± 10	67.2 ± 9.9	69.4 ± 8.8	67 ± 10	66 ± 9
Male, %	105 (77)	88 (67)	88 (80.7)	86 (81.1)	127 (82)	130 (84)	122 (77.7)	49 (68.1)	61 (70.9)	62 (72.1)
Diabetes mellitus, %	56 (41)	61 (47)	44 (40.4)	35 (33.0)	75 (49)	66 (43)	48 (30.6)	24 (33.3)	43 (50.0)	38 (44.2)
Hypertension, %	105 (77)	101 (77)	78 (71.6)	69 (65.1)	110 (71)	121 (78)	144 (91.7)	70 (97.2)	60 (69.8)	65 (75.6)
Hyperlipidemia, %	108 (79)	103 (79)	38 (34.9)	35 (33.0)	110 (71)	121 (78)	134 (85.4)	62 (86.1)	49 (57.0)	53 (61.6)
Current and/or smoker, %	19 (14)	15 (11)	23 (21.1)	27 (25.5)	89 (58)	87 (56)	104 (66.2)	42 (58.3)	40 (46.5)	37 (43.0)
LVEF, %	53.6 ± 9.8	54.5 ± 9.9	61.7 ± 8.5	62.3 ± 8.6	58 ± 12	59 ± 11	NA	NA	59.4 ± 8.4	59.9 ± 7.8
Lesion										
Target lesion, %										
LAD	59 (34)	50 (30)	47 (41.6)	61 (56.5)	77 (50)	71 (46)	NA	NA	48 (55.8)	52 (60.5)
LCX	54 (31)	61 (36)	21 (18.6)	13 (12.0)	27 (18)	34 (22)	NA	NA	13 (15.1)	11 (12.8)
RCA	59 (34)	56 (33)	45 (39.8)	34 (31.5)	43 (28)	45 (29)	NA	NA	24 (27.9)	21 (24.4)
LM	0	1 (1)	0	0	0	0	0	0	0	2 (2.3)
Quantitative features										
MLD, mm	0.97 ± 0.48	0.93 ± 0.50	0.85 ± 0.38	0.86 ± 0.41	0.79 ± 0.4	0.75 ± 0.4	1.0 ± 0.5	0.9 ± 0.5	0.63 ± 0.4	0.63 ± 0.42
DS%	64.4 ± 16.8	66.7 ± 16.5	68.26 ± 12.47	68.43 ± 13.25	69 ± 17	72 ± 15	67.2 ± 13.5	68.9 ± 14.7	77 ± 17	79 ± 13
Lesion length, mm	NA	NA	12.52 ± 6.55	13.08 ± 7.13	10.4 ± 5.6	10.7 ± 5.4	5.8 ± 4.0	7.2 ± 6.1	18.1 ± 9.7	17.4 ± 11.4
Procedure										
Predilation, %	139 (81)	145 (86)	112 (99.1)	107 (99.1)	NA	NA	160 (98.2)	77 (96.3)	65 (75.6)	72 (83.7)
Cutting/scoring balloon, %	2 (1)	2 (1)	NA	NA	7 (4)	5 (3)	NA	NA	NA	NA
Device length, mm	NA	NA	19.73 ± 5.88	20.12 ± 7.07	19 ± 6	19 ± 8	20.4 ± 5.0	20.5 ± 6.5	28.5 ± 14.7	25.5 ± 11.5
Device diameter, mm	NA	NA	3.06 ± 0.39	2.98 ± 0.39	NA	NA	3.2 ± 0.4	3.0 ± 0.5	2.98 ± 0.40	3.14 ± 0.35
DAPT protocol, months	>6	>6	>12	>12	>3	>12	NA	NA	>6	>6

The baseline data of patients presenting DES-ISR was not available from BIOLUX, therefore we used the baseline data of general participant (BMS-ISR and DES-ISR) instead.

ISR, in-stent restenosis; DCB, drug-coated balloon; DES, drug-eluting stent; LVEF, left ventricular ejection fraction; LAD, left anterior descending artery; LCX, left circumflex artery; RCA, right coronary artery; LM, left main; MLD, minimum lumen diameter; DS%, percent diameter stenosis; DAPT, dual antiplatelet therapy; NA, not applicable; BMS, bare-mental stent.

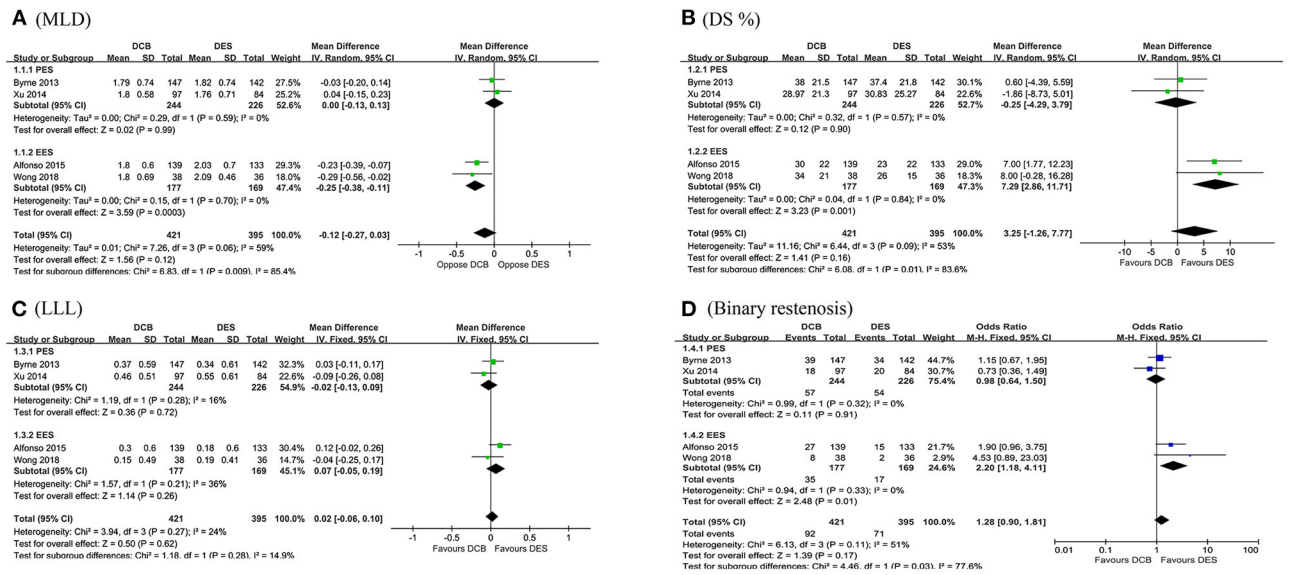

FIGURE 2 | Forest plot of comparing angiographic outcomes in MLD **(A)**, DS% **(B)**, LLL **(C)**, and binary restenosis **(D)** between repeat DES implantation and DCB angioplasty. MLD, minimum lumen diameter; DS%, percent diameter stenosis; LLL, late lumen loss; DES, drug-eluting stents; DCB, drug-coated balloon; PES, paclitaxel-eluting stents; EES, everolimus-eluting stents.

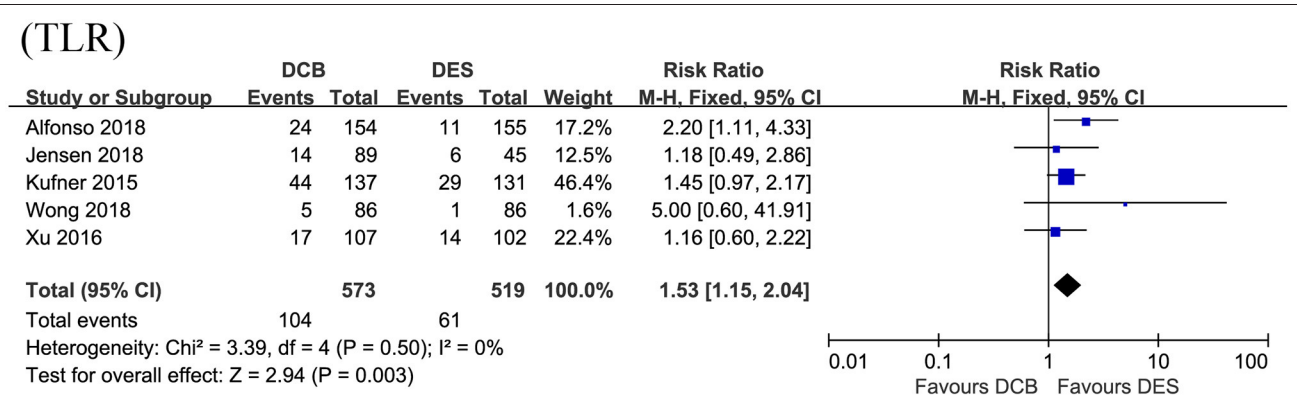

FIGURE 3 | Forest plot of comparing the risk of TLR between repeat DES implantation and DCB angioplasty. TLR, target lesion revascularization; DES, drug-eluting stents; DCB, drug-coated balloon.

deployment (5, 20). In addition, the pathophysiology underlying DES-ISR may be more complex. In addition to neointimal hyperplasia and stent under-expansion, which were considered as the dominant risk factors for BMS-ISR, neo-atherosclerosis seems to be another factor contributing to DES-ISR (8, 9). Furthermore, DES-ISR continues to be a therapeutic challenge and trials designed to determine the optimal treatment strategy for patients with DES-ISR were limited.

Although repeat stenting with DES and DCB angioplasty has been recommended by current guidelines, the consensus was lacking regarding the best treatment for DES-ISR. Bajraktari et al. performed a meta-analysis of seven studies (three of which were RCTs) and reported DEB was comparable to DES in terms of clinical outcomes (MACEs, cardiac death, MI, stent thrombosis, TLR, and TVR) for the treatment of DES-ISR (21). However, Giacoppo et al. reported, in the meta-analysis of individual patient data from all available RCTs (DAEDALUS), DCB angioplasty is significantly associated with a higher risk of TLR compared to repeat stenting with DES for the treatment of DES-ISR at 3-year follow-up (22). In addition, the primary safety endpoint (a composite of all-cause mortality, MI, and target lesion thrombosis) was similar between the two groups (22). In consistent with the study DAEDALUS, this study also confirmed repeat DES implantation was superior to DCB angioplasty in terms of TLR. Moreover, this trend still persisted when we compared PES with DCB, but it was marginally significant. To extend previous studies, this meta-analysis further confirmed EES, not PES, outperforms DCB in terms of MLD, DS%, and binary restenosis.

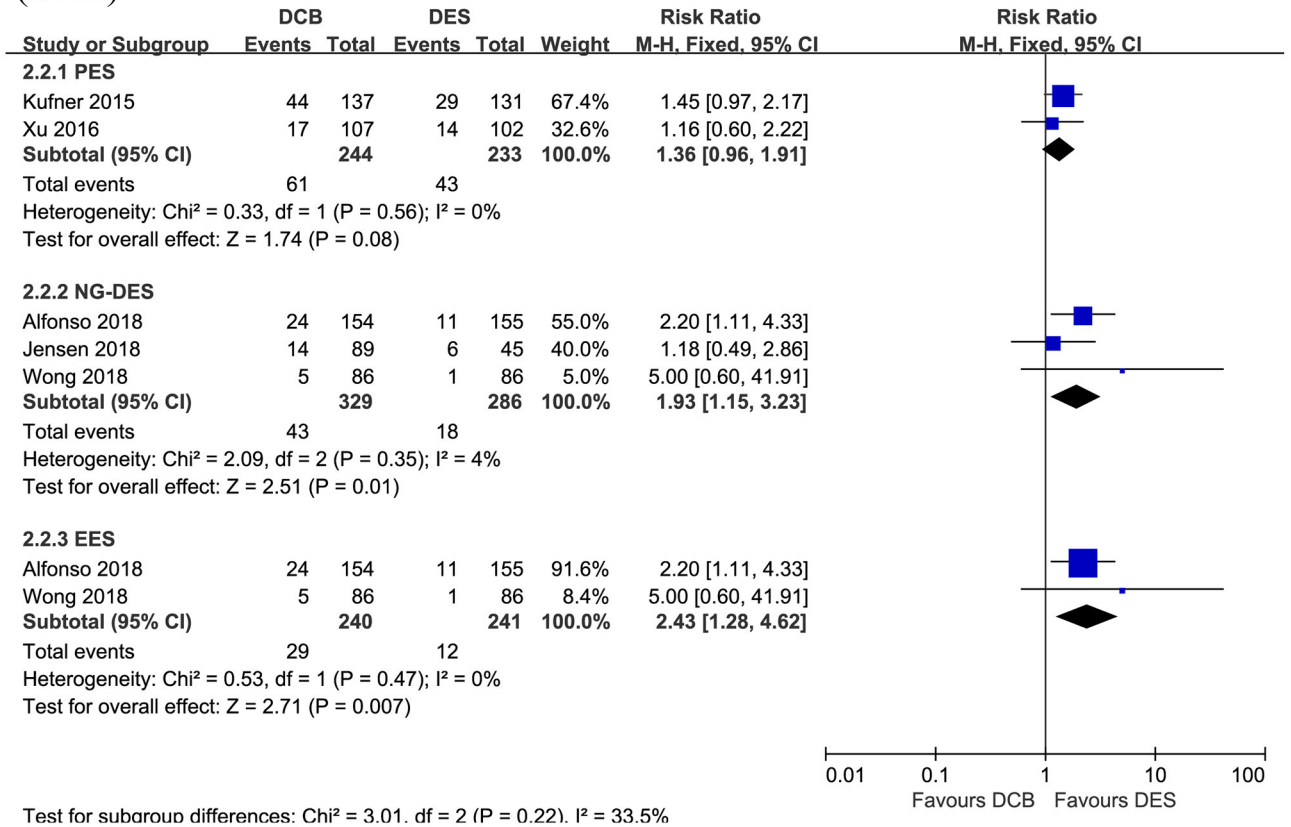

FIGURE 4 | Subgroup analysis for the primary endpoint TLR according to the type of DES used. TLR, target lesion revascularization; DES, drug-eluting stents; PES, paclitaxel-eluting stents; NG-DES, new-generation DES; EES, everolimus-eluting stents.

Our conclusions were reliable and stable because we only included RCTs and the sensitivity analysis and subgroup analysis were performed. But we should keep in mind our conclusions may not generalize to the patients with target lesions located in the left main artery or aorto-ostial coronary. Because few such patients were included in this study. Therefore, multicenter, prospective, and RCTs are needed to figure out this knowledge gap.

Future Perspectives

DES, especially new-generation (NG-DES)/EES, was superior to DCB in reducing the risk of TLR in this meta-analysis. But treatment with DCB for DES-ISR could avoid multilayers of metal stents in the coronary artery, which poses difficulty for further treatment of recurrent restenosis and is associated with a poor prognosis (23–25). In addition, DCB may be more suitable for patients who are intolerable of long-term DAPT or at a high risk of bleeding (26, 27). Therefore, further investigating and refining DCB technology were warranted. First, future RCTs should focus on the strategy of DCB angioplasty combined with neointimal modification by scoring/cutting balloon, rotablation, and excimer laser. In addition, Kufner et al. have confirmed in patients with DES-ISR, neointimal modification with scoring balloon before DCB was superior over DCB angioplasty alone (28). Second, to extend the previous study from Ali et al. (29), RCTs with large sample sizes and extended clinical follow-up time are required to verify the efficacy and safety of sirolimus-coated balloon (SCB) in patients with DES-ISR. Third, compared to DCB, bioresorbable vascular scaffolds (BVS) could prevent early recoil without adding another layer of metal. Alfonso et al. have confirmed BVS was similar to DCB but inferior to EES in late angiographic and clinical results for the treatment of any ISR in RIBS trial VI (30). In addition, Moscarella et al. also reported BVS was associated with a numerically higher rate of device-oriented cardiovascular events (DOCE) compared with EES while a similar rate compared to DCB for the treatment for any ISR in the BIORESOLVE-ISR Study (31). But the value of BVS in the scenario of DES-ISR remains unsettled and future trials are needed to investigate it.

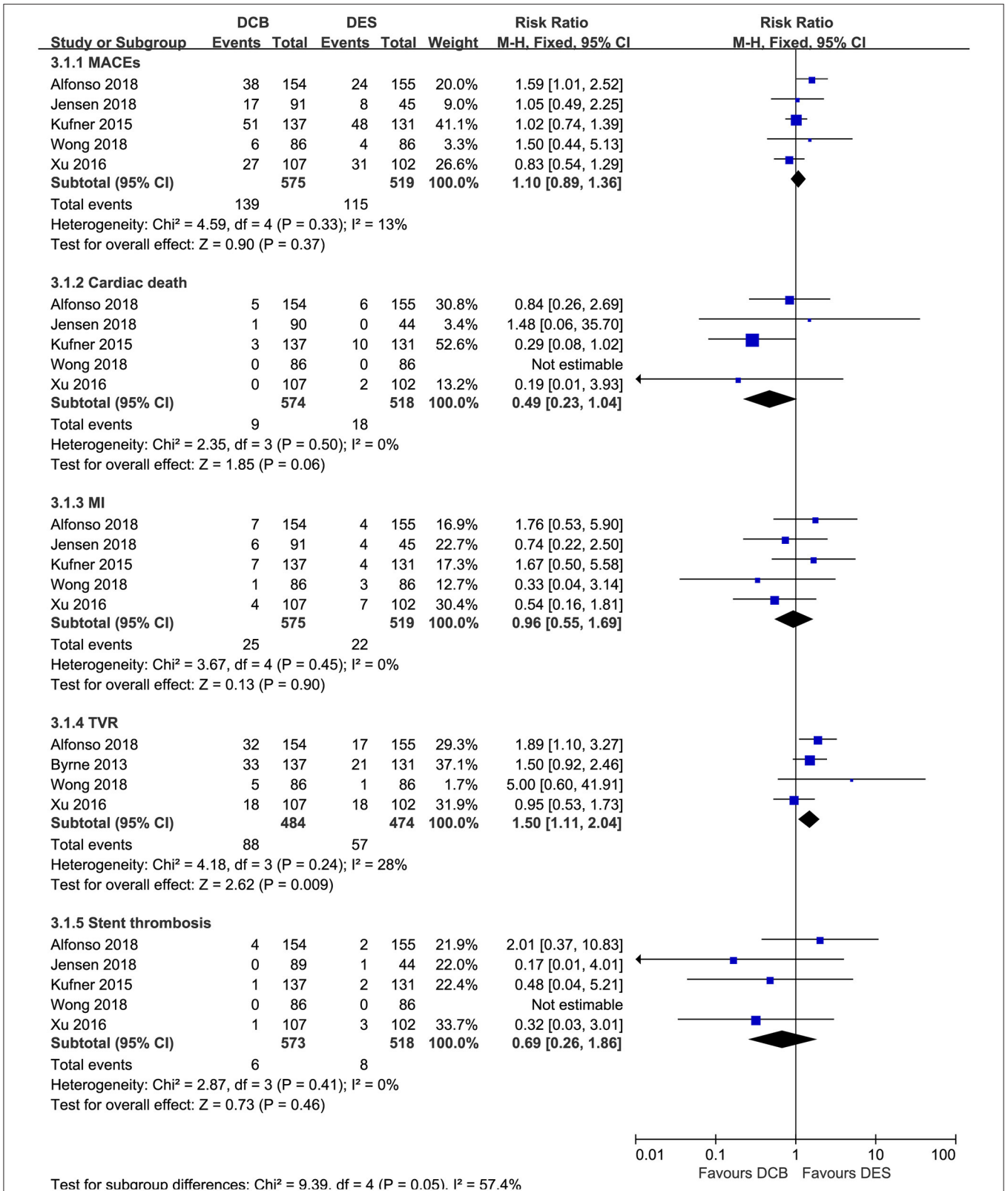

FIGURE 5 | Forest plot comparing secondary outcomes between repeat DES implantation and DCB angioplasty. DES, drug-eluting stents; DCB, drug-coated balloon; MACEs, major adverse cardiac events; MI, myocardial infarction; TVR, target vessel revascularization.

TABLE 4 | Subgroup analysis for secondary outcomes.

	Number of studies	RR (95% CI)	*P* for test	I^2	*P* for heterogeneity
MACEs					
PES	2	0.94 (0.73, 1.22)	0.65	0%	0.46
NG-DES	3	1.43 (0.99, 2.08)	0.06	0%	0.65
Only EES	2	1.58 (1.03, 2.43)	**0.04**	0%	0.93
Cardiac death					
PES	2	0.27 (0.08, 0.86)	**0.03**	0%	0.81
NG-DES	3	0.90 (0.30, 2.69)	0.86	0%	0.74
Only DES	2	0.84 (0.26, 2.69)	0.77	-	-
MI					
PES	2	0.95 (0.42, 2.16)	0.91	40%	0.20
NG-DES	3	0.97 (0.45, 2.09)	0.94	0%	0.37
Only EES	2	1.15 (0.42, 3.12)	0.79	39%	0.20
TVR					
PES	2	1.25 (0.86, 1.82)	0.25	25%	0.25
NG-DES (EES)	2	2.07 (1.22, 3.50)	**0.007**	0%	0.41
Stent thrombosis					
PES	2	0.38 (0.07, 1.95)	0.25	0%	0.81
NG-DES	3	1.09 (0.30, 4.00)	0.90	46%	0.17
Only EES	2	2.01 (0.37, 10.83)	0.42	-	-

RR, risk ratio; CI, confidence interval; MACEs, major adverse cardiac events; PES, paclitaxel-eluting stents; NG-DES, new-generation drug-eluting stent; EES, everolimus-eluting stents; MI, myocardial infarction; TVR, target vessel revascularization.

Limitations

Several limitations should be acknowledged in this meta-analysis. First, the type of restenotic DES, generation of DES used, time from implantation to admit for DES-ISR, and antithrombotic strategy after intervention for DES-ISR were not uniformly across the included RCTs, which may cause heterogeneity. Second, this meta-analysis only included five RCTs. Therefore, some subgroups were not powered to detect differences and publication bias was not evaluated. Third, this meta-analysis was based on the study level rather than the patient level. In addition, the ratio of follow-up angiography at the scheduled time was suboptimal and the exact reasons were not reported. Finally, the follow-up time for the main analysis was limited up to 3 years in this meta-analysis. Future studies with an extended follow-up duration could provide an additional value to assess the efficacy and safety of DES vs. DCB for DES-ISR.

CONCLUSION

Angioplasty with DCB was moderately less effective than repeat DES implantation in reducing the TLR for patients with coronary DES-ISR at long-term follow-up. In addition, this trend was more obvious when compared with NG-DES/EES. In addition, repeat stenting with EES could also provide better angiographic outcomes than DCB angioplasty. To confirm our findings, RCTs with a large sample size and extended follow-up duration are required in the future.

DATA AVAILABILITY STATEMENT

The original contributions presented in the study are included in the article/supplementary material, further inquiries can be directed to the corresponding authors.

AUTHOR CONTRIBUTIONS

Data analysis, interpretation, and manuscript writing were performed by YZhu. Literature search, study selection, data extraction, and quality assessment were performed by YZhu, KL, XK, YL, AG, and YZha. YZha, JZ, and HH were responsible for the conception and design of the study. JN and HL revised the manuscript carefully. All authors read and approved the final manuscript.

FUNDING

This work was supported by the grant from the National Key Research and Development Program of China (2017YFC0908800), the Beijing Municipal Administration of Hospitals Ascent Plan (DFL20150601) and Mission Plan (SML20180601), and the Beijing Municipal Health Commission Project of Science and Technology Innovation Center (PXM2019_026272_000006) (PXM2019_026272_000005).

REFERENCES

1. Stefanini GG, Holmes DR, Jr. Drug-eluting coronary-artery stents. *N Engl J Med.* (2013) 368:254–65. doi: 10.1056/NEJMra1210816
2. Serrador Frutos AM, Jiménez-Quevedo P, Pérez De Prado A, Pan Álvarez-Ossorio M. Spanish cardiac catheterization and coronary intervention registry. 26th Official report of the spanish society of cardiology working group on cardiac catheterization and interventional cardiology (1990-2016). *Rev Esp Cardiol (Engl Ed).* (2017) 70:1110–20. doi: 10.1016/j.rec.2017.10.017
3. Neumann FJ, Sousa-Uva M, Ahlsson A, Alfonso F, Banning AP, Benedetto U, et al. 2018 ESC/EACTS Guidelines on myocardial revascularization. *Eur Heart J.* (2019) 40:87–165. doi: 10.1093/eurheartj/ehy855
4. Basavarajaiah S, Naganuma T, Latib A, Sticchi A, Ciconte G, Panoulas V, et al. Treatment of drug-eluting stent restenosis: comparison between drug-eluting balloon versus second-generation drug-eluting stents from a retrospective observational study. *Catheter Cardio Interv.* (2016) 88:522–8. doi: 10.1002/ccd.26368
5. Alfonso F, Pérez-Vizcayno MJ, Cuesta J, García Del Blanco B, García-Touchard A, López-Mínguez JR, et al. 3-Year clinical follow-up of the RIBS IV clinical trial. *JACC Cardiovasc Interv.* (2018) 11:981–91. doi: 10.1016/j.jcin.2018.02.037
6. Steinberg DH, Gaglia MA, Pinto Slottow TL, Roy P, Bonello L, De Labriolle A, et al. Outcome differences with the use of drug-eluting stents for the treatment of in-stent restenosis of bare-metal stents versus drug-eluting stents. *Am J Cardiol.* (2009) 103:491–5. doi: 10.1016/j.amjcard.2008.09.107
7. Alfonso F, Pérez-Vizcayno MJ, García Del Blanco B, García-Touchard A, López-Mínguez J, Masotti M, et al. Everolimus-eluting stents in patients with bare-metal and drug-eluting in-stent restenosis. *Circulation Cardiovasc Interv.* (2016) 9:e003479. doi: 10.1161/CIRCINTERVENTIONS.115.003479
8. Alfonso F, Byrne RA, Rivero F, Kastrati A. Current treatment of in-stent restenosis. *J Am Coll Cardiol.* (2014) 63:2659–73. doi: 10.1016/j.jacc.2014.02.545
9. Shlofmitz E, Iantorno M, Waksman R. Restenosis of drug-eluting stents. *Circulation Cardiovasc Interv.* (2019) 12:e007023. doi: 10.1161/CIRCINTERVENTIONS.118.007023
10. Byrne RA, Neumann F, Mehilli J, Pinieck S, Wolff B, Tiroch K, et al. Paclitaxel-eluting balloons, paclitaxel-eluting stents, and balloon angioplasty in patients with restenosis after implantation of a drug-eluting stent (ISAR-DESIRE 3): a randomised, open-label trial. *Lancet.* (2013) 381:461–7. doi: 10.1016/S0140-6736(12)61964-3
11. Xu B, Gao RL, Wang J'An, Yuejin Y, Chen SL, Liu B, et al. A prospective, multicenter, randomized trial of paclitaxel-coated balloon versus paclitaxel-eluting stent for the treatment of drug-eluting stent in-stent restenosis: results from the PEPCAD China ISR trial. *JACC Cardiovasc Interv.* (2014) 7:204–11. doi: 10.1016/j.jcin.2013.08.011
12. Alfonso F, Perez-Vizcayno MJ, Cardenas A, Garcia DBB, Garcia-Touchard A, Lopez-Minguez JR, et al. A Prospective randomized trial of drug-eluting balloons versus everolimus-eluting stents in patients with in-stent restenosis of drug-eluting stents: the RIBS IV randomized clinical trial. *J Am Coll Cardiol.* (2015) 66:23–33. doi: 10.1016/j.jacc.2015.04.063
13. Wong YTA, Kang DY, Lee JB, Rha SW, Hong YJ, Shin ES, et al. Comparison of drug-eluting stents and drug-coated balloon for the treatment of drug-eluting coronary stent restenosis: a randomized RESTORE trial. *Am Heart J.* (2018) 197:35–42. doi: 10.1016/j.ahj.2017.11.008
14. Jensen CJ, Richardt G, Tölg R, Erglis A, Skurk C, Jung W, et al. Angiographic and clinical performance of a paclitaxel-coated balloon compared to a second-generation sirolimus-eluting stent in patients with in-stent restenosis: the BIOLUX randomised controlled trial. *EuroIntervention.* (2018) 14:1096–103. doi: 10.4244/EIJ-D-17-01079
15. Katsanos K, Spiliopoulos S, Kitrou P, Krokidis M, Karnabatidis D. Risk of death following application of paclitaxel-coated balloons and stents in the femoropopliteal artery of the leg: a systematic review and meta-analysis of randomized controlled trials. *J Am Heart Assoc.* (2018) 7:e011245. doi: 10.1161/JAHA.118.011245
16. Kufner S, Cassese S, Valeskini M, Neumann FJ, Schulz-Schupke S, Hoppmann P, et al. Long-term efficacy and safety of paclitaxel-eluting balloon for the treatment of drug-eluting stent restenosis: 3-year results of a randomized controlled trial. *JACC Cardiovasc Interv.* (2015) 8:877–84. doi: 10.1016/j.jcin.2015.01.031
17. Xu B, Qian J, Ge J, Wang J, Chen F, Chen J, et al. Two-year results and subgroup analyses of the PEPCAD China in-stent restenosis trial: a prospective, multicenter, randomized trial for the treatment of drug-eluting stent in-stent restenosis. *Catheter Cardio Interv.* (2016) 87:624–9. doi: 10.1002/ccd.26401
18. Da Silva A, Caldas APS, Hermsdorff HHM, Bersch-Ferreira ÂC, Torreglosa CR, Weber B, et al. Triglyceride-glucose index is associated with symptomatic coronary artery disease in patients in secondary care. *Cardiovasc Diabetol.* (2019) 18:89. doi: 10.1186/s12933-019-0893-2
19. Sun Z, Cao Y, Li H. Multislice computed tomography angiography in the diagnosis of coronary artery disease. *J Geriatr Cardiol.* (2011) 8:104–13. doi: 10.3724/SP.J.1263.2011.00104
20. Bønaa KH, Mannsverk J, Wiseth R, Aaberge L, Myreng Y, Nygård O, et al. Drug-eluting or bare-metal stents for coronary artery disease. *N Engl J Med.* (2016) 375:1242–52. doi: 10.1056/NEJMoa1607991
21. Bajraktari G, Jashari H, Ibrahimi P, Alfonso F, Jashari F, Ndrepepa G, et al. Comparison of drug-eluting balloon versus drug-eluting stent treatment of drug-eluting stent in-stent restenosis: a meta-analysis of available evidence. *Int J Cardiol.* (2016) 218:126–35. doi: 10.1016/j.ijcard.2016.05.040
22. Giacoppo D, Alfonso F, Xu B, Claessen BEPM, Adriaenssens T, Jensen C, et al. Paclitaxel-coated balloon angioplasty vs. drug-eluting stenting for the treatment of coronary in-stent restenosis: a comprehensive, collaborative, individual patient data meta-analysis of 10 randomized clinical trials (DAEDALUS study). *Eur Heart J.* (2020) 41:3715–28. doi: 10.1093/eurheartj/ehz861
23. Singh AD, Singal AK, Mian A, Kapadia SR, Hedrick DP. Kanaa'N A, et al. Recurrent drug-eluting stent in-stent restenosis: a state-of-the-art review of pathophysiology, diagnosis, and management. *Cardiovasc Revasc Med.* (2020) 21:1157–63. doi: 10.1016/j.carrev.2020.01.005
24. Wang G, Zhao Q, Chen Q, Zhang X, Tian L, Zhang X. Comparison of drug-eluting balloon with repeat drug-eluting stent for recurrent drug-eluting stent in-stent restenosis. *Coron Artery Dis.* (2019) 30:473–80. doi: 10.1097/MCA.0000000000000784
25. Kawamoto HM, Ruparelia NMD, Latib AM, Miyazaki TM, Sato KM, Mangieri AM, et al. Drug-coated balloons versus second-generation drug-eluting stents for the management of recurrent multimetal-layered in-stent restenosis. *JACC Cardiovasc interv.* (2015) 8:1586–94. doi: 10.1016/j.jcin.2015.04.032
26. Roncalli J, Godin M, Boughalem K, Shayne J, Piot C, Huret B, et al. Paclitaxel drug-coated balloon after bare-metal stent implantation, an alternative treatment to drug-eluting stent in high bleeding risk patients (the panelux trial). *J Invasive Cardiol.* (2019) 31:94–100.
27. Scheller B. Antithrombozytäre therapie und PCI. *Herz.* (2014) 39:819–21. doi: 10.1007/s00059-014-4158-2
28. Kufner S, Joner M, Schneider S, Tolg R, Zrenner B, Repp J, et al. Neointimal modification with scoring balloon and efficacy of drug-coated balloon therapy in patients with restenosis in drug-eluting coronary stents: a randomized controlled trial. *JACC Cardiovasc Interv.* (2017) 10:1332–40. doi: 10.1016/j.jcin.2017.04.024
29. Ali RM, Abdul Kader MASK, Wan Ahmad WA, Ong TK, Liew HB, Omar A, et al. Treatment of coronary drug-eluting stent restenosis by a sirolimus- or paclitaxel-coated balloon. *JACC Cardiovasc Interv.* (2019) 12:558–66. doi: 10.1016/j.jcin.2018.11.040
30. Alfonso F, Cuesta J, Pérez-Vizcayno MJ, García Del Blanco B, Rumoroso JR, Bosa F, et al. Bioresorbable vascular scaffolds

for patients with in-stent restenosis: the RIBS VI study. *JACC Cardiovasc interv.* (2017) 10:1841–51. doi: 10.1016/j.jcin.2017.06.064

31. Moscarella E, Tanaka A, Ielasi A, Cortese B, Coscarelli S, De Angelis MC, et al. Bioresorbable vascular scaffold versus everolimus-eluting stents or drug eluting balloon for the treatment of coronary in-stent restenosis: 1-Year follow-up of a propensity score matching comparison (the BIORESOLVE-ISR Study). *Catheter Cardio Inter.* (2018) 92:668–77. doi: 10.1002/ccd.27473

Conflict of Interest: The authors declare that the research was conducted in the absence of any commercial or financial relationships that could be construed as a potential conflict of interest.

Publisher's Note: All claims expressed in this article are solely those of the authors and do not necessarily represent those of their affiliated organizations, or those of the publisher, the editors and the reviewers. Any product that may be evaluated in this article, or claim that may be made by its manufacturer, is not guaranteed or endorsed by the publisher.

frontiers in Cardiovascular Medicine

ORIGINAL RESEARCH
published: 14 December 2021
doi: 10.3389/fcvm.2021.792180

A Link Between Methylglyoxal and Heart Failure During HIV-1 Infection

*Prasanta K. Dash[1†], Fadhel A. Alomar[2†], Jesse L. Cox[3], JoEllyn McMillan[1], Bryan T. Hackfort[4], Edward Makarov[1], Brenda Morsey[5], Howard S. Fox[5], Howard E. Gendelman[1], Santhi Gorantla[1] and Keshore R. Bidasee[1,6,7]**

[1] Departments of Pharmacology and Experimental Neuroscience, University of Nebraska Medical Center, Omaha, NE, United States, [2] Department of Pharmacology and Toxicology, College of Clinical Pharmacy, Imam Abdulrahman Bin Faisal University, Dammam, Saudi Arabia, [3] Departments of Pathology and Microbiology, University of Nebraska Medical Center, Omaha, NE, United States, [4] Departments of Cellular and Integrative Physiology, University of Nebraska Medical Center, Omaha, NE, United States, [5] Departments of Neurological Sciences, University of Nebraska Medical Center, Omaha, NE, United States, [6] Departments of Environment and Occupational Health, University of Nebraska Medical Center, Omaha, NE, United States, [7] Nebraska Redox Biology Center, Lincoln, NE, United States

OPEN ACCESS

Edited by:
Jingyan Han,
Boston University, United States

Reviewed by:
Cinzia Antognelli,
University of Perugia, Italy
Rongxue Wu,
University of Chicago, United States

***Correspondence:**
Keshore R. Bidasee
kbidasee@unmc.edu

[†]These authors have contributed equally to this work

Specialty section:
This article was submitted to Cardiovascular Therapeutics, a section of the journal Frontiers in Cardiovascular Medicine

Received: *09 October 2021*
Accepted: *22 November 2021*
Published: *14 December 2021*

Citation:
Dash PK, Alomar FA, Cox JL, McMillan J, Hackfort BT, Makarov E, Morsey B, Fox HS, Gendelman HE, Gorantla S and Bidasee KR (2021) A Link Between Methylglyoxal and Heart Failure During HIV-1 Infection. Front. Cardiovasc. Med. 8:792180. doi: 10.3389/fcvm.2021.792180

Early-onset heart failure (HF) continues to be a major cause of morbidity and mortality in people living with human immunodeficiency virus type one (HIV-1) infection (PLWH), yet the molecular causes for this remain poorly understood. Herein NOD.Cg-Prkdc^{scid}Il2rg^{tm1Wjl}/SzJ humanized mice (Hu-mice), plasma from PLWH, and autopsied cardiac tissues from deceased HIV seropositive individuals were used to assess if there is a link between the glycolysis byproduct methylglyoxal (MG) and HF in the setting of HIV-1 infection. At five weeks post HIV infection, Hu-mice developed grade III-IV diastolic dysfunction (DD) with an associated two-fold increase in plasma MG. At sixteen-seventeen weeks post infection, cardiac ejection fraction and fractional shortening also declined by 26 and 35%, and plasma MG increased to four-fold higher than uninfected controls. Histopathological and biochemical analyses of cardiac tissues from Hu-mice 17 weeks post-infection affirmed MG increase with a concomitant decrease in expression of the MG-degrading enzyme glyoxalase-1 (Glo1). The endothelial cell marker CD31 was found to be lower, and coronary microvascular leakage and myocardial fibrosis were prominent. Increasing expression of Glo1 in Hu-mice five weeks post-infection using a single dose of an engineered AAV2/9 (1.7×10^{12} virion particles/kg), attenuated the increases in plasma and cardiac MG levels. Increasing Glo1 also blunted microvascular leakage, fibrosis, and HF seen at sixteen weeks post-infection, without changes in plasma viral loads. In plasma from virally suppressed PLWH, MG was also 3.7-fold higher. In autopsied cardiac tissues from seropositive, HIV individuals with low viral log, MG was 4.2-fold higher and Glo1 was 50% lower compared to uninfected controls. These data show for the first time a causal link between accumulation of MG and HF in the setting of HIV infection.

Keywords: HIV-1, heart failure, humanized mice, methylglyoxal, echocardiography

INTRODUCTION

Modern antiretroviral drug therapies (ART) have profoundly reduced morbidities and mortality in human immunodeficiency virus type one (HIV-1) infected individuals (1, 2). However, by contemporary estimates more than 40% of persons living with HIV-1 infection (PLWH) on long-term combination ART therapies are developing early-onset heart failure (HF) (3–7). This disease which starts at least a decade earlier in PLWH compared to uninfected individuals and is independent of arteriosclerosis, and/or myocardial infarction. This HF also starts earlier in women than in men (6, 8–13). To date, pharmacological strategies to blunt/slow the development HF in PLWH remain virtually non-existent, in part because of an incomplete understanding of the mechanisms involved.

Available data suggest that the pathophysiology of early-onset HF in PLWH is multifactorial, arising from persistent systemic immune activation, elevation in inflammation and oxidative stress, off-target effects of antiretroviral drugs, alcohol, aging, illicit drug use and the composition of the gut microbiome (5, 14–22). However, specific molecular pathways by which these cues negatively impact cardiac function are not well-defined. Some investigators using transgenic rodents have suggested that the HIV-1 auxiliary proteins Nef, gp120 and Tat contribute to the early-onset HF by impairing mitochondria and contractile functions of myocytes (23–28). However, to the best of our knowledge, plasma levels of HIV viral proteins in PLWH on ART are significantly lower than that in the transgenic rodent models (29–31). Also, the low-grade systemic inflammation seen in PLWH is minimally observed in these transgenic rodents, raising concerns about the disease relevance of the latter. Whether EcoHIV mice, another model in which gp120 from HIV-1 is replaced with murine leukemia virus gp80 for cell entry, also develops HF remains unclear (32). Others have suggested that off-target effects of antiretroviral drugs, alcohol and illicit drug use, and accelerated aging could exacerbate traditional risk factors of cardiovascular diseases and HF potentiating dyslipidemia, hyperglycemia, and endothelial dysfunction (5, 14–21, 33). However, the effects of antiretroviral drugs, alcohol, and illicit drugs, and aging on cardiac function in the setting of HIV-1 infection are limited, making delineation of mechanisms that trigger HF development in HIV-1 setting challenging.

There are some studies in the literature showing that prior to the onset of antiretroviral therapy, HIV-infected individuals usually develop dyslipidemia, hypertension, and metabolic syndrome (34–38). Some ART-naive patients also developed left ventricular stiffness, suggesting that HIV infection itself could be initiating/triggering HF (39–42). HIV-1, like all RNA viruses depends on the host cells they infect for the metabolic resources needed for replication. Immunocytes (mononuclear phagocytes and lymphocytes) that express the CD4, CCR5 and CXCR4 are principal targets for HIV-1 infection (43). Following viral infection, glucose transporter 1 (GLUT1) is upregulated in immunocytes to facilitate the increase in glycolysis needed for viral replication and the release of new viruses (44–46). In addition to the two pyruvate and two ATP molecules (47), glycolysis also generates a cytotoxic byproduct, namely methylglyoxal (MG) from breakdown of triose intermediates, glyceraldehyde 3-phosphate and dihydroxyacetone phosphate (48). In healthy individuals, MG is kept low (between ∼250 nM in plasma, and ∼3 μM in tissues, respectively) by the actions of dual-enzyme, glyoxalase degradation system (49–51). In the first step, the rate-limiting glyoxalase-I (*GLOI,* EC4.4.1.5, Glo1) converts a hemi-thioacetal formed between MG and reduced glutathione (MG-GSH) into S,D-lactoylglutathione which is then degraded by glyoxalase-II (*GLOII,* EC3.1.2.6, Glo-II) in the presence of water into D-lactic acid and GSH (49–51).

MG is a potent activator of the inflammation transcription factor, nuclear factor kappa-light-chain-enhancer of activated B cells (NF-κB), the NLR family pyrin domain containing 3 (NRLP3) inflammasome and mitochondria production of reactive oxygen species (ROS) (52, 53). Glo1 expression is also negatively regulated by inflammation and oxidative stress (49, 54–57). Thus, as MG levels increase it can activate NF-kB and the NRLP3 inflammasome, increase oxidative stress and downregulate Glo1, resulting in accumulation of MG. At high levels MG can also diffuse from infected immunocytes into the microenvironment. Earlier we showed that acute exposure of vascular endothelial cells and cardiac myocytes to supraphysiologic levels of MG, perturb their intracellular Ca^{2+} homeostasis and increase ROS production (58, 59). Long-term exposure of vascular endothelial cells to MG also diminished their responses to vasodilators and expression of tight junction proteins, established causes of microvascular leakage, decreased microvascular perfusion, fibrosis, and HF (58–60).

Earlier we showed that NOD.Cg-Prkdc^{scid}Il2rg^{tm1Wjl}/SzJ mice reconstituted with human CD34+ hematopoietic stem cells obtained from umbilical cord blood (Hu-mice) can be productively infected with the HIV-1 virus (61–63). These Hu-mice also develop a progressive HF with microvascular leakage and ischemia, akin to that reported in PLWH (64–67), suggesting commonalities in the pathogenesis of HF in Hu-mice and PLWH. Herein, we investigated if the microvascular leakage, fibrosis, ischemia, and HF seen in HIV-infected Hu-mice could be arising from accumulation of MG. Plasma from PLWH and cardiac tissues from deceased HIV-seropositive individuals with HF were also used to confirm elevation in MG.

RESULTS

General Characteristics of Hu-Mice

The general characteristics of the animals used in this study are shown in **Table 1**. Intraperitoneal injection of HIV-1 into Hu-mice led to productive infection; the plasma HIV viral loads four weeks post-infection was 1.5–1.64 × 10^6 RNA copies/mL and remained elevated during the 16-week period. The percentage of CD4+ T cells in blood declined in HIV-1 infected Hu-mice from 76.6 ± 0.4% to 55.2 ± 2.1% during the course of the study (**Supplementary Figure S1A**). CD4+ T cells in blood of HIV-infected Hu-mice treated with AAV2/9-Endo Glo1 also declined to 50.2 ± 3.1%. CD8+ T cells increased in blood of HIV-1 infected Hu-mice and HIV-infected Hu-mice treated with AAV2/9-Endo-Glo1 after 16 weeks of infection (**Supplementary Figure S1B**). The gating strategy

used was CD45→ CD3→ CD4/CD8, and the total CD45 and CD3+ T cells did not notably change during the study (**Supplementary Figures S1C,D**). None of the animals used for this study had to be sacrificed prematurely due to weight loss or graft-vs. host disease.

AAV2/9-Endo-Glo1 Treatment Blunt Lefted Ventricular Function in HIV-1 Infected Hu-Mice

Non-invasive, multi-modal echocardiography (pulsed-wave, tissue Doppler, M-mode, and speckle tracking) did not reveal any impairments in diastolic or systolic functions of the uninfected humanized mice at the start of the study. At five weeks post-infection, all hu-mice (males and females) developed DD characterized by a reduction in peak late-diastolic transmitral velocity (A-wave), an increase in E:A ratio and an increase in E wave deceleration time [**Figure 1B**(ii) $t = 5$ weeks and **Figures 2B-D**]. E:e' ratio and isovolumetric relaxation (IVRT) did not change significantly after five weeks of infection (**Figures 2E,F**). Other parameters of diastolic functions assayed including, isovolumetric contraction (IVCT), mitral valve ejection time (MV-ET), aortic ejection time (AET), and no flow times (NFT) also did not change after five weeks of infection (data not shown). Consistent with DD, speckle tracking (ST) analyses of B-mode images also revealed a significant lowering in global longitudinal strain (**Figure 3A**), and a decrease in reverse longitudinal strain (Pk, %) using the reverse peak algorithm (**Figure 3B**) (63). After five weeks of infection, M-mode Doppler recordings did not show any significant changes in left ventricular systolic functions (percent fractional shortening (FS), percent ejection fraction (EF), left ventricular end diameter–diastole (LVED-diastole), left ventricular end diameter–systole (LVED-systole), and cardiac output (**Figure 4**).

After sixteen weeks of infection, pulsed wave and tissue Doppler revealed worsened DD in HIV-1-infected Hu-mice (males and females) with significant declines in E-wave, A-wave and E-wave deceleration time (**Figures 1**, **2**). L-waves were also pronounced in 4/6 HIV-1 infected Hu-mice [**Figure 1B**(ii), middle right panel, yellow arrow]. E:A ratio, E:e' and IVRT also increased sixteen weeks post-infection (**Figure 2**) as did global longitudinal strain and global circumferential strain (**Figures 3A,C**). Reverse global longitudinal strain decreased further (**Figure 3B**). Strain analyses of long and short axes B-mode images during systole revealed dyskinesis (expansion of a wall segment during systole **Figure 4** left panels, red arrows) and dyssynchrony (opposite walls moving in counter directions, **Figure 4**, right panels blue arrows). After 16 weeks of infection, M-mode echocardiography revealed small but significant declines in FS, EF and cardiac output, and an increase in LVED-diastole and LVED-systole (**Figure 5**).

A single intravenous injection of AAV2/9-Endo-Glo1 to express the Glo1 five weeks after HIV infection, attenuated impairments in myocardial diastolic and systolic dysfunctions that developed 16 weeks post-infection (**Figures 2**, **3**, **5**). Administration of AAV2/9-Endo-Glo1 also attenuated the dyskinesia and the dyssynchrony (**Figure 4**). Video recordings of parasternal long- and short-axis loops showing direction and magnitude of endocardial deformation between uninfected control, HIV-infected Hu-mice and HIV-infected mice treated with AAV2/9-Endo-1, are shown in **Supplementary Videos Files, Videos 1–6**. The non-specific virus AAV2/9-Endo-eGFP had no effect on diastolic and systolic parameters (data not shown). In this study, uninfected Hu-NSG mice also did not develop diastolic and systolic deficits during the 16-week study period. Animals used in this study also did not show physical signs of graft-vs-host disease including hair loss, hunch back or reduced mobility.

AAV2/9-Endo-Glo1 Treatment Blunted Plasma Elevation of MG and Semicarbazide-Sensitive Amine Oxidase (SSAO) in HIV-1 Infected Hu-Mice

After five weeks of HIV-1 infection, MG level was 100.0 ± 6.8% higher in plasma of HIV-1 infected Hu-mice compared to uninfected controls. The activity of the non-selective inflammation enzyme SSAO (the soluble form of vascular adhesion protein-1, VAP-1) was also 38.7 ± 2.3% higher in plasma of HIV-1 infected Hu-mice compared to uninfected controls. After 16 weeks of infection, plasma MG increased further to 250.0 ± 10.3% and SSAO activity increased 84.2 ± 4.3%. A single intravenous injection of AAV2/9-Endo-Glo1 five weeks after HIV-1 infection, attenuated the increases in plasma MG and SSAO as observed at 16 weeks of infection with minimal change in HIV-1 viremia. Uninfected Hu mice showed minimal change in plasma MG and SSAO activity during the study period (**Table 1**).

AAV2/9-Endo-Glo1 Treatment Blunted Leakage of Microvessels and Restored Vascular Perfusion in HIV-1 Infected Hu-Mice

In uninfected control animals, the green fluorescence of injected FITC-labeled BSA (FITC-BSA) appeared throughout the vascular network of mice, indicative of perfusion of the coronary microvessels. Larger diameter vessels which typically contain more blood had more FITC-BSA fluorescence compared to the smaller capillaries (**Figure 6A,** yellow arrow). There was also minimal leakage of the FITC-BSA from the vasculature into the myocardium of uninfected mice. Interestingly, in ventricular tissues in HIV-1 infected animals, FITC-BSA fluorescent was present as "blobs" in some regions, indicative of leakage from the confines of the microvessels into the myocardium (**Figure 6A**, white arrows). Intravenous administration of AAV2/9-Endo-Glo1 to Hu-mice five weeks after HIV-1 infection blunted the impairment in microvascular permeability and microvascular leakage seen in heart at seventeen weeks post-infection (**Figure 6A**, lower right panel). Quantitation of microvascular leakage is shown in **Figure 6B**.

Myocardial tissues from hu-mice seventeen weeks following viral infection contained extensive perivascular and interstitial fibrosis. This was indicated by blue Masson's Trichrome

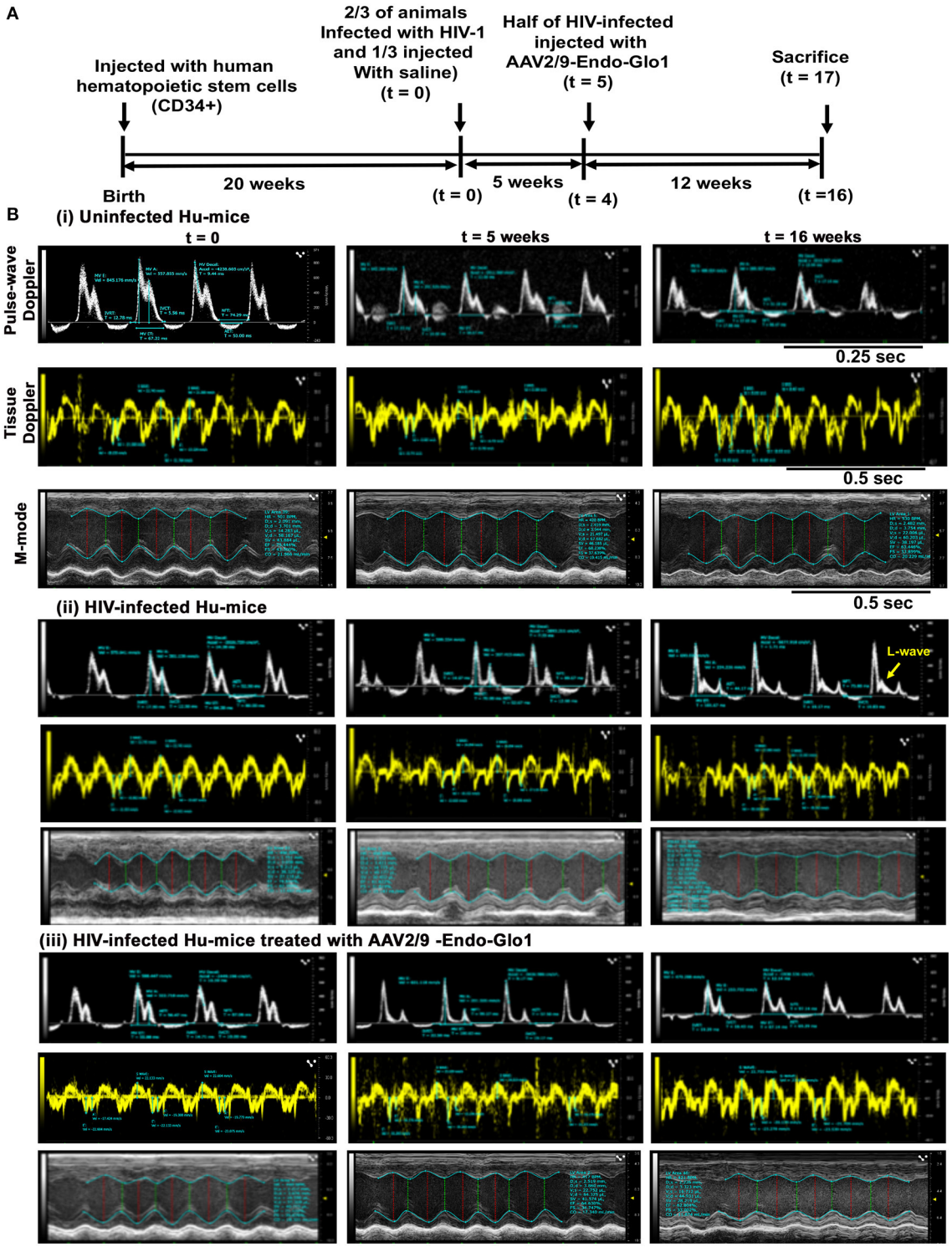

FIGURE 1 | Administration of AAV2/9-Endo-Glo1 shortly after HIV-1 infection attenuated the development of heart failure in humanized mice. **(A)** Experimental scheme for human CD34+ HSC reconstitution, HIV-1 infection, ECHO analysis, Endo-Glo-1 administration, immune cell profiling, and histological evaluations are shown. **(B)** Raw echocardiographic data obtained using Pulse-wave, M-Mode, tissue Doppler in (i) uninfected, (ii) HIV-infected (iii) HIV-infected and treated with AAV2/9-Endo-Glo1. Administration of a single injection of AAV2/9-Endo-Glo1 to hu-mice 5-weeks after HIV-infection attenuated the development of both diastolic and systolic dysfunction as shown at study end. Administration of AAV2/9-Endo-Glo1 also blunted the development of mitral regurgitation (seen as L-wave, yellow arrow).

TABLE 1 | General characteristics of animals used in the study.

Parameter	Uninfected Hu-NSG mice ($n = 6$)	HIV-infected Hu-NSG mice ($n = 6$)	HIV-infected Hu-NSG Treated with AAV2/9-Endo-Glo1 ($n = 6$)
Duration of infection (weeks)	NA	16	16
Body weight (g)			
4-Weeks	18.3 ± 0.4	18.4 ± 0.3	18.3 ± 0.3
16-Weeks	19.2 ± 0.4	19.0 ± 0.3	19.3 ± 0.5
Plasma HIV viral load (RNA copies/mL)			
4-Weeks	NA	$1.6 \pm 0.1 \times 10^5$	$1.5 \pm 0.1 \times 10^5$
16-Weeks	NA	$1.5 \pm 0.1 \times 10^5$	$1.6 \pm 0.3 \times 10^5$
Plasma SSAO activity (units/mL/2 h)			
4-Weeks	3.1 ± 0.1	4.3 ± 0.1*	3.2 ± 0.1**
16-Weeks	3.3 ± 0.4	6.1 ± 0.3*	4.2 ± 0.3**
Plasma HSA-MG eq (μg/ml)			
4-Weeks	30.1 ± 8.1	60.1 ± 10.1*	37.2 ± 10.2**
16-Weeks	35.2 ± 7.1	88.5 ± 12.3*	40.5 ± 9.2**

NA, not applicable.
**significantly different from uninfected controls ($p < 0.05$).*
***Significantly different from HIV-1-infected ($p < 0.05$).*

staining (**Figure 6C**, middle panels, blue staining, yellow arrows), as compared to uninfected controls which exhibited minimal Masson's Trichrome blue staining (**Figure 6C**, upper left panel). Administration of AAV2/9-Endo-Glo1 five weeks after HIV-1 infection blunted the increase in interstitial and perivascular fibrosis seen after 17 weeks post-infection (**Figure 6C**). Quantitation of data are shown in **Figures 6D,E**.

After seventeen weeks of infection, the MG adduct (MG-hydroxyimidazole, isomer 1, MG-H1) was also increased by 400% in ventricular tissues [**Figure 7**(i), middle panels, yellow arrow]. Glo1 immunofluorescence was also reduced by 40%, compared to uninfected controls [**Figure 7**(ii), middles panels]. VAP-1 was upregulated in vascular smooth muscle cells [**Figure 7**(iii), middle panels]. Administration of AAV2/-Endo-Glo1 five weeks post-HIV-1 infection blunted the upregulation of MG-H1, VAP-1 and the loss of Glo1 seen in hearts of Hu-mice, seventeen weeks post-HIV-1 infection (**Figure 7**, right panels).

AAV2/9-Endo-Glo1 Treatment Blunted Endothelial Cell Dysfunction in HIV-1 Infected Hu-Mice

Immunofluorescence staining was also conducted for the endothelial cell marker CD31, to assess the integrity of endothelial cells (ECs) in the coronary microvasculature. After seventeen weeks of infection, CD31 immunofluorescence was reduced by 27.8 ± 2.1% in ventricular sections from HIV-infected animals compared to uninfected controls (**Figure 8A**, and graphs on right, and **Figure 8B**). Administration of AAV2/-Endo-Glo1 blunted the upregulation of the loss of CD31 seen in the myocardium of Hu-mice 16 weeks post-HIV-1 infection (**Figure 8A**).

AAV2/9-Endo-Glo1 Treatment Restored Glo1 and Decreased VAP-1 Protein in Ventricular Homogenates From HIV-Infected Hu-Mice

Western blot analyses conducted to validate changes in ventricular levels of Glo1 and VAP-1 seen in immunofluorescence assays. In this study we found that after seventeen weeks of HIV-1 infection, cardiac Glo1 level was 40.2 ± 3.5% lower than that in control animals (**Figure 8C**). Myocardial VAP-1 level also increased by 58.6 ± 6.5%. A single intravenous injection of AAV2/9-Endo-Glo1 to hu-mice five weeks after HIV-1 infection, increased myocardial Glo1 protein and attenuated the increase in VAP-1 as observed at seventeen weeks following viral infection (**Figure 8D**).

Increased MG and SSAO in PLWH Plasma and Increased MG, Glo1, and VAP-1 in Autopsied Cardiac Tissues in HIV+ Individuals

The amount of MG and SSAO activity in plasma of PLWH, and MG-H1, Glo1 and VAP-1 in autopsied cardiac tissues from deceased HIV-1 sero-positive individuals with HF were assessed to validate the clinical significance of our pre-clinical findings. In plasma of PLWH (age 48.9 ± 3.5 years, duration of infection, 8.55 ± 2.12 years, plasma viral load < 20 RNA copies/ml, **Supplementary Excel File**, patient plasma), MG was 3.2-fold higher when compared to uninfected controls (1607.2

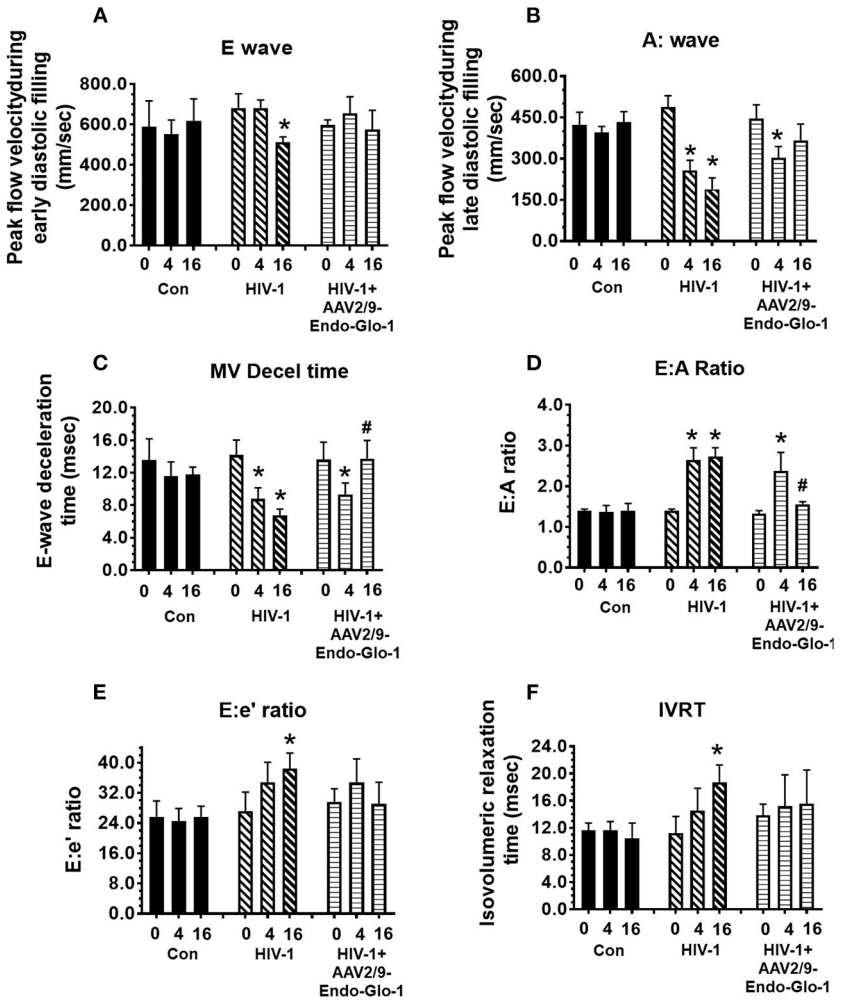

FIGURE 2 | Longitudinal pulse-wave and tissue doppler echocardiography before and after administration of AAV2/9-Endo-Glo1 to Hu-mice after HIV-1 infection reversed/attenuated the development of diastolic dysfunction. The panels below show **(A)** E:wave velocity, **(B)** A:wave velocity, **(C)** E:A ratio, **(D)** E:wave deceleration time, **(E)** E:e ratio and **(F)** isovolumetric relaxation time (IVRT) in uninfected control animals (■) before (0), 5 weeks after and sixteen weeks after injection of saline; in HIV-infected mice (▒) before, 5 weeks and sixteen weeks after HIV-1 infection, and in AAV2/9-Endo-Glo1-treated HIV-infected Hu-mice (▤) before, 5 weeks after infection with HIV-1, and eleven weeks after administration of AAV2/9-Endo Glo1. Data shown on graphs are mean ± SEM from $n \geq 6$ mice per group. *Denotes significantly different from uninfected Hu-NSG mice ($p < 0.05$). #denotes significantly different from HIV-1 infected Hu-mice ($p < 0.05$).

± 89.3 HSA-MG eq (μg/mL) compared to 502.6 ± 61.8 HSA-MG eq (μg/mL)). Mean SSAO activity was also 60% higher compared to uninfected controls (15.5 ± 1.6 units/mL/2 vs. 5.0 ± 0.5 units/mL/2 h, **Supplementary Excel File**, patient plasma). In autopsied ventricular tissues from HIV+ patients with HF MG-H1 was 4.2 ± 0.3-fold higher in vascular smooth muscle cells than control HIV-1 seronegative samples with no HF and 2.0 ± 0.2-fold higher than HIV- patients with atherosclerosis and HF (**Figure 9**, upper panels and graph bottom left, also see **Supplementary Excel File**, autopsied tissues). Glo1 levels were about 50% lower in cardiac tissues from HIV+ with HF as compared to HIV- with no HF and 35 ± 5.1% lower than HIV- group with atherosclerosis and HF (**Figure 9**, middle panels and middle graph). VAP-1 was 5.0 ± 0.3-fold higher in HIV-1 seropositive group with HF as compared to HIV-1 seronegative with no HF and 3.1 ± 0.2-fold higher in HIV-1 seronegative patients with atherosclerosis and HF.

DISCUSSION

HF remains a major cause of morbidity and mortality in >40% of PLWH (4–13). Drugs to blunt or slow the progression of HF in PLWH are not available in part to an incomplete understanding of its underlying cause(s). Herein, we demonstrate for the first time that elevation of the cytotoxic glycolysis byproduct MG is an initiating cause for HF during HIV-1 infection. This conclusion is based on new findings obtained from infected Hu-mice, plasma from PLWH and autopsied cardiac tissues from deceased HIV-1

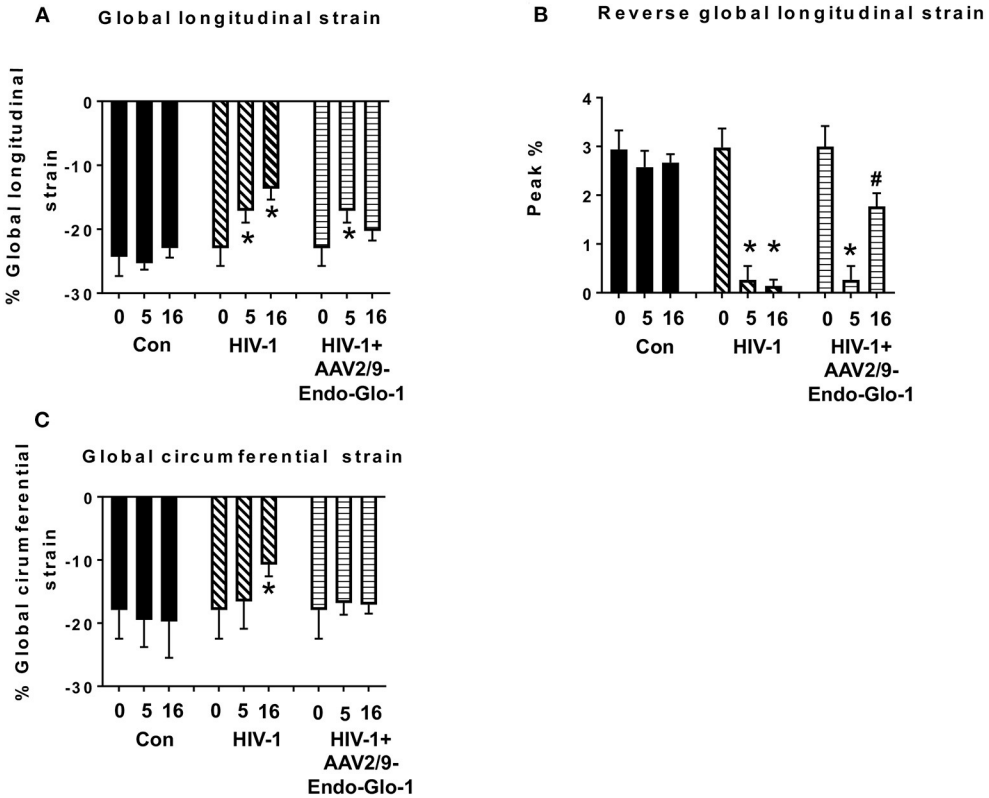

FIGURE 3 | Speckle tracking analysis revealed that administration of AAV2/9-End-Glo1 to Hu-mice after HIV-1 infection attenuated/blunted myocardial strain. **(A)** Global longitudinal strain, **(B)** Reversed global longitudinal strain and **(C)** global circumferential strain in uninfected control animals before injection, 5 weeks, and sixteen weeks after injection of saline; in HIV-infected mice prior to infection with HIV-1, 5 weeks and sixteen weeks after HIV-1 infection, and in AAV2/9-Endo-Glo1-treated HIV-infected Hu-mice before infection, 5 weeks after infection with HIV-1, and eleven weeks after administration of AAV2/9-Endo Glo1 (16 WPI). Data in graphs are mean ± S.E.M from $n \geq 6$ mice per group female mice per group. *Denotes significantly different from uninfected Hu-mice ($p < 0.05$). #Denotes significantly different from HIV-1 infected Hu-mice ($p < 0.05$).

seropositive individuals with HF. MG has been previously linked to HF in other inflammatory diseases (60, 68).

In this study we confirmed our HIV-infected Hu-mice developed a progressive HF using longitudinal echocardiography and histopathological analyses (63). At five weeks post-infection, HIV-infected Hu-mice developed diastolic dysfunction with/without mitral regurgitation that progressed to systolic dysfunction as the duration of infection increased (63). We also found for the first time a progressive increase in plasma MG with worsening HF. Prior studies have reported that following HIV-1 infection, immunocytes upregulate glucose transporter 1 (GLUT1) and increase aerobic glycolysis to generate the necessary substrates needed for HIV-1 replication (43–46). Since 0.1% of glucotriose flux is converted to MG (49, 50), an increase in glycolysis in immunocytes could account in part for the increase in MG. However, additional work is needed to confirm this. Accumulation of MG in plasma and cardiac tissues could also arise from a reduction in its degradation. Using immunofluorescence and Western blot assays, in this study we found for the first time a reduction in Glo1 protein in hearts of Hu-mice seventeen weeks post-infection. These data indicate that the accumulation of MG during HIV-1 infection is also arising in part from a reduction in its degradation.

Next, we assessed if increasing expression of Glo1 would blunt accumulation of MG in HIV-infected hu-mice. Under non-stressed conditions, the nuclear factor erythroid 2-related factor 2 (Nrf2) binds to the antioxidant response element (ARE) on the promoter region of the Glo1 gene induces expression of Glo1 (54, 69). However, under inflammatory as is the case in HIV-1 infection, activated NF-κB would compete with Nrf2 to suppress Glo1 expression (49, 56, 57). As such, to induce expression of Glo1 under inflammatory conditions, we replaced the endogenous CMV promoter of AAV2/9 with the promoter of inflammation-induced protein endothelin-1 (58, 60). Using this strategy, we show for the first time that increasing expression of Glo1 in hearts of HIV-infected Hu-mice decreased MG and blunted the HF seen 16 weeks post-infection, establishing that elevated MG is an underlying cause of HF in HIV-1-infected Hu-mice. It should be mentioned that in this study AAV2/9-Endo-Glo1 was not given to uninfected Hu-mice as these mice have low systemic and

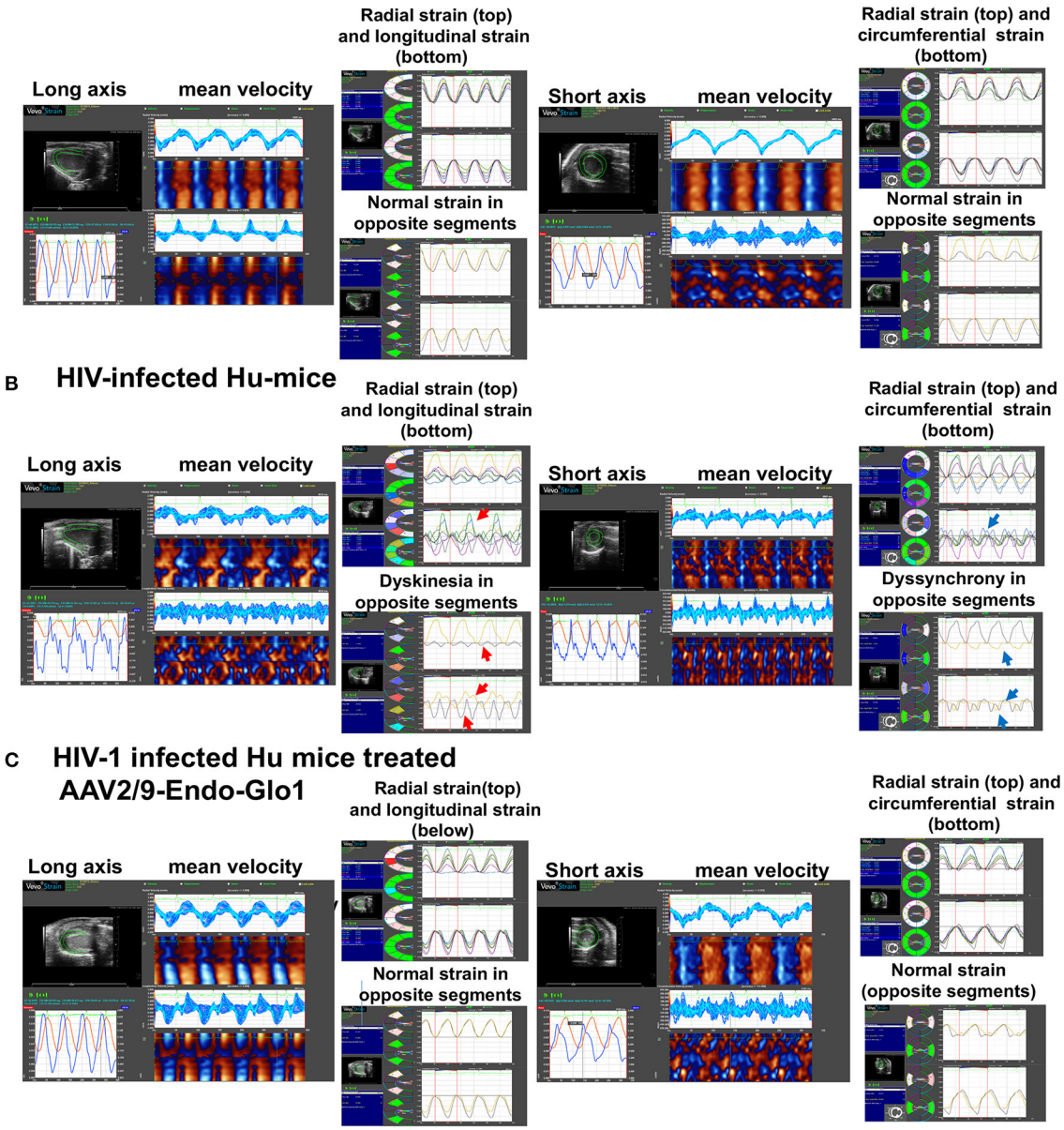

FIGURE 4 | Speckle tracking analysis revealed that administration of AAV2/9-End-Glo1 to Hu-mice after HIV-1 infection attenuated/blunted dyskinesia and dyssynchrony. **(A–C)** Show representative raw data from long (left side) and short axis (right side) velocities during three to four consecutive cardiac cycles (left) in uninfected control animals ($n = 6$) sixteen weeks after injection of saline; HIV-infected hu-mice sixteen weeks after infection ($n = 7$) and HIV-1 infected mice eleven weeks after administration of AAV2/9-Endo Glo1 which is equivalent to 16 weeks post-HIV-infection ($n = 5$). The data shows that 16 weeks after HIV-1 infection, Hu-mice developed dyskinesia [expansion of a wall segment during systole **(B)**, red arrows] and dyssynchrony [opposite walls moving in counter directions **(B)**, blue arrows]. The dyskinesia and dyssynchrony were attenuated in HIV-infected Hu-mice treated with AAV2/9-Endo Glo1.

tissue inflammation, and as such this viral construct would not express Glo1 (58, 60).

Studies were then conducted to delineate mechanisms by which elevated MG elicited HF during HIV-1 infection. First, we found that increasing Glo1 expression blunted the loss of CD31, and microvascular leakage seen in HIV-1 infected Hu-mice, indicating that Glo1 was protected vascular endothelial cells (ECs) in the heart from MG insults. Earlier we showed that microvascular ECs are especially susceptible to elevation in plasma MG due to their low expression of Glo1 (58). We also showed that chronic exposure of microvascular ECs to MG decreased expression of their tight junction proteins (58). Second, we found that increasing Glo1 in the heart of HIV-1-infected hu-mice attenuated perivascular and interstitial fibrosis

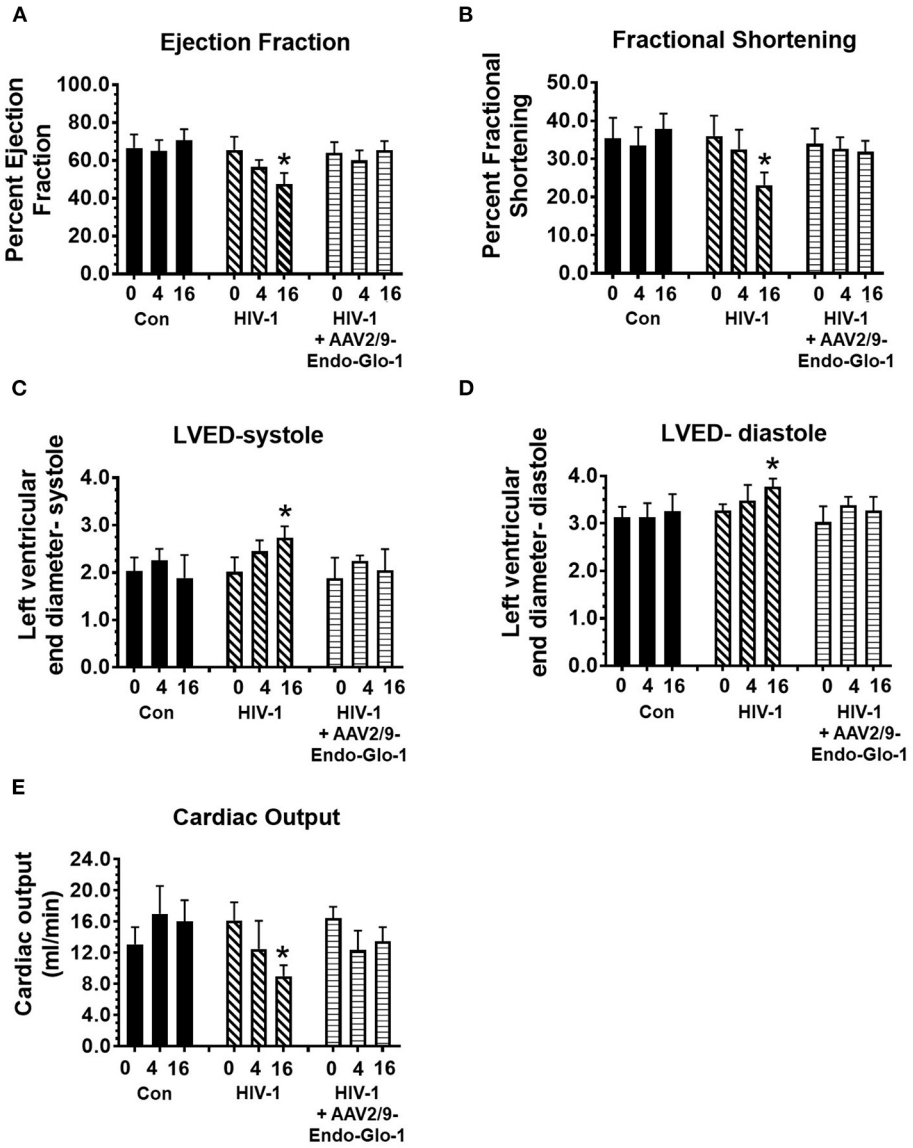

FIGURE 5 | Longitudinal M-Mode echocardiography revealed administration of AAV2/9-Endo-Glo1 to Hu-mice after HIV-1 infection attenuated/blunted systolic dysfunction. **(A)** ejection fraction, **(B)** fractional shortening**, (C)** left ventricular end diameter in systole, **(D)** left ventricular end diameter in diastole , and **(E)** cardiac output in uninfected control animals before injection, 5 weeks and sixteen weeks after injection of saline; in HIV-infected mice before, 5 weeks and sixteen weeks after HIV-1 infection, and in AAV2/9-Endo-Glo1-treated HIV-infected Hu-mice prior to infection with HIV-1, 5 weeks after infection with HIV-1, and eleven weeks after administration of AAV2/9-Endo Glo1. Data in graphs are mean ± S.E.M from $n \geq 6$ mice per group female mice per group. *Denotes significantly different from uninfected Hu-NSG mice ($p < 0.05$).

(60) indicating that the myocardial fibrosis that developed in hearts of HIV-infected Hu-mice were linked to elevated MG. Although the specific molecular pathways by which elevated MG induce fibrosis is not clear, we posit that MG-induced reduction in tight junction proteins would increase extravasation of blood substances and immunocytes into the cardiac interstitium, triggering inflammation, activating matrix metalloproteinases and the deposition of collagen fibers (70). Third, in this study we found that increasing Glo1 expression in hearts of HIV-1 infected mice blunted plasma SSAO and cardiac VAP-1 expression, consistent with the notion that elevation in MG is contributing to systemic and cardiac inflammation (71–73). However, additional studies are needed to determine the cause-effect relationships between MG, cardiac inflammation, NF-κB and NRLP3 inflammasome activation (52, 53).

Plasma from PLWH and autopsied cardiac tissues were assayed for MG, Glo1, SSAO, and VAP-1 to define the clinical relevance of our findings. In plasma from PLWH with low HIV-viremia and autopsied tissues from deceased HIV-1 seropositive individuals, MG levels were 3.7-fold and 4.2-fold higher than

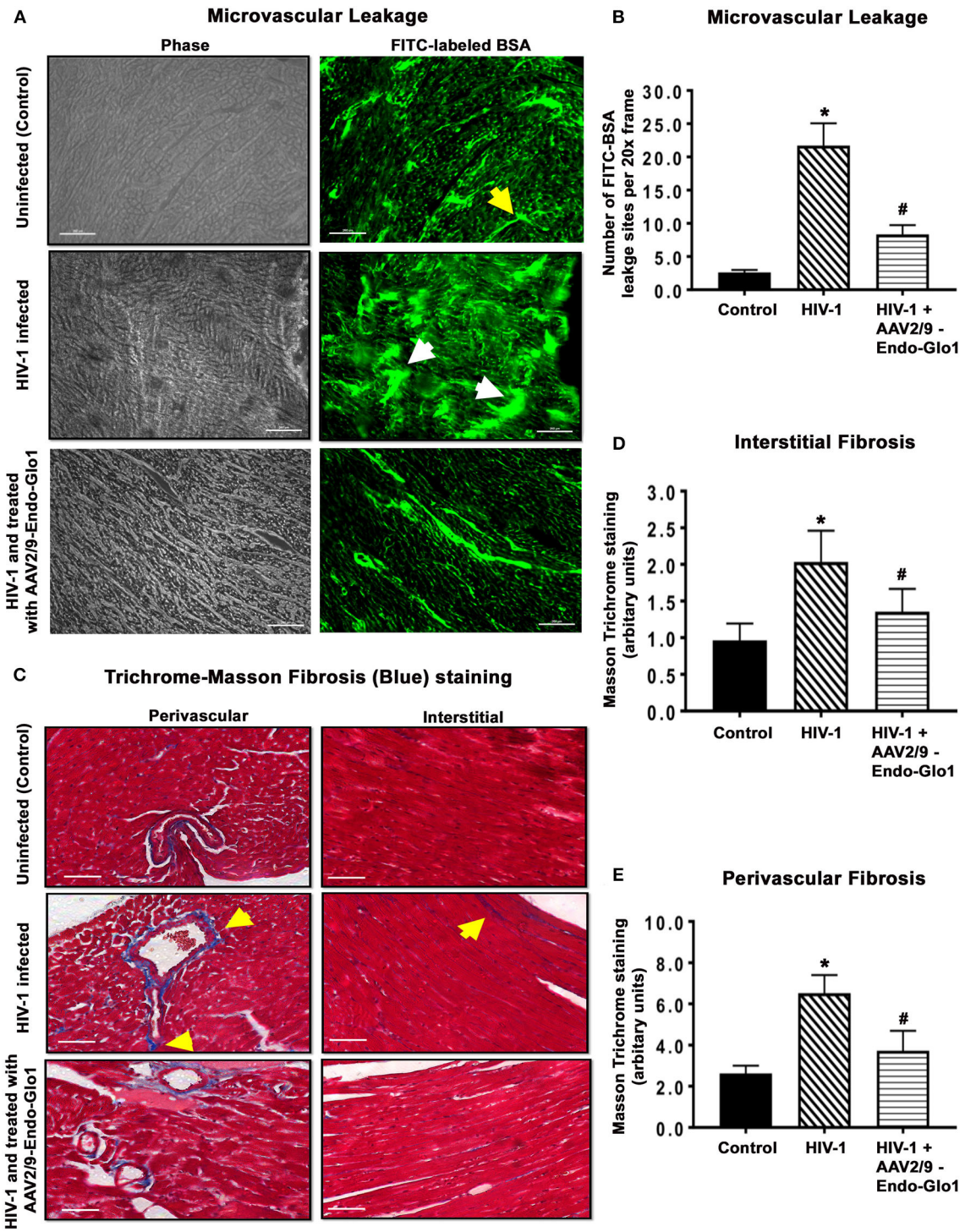

FIGURE 6 | Immunofluorescence and Trichrome-Masson staining revealed administration of AAV2/9-End-Glo1 to Hu-mice shortly after HIV-1 infection attenuated coronary microvascular leakage and fibrosis. **(A)** Representative FITC-BSA images from ventricular sections from uninfected, HIV-infected and AAV2/9-Endo Glo1-treated HIV-infected hu-mice. Yellow arrow points to a perfuse microvessel. White arrows point to microvascular leakage. Graph on right **(B)** shows the relative density of microvessels (<25 μm) perfused with BSA-FITC per 20-x frame. Data in graphs are mean ± SEM from $n > 20$ sections from $n \geq 3$ mice per group. **(C)** Representative Trichrome-Masson staining for fibrosis in left ventricular sections (interstitial and perivascular) from uninfected, HIV-infected and AAV2/9-Endo-Glo1-treated HIV-infected hu-mice at seventeen-weeks study protocol. Graphs on right **(D,E)** are mean ± S.E.M from $n \geq 3$ mice per group. *Denote significantly different ($p < 0.05$) compared to saline injected humanized mice. #Denotes significantly different from HIV-1 infected Hu-mice ($p < 0.05$). White scale bar indicates 200 μm.

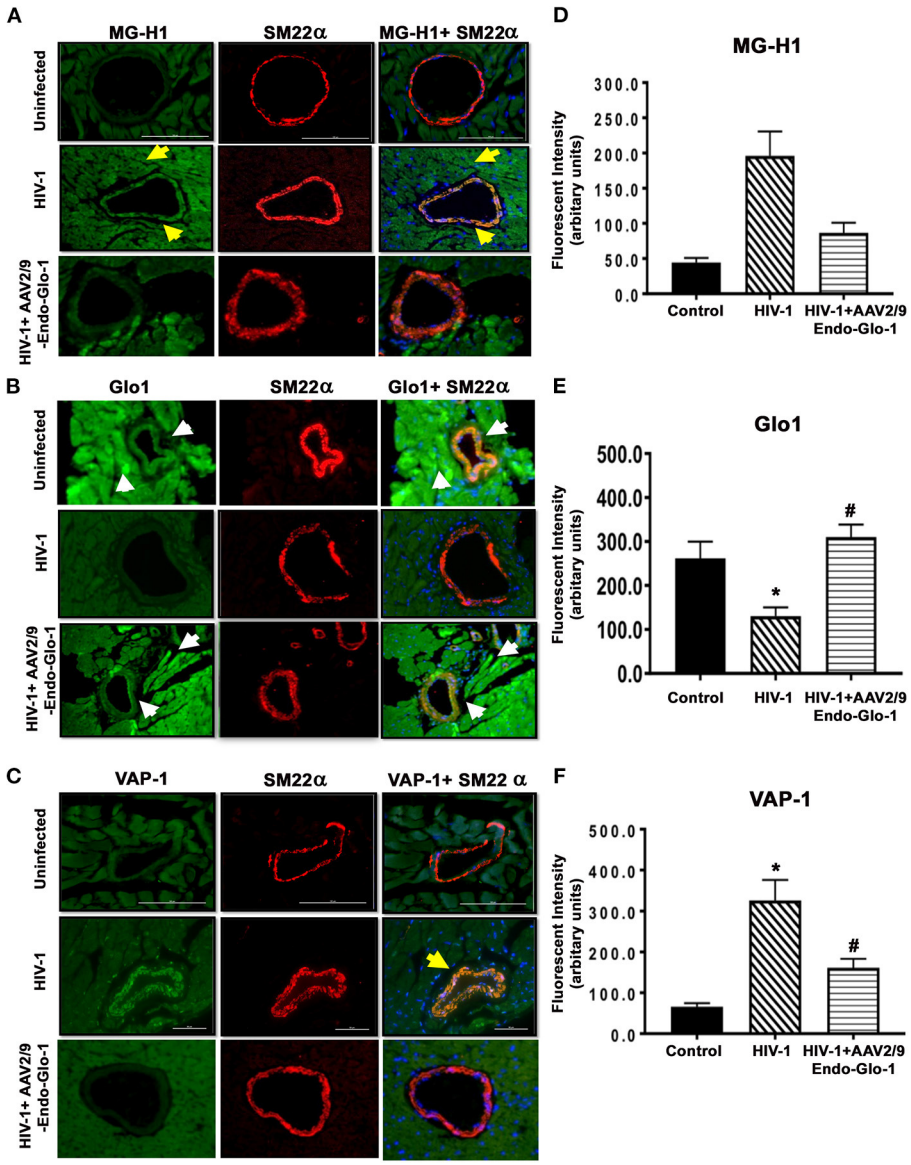

FIGURE 7 | Immunofluorescence assays revealed increasing expression of Glo1 in HIV-infected Hu-mice using AAV2/9-Endo-Glo1 attenuated MG-H1 adduct and the inflammation-induced protein VAP-1. **(A–C)** Shows representative MG-H1, Glo1, and VAP1 immunofluorescence staining in ventricular sections from uninfected, HIV-infected and AAV2/9-Endo Glo1-treated HIV-infected Hu-mice. Yellow arrows in **(A)** shows high immuno-fluorescence for MG-H1 in ventricular tissues from uninfected control tissues. White arrows in **(B)** shows high levels of Glo1 in ventricular shows from uninfected control and AAV2/9-Endo Glo1-treated HIV-infected Hu-mice. Yellow arrow in **(B)** shows high immuno-fluorescence for VAP-1 in ventricular tissues HIV-infected Hu-mice. Graph on right **(D–F)** are mean ± S.E.M for $n \geq 15$ sections obtained from minimum of ($n \geq 3$) animals per group. *Denote significantly different ($p < 0.05$) compared to saline control. #Denotes significantly different from HIV-1 infected Hu-mice ($p < 0.05$).

that in uninfected controls, respectively. SSAO was also 60% higher in plasma of PLWH compared to uninfected controls. In autopsied cardiac tissues from deceased HIV+ individuals, VAP-1 was 5.0-fold higher and Glo1 was 50% lower as compared to uninfected controls without HF. Thus, the elevation in MG and the reduction in Glo1 observed in Hu-mice is of clinical relevance to HF for PLWH.

There are some limitations with the present study. First, although our data show that MG (measured as its surrogate MG-H1) is elevated in plasma and cardiac tissues from HIV-infected Hu-mice, PLWH and autopsied cardiac tissues from HIV-seropositive deceased individuals, the underlying cause for this is not well-delineated. In the present study, we focused on expression of Glo1. However, Glo-1 degrades the hemiacetal formed between MG and reduced glutathione, GSH (49, 50). Thus, a reduction in GSH could result in MG accumulation. As such, additional studies will be needed to determine total glutathione, the ratio of reduced and oxidized glutathione, and

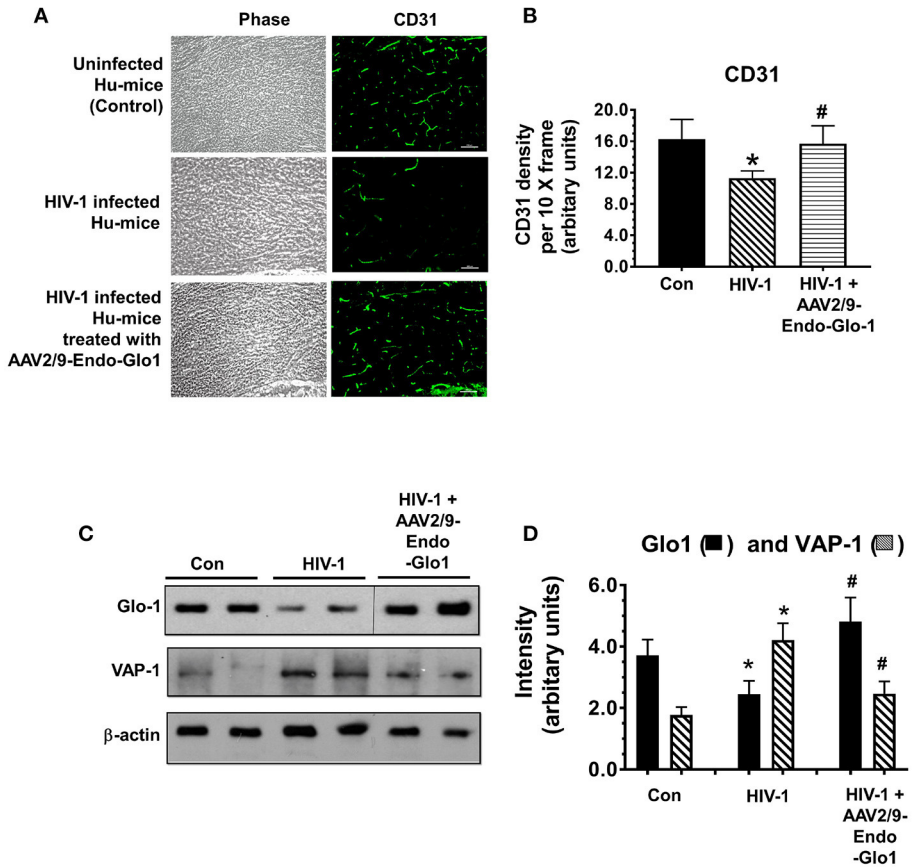

FIGURE 8 | Increasing expression of Glo1 in hearts of HIV-infected Hu-mice using AAV2/9-Endo-Glo1 attenuate loss of CD31 and decrease in VAP-1. **(A)** Immuno-fluorescence analysis to look for the endothelial cell marker CD31 in ventricular tissues from uninfected, HIV-infected, and AAV2/9-Endo Glo1-treated HIV-infected hu-mice. Graph on right **(B)** shows mean ± S.E.M relative intensity from $n > 15$ sections from $n \geq 3$ mice per group, per 10-x frame. **(C)** Representative autoradiograms for Glo1 and VAP1 in ventricular homogenates from uninfected, HIV-infected and AAV2/9-Endo Glo1-treated HIV-infected Hu-mice. Graph on right **(D)** are mean ± S.E.M for ventricular homogenates from ($n \geq 3$) animals per group and done in duplicates. *Denote significantly different from control ($p < 0.05$), #Denote significantly different from T1DM ($p < 0.05$). Scale bar at bottom of each image = 50 μm.

the activities of the two enzymes involved in the synthesis of GSH, namely γ-glutamylcysteine ligase (ligates L-glutamate and L-cysteine), and glutathione synthetase (adds glycine to γ-glutamylcysteine) in hearts of HIV-infected Hu-mice. Second, ischemic regions were observed in hearts of HIV-1 infected Hu-mice as well as in PLWH (63, 66, 67). Under normoxia, the heterodimeric transcription factor that regulates cellular and systemic adaptive responses hypoxia-inducible factor 1α (HIF-1α) is targeted for degradation by the proteasome via hydroxylation of proline residues, mediated by the oxygen-dependent prolyl hydroxylase domain (PHD) family of enzymes (74, 75). When oxygen delivery is compromised, as is the case with ischemia, the PHD enzymes are inhibited, and HIF-1α escapes hydroxylation, allowing it to migrate to the nucleus and induce transcription of HIF-1 target genes, including those involved in glycolysis and erythropoiesis. HIF-1α also binds to the antioxidant response element (ARE) on the promoter region of the *GLO1* gene to inhibit Glo1 expression (49, 56, 57). Thus, ischemia and activation of HIF-1α will also inadvertently lead to an increase in MG. Additional work will also be needed to investigate if inhibitors of HIF-1α are cardio-protective in the setting of HIV-1 infection. Third, the present study focused on EC dysfunction and microvascular leakage, vascular changes that are known mediators of inflammation, fibrosis, and HF. However, supraphysiologic level of MG can also perturb intracellular Ca^{2+}, induce reactive oxygen species (ROS), and form adducts on accessible basic moieties of proteins that could negatively impact the function of cardiac myocytes (59). In the future, we will assess if myocytes from HIV-1 infected Hu-mice have impaired Ca^{2+} homeostasis, increased ROS production, and diminished contractile properties.

In conclusion, the present study shows for the first time that early-onset HF seen in HIV-1-infected Hu-mice is arising in part from accumulation of the cytotoxic glycolysis metabolite MG. We also showed that this elevation in MG is arising in part from a decrease in its degradation and precipitating dysregulation of

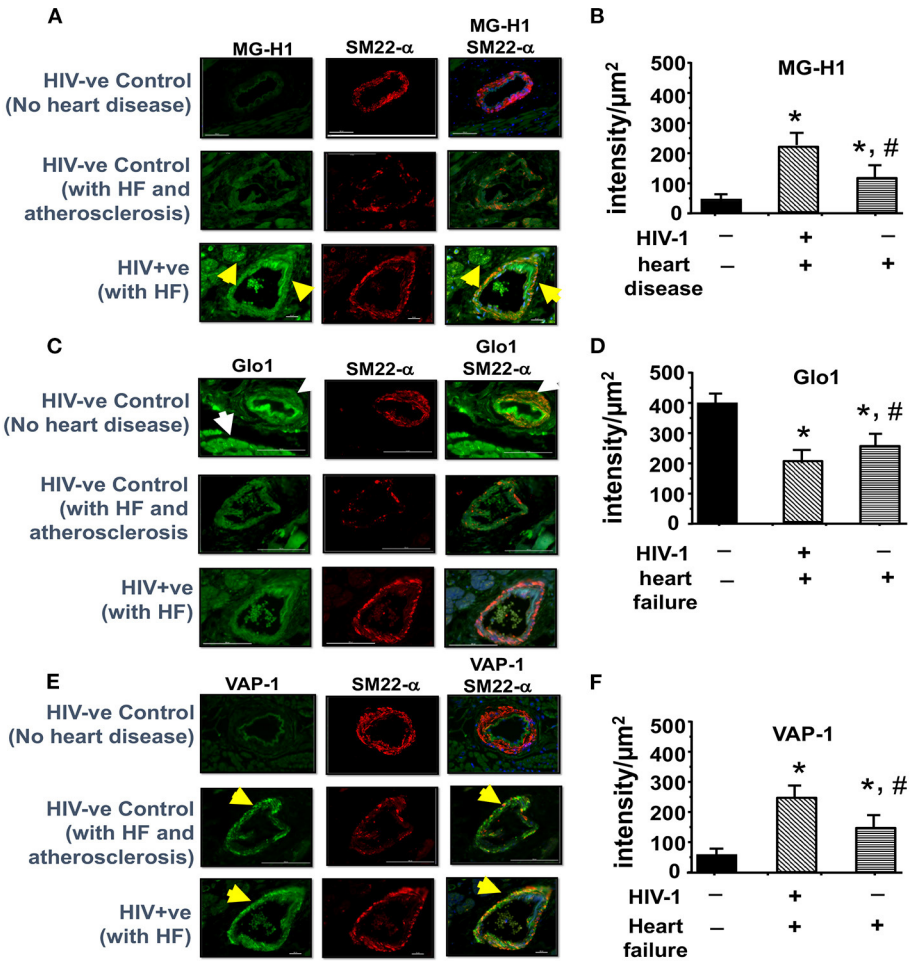

FIGURE 9 | Immunofluorescence revealed increasing expression of MG-H1 and VAP-1 and decreased Glo1 in autopsied left ventricular tissues from decreased HIV+ patients. **(A,C,E)** shows representative MG-H1, Glo1, and VAP1 immunofluorescence staining in autopsied ventricular sections from deceased HIV- patients without heart failure, uninfected controls with atherosclerosis, and HIV+ patients with heart failure. Yellow arrows in **(A,C)** show elevated MG-H1 and VAP-1 in autopsied ventricular sections from non-HIV-infected controls with atherosclerosis and HIV+. White arrows in **(B)** shows elevated Glo1 in autopsied ventricular sections from deceased uninfected patients without heart failure. Graph on right **(B,D,F)** are mean ± S.E.M for ($n \geq 6$) sections obtained from $n = 7$ patients per group. *Denote significantly different ($p < 0.05$) compared to uninfected control without HF. #Denotes significantly different from HIV+ ($p < 0.05$).

coronary microvascular ECs, microvascular leakage, and fibrosis (**Figure 10**). We posit that an elevation in MG could also be an underlying cause increase in systemic and cardiac inflammation seen during HIV-1 infection by activating NF-κB and NRLP3 (4, 5, 19–21). These data also suggest that therapeutic strategies to lower MG levels may be useful in reducing inflammation and HF during HIV-1 infection.

MATERIALS AND METHODS

Antibodies and Reagents

Human hematopoietic stem cell enrichment was done using magnetic beads conjugated CD34+ antibodies from Miltenyi Biotec Inc. (Auburn, CA, USA). The human immune cell reconstitution in mice was assessed by flow cytometry using fluorescence conjugated primary antibodies to the human antigens CD45, CD3, CD19, CD4, CD8, and CD14 from BD Pharmingen (San Diego, CA, USA). Antibodies for immunohistochemistry were obtained from AbCam Inc., Cambridge MA [anti-VAP-1, rabbit polyclonal, Cat # Ab187202; anti-TAGLN (SM22α), goat polyclonal, Cat # Ab10135]; Hycult Biotech, Wayne PA (mouse monoclonal, MG-H1, Cat # HM5017) and Santa Cruz Biotechnology Inc., Santa Cruz, CA [Glo-I [FL-184]], rabbit polyclonal, Cat # SC-67351; the non-selective inflammation-induced protein VAP-1 [E-19], goat polyclonal, Cat # sc-13741; and actin (1–19), goat polyclonal Cat # SC-1616). Secondary antibodies were obtained from Invitrogen Life Technologies (chicken anti-rabbit IgG coupled to Alexa Fluor 488, Cat # A21441; chicken-anti-mouse IgG coupled to Alexa Fluor 488, Cat # A21200; donkey anti-goat IgG coupled to Alexa 594 Cat # A11058); Santa Cruz Biotechnology, Inc. (Donkey anti-rabbit IgG-HRP, Cat # sc-2305 Donkey anti goat IgG-HRP Cat # sc-2304). Fluorescein isothiocyanate-labeled bovine serum

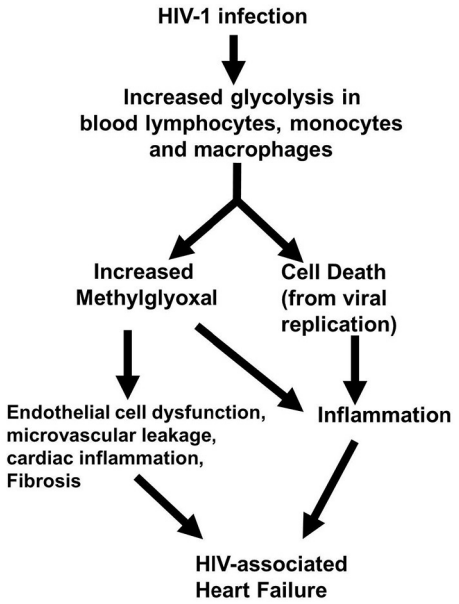

FIGURE 10 | Working hypothesis by which elevation in MG induces HF during HIV-1 infection.

albumin labeled with (FITC-BSA, Cat # A9771), Trichrome-Masson staining kit (Cat # HT15-1KT) and Fluoroshield with DAP1, (Cat # F6057) were from Sigma-Aldrich (St Louis, MO). Semicarbazide-sensitive amine oxidase (soluble form of VAP-1) assay kits (Cat # SSAO100) was obtained from Cell Technology, Inc. (Mountain View, CA). OxiSelect^{TM} MGO competitive ELISA kit (Cat # STA-811) was obtained from Cell BioLabs Inc., San Diego CA. All other reagents were from commercial sources.

Ethics Statement

All experimental protocols involving the use of laboratory animals were approved by the University of Nebraska Medical Center (UNMC) Institutional Animal Care and Use Committee (IACUC) ensuring the ethical care and use of laboratory animals in experimental research. All animal studies were performed in compliance with UNMC institutional policies and NIH guidelines for laboratory animal housing and care. Human CD34+ Hu-NSG were isolated from umbilical cord blood obtained from UNMC labor and delivery department at UNMC with written consents from adult parents to use the remaining or discarded biological material for research. Samples were collected without identifiers under UNMC Institutional Review Board (IRB) exempt. The UNMC institutional IRB determined that these studies using anonymized cord blood samples doesn't constitute human subject research as defined at 45CFR46.102(f). We regularly collect the cord blood samples and isolate CD34+ hematopoietic cells which are either injected immediately into mice or stored in liquid nitrogen for future human reconstitution. NOD.Cg-PrkdcscidIl2rgtm1Wjl/SzJ, NSG mice were obtained from the Jackson Laboratories (Bar Harbor, Maine, USA; stock number 005557), and a breeding colony was developed at the University of Nebraska Medical Center. All animal procedures are approved under the IACUC protocols 18-110-08 and 10-107-01 for ECHO procedures (61–63).

Autopsied Ventricular Tissues From Deceased HIV+ Individuals and Plasma From PLWH

De-identified, autopsied left ventricular tissues on glass slides (consecutive sections) from seven de-identified HIV+ patients with myocardial dysfunction (4 males and 3 females) were obtained from the National NeuroAIDS Tissue Consortium (NNTC), under approved protocol # R605. Age, HIV-1 infection duration, plasma viral load and ARDs taken are in **Supplementary Excel File-a**. Deidentified autopsied cardiac tissues from seven patients with cardiac hypertrophy and atherosclerosis (4 males and 3 females) and from seven uninfected individuals who died in accidents with no reported history of heart diseases were obtained from the tissue bank at the UNMC. De-identified plasma from ten HIV-infected and uninfected "control" patients were also obtained from the UNMC tissue bank. Plasma viral load and ART taken are in **Supplementary Excel File-b**.

Construction of Adeno-Associated Virus Containing Glo1

The University of Pennsylvania Vector Core Facility constructed an adeno-associated virus, AAV2/9 containing glyoxalase-1 driven by the promoter of the inflammation-induced protein, endothelin-1 (AAV2/9-Endo-Glo1) with support from the Gene Therapy Resource Program, GTRP # 1053 (58, 60).

Generation of Humanized Mice

Humanized mice (Hu-mice) were prepared as described in prior publications (61–63). Shortly after birth, NOD.Cg-Prkdc^{scid} Il2rgt^{m1Wjl}/SzJ mice were briefly irradiated with a sub-lethal dose of radiation (1Gy) using a RS-2000 X-Ray Irradiator (Rad Source Technologies). CD34+ cells (50,000 cells/mouse) enriched from human cord blood (>90%) were then injected intra-hepatically and left for humanization. At monthly intervals mice were bled via a submandibular vein into EDTA-coated tubes and screened for human immune cells using flow cytometry (LSR-II FACS analyzer, BD Biosciences, Mountain View, CA, USA). The CD45 percentage in humanized mice used in this study ranged from 25 to 50%. About 5% of our Hu mice develop graft vs.-host disease (GVHD) and these mice were excluded from our study.

Infection of Hu-Mice With HIV-1

Twenty weeks after humanization, 12 Hu-mice were infected intraperitoneally (IP) with 2×10^4 tissue culture infectious dose 50 ($TCID_{50}$) of HIV-1_{ADA} (a macrophage tropic viral strain) (61–63). An additional six Hu-mice served as uninfected aged-matched controls. Peripheral blood samples were collected every four weeks via submandibular vein bleeding to assess HIV-1 viral RNA and to assess the dynamics of human immune cell markers by flow cytometric analysis. Plasma HIV-1 RNA levels were

measured using an automated COBAS Ampliprep V2.0/Taqman-48 system (Roche Molecular Diagnostics, Basel, Switzerland) as per the manufacturer's instructions. The detection limit after dilution factor adjustment was 200 viral RNA copies/mL.

Glo1 Gene Transfer to HIV-1 Infected Hu-Mice

Five weeks post-HIV-1 infection, Hu mice were divided into two groups. Animals in Group-1 received a single intravenous injection of AAV2/9-Endo-Glo1 (1.7×10^{12} virion particles/kg in sterile physiologic saline solution), while animals in Group-2 received saline (58, 60). Uninfected animals were injected with saline and were kept for the whole duration of the study (4 months total). The dose (multiplicity of infection) of AAV used in this study was selected from our earlier (60) and other previous studies (76, 77). AAV2/9 was selected because of its high tropism for cardiac myocytes and endothelial cells (76, 77). The endothelin-1 promoter was used to induce expression of Glo1 in these cells under inflammatory conditions.

Assessment of Longitudinal Cardiac Function Using Echocardiography

Transthoracic conventional echocardiography was performed using a Fujifilm VisualSonics Vevo 3100 system (Fujifilm VisualSonics, Toronto, ON, CAN), employing a MX550D transducer with a center frequency of 40 Hz and an axial resolution of 40 μM, prior to, 5 and 16 weeks after infection with HIV-1 or saline injection (63). For this, hair on chests of mice were removed (Nair, Church & Dwight Co., Inc. NJ, USA). Twenty-four hours later, mice were anesthetized with 1–2% isoflurane (Cardinal Health, Dublin OH, USA) and taped in the supine position on a heated 37°C pad. Anesthesia was maintained with 0.5–3% isoflurane via a nose cone. Feet of mice were connected to ECG leads, and pulsed-wave Doppler images were acquired in the apical four chamber view with appropriate stage tilt and probe tilt to acquire maximum flow and digitally stored in cine loops. The offline Program Vevo LAB 3.1.1 was then used to assess peak early- and late-diastolic transmitral velocities (E and A waves), E-wave deceleration time, isovolumetric relaxation time (IVRT), isovolumetric contraction time (IVCT), mitral valve ejection time (MV ET), aortic ejection time (AET), and no flow time (NFT) as indices of diastolic function. E/A ratio was also calculated. Early diastolic tissue relaxation velocity (E') was measured using tissue Doppler, and E/e′ ratio was calculated. M-mode images were acquired from parasternal short-and long-axes views. Parameters measured include, left ventricular end-diastolic diameter (LVEDD), left ventricular end-systolic diameter (LVESD), left ventricular anterior wall thickness-diastole (LVAW;d), left ventricular anterior wall thickness-systolic (LVAW;s), left ventricular posterior wall thickness-diastolic (LVPW;d), posterior wall thickness-systolic (LVPW;s), mass, fractional shortening (FS), and ejection fraction (EF). Early diastolic tissue relaxation velocity (E') was measured using tissue Doppler, and E:e′ ratio was calculated. All ultrasound imaging and analyses were done in a blinded manner then decoded for statistical evaluation.

Speckle Tracking

Parasternal long-axis and short axis B-mode echocardiographic images were obtained at a rate of >300 frames/second using the Fuji VisualSonics Vevo 3100 system and digitally stored in cine loops (60). Vevo LAB 3.1.1 was used to determine global longitudinal, radial, and circumferential strain using three to four consecutive cardiac cycles. The Vevo Strain Software was used to determine longitudinal, radial strain/strain rates, dyskinesis, and dyssynchrony during systole using six segment (anterior base, AB; anterior middle, AM; anterior apex, AP, posterior base, PB; posterior middle, PM; and posterior apex PA) analyses. All analyses were done in a blinded manner but decoded for statistical analyses.

Microvessels Perfusion and Permeability in Cardiac Tissue

One week after the last echocardiographic measurement (17 weeks post-infection), half of mice from each group were injected with fluorescein isothiocyanate-labeled bovine serum albumin (FITC-BSA 40 mg/kg in sterile 1X PBS buffer, 50 μL) via tail vein (58, 60) and was allowed to circulate for 10 min, after which animals were anesthetized with 5% isoflurane. Chest cavities were opened and hearts were quickly removed and immersed in 4% paraformaldehyde for 24 h at 4°C. Hearts were then cut longitudinally into three sections, and the right 1/3 was transferred to 4% paraformaldehyde/15% sucrose solution for 24 h, followed by 4% paraformaldehyde/30% sucrose solution for 24 h, and then 30% sucrose solution for 24 h. Cryoprotected hearts were cut into 20 μm thick longitudinal/coronal sections on a microtome (Leica EM-UC 6, Leica Microsystems, Wien, Austria) and mounted onto pre-cleaned glass slides. Cardiac sections were then washed three times with 1X PBS to remove cutting medium. Vectashield™ mounting medium containing DAPI was added to the sections, and slides were cover slipped and dried overnight. Next day slides were placed on the head stage of a Nikon TE2000 microscope attached to a Coolsnap HQ2 CCD camera (Photometrics, Tuscon AZ, USA) and images were collected to assess the density of microvessels perfused with BSA-FITC and microvascular leakage. Analyses were done in a blinded manner but decoded for statistical evaluation.

Masson-Trichrome and Immunofluorescence Staining in Cardiac Tissue

The left longitudinal 1/3rd of hearts from Hu-mice were also placed in 4% paraformaldehyde for 24 h and then processed and embedded in paraffin as described earlier (63). Five micrometer sections were then cut and placed onto glass slides. Slides were de-paraffinized with xylene (3 changes, ten minutes each) and rehydrated in decreasing concentrations of ethanol (100, 95, 70% and distilled water, three minutes each) followed

by a saline wash. Masson Trichrome staining was conducted using rehydrated sections without modification to assess fibrosis (Sigma-Aldrich, St Louis, MO, USA). Sections were then cover slipped with Prolong Gold Anti-fade reagent. Images were then taken with a Nikon inverted fluorescence microscope (TE 2000) equipped with a CoolSNAP HQ2 CCD Camera (Photometrics, Tucson, AZ, USA). Image analysis software quantitated changes. This was completed in a blinded manner then decoded for statistical evaluation. Immunofluorescence staining was performed on cardiac tissues from Hu-mice (uninfected, HIV-1-infected and HIV-1-infected and treated with AAV2/9-Endo-Glo1) and from autopsied cardiac tissues obtained from uninfected and HIV-1 seropositive persons to determine the levels of the MG (hydroimidazolone isomer 1), Glo1, CD31 (measure of endothelial cell) and VAP-1 (a non-selective, inflammation-induced protein). Calponin-related protein (SM22α), a marker of contractile smooth muscle cells, served as reference to define microvessels. Primary antibodies were used at concentrations of 1:100 to 1:200 while secondary antibodies concentrations were 1:250 to 1:500. Horse serum (10%) was used as the blocking agents to reduce non-specific interactions. Images were taken with a Nikon inverted fluorescence microscope (TE 2000). Nikon Elements image analysis software was used to quantitate changes of VAP-1, MG-H1 and Glo1 immunoreactivities using 20× frames.

MG and Semicarbazide-Sensitive Amine Oxidase (SSAO) in Plasma

MG levels (as surrogate MG-H1, OxiSelect™ Methylglyoxal Competitive ELISA, Cell Biolabs Inc, San Diego CA) in plasma were measured from Hu-mice (6 and 16 weeks, uninfected, HIV-infected and AAV2/9-Endo-Glo1-treated), and from uninfected healthy controls and PLWH as per manufacturers' instruction inside a BSL2+ Facility at UNMC. The activity of the non-selective inflammation marker, semicarbazide-sensitive amine oxidase (the soluble form of VAP-1) in plasma from Hu-mice was measured from (uninfected, HIV-infected and AAV2/9-Endo-Glo1-treated), and from uninfected healthy controls and PLWH using Fluoro-SSAO™ (Cell Technology, Mountain View CA) as per manufacture's instruction.

Glo1 and VAP-1

Glo1 and VAP-1 levels in ventricular homogenates were also determined using Western blot assays (59). For this, cardiac tissues (50 mg) were chopped into small pieces, placed into 200 μL of cell lysis buffer (MicroRotofor Cell Lysis Kit (mammals), BioRad Inc., Burlingame CA) and sonicated 3 × 3 s with 10 s intervals on ice in between. Samples were then centrifuged at 3,000 × g for 5 min and the supernatants were collected and protein concentration was determined using Bradford Protein Assay Kit (BioRad Inc., Burlingame CA). Western blots were then carried out as described in earlier publications. Primary antibody concentrations were used at 1:1,000 dilutions and incubated for 16 h at 4°C and secondary antibody were used at 1:2,00 and incubated for 2 h at room temperature. β-actin served as the internal control to correct for variations in sample loading.

Statistical Analyses

Data were analyzed using GraphPad Prism 7.0 software (La Jolla, CA) and presented in text as the mean ± the standard error of the mean. All experiments listed in this manuscript were performed using a minimum of three biologically distinct replicates. One-way ANOVA with Bonferroni correction for multiple comparisons were used. For studies with multiple time points, two-way factorial ANOVA and Bonferroni's *post-hoc* tests for multiple comparisons were performed. Studies were from six animals per group. Significant differences were determined at $p < 0.05$.

DATA AVAILABILITY STATEMENT

The original contributions presented in the study are included in the article/**Supplementary Material**, further inquiries can be directed to the corresponding author/s.

ETHICS STATEMENT

The studies involving human participants were reviewed and approved by Human CD34+ Hu-NSG were isolated from umbilical cord blood obtained from UNMC labor and delivery department at UNMC with written consents from adult parents to use the remaining or discarded biological material for research. Samples were collected without identifiers under UNMC Institutional Review Board (IRB) exempt. The UNMC institutional IRB determined that these studies using anonymized cord blood samples doesn't constitute human subject research as defined at 45CFR46.102(f). We regularly collect the cord blood samples and isolate CD34+ hematopoietic cells which are either injected immediately into mice or stored in liquid nitrogen for future human reconstitution. The patients/participants provided their written informed consent to participate in this study. The animal study was reviewed and approved by University of Nebraska Medical Center (UNMC) Institutional Animal Care and Use Committee (IACUC). All animal procedures are approved under the IACUC protocols 18-110-08 and 10-107-01 for ECHO procedures. Written informed consent was obtained from the individual(s) for the publication of any potentially identifiable images or data included in this article.

AUTHOR CONTRIBUTIONS

KB conceived the experiments and planned along with all other authors. SG created humanized mice. PD, FA, BH, and KB conducted echocardiography and histopathological assays and interpreted the data sets for the humanized mice. PD and KB performed molecular, virologic and immunological studies, and related data analyses. JC, HF, and BM assisted with obtaining the de-identified human plasma and tissues. KB, EM, and SG performed

and analyzed the microvascular permeability and fibrosis tests and analyses. FA, PD, JM, JC, BM, HG, HF, and SG interpreted the data and wrote the manuscript with editing. All authors contributed to the article and approved the submitted version.

FUNDING

This work was supported in part by a pilot project from UNMC Center for Chronic HIV infection and Aging in NeuroAIDS (NIH P30 MH062261) and R56 HL151602-01A1.

ACKNOWLEDGMENTS

The authors are thankful to Hang Su for technical assistance, Emiko Waight for proof-reading the article and Lili Guo for generation of humanized mice.

SUPPLEMENTARY MATERIAL

The Supplementary Material for this article can be found online at: https://www.frontiersin.org/articles/10.3389/fcvm.2021.792180/full#supplementary-material

Supplementary Figure S1 | Time frame of observation of immune status of animals used in the study.

Supplementary XLSX | Showing (Sheet-1)—Patient data details from whom Plasma is analyzed. (Sheet-2)—Patient data details from whom autopsied tissues were used for the study.

Video 1 | Uninfected control Hu-mice Video Short axis.

Video 2 | Uninfected control Hu-mice Video Long axis.

Video 3 | HIV-1 infected Hu-mice Video Short axis.

Video 4 | HIV-1 infected Hu-mice Video Long axis.

Video 5 | HIV-1 infected and AAV2/9-Endo-Glo1 injected mice Video short axis.

Video 6 | HIV-1 infected and AAV2/9-Endo-Glo1 injected mice Video Long axis.

REFERENCES

1. Cattaneo D, Baldelli S, Cozzi V, Clementi E, Marriott DJE, Gervasoni C, et al. Impact of therapeutic drug monitoring of antiretroviral drugs in routine clinical management of people living with HIV: a narrative review. *Ther Drug Monit*. (2020) 42:64–74. doi: 10.1097/FTD.0000000000000684
2. Mu Y, Kodidela S, Wang Y, Kumar S, Cory TJ. The dawn of precision medicine in HIV: state of the art of pharmacotherapy. *Expert Opin Pharmacother*. (2018) 19:1581–95. doi: 10.1080/14656566.2018.1515916
3. Erqou S, Lodebo BT, Masri A, Altibi AM, Echouffo-Tcheugui JB, Dzudie A, et al. Cardiac dysfunction among people living with HIV: a systematic review and meta-analysis. *JACC Heart Fail*. (2019) 7:98–108. doi: 10.1016/j.jchf.2018.10.006
4. Butler J, Kalogeropoulos AP, Anstrom KJ, Hsue PY, Kim RJ, Scherzer R, et al. Diastolic dysfunction in individuals with human immunodeficiency virus infection: literature review, rationale and design of the characterizing heart function on antiretroviral therapy (CHART) study. *J Card Fail*. (2018) 24:255–65. doi: 10.1016/j.cardfail.2018.02.001
5. Hsue PY, Waters DD. Heart failure in persons living with HIV infection. *Curr Opin HIV AIDS*. (2017) 12:534–9. doi: 10.1097/COH.0000000000000409
6. Savvoulidis P, Butler J, Kalogeropoulos A. Cardiomyopathy and heart failure in patients with HIV infection. *Can J Cardiol*. (2019) 35:299–309. doi: 10.1016/j.cjca.2018.10.009
7. Freiberg MS, Chang CH, Skanderson M, Patterson OV, DuVall SL, Brandt CA, et al. Association between HIV infection and the risk of heart failure with reduced ejection fraction and preserved ejection fraction in the antiretroviral therapy era: results from the veterans aging cohort study. *JAMA Cardiol*. (2017) 2:536–46. doi: 10.1001/jamacardio.2017.0264
8. Moayedi Y, Walmsley SL. Heart failure with preserved ejection fraction in women living with HIV: another inflammatory comorbidity? *J Infect Dis*. (2020) 221:1219–22. doi: 10.1093/infdis/jiz185
9. Al-Kindi SG, ElAmm C, Ginwalla M, Mehanna E, Zacharias M, Benatti R, et al. Heart failure in patients with human immunodeficiency virus infection: epidemiology and management disparities. *Int J Cardiol*. (2016) 218:43–6. doi: 10.1016/j.ijcard.2016.05.027
10. Volpe M, Uglietti A, Castagna A, Mussini C, Marchetti G, Bellagamba R, et al. Cardiovascular disease in women with HIV-1 infection. *Int J Cardiol*. (2017) 241:50–6. doi: 10.1016/j.ijcard.2017.02.117
11. Stone L, Looby SE, Zanni MV. Cardiovascular disease risk among women living with HIV in North America and Europe. *Curr Opin HIV AIDS*. (2017) 12:585–93. doi: 10.1097/COH.0000000000000413
12. Russell E, Albert A, Cote H, Hsieh A, Nesbitt A, Campbell AR, et al. Rate of dyslipidemia higher among women living with HIV: a comparison of metabolic and cardiovascular health in a cohort to study aging in HIV. *HIV Med*. (2020) 21:418–28. doi: 10.1111/hiv.12843
13. Kendall CE, Wong J, Taljaard M, Glazier RH, Hogg W, Younger J, et al. A cross-sectional, population-based study measuring comorbidity among people living with HIV in Ontario. *BMC Public Health*. (2014) 14:161. doi: 10.1186/1471-2458-14-161
14. Hsue PY, Waters DD. Time to recognize HIV infection as a major cardiovascular risk factor. *Circulation*. (2018) 138:1113–5. doi: 10.1161/CIRCULATIONAHA.118.036211
15. Losina E, Hyle EP, Borre ED, Linas BP, Sax PE, Weinstein MC, et al. Projecting 10-year, 20-year, and lifetime risks of cardiovascular disease in persons living with human immunodeficiency virus in the United States. *Clin Infect Dis*. (2017) 65:1266–71. doi: 10.1093/cid/cix547
16. Desai N, Burns L, Gong Y, Zhi K, Kumar A, Summers N, et al. An update on drug-drug interactions between antiretroviral therapies and drugs of abuse in HIV systems. *Expert Opin Drug Metab Toxicol*. (2020) 16:1005–18. doi: 10.1080/17425255.2020.1814737
17. Hershow RB, Zuskov DS, Vu Tuyet Mai N, Chander G, Hutton HE, Latkin C, et al. "[Drinking is] Like a Rule That You Can't Break": perceived barriers and facilitators to reduce alcohol use and improve antiretroviral treatment adherence among people living with HIV and alcohol use disorder in Vietnam. *Subst Use Misuse*. (2018) 53:1084–92. doi: 10.1080/10826084.2017.1392986
18. Longo-Mbenza B, Longokolo Mashi M, Lelo Tshikwela M, Mokondjimobe E, Gombet T, Ellenga-Mbolla B, et al. Relationship between younger age, autoimmunity, cardiometabolic risk, oxidative stress, HAART, and ischemic stroke in Africans with HIV/AIDS. *ISRN Cardiol*. (2011) 2011:897908. doi: 10.5402/2011/897908
19. de Leuw P, Arendt CT, Haberl AE, Froadinadl D, Kann G, Wolf T, et al. Myocardial fibrosis and inflammation by CMR predict cardiovascular outcome in people living with HIV. *JACC Cardiovasc Imaging*. (2021) 4:1548–57. doi: 10.1016/j.jcmg.2021.01.042
20. Maritati M, Alessandro T, Zanotta N, Comar M, Bellini T, Sighinolfi L, et al. A comparison between different anti-retroviral therapy regimes on soluble inflammation markers: a pilot study. *AIDS Res Ther*. (2020) 17:61. doi: 10.1186/s12981-020-00316-w
21. Vallejo A, Molano M, Monsalvo-Hernando M, Hernandez-Walias F, Fontecha-Ortega M, Casado JL. Switching to dual antiretroviral regimens is associated with improvement or no changes in activation and inflammation markers in virologically suppressed HIV-1-infected patients: the TRILOBITHE pilot study. *HIV Med*. (2019) 20:555–60. doi: 10.1111/hiv.12749
22. Colaco NA, Wang TS, Ma Y, Scherzer R, Ilkayeva OR, Desvigne-Nickens P, et al. Transmethylamine-N-oxide is associated with diffuse

cardiac fibrosis in people living with HIV. *J Am Heart Assoc*. (2021) 10:e020499 doi: 10.1161/JAHA.120.020499
23. Lewis W. Use of the transgenic mouse in models of AIDS cardiomyopathy. *AIDS*. (2003) 17(Suppl 1.):S36–45. doi: 10.1097/00002030-200304001-00006
24. Otis JS, Ashikhmin YI, Brown LA, Guidot DM. Effect of HIV-1-related protein expression on cardiac and skeletal muscles from transgenic rats. *AIDS Res Ther*. (2008) 5:8. doi: 10.1186/1742-6405-5-8
25. Kay DG, Yue P, Hanna Z, Jothy S, Tremblay E, Jolicoeur P. Cardiac disease in transgenic mice expressing human immunodeficiency virus-1 NEF in cells of the immune system. *Am J Pathol*. (2002) 161:321–35. doi: 10.1016/S0002-9440(10)64184-3
26. Lund AK, Lucero J, Herbert L, Liu Y, Naik JS. Human immunodeficiency virus transgenic rats exhibit pulmonary hypertension. *Am J Physiol Lung Cell Mol Physiol*. (2011) 301:L315–26. doi: 10.1152/ajplung.00045.2011
27. Cheung JY, Gordon J, Wang J, Song J, Zhang XQ, Prado FJ, et al.: Mitochondrial dysfunction in human immunodeficiency virus-1 transgenic mouse cardiac myocytes. *J Cell Physiol*. (2019) 234:4432–44. doi: 10.1002/jcp.27232
28. Cheung JY, Gordon J, Wang J, Song J, Zhang XQ, Tilley DG, et al. Cardiac dysfunction in HIV-1 transgenic mouse: role of stress and BAG3. *Clin Transl Sci*. (2015) 8:305–10. doi: 10.1111/cts.12331
29. Henderson LJ, Johnson TP, Smith BR, Reoma LB, Santamaria UA, Bachani M, et al. Presence of Tat and transactivation response element in spinal fluid despite antiretroviral therapy. *AIDS*. (2019) 33(Suppl. 2):S145–57. doi: 10.1097/QAD.0000000000002268
30. Khan MB, Lang MJ, Huang MB, Raymond A, Bond VC, Shiramizu B, et al. Nef exosomes isolated from the plasma of individuals with HIV-associated dementia (HAD) can induce Abeta(1-42) secretion in SH-SY5Y neural cells. *J Neurovirol*. (2016) 22:179–90. doi: 10.1007/s13365-015-0383-6
31. Johnson TP, Patel K, Johnson KR, Maric D, Calabresi PA, Hasbun R, et al. Induction of IL-17 and nonclassical T-cell activation by HIV-Tat protein. *Proc Natl Acad Sci USA*. (2013) 110:13588–93. doi: 10.1073/pnas.1308673110
32. Potash MJ, Chao W, Bentsman G, Paris N, Saini M, Nitkiewicz J, et al. A mouse model for study of systemic HIV-1 infection, antiviral immune responses, and neuroinvasiveness. *Proc Natl Acad Sci USA*. (2005) 102:3760–5. doi: 10.1073/pnas.0500649102
33. Chen M, Hung CL, Yun CH, Webel AR, Longenecker CT. Sex differences in the association of fat and inflammation among people with treated HIV infection. *Pathog Immun*. (2019) 4:163–79. doi: 10.20411/pai.v4i1.304
34. Waters DD, Hsue PY. Lipid abnormalities in persons living with HIV infection. *Can J Cardiol*. (2019) 35:249–59. doi: 10.1016/j.cjca.2018.11.005
35. Padmapriyadarsini C, Shet A, Srinivasan R, Ramachandran G, Sanjeeva GN, Devi P, et al. High prevalence of lipid abnormalities and insulin resistance among antiretroviral naive HIV-infected children in India. *Pediatr Infect Dis J*. (2018) 37:253–7. doi: 10.1097/INF.0000000000001829
36. Calza L, Colangeli V, Magistrelli E, Rossi N, Rosselli Del Turco E, et al. Prevalence of metabolic syndrome in HIV-infected patients naive to antiretroviral therapy or receiving a first-line treatment. *HIV Clin Trials*. (2017) 18:110–7. doi: 10.1080/15284336.2017.1311502
37. Shen Y, Wang J, Wang Z, Qi T, Song W, Tang Y, et al. Prevalence of dyslipidemia among antiretroviral-naive HIV-infected individuals in China. *Medicine*. (2015) 94:e2201. doi: 10.1097/MD.0000000000002201
38. Mocumbi AO, Dobe I, Candido S, Kim N. Cardiovascular risk and D-dimer levels in HIV-infected ART-naive Africans. *Cardiovasc Diagn Ther*. (2020) 10:526–33. doi: 10.21037/cdt.2019.12.02
39. Karavidas A, Xylomenos G, Matzaraki V, Papoutsidakis N, Leventopoulos G, Farmakis D, et al. Myocardial deformation imaging unmasks subtle left ventricular systolic dysfunction in asymptomatic and treatment-naive HIV patients. *Clin Res Cardiol*. (2015) 104:975–81. doi: 10.1007/s00392-015-0866-8
40. Fontes-Carvalho R, Mancio J, Marcos A, Sampaio F, Mota M, Rocha Goncalves F, et al. HIV patients have impaired diastolic function that is not aggravated by anti-retroviral treatment. *Cardiovasc Drugs Ther*. (2015) 29:31–9. doi: 10.1007/s10557-015-6573-x
41. Bergersen BM, Sandvik L, Dunlop O, Birkeland K, Bruun JN. Prevalence of hypertension in HIV-positive patients on highly active retroviral therapy (HAART) compared with HAART-naive and HIV-negative controls: results from a Norwegian study of 721 patients. *Eur J Clin Microbiol Infect Dis*. (2003) 22:731–6. doi: 10.1007/s10096-003-1034-z
42. Barbaro G, Barbarini G, Di Lorenzo G. Early impairment of systolic and diastolic function in asymptomatic HIV-positive patients: a multicenter echocardiographic and echo-Doppler study. The Gruppo Italiano Per lo Studio Cardiologico dei Pazienti Affetti da AIDS. *AIDS Res Hum Retroviruses*. (1996) 12:1559–63. doi: 10.1089/aid.1996.12.1559
43. Hegedus A, Kavanagh Williamson M, Huthoff H. HIV-1 pathogenicity and virion production are dependent on the metabolic phenotype of activated CD4+ T cells. *Retrovirology*. (2014) 11:98. doi: 10.1186/s12977-014-0098-4
44. Palmer CS, Ostrowski M, Gouillou M, Tsai L, Yu D, Zhou J, et al. Increased glucose metabolic activity is associated with CD4+ T-cell activation and depletion during chronic HIV infection. *AIDS*. (2014) 28:297–309. doi: 10.1097/QAD.0000000000000128
45. Kang S, Tang H. HIV-1 infection and glucose metabolism reprogramming of T cells: another approach toward functional cure and reservoir eradication. *Front Immunol*. (2020) 11:572677. doi: 10.3389/fimmu.2020.572677
46. Loisel-Meyer S, Swainson L, Craveiro M, Oburoglu L, Mongellaz C, Costa C, et al. Glut1-mediated glucose transport regulates HIV infection. *Proc Natl Acad Sci USA*. (2012) 109:2549–54. doi: 10.1073/pnas.1121427109
47. Palmer CS, Cherry CL, Sada-Ovalle I, Singh A, Crowe SM. Glucose metabolism in T cells and monocytes: new perspectives in HIV pathogenesis. *EBioMedicine*. (2016) 6:31–41. doi: 10.1016/j.ebiom.2016.02.012
48. Richard JP. Mechanism for the formation of methylglyoxal from triosephosphates. *Biochem Soc Trans*. (1993) 21:549–53. doi: 10.1042/bst0210549
49. Schalkwijk CG, Stehouwer CDA. Methylglyoxal, a highly reactive dicarbonyl compound, in diabetes, its vascular complications, and other age-related diseases. *Physiol Rev*. (2020) 100:407–61. doi: 10.1152/physrev.00001.2019
50. Thornalley PJ. The glyoxalase system in health and disease. *Mol Aspects Med*. (1993) 14:287–371. doi: 10.1016/0098-2997(93)90002-U
51. Sousa Silva M, Gomes RA, Ferreira AE, Ponces Freire A, Cordeiro C. The glyoxalase pathway: the first hundred years and beyond. *Biochem J*. (2013) 453:1–15. doi: 10.1042/BJ20121743
52. Lin CC, Chan CM, Huang YP, Hsu SH, Huang CL, Tsai SJ. Methylglyoxal activates NF-kappaB nuclear translocation and induces COX-2 expression via a p38-dependent pathway in synovial cells. *Life Sci*. (2016) 149:25–33. doi: 10.1016/j.lfs.2016.02.060
53. Hishida E, Ito H, Komada T, Karasawa T, Kimura H, Watanabe S, et al. Crucial role of NLRP3 inflammasome in the development of peritoneal dialysis-related peritoneal fibrosis. *Sci Rep*. (2019) 9:10363. doi: 10.1038/s41598-019-46504-1
54. Xue M, Rabbani N, Momiji H, Imbasi P, Anwar MM, Kitteringham N, et al. Transcriptional control of glyoxalase 1 by Nrf2 provides a stress-responsive defence against dicarbonyl glycation. *Biochem J*. (2012) 443:213–22. doi: 10.1042/BJ20111648
55. Bellier J, Nokin MJ, Larde E, Karoyan P, Peulen O, Castronovo V, et al. Methylglyoxal, a potent inducer of AGEs, connects between diabetes and cancer. *Diabetes Res Clin Pract*. (2019) 148:200–11. doi: 10.1016/j.diabres.2019.01.002
56. Antognelli C, Talesa VN. Glyoxalases in urological malignancies. *Int J Mol Sci*. (2018) 19:415. doi: 10.3390/ijms19020415
57. Ranganathan S, Ciaccio PJ, Walsh ES, Tew KD. Genomic sequence of human glyoxalase-I: analysis of promoter activity and its regulation. *Gene*. (1999) 240:149–55. doi: 10.1016/S0378-1119(99)00420-5
58. Alomar F, Singh J, Jang HS, Rozanzki GJ, Shao CH, Padanilam BJ, et al. Smooth muscle-generated methylglyoxal impairs endothelial cell-mediated vasodilatation of cerebral microvessels in type 1 diabetic rats. *Br J Pharmacol*. (2016) 173:3307–26. doi: 10.1111/bph.13617
59. Shao CH, Tian C, Ouyang S, Moore CJ, Alomar F, Nemet I, et al. Carbonylation induces heterogeneity in cardiac ryanodine receptor function in diabetes mellitus. *Mol Pharmacol*. (2012) 82:383–99. doi: 10.1124/mol.112.078352
60. Alomar FA, Al-Rubaish A, Al-Muhanna F, Al-Ali AK, McMillan J, Singh J, et al. Adeno-associated viral transfer of glyoxalase-1 blunts carbonyl and oxidative stresses in hearts of type 1 diabetic rats. *Antioxidants*. (2020) 9:592–614. doi: 10.3390/antiox9070592
61. Gorantla S, Poluektova L, Gendelman HE. Rodent models for HIV-associated neurocognitive disorders. *Trends Neurosci*. (2012) *35*:197–208. doi: 10.1016/j.tins.2011.12.006

62. Dagur RS, Wang W, Cheng Y, Makarov E, Ganesan M, Suemizu H, et al. Human hepatocyte depletion in the presence of HIV-1 infection in dual reconstituted humanized mice. *Biol Open*. (2018) 7:bio029785. doi: 10.1242/bio.029785
63. Dash PK, Alomar FA, Hackfort BT, Su H, Conaway A, Poluektova LY, et al. HIV-1-associated left ventricular cardiac dysfunction in humanized mice. *Sci Rep*. (2020) 10:9746. doi: 10.1038/s41598-020-65943-9
64. Zanni MV, Awadalla M, Toribio M, Robinson J, Stone LA, Cagliero D, et al. Immune correlates of diffuse myocardial fibrosis and diastolic dysfunction among aging women with human immunodeficiency virus. *J Infect Dis*. (2019) 221:1315–20. doi: 10.1093/infdis/jiz184
65. Mak IT, Kramer JH, Chen X, Chmielinska JJ, Spurney CF, Weglicki WB. Mg supplementation attenuates ritonavir-induced hyperlipidemia, oxidative stress, and cardiac dysfunction in rats. *Am J Physiol Regul Integr Comp Physiol*. (2013) 305:R1102–11. doi: 10.1152/ajpregu.00268.2013
66. Pocock MO, Dorrell L, Cicconi P. Pathophysiology of ischaemic heart disease. *Curr Opin HIV AIDS*. (2017) 12:548–53. doi: 10.1097/COH.0000000000000411
67. Triant VA, Grinspoon SK. Epidemiology of ischemic heart disease in HIV. *Curr Opin HIV AIDS*. (2017) 12:540–7. doi: 10.1097/COH.0000000000000410
68. Kuhla B, Luth HJ, Haferburg D, Boeck K, Arendt T, Munch G. Methylglyoxal, glyoxal, and their detoxification in Alzheimer's disease. *Ann N Y Acad Sci*. (2005) 1043:211–6. doi: 10.1196/annals.1333.026
69. He F, Ru X, Wen T. NRF2, a transcription factor for stress response and beyond. *Int J Mol Sci*. (2020) 21:4777. doi: 10.3390/ijms21134777
70. Li YY, McTiernan CF, Feldman AM. Interplay of matrix metalloproteinases, tissue inhibitors of metalloproteinases and their regulators in cardiac matrix remodeling. *Cardiovasc Res*. (2000) 46:214–24. doi: 10.1016/S0008-6363(00)00003-1
71. Jalkanen S, Salmi M. Vascular adhesion protein-1 (VAP-1)-a new adhesion molecule recruiting lymphocytes to sites of inflammation. *Res Immunol*. (1993) 144:746–9; discussion 54–62. doi: 10.1016/0923-2494(93)80060-C
72. Salmi M, Jalkanen S. VAP-1: an adhesin and an enzyme. *Trends Immunol*. (2001) 22:211–6. doi: 10.1016/S1471-4906(01)01870-1
73. Stolen CM, Yegutkin GG, Kurkijarvi R, Bono P, Alitalo K, Jalkanen S. Origins of seum semicarbazide-sensitive amine oxidase. *Circ Res*. (2004) 95:50–7. doi: 10.1161/01.RES.0000134630.68877.2F
74. Schofield CJ, Ratcliffe PJ. Oxygen sensing by HIF hydroxylases. *Nat Rev Mol Cell Biol*. (2004) 5:343–354 doi: 10.1038/nrm1366
75. Epstein AC, Gleadle JM, McNeill LA, Hewitson KS, O'Rourke J, Mole DR, et al. C. elegans EGL-9 and mammalian homologs define a family of dioxygenases that regulate HIF by prolyl hydroxylation. *Cell*. (2001) 107:43–54. doi: 10.1016/S0092-8674(01)00507-4
76. Bish LT, Morine K, Sleeper MM, Sanmiguel J, Wu D, Gao G, et al. Adeno-associated virus (AAV) serotype 9 provides global cardiac gene transfer superior to AAV1, AAV6, AAV7, and AAV8 in the mouse and rat. *Hum Gene Ther*. (2008) 19:1359–68. doi: 10.1089/hum.2008.123
77. Timiri Shanmugam PS, Dayton RD, Palaniyandi S, G Abreo F, Caldito, Klein RL, et al. Recombinant AAV9-TLK1B administration ameliorates fractionated radiation-induced xerostomia. *Hum Gene Ther*. (2013) 24:604–12. doi: 10.1089/hum.2012.235

Conflict of Interest: The authors declare that the research was conducted in the absence of any commercial or financial relationships that could be construed as a potential conflict of interest.

frontiers in Cardiovascular Medicine

ORIGINAL RESEARCH
published: 24 December 2021
doi: 10.3389/fcvm.2021.792804

Impact of RAAS Inhibitors on Clinical Outcome and Mortality in Patients With STEMI During the COVID-19 Era: A Multicenter Observational Study

Lucia Barbieri[1], Daniela Trabattoni[2], Giulio G. Stefanini[3,4], Enrico Vizzardi[5], Gabriele Tumminello[1], Emilio Assanelli[2], Marianna Adamo[5], Carlo A. Pivato[3], Giovanni Provenzale[1], Domitilla Gentile[1], Marco Metra[5] and Stefano Carugo[1]*

[1] Cardiology Unit, Fondazione IRCCS Ca' Granda Ospedale Maggiore Policlinico, Milan, Italy, [2] Centro Cardiologico Monzino, IRCCS, Milan, Italy, [3] Department of Biomedical Sciences, Humanitas University, Milan, Italy, [4] IRCCS Humanitas Research Hospital, Milan, Italy, [5] Cardiology, ASST Spedali Civili, Department of Medical and Surgical Specialties, Radiological Sciences, and Public Health, University of Brescia, Brescia, Italy

OPEN ACCESS

Edited by:
Xiaofeng Yang,
Temple University, United States

Reviewed by:
Mladen Vidovich,
University of Illinois at Chicago, United States
Gennaro Galasso,
University of Salerno, Italy

***Correspondence:**
Lucia Barbieri
lb.luciabarbieri@gmail.com

Specialty section:
This article was submitted to Cardiovascular Therapeutics, a section of the journal Frontiers in Cardiovascular Medicine

Received: *11 October 2021*
Accepted: *30 November 2021*
Published: *24 December 2021*

Citation:
Barbieri L, Trabattoni D, Stefanini GG, Vizzardi E, Tumminello G, Assanelli E, Adamo M, Pivato CA, Provenzale G, Gentile D, Metra M and Carugo S (2021) Impact of RAAS Inhibitors on Clinical Outcome and Mortality in Patients With STEMI During the COVID-19 Era: A Multicenter Observational Study. Front. Cardiovasc. Med. 8:792804. doi: 10.3389/fcvm.2021.792804

Conflicting results are available regarding the influence of ACEi/ARBs on the risk of COVID-19 infection, while less is known about their impact on the clinical outcome of patients with STEMI diagnosed with COVID-19. Our aim was to evaluate the impact of ACEi/ARBs therapy on in-hospital mortality and clinical outcomes of patients with STEMI during the COVID-19 pandemic. We retrospectively analyzed consecutive patients with STEMI hospitalized from February 20 to May 10, 2020 in four Hospitals in Lombardy. SARS-COV-2 diagnosis was performed by nasopharyngeal swab test. Procedural outcome, respiratory complications, and in-hospital mortality were reported. Univariate and multivariate analyses were performed by logistic regressions. Our population was represented by 182 patients with STEMI, 76.9% of which were males, and mean age was 67 ± 12.5. Hypertension was reported in 53.3%, and 29.1% was treated with ACEi/ARBs. COVID-19 diagnosis was confirmed in 17.1% of the patients. In-hospital mortality (13.2%) was significantly higher in patients with COVID-19 (31 vs. 10%, $p = 0.003$), even if ejection fraction [OR 0.93 (95% CI) 0.87–0.99; $p = 0.03$] and respiratory complications [OR 9.39 (95% CI) 1.91–45.9; $p = 0.006$] were the only two independent predictors. The incidence of COVID-19 infection was not influenced by ACEi/ARBs (16.5 in naïve vs. 18.8%) whose presence on admission did not correlate with respiratory complications or mortality both in the case of discontinuation and maintenance. In conclusion, in a high-risk population, such as that of patients with STEMI, the potential benefit of ACEi/ARB discontinuation in patients with COVID-19 is overcome by its detrimental effect. Intensive care, additional preventive respiratory investigations, regardless of swab test result, should be suggested for all patients admitted for STEMI during the pandemic.

Keywords: STEMI patients, COVID-19, RAAS inhibitors, mortality, outcome

INTRODUCTION

Coronavirus disease-2019 (COVID-19) is a global pandemic that has affected more than 239,000,000 patients worldwide (WHO data report, October 14th, 2021). Italy was one of the most affected countries in Europe, especially in Lombardy. COVID-19 is caused by severe acute respiratory syndrome coronavirus 2 (SARS-CoV-2), which penetrates cells through the angiotensin-converting enzyme 2 receptor (ACE-2) (1). ACE-2 is largely expressed in the vascular endothelium and in the lungs (2). After ACE-2 was confirmed to be the SARS-CoV-2 receptor (3), it was supposed that treatment with angiotensin converting enzyme inhibitors (ACEis) and angiotensin receptor blockers (ARBs) would be harmful for COVID-19 patients. Few animal models have shown different results regarding the use of ARBs on ACE-2 with limited data in humans studying the effects of renin-angiotensin-aldosterone system (RAAS) inhibition on ACE-2 expression (4). There is a potential rather than harmful benefit in the use of ACE inhibitors. Meng et al. (5) suggested that the use of ACEi might be protective against respiratory complications. The binding of SARS-CoV-2 to ACE-2 exhausts ACE-2, with a consequent imbalance of the RAAS, which spirals into acute severe pneumonia. Blocking the RAAS by ACEi might reduce inflammation with potential reduction in mortality. Moreover, abrupt withdrawal of RAAS inhibitors in high-risk patients, like those affected by stage 3 hypertension, heart failure, or chronic coronary syndrome, may result in clinical instability and adverse clinical outcomes (6). The impact of RAAS inhibitors on clinical outcome has never been investigated on patients with COVID-19 presenting with ST-segment-elevation myocardial infarction (STEMI). Although it is well-known that all-cause mortality is reduced by 36% with an absolute reduction of 11.4% by the use of ACEi in post-infarct patients, their safety and effectiveness in patients with COVID-19 affected by acute myocardial infarction is unclear (7). The aim of this study was to evaluate the impact of RAAS-inhibitors on in-hospital mortality and clinical outcomes of patients with STEMI patients during the pandemic.

METHODS

We retrospectively included consecutive patients with STEMI who were hospitalized from February 20 to May 10, 2020 in four hospitals with 24/7 cath lab service in Lombardy. All clinical, demographic, and procedural characteristics were collected from a dedicated database. The study was performed in accordance with the Declaration of Helsinki. All the patients signed specific consent and disclosure for the use of personal data that were collected anonymously. The diagnosis of SARS-COV-2 was performed by nasopharyngeal swab test. Hypertension was defined as systolic $\geq$140 mmHg and/or diastolic blood pressure $\geq$90 mmHg or if on-treatment with antihypertensive medications (8). For patients on therapy with ACEi or ARBs, specific molecule and relative dose were reported, as well as discontinuation of such therapies after admission. For each patient procedural outcome, respiratory complications and in-hospital mortality were reported. Respiratory complication was defined as acute respiratory failure with a need for non-invasive and mechanical invasive ventilatory support. Ischemic stroke, non-fatal myocardial infarction (MI) and major bleeding, defined from types 3–5 according to Bleeding Academic Research Consortium (BARC) criteria, were identified as in-hospital adverse events (9). A statistical analysis was performed with the SPSS 23 statistical package. Continuous data were expressed as mean $\pm$ SD, and categorical data as percentage. For continuous and categorical variables, analysis of variance and chi-square test, respectively, were performed. Univariate and multivariate analyses were performed by logistic regressions, and a p-value $<$ 0.05 was considered significant.

RESULTS

Our population was represented by 182 patients with STEMI, 76.9% were males with a mean age of 67.01 $\pm$ 12.5 years, and ranged from 40 to 92 years old. Baseline clinical and demographical characteristics are detailed in **Table 1** for the whole population and divided in two subgroups according to COVID-19 infection. Hypertension was reported in 53.3% of cases treated with ACEi or ARBs in 18.7 and 10.4% respectively. The most used ACEi molecule was ramipril (61.7%), while olmesartan (26.3%) was for ARBs. ACEi's discontinuation was observed in 3/34 patients, due to hypotension and one of these patients resulted COVID-19 positive, while 9/19 patients in therapy with ARBs discontinued due to hypotension (4/19) or to ACEi switch (5/19). Regarding COVID-19 infection, a total of 169/182 patients were tested with nasopharyngeal swab test, with confirmed diagnosis in 17.1% of cases. Patients with COVID-19 showed higher baseline glycaemia on admission (151 $\pm$ 47 vs. 129 $\pm$ 51, $p = 0.03$), and lower rate of multivessel disease (21.4 vs. 52.9%, $p = 0.002$). Procedural and event characteristics are shown in **Table 2**. In the majority of cases STEMI diagnosis was assessed in a pre-hospital setting (51.6%), cardiogenic shock on admission was present in 8.8%, while 7.7% of the patients experienced out-of-hospital cardiac arrest. Anterior MI was the most represented (51.5%), and 12.6% of the patients needed intraaortic balloon pump support during primary PCI. Multivessel disease was detected in 47.8% of the cases, with complete revascularization in 22.9% during "index procedure" and in 42.5% staged before hospital discharge. In-hospital mortality was 13.2%, and in the multivariate analysis, ejection fraction [OR 0.93 (95% CI) 0.87–0.99; $p = 0.03$] and respiratory complications [OR 9.39 (95% CI) 1.91–45.9; $p = 0.006$] were the only two independent predictors. In our population, patients with defined diagnosis of COVID-19 showed higher incidence of respiratory complications and mortality rate (20.7 vs. 4.3% and 31 vs. 10%, $p = 0.002$ and $p = 0.003$ respectively) without significative increase in global in-hospital adverse events (34.5 vs. 19.3, $p =$ ns). Nevertheless, the infection did not result as an independent predictor of mortality in both the multivariate and univariate analyses. The incidence of COVID-19 infection was not influenced by the presence of previous ACEi/ARBs therapy (16.5% in naïve patients vs. 18.8%; $p = 0.73$). We did not find any significant correlation between ACEi/ARBs therapy and respiratory complications [OR

TABLE 1 | Baseline characteristics of the population.

Clinical characteristics (*n*)	Total (182)	COVID – (153)	COVID + (29)	*P*
Age (mean ± SD)	67.01 ± 12.5	66.3 ± 12.9	67.7 ± 10.5	Ns
Male gender % (*n*)	76.9 (140)	77.1 (118)	75.9 (22)	Ns
Diabetes % (*n*)	14.3 (26)	14.3 (24)	6.9 (2)	Ns
Hypertension % (*n*)	53.3 (97)	51.4 (79)	62.1 (18)	Ns
Family history of CAD % (*n*)	18.7 (34)	17.1 (26)	27.6 (8)	Ns
Active smoke % (*n*)	28.6 (52)	32.1 (48)	13.8 (4)	Ns
Previous smoke % (*n*)	4.4 (8)	2.9 (6)	6.9 (2)	Ns
Dyslipidemia % (*n*)	24.7 (45)	25.7 (40)	17.2 (5)	Ns
Ejection fraction (mean ± SD)	46.3 ± 10.5	46.8 ± 10.5	42.5 ± 9.2	Ns
Previous PCI % (*n*)	16.5 (30)	18.6 (26)	13.8 (4)	Ns
Previous MI % (*n*)	13.7 (25)	15.0 (21)	13.8 (4)	Ns
Previous CABG % (*n*)	1.6 (3)	2.1 (3)	0	Ns
Chronic kidney disease % (*n*)	17 (31)	17.1 (25)	20.7 (6)	Ns
COPD % (*n*)	10.4 (19)	8.6 (15)	13.8 (4)	Ns
COVID + % (*n*)	17.2 (29)	–	100 (29)	Na
Biochemistry				
Hemoglobin (g/dL) (mean ± SD)	13.5 ± 1.9	13.6 ± 1.8	12.9 ± 1.9	Ns
White Blood Cells (10∧3/uL) (mean ± SD)	11.3 ± 4.3	11.2 ± 4.0	12.5 ± 5.4	Ns
Lymphocytes (10∧3/uL) (mean ± SD)	2.2 ± 1.8	2.2 ± 1.8	1.7 ± 1.3	Ns
Platelet count (10∧3/uL) (mean ± SD)	243 ± 77	238 ± 68	280 ± 105	0.04
Creatinine (mg/dL) (mean ± SD)	1.04 ± 0.54	1.04 ± 0.57	1.09 ± 0.42	Ns
Creatinine peak (mg/dL) (mean ± SD)	1.39 ± 0.92	1.40 ± 0.99	1.43 ± 0.72	Ns
Creatinine Kinase MB (ug/L) (mean ± SD)	183 ± 316	201 ± 344	59 ± 59	Ns
Glycaemia (mg/dL) (mean ± SD)	134 ± 52	129 ± 51	151 ± 47	0.03
Reactive protein C (mg/dL) (mean ± SD)	32 ± 62	31 ± 61	43 ± 72	Ns
Pharmacological therapy at admission				
Acetylsalicylic acid % (*n*)	24.7 (45)	25.7 (38)	24.1 (7)	Ns
Vitamin K antagonists % (*n*)	1.1 (2)	2.2 (2)	0	Ns
Direct oral anticoagulants % (*n*)	3.3 (6)	3.3 (4)	12.5 (2)	Ns
Beta-blockers % (*n*)	24.2 (44)	25.0 (36)	27.6 (8)	Ns
Calcium channel blockers % (*n*)	15.4 (28)	17.1 (24)	13.8 (4)	Ns
Angiotensin converting enzyme inhibitors % (*n*)	18.7 (34)	18.6 (28)	20.7 (6)	Ns
Angiotensin receptor blockers % (*n*)	10.4 (19)	9.3 (16)	10.3 (3)	Ns
Statins % (*n*)	33 (60)	37.1 (53)	24.1 (7)	Ns
Aldosterone antagonists % (*n*)	8.8 (16)	9.3 (13)	10.3 (3)	Ns
Diuretics % (*n*)	27.5 (50)	27.9 (40)	34.5 (10)	Ns

M-SD, mean-standard deviation; CAD, coronary artery disease; PCI, percutaneous coronary intervention; MI, myocardial infarction; CABG, coronary artery by-pass graft; COPD, chronic obstructive pulmonary disease.

TABLE 2 | Event characteristics.

Site of diagnosis	Total (182)	COVID – (153)	COVID + (29)	*P*
Pre hospital setting % (*n*)	51.6 (94)	52.9 (83)	37.9 (11)	Ns
Emergency department % (*n*)	41.2 (75)	40.7 (61)	48.3 (14)	
Spoke center % (*n*)	6.6 (12)	6.4 (9)	10.3 (3)	
Hub hospital department % (*n*)	0.5 (1)	0.0 (-)	3.4 (1)	
Out of hospital cardiac arrest % (*n*)	7.7 (14)	8.6 (13)	3.4 (1)	Ns
Killip class $\geq$3% (*n*)	11.5 (21)	9.8 (15)	22.2 (6)	Ns
Cardiogenic shock % (*n*)	8.8 (16)	7.1 (11)	17.2 (5)	Ns
Procedural characteristics				
MI type				
Anterior MI % (*n*)	51.5 (92)	49.3 (76)	55.2 (16)	Ns
Inferior MI % (*n*)	32.3 (57)	34.3 (49)	27.6 (8)	
Lateral MI % (*n*)	10.8 (18)	8.6 (16)	6.9 (2)	
Posterior MI % (*n*)	5.4 (8)	4.3 (7)	3.4 (1)	
Radial Approach % (*n*)	86.8 (158)	88.6 (137)	75.0 (21)	Ns
Multivessel disease % (*n*)	47.8 (87)	52.9 (81)	21.4 (6)	0.002
Left main % (*n*)	4.9 (9)	6.4 (9)	0	Ns
Left anteriore descending % (*n*)	62.1 (113)	61.4 (96)	60.7 (17)	Ns
Left circumflex % (*n*)	35.7 (65)	37.1 (59)	21.4 (6)	Ns
Right coronary artery % (*n*)	46.2 (84)	50.0 (74)	35.7 (10)	Ns
IABP % (*n*)	12.6 (23)	12.1 (18)	17.9 (5)	Ns
Final TIMI flow 3 % (*n*)	95.1 (175)	96.4 (147)	96.3)26	Ns
In hospital complete revascularization % (*n*)	42.5 (37)	40.5 (35)	40.0 (2)	Ns
Index procedure complete revascularization % (*n*)	22.9 (20)	23.3 (20)	0	Ns
Main time components of STEMI care				
Symptoms to first allarm (min) (mean ± SD)	437 ± 920	387 ± 87	83 ± 1486	Ns
Door to balloon (min) (mean ± SD)	57 ± 163	61 ± 183	37 ± 38	Ns
Total ischemic time (min) (mean ± SD)	514 ± 975	465 ± 71	899 ± 502	Ns
In hospital outcome				
In hospital adverse events % (*n*)	20.9 (38)	19.3 (28)	34.5 (10)	Ns
Respiratory complications % (*n*)	7.1 (13)	4.3 (7)	20.7 (6)	0.002
In hospital mortality % (*n*)	13.2 (24)	10.0 (15)	31.0 (9)	0.003

IABP, intra aortic balloon pump; STEMI, ST segment elevation myocardial infarction.

1.08 (95% CI) 0.32–3.7; $p = 0.89$] or mortality [OR 0.45 (95% CI) 0.14–1.37; $p = 0.15$] in the whole population or in the COVID-19 subgroup [OR 2.83 (95% CI) 0.44–18.04; $p = 0.27$; OR 0.15 (95% CI) 0.01–1.46; $p = 0.1$; respiratory complications and mortality, respectively]. Among patients who discontinued ACEi/ARBs therapy, there was no more incidence of mortality (8.3 vs. 10%, $p = 0.89$) or respiratory complications (16.7 vs. 10%, $p = 0.65$).

DISCUSSION

Among the patients with STEMI s during the COVID-19 pandemic, our study did not find any association between ACEi/ARBs use and mortality, and does not suggest the need to change our clinical practice. A report underlined the theoretical mechanism of action of ACEi and ARBs on RAAS and their potential influence on COVID-19 pathophysiology (6). The authors concluded the need for more data on this issue due to the potential positive effects of both discontinuation and maintenance of ACEs/ARBs during COVID-19 infection. The idea that ACE-2 receptor induction by ACEi/ARBs inhibition may be harmful during COVID-19 infection is based on animal models. Although no randomized trials or systematic analyses are available on the effects of RAAS blockers during the course of COVID-19 disease, and the European Society of Cardiology (ESC) and The American College of Cardiology (ACC) suggested physicians to continue the treatment in patients who are already on RAAS blockers. Nevertheless, it has also been recommended to individualize treatment decisions according to each patient's hemodynamic status and clinical presentation (10). The impact of arterial hypertension on cardiovascular disease risk is estimated to be up to 40% (11), which is reduced by the use of ACEI and ARB's. To date, it is still controversial, without any evidence, whether ACEI and ARB's could be harmful to patients with COVID-19. The high debate in social media, and popular and scientific journals forced major international societies to issue position statements. Fang et al. reported a possible impact of ACEI and ARBs on patients with

COVID-19, which led to spread of alarm among physicians and patients (12). This finding was complicated by the evidence that arterial hypertension and diabetes mellitus are the highest co-morbidity of patients with COVID-19. In a case series of hypertensive patients from Wuhan, the absence of association between ACEi/ARBs and severity or mortality of COVID-19 was reported (13). Similar results were found in other studies from Italy (14) and North America (15, 16). ACEi/ARBs treatment is the cornerstone of cardiovascular therapy found to be effective in reducing death and cardiovascular end points in several settings. Early RAAS inhibition in patients with STEMI is safe and is associated with significant reduction in 30-day mortality (17). Clinical trials (18, 19), in the non-COVID-19 era, have shown that the discontinuation of ACEi/ARBs, especially after MI, correlates with worse prognosis. STEMI is a specific setting where hemodynamic impact plays a central role in the pathophysiology of the disease and may influence the underlying mechanism and prognosis (20). Li et al. since 2003 suggested that ACE-2 is a functional receptor of the SARS-CoV virus (21). Two years later, it was evidenced that virus–ACE-2 receptor binding plays a crucial role in cell penetration and consequent disease development (1). After the spread of COVID-19, several studies have confirmed that the SARS-CoV2 receptor-binding domain interacts with ACE-2 (22). On the other hand, ARBs might prevent inflammation of the lungs, as shown in animal models. Based on these data, reviews speculated that ARBs could be a possible treatment tool in patients with COVID-19 (23). A recent large observational study supports that, when clinically indicated, ACEi/ARB therapy should be continued in the setting of COVID-19 unless the patient is hemodynamically unstable (24). Even in this peculiar cardiovascular condition, with the co-presence of COVID-19 infection (25, 26), this study confirms that the use of ACEi/ARBs does not correlate with a worse in-hospital prognosis. Conversely, as the pre-COVID-19 era literature shows, untreated patients showed a doubled in-hospital mortality vs. patients receiving ACEi/ARBs, despite these data being not statistically significant. The multivariate analysis showed that ejection fraction and respiratory complications are the only variables correlating with in-hospital mortality. On the other hand, even if patients with COVID-19 had doubled mortality, the infection did not correlate in the multivariate analysis. The low negative predictive value of nasal swab test (27) may explain these findings. Therefore, regardless of swab test result, our results suggest the need for more attention to patient with STEMI and concomitant respiratory impairment, and an early preventive diagnostic and therapeutic approach. Contrary to the recent literature, in our study, patients treated with ACEi/ARBs did not show higher prevalence of COVID-19 infection, and therapy discontinuation did not influence both in-hospital mortality and respiratory complications. Therefore, the well-known beneficial effect of ACEi/s therapy in patients with STEMI is not balanced by the potential and not yet confirmed positive effect of discontinuation in the presence of COVID-19 infection.

LIMITATIONS

The routine use of nasopharyngeal swab as the only screening test for COVID-19 detection may have underestimated the real incidence of infection in our population. Moreover, the sample size may have influenced the significance of some analysis as the difference in mortality in patients treated with ACEi/ARBs or naïve.

CONCLUSIONS

In conclusion, in a high risk population, such as that of patients with STEMI, the potential benefit of ACEi/ARB discontinuation in patients with COVID-19 may be overcome by its detrimental effect. Therefore, our clinical practice should not be modified regarding the treatment of acute ischemic injury among the COVID-19 subpopulation. Strict respiratory monitoring, intensive care and aggressive life support, regardless from swab test result, should be routinely used among patients admitted for STEMI during pandemic.

DATA AVAILABILITY STATEMENT

The raw data supporting the conclusions of this article will be made available by the authors without undue reservation.

ETHICS STATEMENT

Ethical review and approval was not required for this study with human participants, in accordance with the local legislation and institutional requirements. The patients/participants provided their written informed consent to participate in this study.

AUTHOR CONTRIBUTIONS

LB, SC, GS, DT, and GT contributed to conception and design of the study. LB and GT organized the database. GT performed the statistical analysis. LB, GT, DG, and GP wrote sections of the manuscript. All authors contributed to manuscript revision, read, and approved the submitted version.

REFERENCES

1. Kuba K, Imai Y, Rao S, Gao H, Guo F, guan B, et al. A crucial role of angiotensin converting enzyme 2 (ACE2) in SARS coronavirus–induced lung injury. *Nat Med.* (2005) 11:875–79. doi: 10.1038/nm1267
2. Hamming I, TimensW, Bulthuis ML, Lely AT, Navis G, van Goor H. Tissue distribution of ACE2, protein, the functional receptor for SARS coronavirus: a first step in understanding SARS pathogenesis. *J Pathol.* (2004) 203:631–7. doi: 10.1002/path.1570
3. Yang J, Zheng Y, Gou X, Pu K, Chen Z, Guo Q, et al. Prevalence of comorbidities and its effects in patients infected with SARS-CoV-2: a systematic review and meta-analysis. *Int J Infect Dis.* (2020) 94:91–5. doi: 10.1016/j.ijid.2020.03.017

4. Hamming I, van Goor H, Turner AJ, Rushworth CA, Michaud AA, Corvol P, et al. Differential regulation of renal Angiotensin-Converting Enzyme (ACE) and ACE2 during ACE inhibition and dietary sodium restriction in healthy rats. *Exp Physiol*. (2008) 93:631–8. doi: 10.1113/expphysiol.2007.041855
5. Meng J, Xiao G, Zhang J, He X, Ou M, Bi J, et al. Renin-angiotensin system inhibitors improve the clinical outcomes of COVID-19 patients with hypertension. *Emerg Microbes Infect*. (2020) 9:757–60. doi: 10.1080/22221751.2020.1746200
6. Vaduganathan M, Vardeny O, Michel T, McMurray JJV, Pfeffer MA, Solomon SD. Renin-angiotensin-aldosterone system inhibitors in patients with COVID-19. *N Engl J Med*. (2020) 382:1653–9. doi: 10.1056/NEJMsr2005760
7. Hall AS, Winter C, Bogle SM, Mackintosh AF, Murray GD, Ball SG. The Acute Infarction Ramipril Efficacy (AIRE) study: rationale, design, organization, and outcome definitions. *J Cardiovasc Pharmacol.* (1991) 18(Suppl. 2):S105–9. doi: 10.1097/00005344-199106182-00022
8. Williams B, Mancia G, Spiering W, Cifkova R, Fagard R, Grassi GGG, et al. The Task Force for the management of arterial hypertension of the European Society of Cardiology (ESC) and the European Society of Hypertension (ESH). 2018 ESC/ESH Guidelines for the management of arterial hypertension. *Eur Heart J*. (2018) 39:3021–104. doi: 10.1093/eurheartj/ehy339
9. Mehran R, Rao SV, Bhatt DL, Gibson CM, Caixeta A, Eikelboom J, et al. Standardized bleeding definitions for cardiovascular clinical trials: a consensus report from the Bleeding Academic Research Consortium. *Circulation*. (2011) 123:2736–47. doi: 10.1161/CIRCULATIONAHA.110.009449
10. Aronson JK, Ferner RE. Drugs and the renin-angiotensin system in COVID-19. *BMJ*. (2020) 369:m1313. doi: 10.1136/bmj.m1313
11. Willey JZ, Moon YP, Kahn E, Rodriguez CJ, Rundek T, Cheung K, et al. Population attributable risks of hypertension and diabetes for cardiovascular disease and stroke in the northern Manhattan study. *J Am Heart Assoc*. (2014) 3:e001106. doi: 10.1161/JAHA.114.001106
12. Fang L, Karakiulakis G, Roth M. Are patients with hypertension and diabetes mellitus at increased risk for COVID-19 infection? *Lancet Respir Med*. (2020) 8:e21. doi: 10.1016/S2213-2600(20)30116-8
13. Li J, Wang X, Chen J, Zhang H, Deng A. Association of renin-angiotensin system inhibitors with severity or risk of death in patients with hypertension hospitalized for coronavirus disease 2019 (COVID-19) infection in Wuhan, China. *JAMA Cardiol*. (2020) 5:825–30. doi: 10.1001/jamacardio.2020.1624
14. Mancia G, Rea F, Ludergnani M, Apolone G, Corrao G. Renin-angiotensin-aldosterone system blockers and the risk of COVID-19. *N Engl J Med*. (2020) 382:2431–40. doi: 10.1056/NEJMoa2006923
15. Mehta N, Kalra A, Nowacki AS, Anjewierden S, Han Z, Bhat P, et al. Association of use of angiotensin-converting enzyme inhibitors and angiotensin ii receptor blockers with testing positive for coronavirus disease 2019 (COVID-19). *JAMA Cardiol*. (2020) 5:1020–6. doi: 10.1001/jamacardio.2020.1855
16. Reynolds HR, Adhikari S, Pulgarin C, Troxel AB, Iturrate E, Johnson SB, et al. Renin-angiotensin-aldosterone system inhibitors and risk of COVID-19. *N Engl J Med*. (2020) 382:2441–8. doi: 10.1056/NEJMoa2008975
17. ACE Inhibitor Myocardial Infarction Collaborative Group. Indications for ACE inhibitors in the early treatment of acute myocardial infarction: systematic overview of individual data from 100,000 patients in randomized trials. *Circulation*. (1998) 97:2202–12. doi: 10.1161/01.CIR.97.22.2202
18. Korhonen MJ, Robinson JG, Annis IE, Hickson RP, Bell JS, Hartikainen J, et al. Adherence tradeoff to multiple preventive therapies and all-cause mortality after acute myocardial infarction. *J Am Coll Cardiol*. (2017) 70:1543–54. doi: 10.1016/j.jacc.2017.07.783
19. Pflugfelder PW, Baird MG, Tonkon MJ, DiBianco R, Pitt B. The Quinapril Heart Failure Trial Investigators. Clinical consequences of angiotensin-converting enzyme inhibitor withdrawal in chronic heart failure: a double-blind, placebo-controlled study of quinapril. *J AmColl Cardiol*. (1993) 22:1557–63. doi: 10.1016/0735-1097(93)90578-O
20. Fosbøl EL, Butt JH, Østergaard L, Andersson C, Selmer C, Kragholm K, et al. Association of angiotensin-converting enzyme inhibitor or angiotensin receptor blocker use with COVID-19 diagnosis and mortality. *JAMA*. (2020) 324:168–77. doi: 10.1001/jama.2020.11301
21. Li W, Moore MJ, Vasilieva N, Sui J, Wong S-K, Berne M, et al. Angiotensin-converting enzyme 2 is a functional receptor for the SARS coronavirus. *Nature*. (2003) 426:450–4. doi: 10.1038/nature02145
22. Chen Y, Guo Y, Pan Y, Zhao ZJ. Structure analysis of the receptor binding of 2019-nCoV. *Biochem Biophys Res Commun*. (2020) 525:135–40. doi: 10.1016/j.bbrc.2020.02.071
23. Zhang H, Penninger JM, Li Y, Zhong N, Slutsky AS. Angiotensin-converting enzyme 2 (ACE2) as a SARS-CoV-2 receptor: molecular mechanisms and potential therapeutic target. *Intensive Care Med*. (2020) 46:586–90. doi: 10.1007/s00134-020-05985-9
24. Rott D, Behar S, Gottlieb S, Boyko V, Hod H. Usefulness of the Killip classification for early risk stratification of patients with acute myocardial infarction in the 1990s compared with those treated in the 1980s. *Am. J. Cardiol*. (1997) 80:859–64. doi: 10.1016/S0002-9149(97)00536-5
25. Stefanini GG, Montorfano M, Trabattoni D, Andreini D, Ferrante G, Ancona M, et al. ST-elevation myocardial infarction in patients with COVID-19: clinical and angiographic outcomes. *Circulation*. (2020) 141:2113–6. doi: 10.1161/CIRCULATIONAHA.120.047525
26. Tam C-CF, Cheung K-S, Lam S, Wong A, Yung A, Sze M, et al. Impact of coronavirus disease 2019 (COVID-19) outbreak on ST-segment elevation myocardial infarction care in Hong Kong, China. *Circ Cardiovasc Qual Outcomes*. (2020) 13:e006631. doi: 10.1161/CIRCOUTCOMES.120.006631
27. Zitek T. The appropriate use of testing for COVID-19. *West J Emerg Med*. (2020) 21:470–2. doi: 10.5811/westjem.2020.4.47370

Conflict of Interest: The authors declare that the research was conducted in the absence of any commercial or financial relationships that could be construed as a potential conflict of interest.

Publisher's Note: All claims expressed in this article are solely those of the authors and do not necessarily represent those of their affiliated organizations, or those of the publisher, the editors and the reviewers. Any product that may be evaluated in this article, or claim that may be made by its manufacturer, is not guaranteed or endorsed by the publisher.

frontiers in Cardiovascular Medicine

ORIGINAL RESEARCH
published: 31 January 2022
doi: 10.3389/fcvm.2021.826687

E-Selectin-Overexpressing Mesenchymal Stem Cell Therapy Confers Improved Reperfusion, Repair, and Regeneration in a Murine Critical Limb Ischemia Model

Hallie J. Quiroz[1], Samantha F. Valencia[1], Hongwei Shao[1], Yan Li[1], Yulexi Y. Ortiz[1], Punam P. Parikh[1], Roberta M. Lassance-Soares[1], Roberto I. Vazquez-Padron[1,2], Zhao-Jun Liu[1,2] and Omaida C. Velazquez[1]**

[1] Division of Vascular Surgery, DeWitt-Daughtry Family Department of Surgery, University of Miami Miller School of Medicine, Miami, FL, United States, [2] Vascular Biology Institute, University of Miami Miller School of Medicine, Miami, FL, United States

OPEN ACCESS

Edited by:
Baohui Xu,
Stanford University, United States

Reviewed by:
Guoping Zheng,
University of Sydney, Australia
Sihai Zhao,
Xi'an Jiaotong University, China
Zhihua Jiang,
University of Florida, United States

***Correspondence:**
Omaida C. Velazquez
ovelazquez@med.miami.edu
Zhao-Jun Liu
zliu@med.miami.edu

Specialty section:
This article was submitted to Cardiovascular Therapeutics, a section of the journal Frontiers in Cardiovascular Medicine

Received: *01 December 2021*
Accepted: *20 December 2021*
Published: *31 January 2022*

Citation:
Quiroz HJ, Valencia SF, Shao H, Li Y, Ortiz YY, Parikh PP, Lassance-Soares RM, Vazquez-Padron RI, Liu Z-J and Velazquez OC (2022) E-Selectin-Overexpressing Mesenchymal Stem Cell Therapy Confers Improved Reperfusion, Repair, and Regeneration in a Murine Critical Limb Ischemia Model. Front. Cardiovasc. Med. 8:826687. doi: 10.3389/fcvm.2021.826687

Aims: Novel cell-based therapeutic angiogenic treatments for patients with critical limb ischemia may afford limb salvage. Mesenchymal stem cells (MSCs) do not overexpress E-selectin; however, we have previously demonstrated the cell-adhesion molecule's vital role in angiogenesis and wound healing. Thus, we created a viral vector to overexpress E-selectin on MSCs to increase their therapeutic profile.

Methods and Results: Femoral artery ligation induced hind limb ischemia in mice and intramuscular injections were administered of vehicle or syngeneic donor MSCs, transduced *ex vivo* with an adeno-associated viral vector to express either GFP^+ (MSC^{GFP}) or E-selectin-GFP^+ ($MSC^{E-selectin-GFP}$). Laser Doppler Imaging demonstrated significantly restored reperfusion in $MSC^{E-selectin-GFP}$-treated mice vs. controls. After 3 weeks, the ischemic limbs in mice treated with $MSC^{E-selectin-GFP}$ had increased footpad blood vessel density, hematoxylin and eosin stain (H&E) ischemic calf muscle sections revealed mitigated muscular atrophy with restored muscle fiber size, and mice were able to run further before exhaustion. PCR array-based gene profiling analysis identified nine upregulated pro-angiogenic/pro-repair genes and downregulated *Tumor necrosis factor (TNF)* gene in $MSC^{E-selectin-GFP}$-treated limb tissues, indicating that the therapeutic effect is likely achieved *via* upregulation of pro-angiogenic cytokines and downregulation of inflammation.

Conclusion: This innovative cell therapy confers increased limb reperfusion, neovascularization, improved functional recovery, decreased muscle atrophy, and thus offers a potential therapeutic method for future clinical studies.

Keywords: cell therapy, E-selectin, adeno-associated virus, limb salvage, angiogenesis

INTRODUCTION

Critical limb ischemia (CLI), the most severe form of peripheral arterial disease (PAD), is the clinical syndrome that includes ischemic rest pain and tissue loss due to severely diminished perfusion to the affected limb. Of all patients with PAD, 11% will go on to develop CLI that confers a 50% 5-year mortality rate and a 70% 10-year mortality rate (1, 2). Risk factors such

as smoking, obesity, and diabetes mellitus increase one's risk of developing PAD. Currently, the treatment modalities available for patients with CLI include medical risk reduction strategies as well as procedural revascularization such as endovascular angioplasty/stenting or bypass surgeries (3). Unfortunately, some patients are not surgical candidates or the revascularization may fail, which results in up to 30% of patients requiring limb amputation within 1 year of diagnosis, and is associated with a postamputation mortality rate up to 25% (4). Due to the reduced quality of life, significant financial costs, and poor survival outcomes among patients with CLI, vascular regenerative therapies that aim to increase limb salvage in these high-risk patients are a promising therapeutic option.

Therapeutic angiogenesis, the therapeutic development of new blood vessels, is an enticing regenerative concept to increase blood perfusion to the affected limb by which to promote tissue repair and regeneration. Gene therapy and cell therapy are two such strategies to employ therapeutic angiogenesis in localized tissues. Stem cell therapy, specifically the use of mesenchymal stem cells (MSCs), is advantageous due to its inherent ability to differentiate into multiple cell lineages required for tissue regeneration or secrete soluble factors or exosomes (paracrine actions) to promote neovascularization and tissue repair. Additionally, the immunomodulatory effects of MSCs may serve to dampen the negative effects of inflammation inherent in ischemic tissues (5, 6). Preclinical studies utilizing MSCs from the bone marrow, placenta, umbilical cord, and adipose tissue have demonstrated improved wound healing (7, 8) and ischemic hind limb reperfusion (9–12). However, treatments with unmodified MSCs in human clinical trials have shown modest translational effects on amputation-free survival (AFS), which has not always been shown to be superior to placebo (13–16). It is hypothesized that the limited therapeutic efficacy may be indicative of low potency in the selected cell populations administered (17–19). Thus, modifications of stem cells based on mechanistic understanding that enrolls regeneration pathways may boost their therapeutic activity resulting in more efficacious cell therapy for CLI.

One method of improving autologous MSC efficacy is by introducing genetic modifications that enhance the MSC's inherent ability to induce neovascularization and promote tissue repair. Our lab has demonstrated that E-selectin, an inducible cell-adhesion molecule that becomes upregulated in ischemic environments, is vital for the neovascularization and tissue repair processes (20, 21). We further demonstrated that coating MSCs, which normally do not express E-selectin, with nanocarrier complexed with soluble E-selectin, improved cell homing to the ischemic environment and improved repair and regeneration in a mouse model of hind limb ischemia (22). This study demonstrated that the MSCs overexpressing E-selectin are more biologically potent and can specifically interact with E-selectin ligands elevated on activated endothelial cells, thus actively contributing to the budding tip of vessel sprouts to promote angiogenesis. While this study was an important proof-of-concept, nanocarrier-coated MSC is not optimal for scale-up and human clinical trials. Moreover, there are potential applicability concerns related to the rapid internalization of nanocarrier bounded on the cell surface. Thus, we designed a viral vector utilizing the adeno-associated virus (AAV), which has been shown to be advantageous for genetic modifications and is a safe vector type already FDA-approved for gene therapy in humans (23, 24). This vector is utilized to transduce cells with resultant overexpression of E-selection on the cell's surface (herein referred to as supercharging), which we hypothesized would augment MSC's neovascularization and regeneration potential. In this work, we characterize biologic effects and explore the mechanisms of action.

MATERIALS AND METHODS

Animals

The generation of the ROSA26-LacZ$^{+/-}$ was performed by crossing C57BL/6 mice with B6; 129S-Gt(ROSA)26Sor/J mice (Jackson Laboratory, Bay Harbor, ME). Mice, hemizygous or homozygous for the ROSA26 retroviral insertion, display no distinguishing phenotype, lacZ is expressed in all tissues of the developing embryo and in most tissues of the adult mouse (25). Six to 8-week-old ROSA26-LacZ$^{+/-}$ male/female mice were utilized for bone marrow extraction and 8–12 week-old male C57/BL6 mice were utilized for CLI-model creation and experimentation. The mice were maintained and bred under standard pathogen-free conditions, cared for and operated following the Policy on Use of Laboratory Animals, and all animal experiments were approved by the institutional animal care committee of the University of Miami (IACUC protocol 16-188). Euthanasia was performed *via* two methods as described by the IACUC protocol *via* CO^2 gas inhalation and cervical dislocation.

Murine Bone Marrow Extraction and Culture of MSCs

Bone marrow was harvested from the femurs of euthanized ROSA26-LacZ$^{+/-}$ mice as previously described (26). Bone marrow cells were cultured in murine MSC MesenCult™ medium with supplement (STEMCELL Technologies, Vancouver, Canada). Non-adherent cells were removed every 96 h by changing the medium. MSCs were harvested at passage 1–2 for use in experiments. Cell growth was determined by different seeding densities and time points in triplicates.

AAV Production

Full length murine genes of *E-selectin* and green-fluorescent protein (*GFP*) were inserted into multiple cloning sites in the pZac vector, respectively, and confirmed by gene sequencing. E-selectin-*ires*-eGFP/pZac and eGFP/pZac plasmids were then sent to University of North Carolina Gene Therapy Vector Core where AAV serotype 2/2 ($AAV_{2/2}$) was packaged and preparations were performed per standard protocol using the 3-plasmid transfection into HEK293 cells (27). Quality assurance and control testing included qPCR quantification of AAV genomes, determination of infectivity titer, and tests for replication competent AAV (RCAAV) (27).

Transduction of MSCs

Mesenchymal stem cells were transduced *ex vivo* with $AAV_{2/2}$ (either E-selectin-*ires*-eGFP/AAV or eGFP/AAV, both under the control of the cytomegalovirus promoter) as previously described (28). Briefly, MSCs were trypsinized and plated in 100 mm cell culture plates at 5×10^5 cell density with 10 ml Mesencult™ medium and were allowed to attach for 24 h before the virus was added directly to the medium at 5,000 viral genomes (VG)/cell. The media was changed after 12 h and every 96 h afterward for the remaining culture period. GFP transgene expression was assessed by immunohistology under fluorescence microscopy to determine transduction success and efficiency 3–4 days after transduction.

Flow Cytometry

Mesenchymal stem cells were detached from culture dish using TrypLE™ express (Thermo Fisher Scientific, Waltham, MA) and collected in Eppendorf tubes. The cells were stained for MSC markers using anti-CD44, PE-Cy5 (BD Biosciences, Franklin Lakes, NJ, #553135), anti-CD73, BV605 (Biolegend, San Diego, CA, #127215), anti-CD105, AF647 (Biolegend, San Diego, CA, #120405), and anti-E-selectin/CD62E, PE (BD Biosciences, Franklin Lakes, NJ, #553751) to assess E-selectin levels. The cells were analyzed on a on a FACSAria II cell sorter using FACSDiva Version 6.1.1 (BD Biosciences) or FlowJo Version 7.6.4 (TreeStar) software.

Creation of a Mouse CLI Model

Creation of hind limb ischemia mouse model was performed as previously described (29). Briefly, 8–10-week-old male mice underwent femoral artery ligation (FAL). To do this, the mice were anesthetized with ketamine 100 mg/kg and xylazine 10 mg/kg Intraperitoneal (IP); then, hair was sheared from the hind limbs and an incision was made to expose the femoral sheath. The femoral artery and vein were dissected and separated from the femoral nerve distally at the sapheno-popliteal bifurcation and proximally below the inguinal ligament. Both artery and vein were ligated at these two locations with 7-0 silk sutures and the intervening segment between sutures severed with a single incision (**Supplementary Figure 1A**). The mice were injected with 100 μl of 5×10^5 MSC^{GFP}, $MSC^{E-selectin-GFP}$, or PBS (vehicle) at 4 points (25 μl/point) in the thigh muscle of the surgical limb after ligation, postoperative day (POD) 1 and POD 2. Finally, the skin incision was closed using 7-0 silk suture in a continuous fashion. A single dose of sustained-release buprenorphine (ZooPharm, 1.0 mg/kg) was subcutaneously administered for postoperative analgesia.

Laser Doppler Imaging

Laser Doppler imaging (LDI) was performed using the LDI2-HR System from Moor Instruments (Wilmington, DE). LDI was performed on the ligated and non-ligated leg preoperatively and immediately after FAL, and subsequently on POD 7, 14, and 21. As previously detailed, the mice were lightly anesthetized (30, 31) and placed on a heating pad to maintain their core body temperature at 37°C. Image of the plantar foot was of particular interest since this area most effectively demonstrates reperfusion on LDI. Hind limb reperfusion index was defined as a ratio of ligated to non-ligated leg for each individual mouse.

Live Animal DiI Perfusion and Confocal Laser Scanning Microscopy

The lipophilic carbocyanine dye DiI (1,1′-dioctadecyl-3,3,3′,3′-tetramethylindocarbocyanine perchlorate (Invitrogen, Carlsbad, CA, #D282) was used for vascular perfusion and staining as previously described (29, 32, 33). Briefly, intramyocardial perfusion of filtered PBS followed by 10 mL of DiI and lastly 10% neutral formalin for tissue fixation was performed on POD 21. The area of interest was the footpad, given our interest in distal hind limb reperfusion. The skinned murine footpad was compressed between two glass micro slides using binder clips for adequate imaging with the Zeiss LSM 510 confocal laser scanning microscope. Z-series obtained from confocal imaging were reconstructed into 3-dimensional images and analyzed using Image J. The intricate network of vessels regenerated in the foot was captured, quantified, and represented by mean capillary density (percentage of volume of total DiI-stained vessels per area within foot) for each mouse.

Histology

Immunofluorescent staining and H&E were performed as per a previously published protocol (34, 35). Slides of tissue sections were deparaffinized, hydrated, washed, and blocked with protein blocking serum (Dako, Carpinteria, CA) for an hour at 25°C. To determine the MSC location within thigh tissue sections, the slides were incubated with anti-GFP (Invitrogen, Carlsbad, CA, #A21312) 1.5 μg/mL in protein blocking serum for 12 h at 4°C. The slides were then washed with 0.1% Tris-buffered saline and polysorbate-20 (TBST) prior to 4′,6-diamidino-2-phenylindole (DAPI) staining (Vector Laboratories, Inc., Burlingame, CA) for nuclei visualization. Confocal laser scanning microscope using 20–40 × magnification was used to image immunofluorescence. For quantification of presence of GFP^+ MSCs, at least 10 random ×40 magnification fields per section were blindly scored and/or measured with Image J or Adobe Photoshop CC. To determine muscular atrophy in the ligated limbs of mice after FAL, H&E staining was performed on paraffin-embedded transverse muscle tissue sections of the treatment groups as previously described (36). Images were then acquired *via* 20X magnification and 10 random myocytes in each field were measured circumferentially based on actual measurement reflected by size bar and total surface area was calculated (μm^2).

Treadmill Exhaustion Test

Exercise treadmill testing was performed on a rodent treadmill as previously described (37, 38) (Columbus Instruments, Columbus, OH, model: Exer3/6) 21 days after FAL to determine the degree of hind limb functionality and recovery after treatment. In this study, our protocol started with a 10° slope at a speed of 10 meters/minute for 5 min. The mice were placed on a horizontal treadmill, and the speed was increased by 5 meters/minute every 5 min until a maximum speed of 30 meters/min was reached. The mice were allowed to run until exhaustion occurred, which was defined as spending 5 consecutive seconds on the stimulus pad or visiting the stimulus

pad a total of 40 times. The total distance (m) traversed prior to exhaustion was then recorded for each mouse.

Gene Expression Analysis by PCR Array

The Murine Angiogenesis RT² Profiler™ PCR array quantitatively profiles the expression of 84 genes involved in angiogenesis (Qiagen, Hilden, Germany, #PAMM-024Z). Total RNA was extracted from the cells and tissues using Trizol® (Invitrogen, Carlsbad, CA, # 15596026) and cDNA was synthesized using RT² First Strand Kits (Qiagen, Hilden, Germany, #330401). PCR array was carried out according to the manufacturer's protocol. The threshold cycle (Ct) values were used to plot a standard curve. All samples were normalized to the relative levels of GAPDH, and results are expressed as fluorescence intensity in relative levels (cultured $MSC^{E-selectin-GFP}$ vs. MSC^{GFP} and ischemic tissue treated with $MSC^{E-selectin-GFP}$ vs. MSC^{GFP}).

Biodistribution of Engrafted MSCs

To detect the biodistribution of locally engrafted MSCs, total RNA was extracted from various tissues, including treated ischemic limbs, lungs, and livers, using Trizol® (Invitrogen, Carlsbad, CA, # 15596026) and cDNA was synthesized using RT² First Strand Kits (Qiagen, Hilden, Germany, #330401). PCR was then performed to detect the presence of GFP (primer: 5′-AAGCTGACCCTGAAGTTCATCTGC-3′, 5′-CTTGTAGTTGCCGTCGTCCTTGAA-3′), GFP/AAV viral DNA was utilized for a positive control and vehicle muscle tissue was negative control. After PCR, gel electrophoresis in 2% agarose gel with ethidium bromide was performed at 90 mV for 40 min. Images of gel were acquired using the Gel Doc XR™ (Bio Rad, Hercules, CA).

Statistical Analysis

Data are presented as mean ± SD. Two-tailed Student's *T*-tests were performed to compare the means of two groups and one-way ANOVA was performed to compare the means of three or more groups, with *post-hoc* Tukey Simultaneous Tests for Differences of Means. An alpha value of $P < 0.05$ was interpreted to denote statistical significance.

RESULTS

Characterization of MSCs With Effective Viral Transduction Utilizing AAV

To ensure that the MSCs were supercharged as intended, several *in vitro* characteristics were assessed before *in vivo* viral transduction took place. The MSCs demonstrated fibroblast-like morphology and were adherent to the cell-culture plate (**Figure 1A**). Flow cytometry demonstrated positive expression of MSC markers CD44, CD73, and CD105 (**Figure 1B**). After transduction with either E-selectin-*ires*-eGFP/AAV or

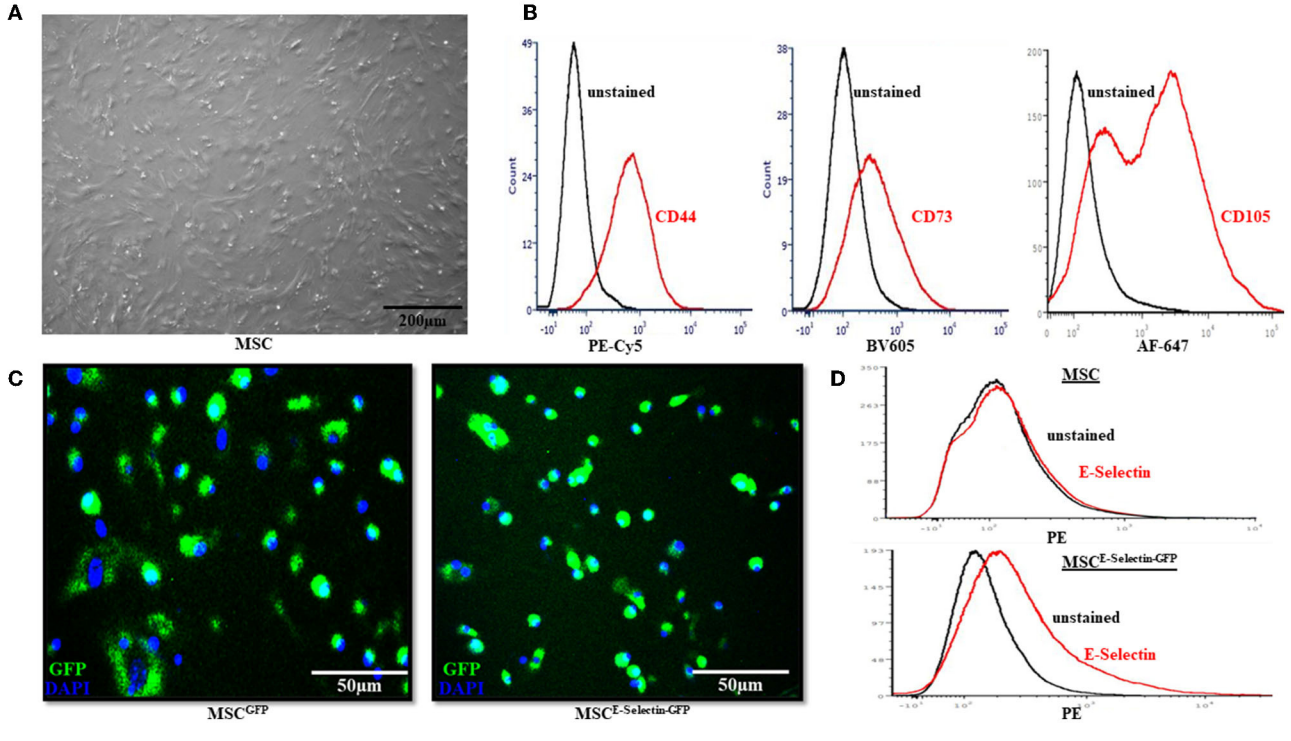

FIGURE 1 | Characterization of Mesenchymal Stem Cells (MSC). **(A)** MSC demonstrated fibroblast-like morphology in the growth medium and were adherent to the cell culture dish. **(B)** Flow cytometry revealed the native MSC had expression of cell-surface molecules CD44, CD73, and CD105. **(C)** After cells were transduced with either GFP/AAV or E-selectin-*ires*-eGFP/AAV, successful cell transduction is demonstrated by expression of GFP under confocal microscopy. **(D)** Flow-cytometry demonstrates a lack of E-selectin expression in untransduced MSC (top) and a gain of E-selectin expression after transduction has been performed (bottom).

eGFP/AAV, fluorescence microscopy was utilized to ensure transgene expression of GFP. Nuclei were stained with DAPI (**Figure 1C**). Almost all cells were successfully transduced by AAV (overlapping of GFP and DAPI), indicating a near 100% transduction efficiency under the utilized transduction conditions. Flow cytometry demonstrated that native MSCs do not express E-selectin (**Figure 1D**, top), while the MSCs transduced with E-selectin-*ires*-eGFP/AAV express elevated levels of E-selectin (**Figure 1D**, bottom).

Supercharging MSCs With AAV-Mediated E-Selectin Expression Enhances the Therapeutic Phenotype

To determine whether supercharging MSCs with E-selectin resulted in a superior therapeutic phenotype, cell proliferation and gene expression profiling were performed. $MSC^{E-selectin-GFP}$ was observed to have increased cell-culture numbers upon harvest from culture plates. We utilized $MSC^{E-selectin-GFP}$ and MSC^{GFP} (control) to compare their growth potentials at two different seeding densities (0.1×10^5 and 0.5×10^5 cells/well). We demonstrate herein that $MSC^{E-selectin-GFP}$ has increased cell proliferation within cell culture compared with MSC^{GFP} at both seeding densities (**Figure 2A**, $P < 0.05$). We then sought to determine genetic expression changes *via* PCR array profiling in $MSC^{E-selectin-GFP}$ vs. MSC^{GFP}. To do this, we extracted RNA from cultured $MSC^{E-selectin-GFP}$ and MSC^{GFP}, and performed RT^2−Profiler PCR array of 84 genes involved in angiogenesis. This analysis demonstrated that compared with MSC^{GFP}, $MSC^{E-selectin-GFP}$ had significantly upregulated genetic expression of 9 genes (*Tbx1, Leptin, IL6, Ilb1, Flt1, F2, Cxcl2, Ccl11, Angpt1*, **Figure 2B**, $P < 0.05$), **Table 1**.

Treatment With $MSC^{E\text{-}Selectin\text{-}GFP}$ Improves Reperfusion Index in Murine Model of Hind Limb Ischemia

We further evaluated the overall effect of $MSC^{E-selectin-GFP}$ therapy on the extent of hind limb ischemia, *in vivo*. Distal hind limb ischemia was surgically induced in mice that were then randomly separated into three groups, each treated with either $MSC^{E-selectin-GFP}$ ($n = 18$), MSC^{GFP} ($n = 20$), or PBS (vehicle, $n = 6$). LDI measurement reflects the vascular perfusion at the skin and subcutaneous tissues of the mice hind limbs, which serves as an overall reflection of the hind limb revascularization process. LDI measurements performed preoperatively and immediately postoperative were comparable between all groups (**Figure 3**). By POD 21, the mice treated with $MSC^{E-selectin-GFP}$ demonstrated statistically significantly increased distal hind limb blood flow, as evidenced by increased reperfusion index (ligated limb / non-ligated limb) on Doppler imaging when compared with mice treated with either MSC^{GFP} or vehicle (**Figure 3A**, $P < 0.01$). *Post-hoc* analysis demonstrated that treatment with MSC^{GFP}

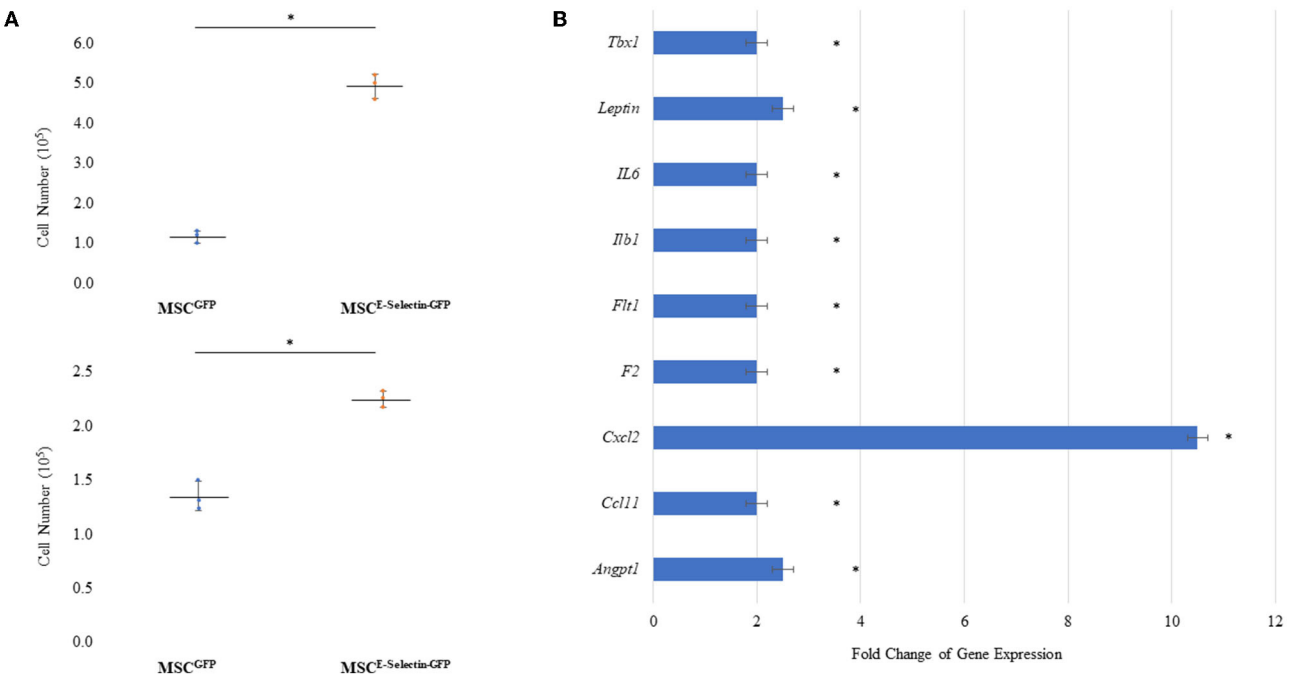

FIGURE 2 | Characteristics of MSC Supercharged with E-selectin. **(A)** Cell growth was enhanced post-transduction with E-selectin in either (top) plating density of 0.5×10^5 or (bottom) 0.1×10^5 when compared to control (mean ± SD of triplicates for each seeding density, $^*P < 0.05$ by Student's *T*-test). **(B)** Expression of several chemokine/cytokine mRNA was significantly higher in the $MSC^{Eselectin-GFP}$ vs. MSC^{GFP} measured by quantitative PCRArray. Equal portions of RNA from three plates in each group were utilized to perform reverse transcription reaction and each experiments was repeated for three times (mean ± SD of fold change $MSC^{E-selectin-GFP}$ vs. MSC^{GFP}, $^*P < 0.05$ by Student's *T*-test).

TABLE 1 | Genes upregulated in E-selectin supercharged mesenchymal stem cells (MSCs) (compared to MSC^{GFP}) and their previously described functions.

Symbol	Gene name	GenBank	Function
Tbx1†	T-box 1	NM_011532	Controls vascular smooth muscle and extracellular matrix investment in great vessel remodeling (39)
Lep†	Leptin	NM_008493	Regulates energy homeostasis (40)
IL6	Interleukin-6	NM_031168	Mediates the immune system and regenerative processes (41)
Ilb1	Interleukin-1β	NM_008361	Mediates inflammation and lymphocyte activation (42)
Flt1	Fms Related Receptor Tyrosine Kinase 1	NM_010228	Acts as a cell-surface receptor for VEGFA, VEGFB, and PGF and regulates cell migration along with post-natal angiogenesis (43–45)
F2†	Coagulation Factor II	NM_010168	Involved in blood homeostasis and wound healing (46)
Cxlc2†	Chemokine (C-X-C motif) ligand 2	NM_009140	Plays a role in improved cellular trafficking and engraftment (47)
Ccl11	C-C Motif Chemokine Ligand 11	NM_011330	Promotes accumulation of eosinophils (48)
Angpt1†	Angiopoietin 1	NM_009640	Promotes endothelial cell survival for angiogenesis (49)

Table listing full name of upregulated genes with the † mark indicating the genes also upregulated in vivo within the ischemic tissue injected with supercharged $MSC^{E-selectin-GFP}$ vs. the ischemic tissue injected with control MSC^{GFP}.
VEGFA, vascular endothelial growth factor a; VEGFB, vascular endothelial growth factor B; PGF, placental growth factor.

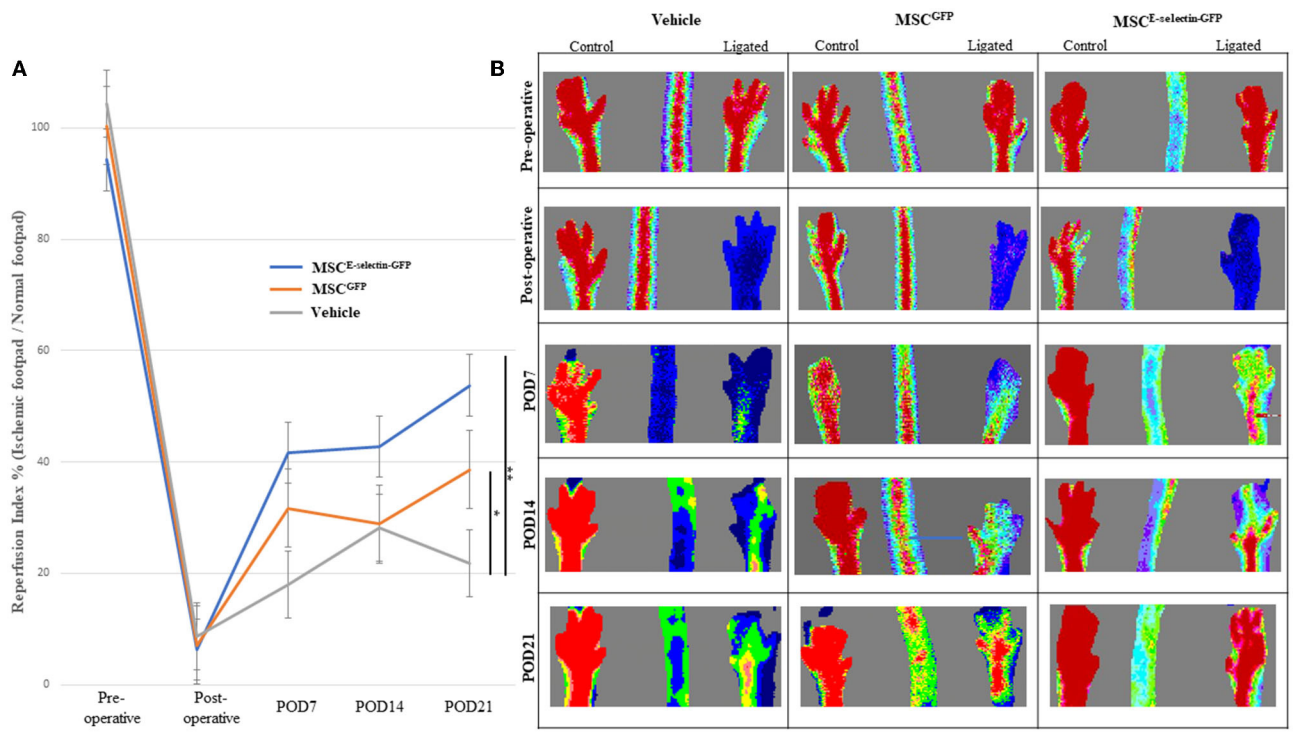

FIGURE 3 | $MSC^{E-selectin-GFP}$ treatment increases ischemic limb reperfusion. **(A)** The quantitative analysis of limb reperfusion measured by LDI (reperfusion index % = ischemic ligated footpad/normal control footpad, mean ± SD; $^{**}P < 0.01$ by ANOVA and $^{*}P < 0.05$ by *post-hoc* analysis, Vehicle $n = 6$, MSC^{GFP} $n = 20$, $MSC^{E-selectin-GFP}$ $n = 18$). **(B)** Representative images of hindlimb reperfusion by LDI obtained preoperatively, immediately after FAL (postoperative), and on postoperative days (POD) 7, 14, and 21.

resulted in superior reperfusion index when compared with vehicle ($P < 0.05$, **Figure 3A**). Overall, these results reveal that there is an increased level of reperfusion in the ischemic hind limb treated with both types of MSCs but the effect is significantly more potent with the E-selectin supercharged MSCs.

$MSC^{E-Selectin-GFP}$ Therapy Increases Vessel Density in the Murine Ischemic Footpad

To determine whether treatment with $MSC^{E-selectin-GFP}$ can increase postnatal neovascularization, 21 days after FAL live animal whole-body DiI perfusion followed by confocal laser

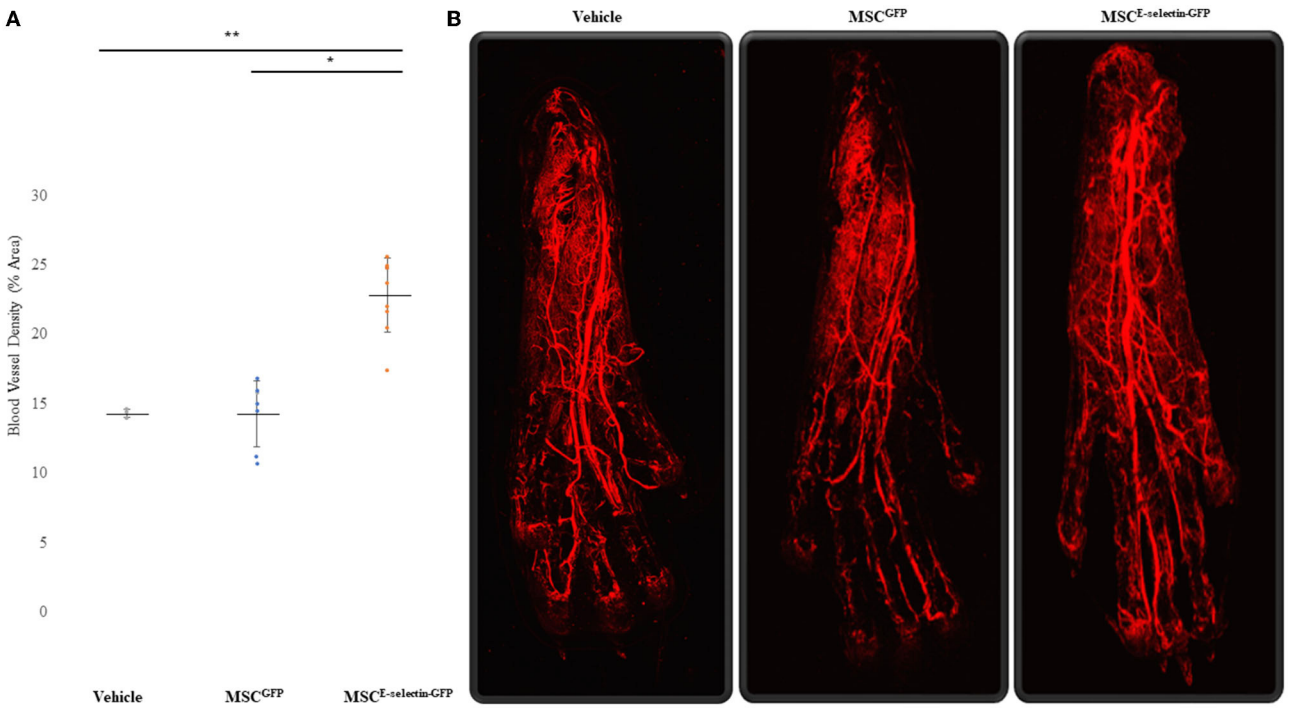

FIGURE 4 | Improved Blood Vessel Density of the Ischemic Distal Footpad after treatment with $MSC^{E-selectin-GFP}$. **(A)** Qualitative analysis of the distal toe vessel density (% area, mean ± SD, $^{**}P < 0.01$ *via* ANOVA, $^{*}P < 0.05$ *post-hoc* Tukey Simultaneous Tests for Differences of Means, Vehicle treatment $n = 3$, MSC^{GFP} $n = 8$, $MSC^{E-selectin-GFP}$ $n = 9$). **(B)** Representative images of Z-stacked images of the ischemic footpads after DiI perfusion *via* Confocal laser microscopy.

scanning photography of the ischemic footpad was performed to evaluate blood vessel density within the murine footpad in mice treated with $MSC^{E-selectin-GFP}$ ($n = 9$), MSC^{GFP} ($n = 8$), or PBS (vehicle, $n = 3$). There was a statistically significant difference in the number of vasculature, including capillaries, in the ischemic footpads of the mice treated by $MSC^{E-selectin-GFP}$ as opposed to treatment with MSC^{GFP} or vehicle (**Figure 4**, $P < 0.01$). Quantitatively, the mean capillary density within the ischemic footpad of mice treated with $MSC^{E-selectin-GFP}$ was 23%, while MSC^{GFP} and vehicle were 14 and 14%, respectively (**Figure 4A**). Taken together, these data demonstrate that treatment with $MSC^{E-selectin-GFP}$ induces increased vessel density in the footpad in mice with surgically induced hind limb ischemia.

$MSC^{E\text{-}Selectin\text{-}GFP}$ Therapy Improves Limb Functional Performance With Improved Exercise Tolerance and Decreased Hind Limb Skeletal Muscle Atrophy

To assess whether cell therapy treatment with $MSC^{E-selectin-GFP}$ would confer increased limb functional performance and decreased muscular atrophy, the treadmill exhaustion test was performed 21 days after induced ischemia in all treatment groups. The treadmill exhaustion test allowed mice in all treatment groups to run to exhaustion. The mice treated with $MSC^{E-selectin-GFP}$ had significantly increased exercise tolerance as evidenced by longer mean distance ran before exhaustion when compared with either MSC^{GFP} or vehicle (**Figure 5A**, $P < 0.01$). The mice treated with $MSC^{E-selectin-GFP}$ ran a mean distance of 162 meters before exhaustion while the mice treated with MSC^{GFP} and vehicle ran mean distances of 111 and 110 m, respectively. The mice treated with $MSC^{E-selectin-GFP}$ consistently stayed on the treadmill and furthest away from the adverse stimuli grid (**Figure 5B**). H&E sections of ischemic calf muscles harvested at POD 21 were examined and less muscle atrophy was noted in the mice treated with $MSC^{E-selectin-GFP}$ compared with those treated by MSC^{GFP} or vehicle. The muscle fibers of mice treated with $MSC^{E-selectin-GFP}$ had a significantly larger cross-sectional surface area when compared with mice treated with MSC^{GFP} or vehicle (**Figures 5C,D**). The muscle fibers in mice treated with $MSC^{E-selectin-GFP}$ had a mean muscle fiber size of 793 μm^2, while mice treated with MSC^{GFP} and vehicle had mean muscle fiber sizes of 526 and 546 μm^2, respectively (**Figure 5C**, $P < 0.01$). Overall, our data demonstrate that cell therapy treatment with $MSC^{E-selectin-GFP}$ improves limb functional recovery while mitigating skeletal muscle atrophy in this murine model of induced CLI.

In vivo Tissue Gene-Expression Profile Changes After Treatment With $MSC^{E\text{-}Selectin\text{-}GFP}$

To elucidate the mechanisms underlying $MSC^{E-selectin-GFP}$ therapy, we examined with an array of genes involved in

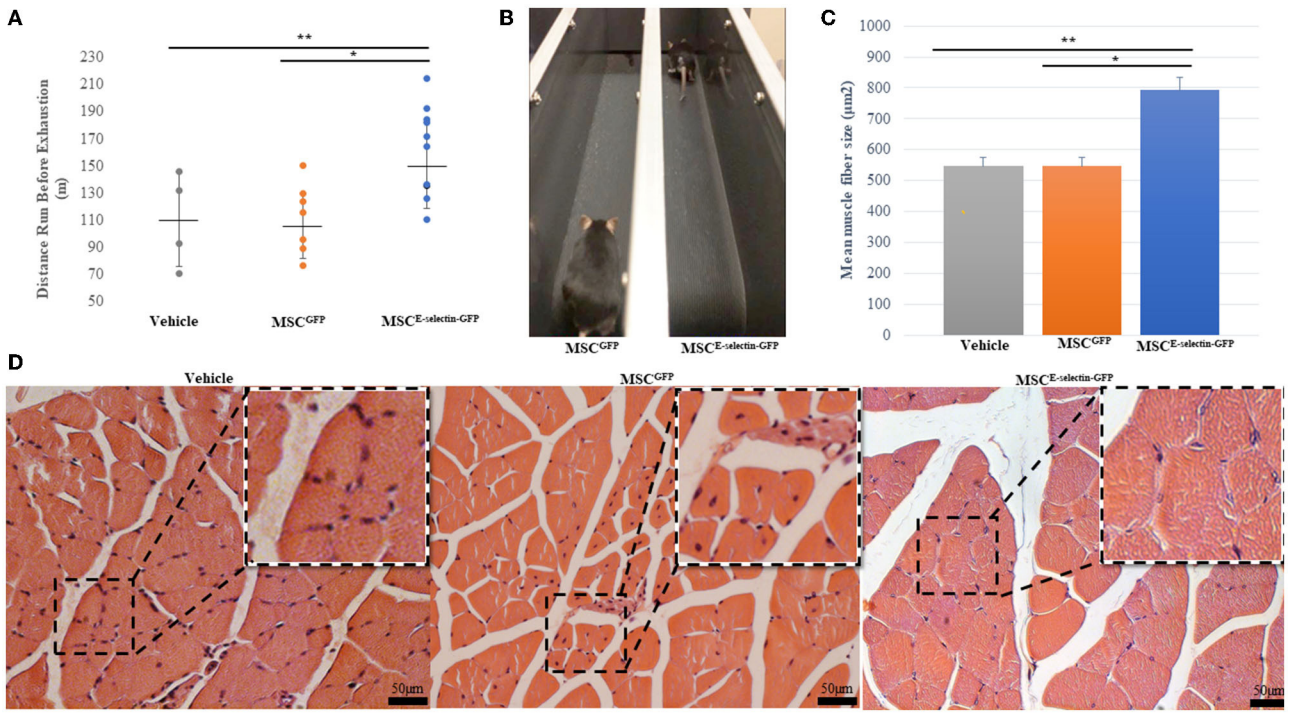

FIGURE 5 | Improved functional and pathologic recovery in ischemic muscles after treatment with $MSC^{E-selectin-GFP}$. **(A)** Quantitative analysis of distance ran (m) prior to exhaustion in treatment groups (Vehicle = 4, MSC^{GFP} = 7, $MSC^{E-selectin-GFP}$ = 10), $^{**}P < 0.01$ *via* ANOVA). **(B)** Representative image of MSC^{GFP} vs. $MSC^{E-selectin-GFP}$ on treadmill. **(C)** Qualitative analysis of the mean myofiber size of the ischemic calf muscle, data are based on 5 section/sample/mouse (μm^2, mean ± SD, $^{**}P < 0.01$ *via* ANOVA, $^{*}P < 0.05$ *post-hoc* Tukey Simultaneous Tests for Differences of Means, Vehicle treatment $n = 3$, MSC^{GFP} treatment $n = 3$, $MSC^{E-selectin-GFP}$ treatment $n = 3$). **(D)** Representative images of transverse H&E sections of ischemic calf muscle in Vehicle, MSC^{GFP}, and $MSC^{E-selectin-GFP}$.

angiogenesis and other functions. We utilized an *RT^2-PCR-Array* analysis of 84 angiogenic and inflammation signaling genes to investigate the genetic expression changes seen in the ischemic limb tissues treated with $MSC^{E-selectin-GFP}$ vs. MSC^{GFP} 21 days after treatment. We demonstrated that the ischemic muscle tissues treated with $MSC^{E-selectin-GFP}$ had significantly upregulated genetic expression of 9 genes (*Vegfb, Tbx1, Serpine1, Leptin, F2, Cxcl5, Cxcl2, Col4a3, and Angpt1*), and significantly downregulated expression of *TNF* gene (**Figure 6A**, $P < 0.05$). Four of those tissue-level genes were also upregulated *in vitro* by the $MSC^{E-selectin-GFP}$ utilized to treat the ischemic limbs: *Tbx1*, *Leptin*, *F2*, and *Cxcl2* (**Figure 6B**). Levels of several angiogenic genes, including VEGF, HGF, and PDGF, were unchanged in the culture $MSC^{E-selectin-GFP}$ compared with MSC^{GFP} *in vitro* according to *RT^2-PCR-Array* (**Supplementary Table 2**). Thus, *Tbx1*, *Leptin*, *F2*, and *Cxcl2* upregulated in treated ischemic limb tissues may be derived directly from the engrafted $MSC^{E-selectin-GFP}$, while likely the upregulation of the other 5 genes (*Vegfb, Serpine1, Cxcl5, Col4a3, and Angpt1*) and downregulation of *TNF* gene in ischemic limb tissues are indirect effects of the supercharged MSC cell therapy, from activation of secondary cell-cell and paracrine signaling cascades. These data suggest that the therapeutic effect of $MSC^{E-selectin-GFP}$ may be mediated through both direct and indirect mechanisms from primary and secondary signaling cascades.

Determining the Persistence, Biodistribution, and Potential Toxicity of MSCs Engrafted in the Ischemic Hind Limb

We performed immunofluorescent staining of the tissue sections treated with either $MSC^{E-selectin-GFP}$, MSC^{GFP}, or vehicle to assess the persistence of MSCs within the ischemic limb tissues harvested at POD 21. Very rare double positive ($DAPI^+/GFP^+$) cells were found within the treated ischemic limb tissues as evidenced by the representative images (**Figure 7A**) and quantification (**Figure 7B**), indicating that a few cells survive at POD 21. To determine the systemic biodistribution of MSCs engrafted in the ischemic hind limb of mice, we employed PCR analysis of remote organs. Lungs and liver represent two organs for engrafted MSCs to spread easiest *via* veins and arteries. These were harvested at POD 21 to detect the expression of *GFP* gene as both $MSC^{E-selectin-GFP}$ and MSC^{GFP} express GFP. First, we extracted total RNA from treated ischemic limb tissues, lungs, and livers, and utilized the cDNA generated by reverse transcription of mRNA for PCR analysis. We demonstrate a positive band (282 bp) within the viral DNA (GFP/AAV, positive control), and an absence of bands for distant organs (liver and lungs) in the treated mice (**Figure 7C**). Additionally, blood tests were performed to examine for potential systemic toxicity of $MSC^{E-selectin-GFP}$ therapy. Among all three treatment groups, there was no leukocytosis, anemia, or alterations in hepatic or

A

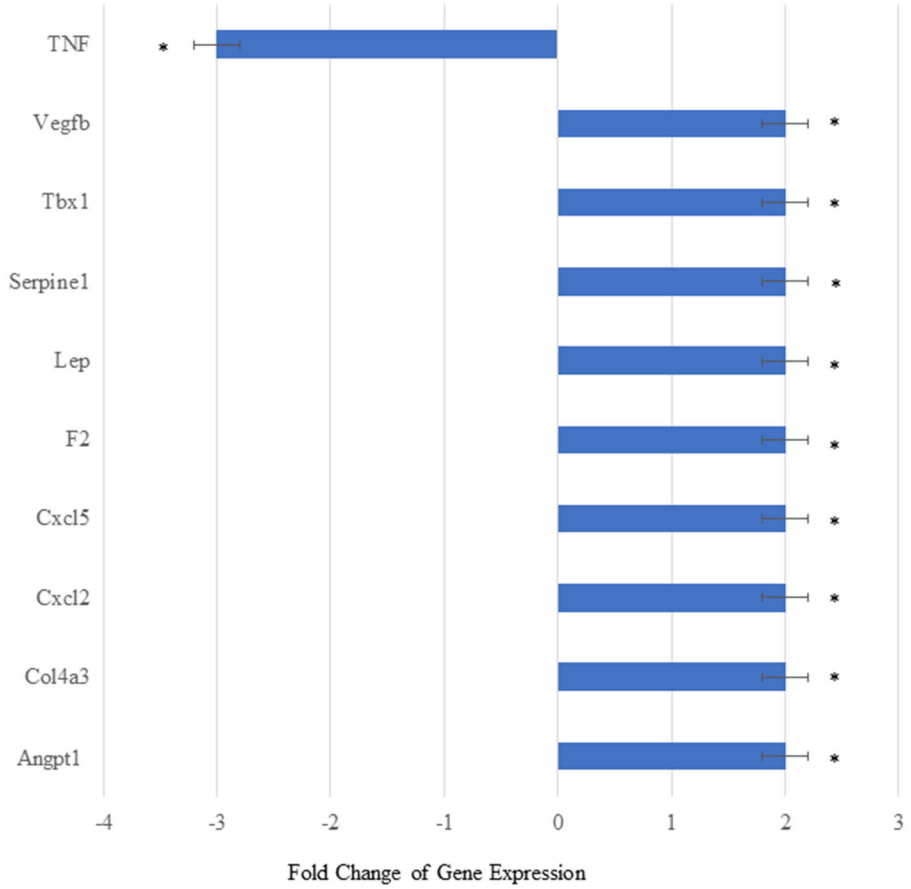

B

Symbol	Gene Name	GenBank
TNF	Tumor necrosis factor	NM_013693
Vegfb	Vascular endothelial growth factor B	NM_011697
Tbx1†	T-box 1	NM_011532
Serpine1	Serine (or cysteine) peptidase inhibitor, clade E, member 1	NM_008871
Lep†	Leptin	NM_008493
F2†	Coagulation Factor II	NM_010168
Cxcl5	Chemokine (C-X-C motif) ligand 5	NM_009141
Cxlc2†	Chemokine (C-X-C motif) ligand 2	NM_009140
Col4a3	Collagen, type IV, alpha 3	NM_007734
Angpt1†	Angiopoietin 1	NM_009640

FIGURE 6 | *In vivo* relative gene expression changes in the ischemic thigh tissue of mice treated with $MSC^{Eselectin-GFP}$ vs. MSC^{GFP}. **(A)** Expression of several chemokine/cytokine mRNA was significantly higher in the ischemic thigh muscle treated with $MSC^{Eselectin-GFP}$ vs. MSC^{GFP} measured by quantitative PCRArray by post-operative day 21. However, tumor necrosis factor (TNF) was significantly downregulated. Equal portions of RNA from three mice in each treatment group were

(Continued)

FIGURE 6 | utilized to perform reverse transcription reaction. Each experiment was repeated three times and data are presented as fold-change of treatment/control (*$P < 0.05$ *via* Student's *T*-test). **(B)** Table listing full name of upregulated genes with the † mark indicating the genes also upregulated *in-vitro* within the injected supercharged $MSC^{E-selectin-GFP}$ vs. the control MSC^{GFP}.

renal metabolism (**Supplementary Table 1**), while there was a trend toward higher AST levels in the vehicle group. Overall, these data demonstrate that the described cell-based therapy is generally not toxic. Most engrafted MSCs disappear by 21 days, which suggests that the therapeutic effect is achieved largely by early direct and indirect paracrine mechanisms. The fact that only a few cells survive in treated limb tissues may also implies that this MSC therapy has a lower theoretical long-term risk for tumorigenesis. Moreover, locally engrafted MSCs do not spread to distant organs (lungs and liver) and do not appear to have systemic toxic effects, indicating early preclinical evidence of biosafety with the $MSC^{E-selectin-GFP}$ therapy.

DISCUSSION

Mesenchymal stem cells throughout the last few decades have demonstrated strong regenerative and therapeutic potentials and have raised a great deal of hope for patients suffering from occlusive PAD. Their utilization as a treatment for CLI has demonstrated feasibility and efficacy in preventing disease progression, while very modest efficacy has been observed for all-cause mortality and amputation rates. However, clinical trials to date have employed unmodified MSCs, which may suggest that autologous MSCs, especially those from older, diseased patients, require additional modification to increase therapeutic efficacy (17, 50). Herein, we utilized a novel strategy of incorporating the pro-angiogenic (34, 51), and pro-healing (29) effects of E-selectin with the immunomodulatory and pro-regenerative properties of MSCs (8, 52) to improve the potential therapeutic efficacy of a stem-cell-based approach to CLI. In this study, we utilized the AAV to induce overexpression of E-selectin on the surface of MSCs. This creates a cell-based product that does not occur in nature, as indicated by the absence of E-selectin on the surface of control MSCs. Genetically modified MSCs have been employed in regenerative medicine, particularly in vascular regenerative preclinical studies to enhance the pro-angiogenic properties inherent in MSCs. Most investigations employ genetic modifications to increase angiogenic growth factors such as stromal cell-derived factor 1(SDF-1α) (53), platelet-derived growth factor (P-DGF) (47), vascular endothelial growth factor (VEGF) (40), and hepatocyte growth factor (HGF) (41), among others (39). These studies have demonstrated improved efficacy when compared with control MSCs, thus indicating MSC efficacy may be enhanced *via* genetic modifications. To our knowledge, this is the first attempt to use an adhesion molecule as the payload for a gene-modified cell-based approach in CLI.

We demonstrated improved therapeutic angiogenesis in hind limb ischemia *via* intramuscular injections of $MSC^{E-selectin-GFP}$ in comparison to MSC^{GFP}. We then further investigated the genetic expression resulting *in vitro* and *in vivo*. Our data demonstrate that treatment with $MSC^{E-selectin-GFP}$ not only improved tissue angiogenesis as evidenced by improved neovascularization on LDI and increased distal blood vessel density on DiI perfusion of murine footpads, but also improved muscular functional recovery and mitigated skeletal muscular atrophy in the ischemic murine hind limb. PCR array gene profiling suggests that treatment with $MSC^{E-selectin-GFP}$ had increased direct and downstream angiogenic chemokines/cytokines in addition to tissue downregulation of TNF, which likely assists in the modulation of the angiogenic response, dampens inflammation, and reduces the ischemia-induced tissue damage.

We utilized a AAV vector to transfer the E-selectin gene into MSCs, which do not normally overexpress E-selectin, to create a gene-modified cell-based therapy that could be applied to CLI. Past attempts at therapeutic angiogenesis utilizing viral vectors have been through gene therapy approaches with recombinant adenovirus (γAd) (42–46). Herein, we utilize the recombinant AAV (γAAV) due to its safety profile (48), high efficiency transduction in MSCs (28), and AAV transduction, which has gained approval for gene therapy from the Federal Drug Administration (FDA) in other disease processes (23, 24). The AAV vector used in this work is a non-pathogenic parvovirus that has the ability to transduce non-dividing and dividing cells with efficient gene expression and with minimal immunologic reaction (49). We demonstrated high-efficiency viral transduction and effective expression of the E-selectin transgene. Under the condition of 5×10^3 viral genome (VG)/cell, we were able to achieve almost 100% transduction efficiency without cellular toxicity. Achieving high transduction efficiency for MSCs *in vitro* with relatively low multiplicity of infection (MOI) of AAV marks this viral vector as a useful tool for gene-modified cell-based stem cell therapy. Supercharging the MSCs with E-selectin resulted in a phenotypic characteristic that increased their therapeutic potential. Specifically, $MSC^{E-selectin-GFP}$ demonstrated increased growth within the cell-culture plates and upregulation of pro-angiogenic genes involved in the production and secretion of chemokines and cytokines necessary for blood vessel development and tissue repair.

Supercharged $MSC^{E-selectin-GFP}$ overexpressed 9 angiogenic genes *in vitro* when compared to MSC^{GFP}. These 9 genes involved in angiogenesis also have multiple additional functions. Chemokine (C-X-C) motif, Ligand 2 (*Cxcl-2*), is known to play a role in improved cellular trafficking and engraftment (54), Leptin regulates energy homeostasis (55), interleukin-6 (*IL-6*) mediates the immune system and regenerative processes (56), while T-box transcription factor-1 (*Tbx1*) regulates arterial

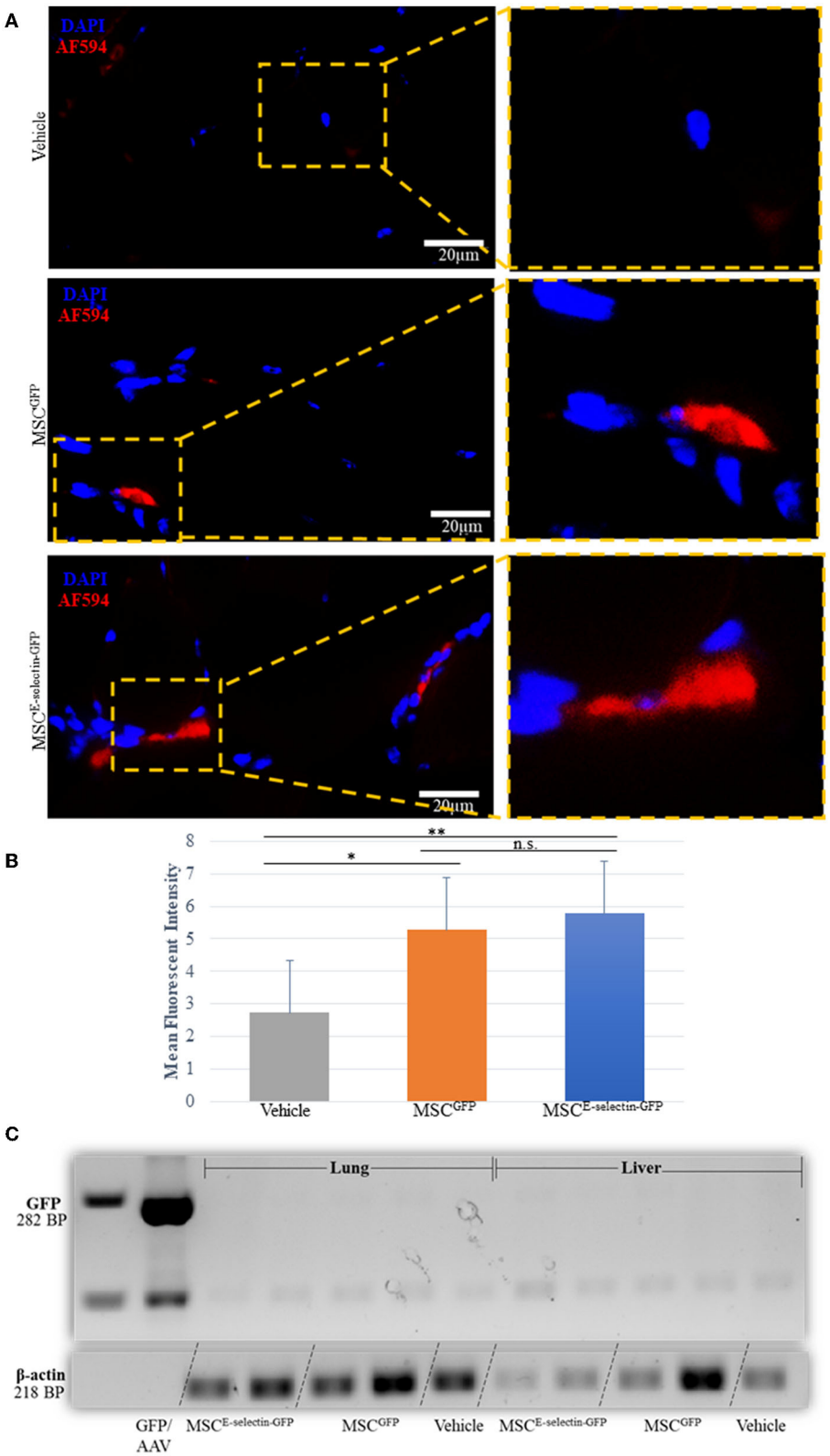

FIGURE 7 | Determining the fate of MSC injected as treatment for hindlimb ischemia 3-weeks after injection into thigh muscle. **(A)**. Representative images of immunohistochemistry co-staining with DAPI and GFP (AF-594), demonstrating that a few of the injected MSC survive at 3-weeks (POD 21). **(B)** Quantitative analysis of mean fluorescent intensity (MFI) in ischemic thigh muscle tissue sections stained for GFP demonstrates significant increased MFI between $MSC^{E-selectin-GFP}$,

(Continued)

FIGURE 7 | MSC^{GFP}, and Vehicle ($n = 30$ sections/group, $^{**}P < 0.001$, $^{*}P < 0.01$, n.s. = not significant *via* ANOVA with *post-hoc* Tukey Simultaneous Tests for Differences of Means) **(C)**. Representative PCR gel electrophoresis of mice lung and liver tissue demonstrating lack of GFP expression (positive control located at 282BP) and positive β-actin for $MSC^{E-selectin-GFP}$, MSC^{GFP}, and Vehicle (at 218BP).

development (57). Interleukin-1β (*Il1b*) mediates inflammation and lymphocyte activation (58), Fms-related Receptor Tyrosine Kinase 1 (*Flt1*) acts as a cell-surface receptor for vascular endothelial growth factor A (VEGFA), vascular endothelial growth factor B (VEGFB), placental growth factor (PGF), and regulates cell migration along with postnatal angiogenesis (59–61), and coagulation factor II (*F2*) is involved in blood homeostasis and wound healing (62). C-C motif Chemokine Ligand 11 (*Ccl11*) promotes accumulation of eosinophils (63), and Angiopoietin-1 (*Angpt1*) promotes endothelial cell survival for angiogenesis (64). MSCs have known immunomodulatory effects (65). Pro-inflammatory MSCs (MSC1) produce cytokines such as IL-1β, IL-6, IL-8/CXCL8, and CCL5, which regulate immune response (66). Many of these pro-inflammatory cytokines increase the recruitment of innate immune cells and progenitor cells that are required for tissue remodeling and blood vessel development (34, 51, 67). $MSC^{E-selectin-GFP}$ demonstrated increased upregulation in the inflammatory cytokines IL-1β and IL-6, indicating that our supercharged stem cells are of the MSC1 phenotype and have increased paracrine effects when compared with control, *in vitro*. Yet, there are other beneficial effects to the immunomodulation induced by the E-Selectin-overexpressing MSCs. We observed that TNF was downregulated in ischemic limb tissues treated with $MSC^{E-selectin-GFP}$ while there was overlap in some pro-angiogenic genes upregulated both in the transduced MSCs and the tissues treated with these cells, the additional effects in gene expression observed only in the treated tissues (and not the cells) point the complex activation of cell-cell and paracrine secondary signaling cascades. Yet, the cells exert the tissue repair within the first 21 days, thereafter mostly being cleared. The LDI imaging quantitative data suggest that the most robust timeframe for angiogenesis occurs in the 1st week, which is likely when the $MSC^{E-selectin-GFP}$ is most actively secreting chemokines/cytokines and modulating the ischemic tissue environment. This augmented angiogenesis is likely due to the enhanced MSCs phenotypes as evidenced by their inflammatory genetic upregulation, which potentially translates into the sustained pro-angiogenic genetic regulation within the ischemic tissues. In fact, a burst of self-limiting inflammation is essential in normal healing (68). Interestingly, although $MSC^{E-selectin-GFP}$ produces increased levels of IL-6 *in vitro*, the treated ischemic limb tissues do not appear to have sustained inflammation and actually by day 21, downregulate TNF. Moreover, tissue levels of IL-6 in treated ischemic limbs are not increased as assessed by PCR array. Future studies are planned to perform transcriptome analysis to further elucidate the alterations seen in the $MSC^{E-selectin-GFP}$ as other therapeutic avenues may yet be uncovered.

The fact that only a limited amount of MSCs survived in ischemic limbs 3 weeks after treatment also supports that the therapeutic effects of engrafted supercharged MSCs are achieved through early direct and paracrine mechanisms rather than permanent cell differentiation and engraftment into tissue. For CLI application, a short period of persistence of these otherwise not naturally occurring MSCs in the treated limb tissues is beneficial since it may imply less risk of long-term tumorigenesis, and thus a safe approach. Biosafety of our E-selectin overexpressing MSC therapy is also suggested by the lack of systemic biodistribution and no evidence of aberrant metabolic changes as indicated by blood tests. Additionally, no untoward side-effects were observed in any of the mice treated with MSCs during the 3-week time frame. Thus, we demonstrate that this supercharged MSC therapy has superior therapeutic efficacy and reassuring biosafety in the mouse model.

In conclusion, this study reports a novel approach at genetic manipulation of MSCs *via* a rAAV vector that induces E-selectin overexpression. These new "supercharged" MSCs grow faster and induced a number of biologic readouts that are relevant to the treatment of CLI. We have shown that our engineered rAAV vector results in efficient expression of E-selectin, which when utilized as a gene-modified cell-based treatment for hind limb ischemia, results in improved functional recovery, muscle size, angiogenesis, and tissue repair. Our study highlights this novel gene therapy approach to CLI as a potential therapeutic option to be tested in future clinical studies.

DATA AVAILABILITY STATEMENT

The raw data supporting the conclusions of this article will be made available by the authors, without undue reservation.

ETHICS STATEMENT

The animal study was reviewed and approved by IACUC protocol 16-188.

AUTHOR CONTRIBUTIONS

HQ: study design, investigation, data analysis, and manuscript writing. RL-S: study design and critical review. YL, SV, YO, PP, and HS: investigation and critical review. RV-P: conceptualization and methodology. Z-JL and OV: conceptualization, methodology, validation, analysis, critical review, and editing of manuscript. All authors contributed to the article and approved the submitted version.

FUNDING

This work was supported by grants from the National Institutes of Health [VITA (NHLBI-CSB-HV-2017-01-JS) and R01DK-071084, R01GM081570].

ACKNOWLEDGMENTS

We thank Histology core and Image core in Miller School of Medicine, University of Miami, for assistance with tissue processing, section, and confocal microscopy.

SUPPLEMENTARY MATERIAL

The Supplementary Material for this article can be found online at: https://www.frontiersin.org/articles/10.3389/fcvm.2021.826687/full#supplementary-material

REFERENCES

1. Nehler MR, Duval S, Diao L, Annex BH, Hiatt WR, Rogers K, et al. Epidemiology of peripheral arterial disease and critical limb ischemia in an insured national population. *J Vasc Surg.* (2014) 60:686–95 e2. doi: 10.1016/j.jvs.2014.03.290
2. Powell RJ. Update on clinical trials evaluating the effect of biologic therapy in patients with critical limb ischemia. *J Vasc Surg.* (2012) 56:264–6. doi: 10.1016/j.jvs.2012.03.255
3. Kinlay S. Management of critical limb ischemia. *Circ Cardiovasc Interv.* (2016) 9:e001946. doi: 10.1161/CIRCINTERVENTIONS.115.001946
4. van Belle E, Nikol S, Norgren L, Baumgartner I, Driver V, Hiatt W, et al. Insights on the role of diabetes and geographic variation in patients with criticial limb ischaemia. *Eur J Vasc Endovasc Surg.* (2011) 42:365–73. doi: 10.1016/j.ejvs.2011.04.030
5. Parikh PP, Liu Z-J, Velazquez OC. A molecular and clinical review of stem cell therapy in critical limb ischemia. *Stem Cells Int.* (2017) 2017:3750829. doi: 10.1155/2017/3750829
6. Parekkadan B, Milwid JM. Mesenchymal stem cells as therapeutics. *Annu Rev Biomed Eng.* (2010) 12:87–117. doi: 10.1146/annurev-bioeng-070909-105309
7. Tark KC, Hong JW, Kim YS, Hahn SB, Lee WJ, Lew DH. Effects of human cord blood mesenchymal stem cells on cutaneous wound healing in leprdb mice. *Ann Plast Surg.* (2010) 65:565–72. doi: 10.1097/SAP.0b013e3181d9aae2
8. Wu Y, Chen L, Scott PG, Tredget EE. Mesenchymal stem cells enhance wound healing through differentiation and angiogenesis. *Stem Cells.* (2007) 25:2648–59. doi: 10.1634/stemcells.2007-0226
9. Gao WH, Gao HY Li YT, Huang PP. Effectiveness of umbilical cord mesenchymal stem cells in patients with critical limb ischemia. *Med Clin.* (2019) 153:341–6. doi: 10.1016/j.medcli.2019.01.031
10. Garcia-Vazquez MD, Herrero de la Parte B, Garcia-Alonso I, Morales MC. Analysis of biological properties of human adult mesenchymal stem cells and their effect on mouse hind limb ischemia. *J Vasc Res.* (2019) 56:77–91. doi: 10.1159/000498919
11. Lu D, Chen B, Liang Z, Deng W, Jiang Y, Li S, et al. Comparison of bone marrow mesenchymal stem cells with bone marrow-derived mononuclear cells for treatment of diabetic critical limb ischemia and foot ulcer: a double-blind, randomized, controlled trial. *Diabetes Res Clin Pract.* (2011) 92:26–36. doi: 10.1016/j.diabres.2010.12.010
12. Wang Z, Zheng L, Lian C, Qi Y, Li W, Wang S. Human umbilical cord-derived mesenchymal stem cells relieve hind limb ischemia by promoting angiogenesis in mice. *Stem Cells Dev.* (2019) 28:1384–97. doi: 10.1089/scd.2019.0115
13. Qadura M, Terenzi DC, Verma S, Al-Omran M, Hess DA. Concise review: cell therapy for critical limb ischemia: an integrated review of preclinical and clinical studies. *Stem Cells.* (2018) 36:161–71. doi: 10.1002/stem.2751
14. Vasa M, Fichtlscherer S, Aicher A, Adler K, Urbich C, Martin H, et al. Number and migratory activity of circulating endothelial progenitor cells inversely correlate with risk factors for coronary artery disease. *Circ Res.* (2001) 89:e1–7. doi: 10.1161/hh1301.093953
15. Wahid SFA, Ismail NA, Jamaludin WFW, Muhamad NA, Hamid MKAA, Harunarashid H, et al. Autologous cells derived from different sources and administered using different regimens for'no-option'critical lower limb ischaemia patients. *Cochr Datab Systemat Rev.* (2018). doi: 10.1002/14651858.CD010747.pub2
16. Teraa M, Gremmels H, Wijnand JGJ, Verhaar MC. Cell therapy for chronic limb-threatening ischemia: current evidence and future directions. *Stem Cells Transl Med.* (2018) 7:842–6. doi: 10.1002/sctm.18-0025
17. Duscher D, Rennert RC, Januszyk M, Anghel E, Maan ZN, Whittam AJ, et al. Aging disrupts cell subpopulation dynamics and diminishes the function of mesenchymal stem cells. *Sci Rep.* (2014) 4:7144. doi: 10.1038/srep07144
18. Dimmeler S, Leri A. Aging and disease as modifiers of efficacy of cell therapy. *Circ Res.* (2008) 102:1319–30. doi: 10.1161/CIRCRESAHA.108.175943
19. Kim H, Han JW, Lee JY, Choi YJ, Sohn Y-D, Song M, et al. Diabetic mesenchymal stem cells are ineffective for improving limb ischemia due to their impaired angiogenic capability. *Cell Transplant.* (2015) 24:1571–84. doi: 10.3727/096368914X682792
20. Mazo IB, Gutierrez-Ramos JC, Frenette PS, Hynes RO, Wagner DD, von Andrian UH. Hematopoietic progenitor cell rolling in bone marrow microvessels: parallel contributions by endothelial selectins and vascular cell adhesion molecule 1. *J Exp Med.* (1998) 188:465–74. doi: 10.1084/jem.188.3.465
21. Schweitzer KM, Dräger AM, van der Valk P, Thijsen SF, Zevenbergen A, Theijsmeijer AP, et al. Constitutive expression of E-selectin and vascular cell adhesion molecule-1 on endothelial cells of hematopoietic tissues. *Am J Pathol.* (1996) 148:165–75.
22. Liu Z-J, Daftarian P, Kovalski L, Wang B, Tian R, Castilla DM, et al. Directing and potentiating stem cell-mediated angiogenesis and tissue repair by cell surface E-selectin coating. *PLoS ONE.* (2016) 11:e0154053. doi: 10.1371/journal.pone.0154053
23. FDA. *Luxterna.* Federal Drug Administration. (2020). Available online at: https://www.fda.gov/vaccines-blood-biologics/cellular-gene-therapy-products/luxturna (accessed November 1, 2021).
24. FDA. *Zolgensma.* Federal Drug Administration. (2020). Available online at: https://www.fda.gov/vaccines-blood-biologics/zolgensma (accessed November 1, 2021).
25. Friedrich G, Soriano P. Promoter traps in embryonic stem cells: a genetic screen to identify and mutate developmental genes in mice. *Genes Dev.* (1991) 5:1513–23. doi: 10.1101/gad.5.9.1513
26. Amend SR, Valkenburg KC, Pienta KJ. Murine hind limb long bone dissection and bone marrow isolation. *JoVE.* (2016) 2016:e53936. doi: 10.3791/53936
27. Clément N, Grieger JC. Manufacturing of recombinant adeno-associated viral vectors for clinical trials. *Mol Ther Method Clin Dev.* (2016) 3:16002. doi: 10.1038/mtm.2016.2
28. Stender S, Murphy M, O'Brien T, Stengaard C, Ulrich-Vinther M, Soballe K, et al. Adeno-associated viral vector transduction of human mesenchymal. *Stem Cells.* (2007) 13:99. doi: 10.22203/eCM.v013a10
29. Parikh PP, Lassance-Soares RM, Shao H, Regueiro MM, Li Y, Liu ZJ, et al. Intramuscular E-selectin/adeno-associated virus gene therapy promotes wound healing in an ischemic mouse model. *J Surg Res.* (2018) 228:68–76. doi: 10.1016/j.jss.2018.02.061
30. Parikh PP, Castilla D, Lassance-Soares RM, Shao H, Regueiro M, Li Y, et al. A reliable mouse model of hind limb gangrene. *Ann Vasc Surg.* (2018) 48:222–32. doi: 10.1016/j.avsg.2017.10.008
31. Faber JE, Zhang H, Lassance-Soares RM, Prabhakar P, Najafi AH, Burnett MS, et al. Aging causes collateral rarefaction and increased severity of ischemic injury in multiple tissues. *Arterioscler Thromb Vasc Biol.* (2011) 31:1748–56. doi: 10.1161/ATVBAHA.111.227314
32. Boden J, Wei J, McNamara G, Layman H, Abdulreda M, Andreopoulos F, et al. Whole-mount imaging of the mouse hindlimb vasculature using the lipophilic carbocyanine dye DiI. *Biotechniques.* (2012) 53:10.2144/000113907. doi: 10.2144/000113907
33. Li Y, Song Y, Zhao L, Gaidosh G, Laties AM, Wen R. Direct labeling and visualization of blood vessels with lipophilic carbocyanine dye DiI. *Nat Protoc.* (2008) 3:1703–8. doi: 10.1038/nprot.2008.172

34. Liu ZJ, Tian R, An W, Zhuge Y, Li Y, Shao H, et al. Identification of E-selectin as a novel target for the regulation of postnatal neovascularization: implications for diabetic wound healing. *Ann Surg.* (2010) 252:625–34. doi: 10.1097/SLA.0b013e3181f5a079
35. Shao H, Cai L, Grichnik JM, Livingstone AS, Velazquez OC, Liu ZJ. Activation of Notch1 signaling in stromal fibroblasts inhibits melanoma growth by upregulating WISP-1. *Oncogene.* (2011) 30:4316–26. doi: 10.1038/onc.2011.142
36. Wang C, Yue F, Kuang S. Muscle histology characterization using H&E staining and muscle fiber type classification using immunofluorescence staining. *Bio Protoc.* (2017) 7:e2279. doi: 10.21769/BioProtoc.2279
37. Castro B, Kuang S. Evaluation of muscle performance in mice by treadmill exhaustion test and whole-limb grip strength assay. *Bio Protoc.* (2017) 7:e2237. doi: 10.21769/BioProtoc.2237
38. Dougherty JP, Springer DA, Gershengorn MC. The treadmill fatigue test: a simple, high-throughput assay of fatigue-like behavior for the mouse. *J Vis Exp.* (2016) 2016:54052. doi: 10.3791/54052
39. Jeong IS, Park Y, Ryu HA, An HS, Han JH, Kim SW. Dual chemotactic factors-secreting human amniotic mesenchymal stem cells *via* TALEN-mediated gene editing enhanced angiogenesis. *Int J Cardiol.* (2018) 260:156–62. doi: 10.1016/j.ijcard.2018.02.043
40. Fierro FA, Magner N, Beegle J, Dahlenburg H, Logan White J, Zhou P, et al. Mesenchymal stem/stromal cells genetically engineered to produce vascular endothelial growth factor for revascularization in wound healing and ischemic conditions. *Transfusion.* (2019) 59:893–7. doi: 10.1111/trf.14914
41. Wu Z, Chen G, Zhang J, Hua Y, Li J, Liu B, et al. Treatment of myocardial infarction with gene-modified mesenchymal stem cells in a small molecular hydrogel. *Sci Rep.* (2017) 7:15826. doi: 10.1038/s41598-017-15870-z
42. Creager MA, Olin JW, Belch JJ, Moneta GL, Henry TD, Rajagopalan S, et al. Effect of hypoxia-inducible factor-1alpha gene therapy on walking performance in patients with intermittent claudication. *Circulation.* (2011) 124:1765–73. doi: 10.1161/CIRCULATIONAHA.110.009407
43. Mohler ER 3rd, Rajagopalan S, Olin JW, Trachtenberg JD, Rasmussen H, Pak R, et al. Adenoviral-mediated gene transfer of vascular endothelial growth factor in critical limb ischemia: safety results from a phase I trial. *Vasc Med.* (2003) 8:9–13. doi: 10.1191/1358863x03vm460oa
44. Rajagopalan S, Olin J, Deitcher S, Pieczek A, Laird J, Grossman PM, et al. Use of a constitutively active hypoxia-inducible factor-1alpha transgene as a therapeutic strategy in no-option critical limb ischemia patients: phase I dose-escalation experience. *Circulation.* (2007) 115:1234–43. doi: 10.1161/CIRCULATIONAHA.106.607994
45. Mäkinen K, Manninen H, Hedman M, Matsi P, Mussalo H, Alhava E, et al. Increased vascularity detected by digital subtraction angiography after VEGF gene transfer to human lower limb artery: a randomized, placebo-controlled, double-blinded phase II study. *Mol Ther.* (2002) 6:127–33. doi: 10.1006/mthe.2002.0638
46. Rajagopalan S, Mohler ER, Lederman RJ, Mendelsohn FO, Saucedo JF, Goldman CK, et al. Regional angiogenesis with vascular endothelial growth factor in peripheral arterial disease. *Circulation.* (2003) 108:1933–8. doi: 10.1161/01.CIR.0000093398.16124.29
47. Capilla-Gonzalez V, Lopez-Beas J, Escacena N, Aguilera Y, de la Cuesta A, Ruiz-Salmeron R, et al. PDGF restores the defective phenotype of adipose-derived mesenchymal stromal cells from diabetic patients. *Mol Ther.* (2018) 26:2696–709. doi: 10.1016/j.ymthe.2018.08.011
48. Berns KI, Linden RMJB. The cryptic life style of adenoassociated virus. *Bioessays.* (1995) 17:237–45. doi: 10.1002/bies.950170310
49. Daya S, Berns KI. Gene therapy using adeno-associated virus vectors. *Clin Microbiol Rev.* (2008) 21:583–93. doi: 10.1128/CMR.00008-08
50. Yan J, Tie G, Wang S, Messina KE, DiDato S, Guo S, et al. Type 2 diabetes restricts multipotency of mesenchymal stem cells and impairs their capacity to augment postischemic neovascularization in db/db mice. *J Am Heart Assoc.* (2012) 1:e002238. doi: 10.1161/JAHA.112.002238
51. Liu ZJ, Tian R, Li Y, Zhang L, Shao H, Yang C, et al. SDF-1alpha-induced dual pairs of E-selectin/ligand mediate endothelial progenitor cell homing to critical ischemia. *Sci Rep.* (2016) 6:34416. doi: 10.1038/srep34416
52. Wu Y, Zhao RCH, Tredget EE. Concise review: bone marrow-derived stem/progenitor cells in cutaneous repair and regeneration. *Stem Cells.* (2010) 28:905–15. doi: 10.1002/stem.420
53. Tang J, Wang J, Yang J, Kong X, Zheng F, Guo L, et al. Mesenchymal stem cells over-expressing SDF-1 promote angiogenesis and improve heart function in experimental myocardial infarction in rats. *Eur J Cardiothorac Surg.* (2009) 36:644–50. doi: 10.1016/j.ejcts.2009.04.052
54. De Filippo K, Dudeck A, Hasenberg M, Nye E, van Rooijen N, Hartmann K, et al. Mast cell and macrophage chemokines CXCL1/CXCL2 control the early stage of neutrophil recruitment during tissue inflammation. *Blood.* (2013) 121:4930–7. doi: 10.1182/blood-2013-02-486217
55. Kelesidis T, Kelesidis I, Chou S, Mantzoros CS. Narrative review: the role of leptin in human physiology: emerging clinical applications. *Ann Intern Med.* (2010) 152:93–100. doi: 10.7326/0003-4819-152-2-201001190-00008
56. Schett G. Physiological effects of modulating the interleukin-6 axis. *Rheumatology.* (2018) 57(suppl.2):ii43–50. doi: 10.1093/rheumatology/kex513
57. Papangeli I, Scambler PJ. Tbx1 genetically interacts with the transforming growth factor-β/bone morphogenetic protein inhibitor Smad7 during great vessel remodeling. *Circ Res.* (2013) 112:90–102. doi: 10.1161/CIRCRESAHA.112.270223
58. Dinarello CA. Overview of the IL-1 family in innate inflammation and acquired immunity. *Immunol Rev.* (2018) 281:8–27. doi: 10.1111/imr.12621
59. Barleon B, Sozzani S, Zhou D, Weich HA, Mantovani A, Marmé D. Migration of human monocytes in response to vascular endothelial growth factor (VEGF) is mediated *via* the VEGF receptor flt-1. *Blood.* (1996) 87:3336–43. doi: 10.1182/blood.V87.8.3336.bloodjournal8783336
60. Cai J, Ahmad S, Jiang WG, Huang J, Kontos CD, Boulton M, et al. Activation of vascular endothelial growth factor receptor-1 sustains angiogenesis and Bcl-2 expression *via* the phosphatidylinositol 3-kinase pathway in endothelial cells. *Diabetes.* (2003) 52:2959–68. doi: 10.2337/diabetes.52.12.2959
61. Ahmad S, Hewett PW, Al-Ani B, Sissaoui S, Fujisawa T, Cudmore MJ, et al. Autocrine activity of soluble Flt-1 controls endothelial cell function and angiogenesis. *Vasc Cell.* (2011) 3:15. doi: 10.1186/2045-824X-3-15
62. Chambers RC, Dabbagh K, McAnulty RJ, Gray AJ, Blanc-Brude OP, Laurent GJ. Thrombin stimulates fibroblast procollagen production via proteolytic activation of protease-activated receptor 1. *Biochem J.* (1998) 333:121–7. doi: 10.1042/bj3330121
63. Kampen GT, Stafford S, Adachi T, Jinquan T, Quan S, Grant JA, et al. Eotaxin induces degranulation and chemotaxis of eosinophils through the activation of ERK2 and p38 mitogen-activated protein kinases. *Blood.* (2000) 95:1911–7. doi: 10.1182/blood.V95.6.1911
64. Song H, Suehiro J, Kanki Y, Kawai Y, Inoue K, Daida H, et al. Critical role for GATA3 in mediating Tie2 expression and function in large vessel endothelial cells. *J Biol Chem.* (2009) 284:29109–24. doi: 10.1074/jbc.M109.041145
65. Waterman RS, Tomchuck SL, Henkle SL, Betancourt AM, A. new mesenchymal stem cell (MSC) paradigm: polarization into a pro-inflammatory MSC1 or an immunosuppressive MSC2 phenotype. *PLoS ONE.* (2010) 5:e10088. doi: 10.1371/journal.pone.0010088
66. Romieu-Mourez R, François M, Boivin MN, Bouchentouf M, Spaner DE, Galipeau J. Cytokine modulation of TLR expression and activation in mesenchymal stromal cells leads to a proinflammatory phenotype. *J Immunol.* (2009) 182:7963–73. doi: 10.4049/jimmunol.0803864
67. Gallagher KA, Liu ZJ, Xiao M, Chen H, Goldstein LJ, Buerk DG, et al. Diabetic impairments in NO-mediated endothelial progenitor cell mobilization and homing are reversed by hyperoxia and SDF-1 alpha. *J Clin Invest.* (2007) 117:1249–59. doi: 10.1172/JCI29710

68. Ross R, Odland G. Human wound repair. II. Inflammatory cells, epithelial-mesenchymal interrelations, and fibrogenesis. *J Cell Biol.* (1968) 39:152–68. doi: 10.1083/jcb.39.1.152

Conflict of Interest: Z-JL and OV along with the University of Miami hold intellectual property of the AAV engineered E-selectin vector and have been licensed to Ambulero, Inc.

The remaining authors declare that the research was conducted in the absence of any commercial or financial relationships that could be construed as a potential conflict of interest.

Publisher's Note: All claims expressed in this article are solely those of the authors and do not necessarily represent those of their affiliated organizations, or those of the publisher, the editors and the reviewers. Any product that may be evaluated in this article, or claim that may be made by its manufacturer, is not guaranteed or endorsed by the publisher.

frontiers in Cardiovascular Medicine

OPINION
published: 25 February 2022
doi: 10.3389/fcvm.2022.801927

What Is the Potential for Lumacaftor as a Chemical Chaperone in Promoting hERG Trafficking?

Zequn Zheng[1,2], *Yongfei Song*[2,3] *and Jiangfang Lian*[2,3]*

[1] Department of Cardiovascular, Medical College, Ningbo University, Ningbo, China, [2] Ningbo Institute for Medicine & Biomedical Engineering Combined Innovation, Ningbo, China, [3] Department of Cardiovascular, Lihuili Hospital Affiliated to Ningbo University, Ningbo, China

Keywords: hERG channel protein, Lumacaftor, gene mutation, retrafficking, therapeutic potential

INTRODUCTION

Endogenous molecular chaperones are essential in the process of going from nascent chain to folded protein (1). Many studies have confirmed that overexpression of specific molecular chaperones promotes the maturation of corresponding substrate proteins, also known as client proteins, which restores intracellular protein homeostasis and is thought to be an effective treatment in a variety of protein conformational diseases such as cystic fibrosis (CF), Alzheimer's disease (AD), Parkinson's disease (PD), amyotrophic lateral sclerosis (ALS), etc (2). Nevertheless, the rescued effect resulting from endogenous molecular chaperones is not specific, since it may have off-target and even deleterious consequences, such as tumor formation (3).

To date, nearly 500 LQT2-associated pathogenic variants have been identified, of which 40% represent nonsense, frame-shift, or splice-site variants that inhibit hERG protein synthesis (Class 1). The remaining 60% are missense variants causing hERG channel loss of function by either disrupting channel trafficking to the membrane (Class 2, trafficking defective), disruption of channel gating (Class 3), and/or negatively affecting channel conductance (Class 4) (4–7). Functional studies revealed that over 80% of missense mutations cause defective hERG protein trafficking. Therefore, exogenous chemical chaperones generating a pharmacological activity that target specific protein conformation diseases represent the most promising therapeutic options. Lumacaftor (LUM), a medicine licensed by the Food and Drug Administration (FDA) for the clinical treatment of CF, appears to be a good representative of this sort of chemical. In a disease-specific human-induced pluripotent stem cell-derived cardiomyocytes (hiPSC-CMs) model, Mehta et al. first examined its effect on different mutation types of hERG. The results showed that for the two variants of A561V and IVS9-28A>G (Class 2), LUM increases the membrane expression of the protein and corrects the cellular phenotype well, but has no effect on the other two variants representing Class 1 (7). We read with great interest a paper published in the journal of *Circulation-Genomic and Precision Medicine* by O'Hare et al., in which they established that the LUM works on three mutants of the *KCNH2*: G604S, N633S, and R685P. They confirmed that LUM affiliates the mature trafficking of hERG mutant proteins in hiPSC-CMs but not in heterologous TSA201 cells (6). This result is consistent with the previous findings from Mehta et al. published in the *European Heart Journal* (7). More recently, LUM has also been shown to correct the phenotype of two additional missense mutations, A561T and N996I, generated by the gene-editing CRISPR-Cas9 (8). Taken together, these results suggest that LUM not only acts as a chemical chaperone in mutants of CF transmembrane conductance regulator (CFTR) proteins but also has a selective phenotypic correction on certain hERG mutants.

However, this is only an exciting result at the beginning. Through phenotypic analysis, the rescue of the G604S mutation may cause more severe prolongation of the QT interval, which is

Edited by:
Xiaofeng Yang,
Temple University, United States

Reviewed by:
Kazuharu Furutani,
Tokushima Bunri University, Japan
Kimberly R. Rebello,
Baylor College of Medicine, United States

***Correspondence:**
Jiangfang Lian
hjmpin@163.com

Specialty section:
This article was submitted to Cardiovascular Therapeutics, a section of the journal Frontiers in Cardiovascular Medicine

Received: *26 October 2021*
Accepted: *31 January 2022*
Published: *25 February 2022*

Citation:
Zheng Z, Song Y and Lian J (2022) What Is the Potential for Lumacaftor as a Chemical Chaperone in Promoting hERG Trafficking? Front. Cardiovasc. Med. 9:801927. doi: 10.3389/fcvm.2022.801927

shown as a prolonged action potential duration at 90% repolarization (APD90) (6). The researchers explained that following LUM, the enhanced trafficking of the mutant hERG channels produced a more pronounced dominant-negative effect. T634S, another hERG point mutation identified as a variant of uncertain significance (VUS), similarly causes intracellular trafficking defects of hERG channel protein that can be rescued by E-4031 rather than LUM (5 μM), indicating that LUM has a selective rescue effect in hERG variants (9). Moreover, LUM did not rescue the *KCNH2*-G601S trafficking mutation in HEK293 cells when administered alone or in combination with novel identified correctors (10, 11).

Obviously, the mutations of *KCNH2* in heterologous systems like HEK293 cells cannot be corrected by LUM, but in hiPSC-CMs, they can. Indeed, autologous disease-specific hiPSC-CMs have irreplaceable advantages over heterologous expression systems or animal models, and the most important of which is that they contain a variety of native cardiac ion channels (12), even if they are still immature, but have well-replicated cardiac electrical activity (13, 14). For the hERG channel, a critical ion channel that functions in the third phase of a cardiac action potential, hiPSC-CMs ensure its relatively accurate gating kinetics and intracellular maturation mechanisms, as well as complete function associated with the auxiliary subunits, β subunits encoded by *KCNE2* (12, 14). Additionally, in the study of O'Hare et al., three hERG variants could not be rescued by LUM in TSA201 cells (data showed only one R685P, and the other two variants were not shown); however, they were all be rescued in the hiPSC-CMs (6). This finding implies that hiPSC-CMs do provide a model advantage for LUM to work in the same mutation context. The model's benefits give us the confidence to conduct clinical translation (15).

The expression of homozygous hERG mutations alone cannot be corrected, whether in homologous or heterologous expression models. Furthermore, there is no indication that chemical chaperones, including LUM, affect the expression of homozygous mutation channels. In O'Hare et al.'s work, however, LUM's rescue of hERG-G604S induced a more serious clinical phenotype, which was attributed to the drug's stronger dominant-negative effect (6). The premise for this explanation is that the three mutants in their investigation are homozygous. When the two alleles are simultaneously mutated and expressed separately, the stable folding effects of LUM generate an approximate wild-type channel, resulting in a longer APD, indicating that the rescue effect of LUM is far less than that of the mutant gene interfering with the corresponding wild-type gene, thus causing deleterious effects. Actually, in their study, this explanation is vague. Since Mehta et al. have demonstrated that LUM affects heterozygous mutations, in this work, almost three variants can be rescued by LUM in hiPSC-CMs (6, 7). Previous studies have shown that when expressed as homozygous, the T634I mutation cannot be corrected, while T634S can, but only E-4031, not LUM, works (9, 16).

Interestingly, the conformation changes generated by certain mutations in the hERG channel may differ in the various mutation sites. As a result, LUM's selectivity appears to be confined not only to the greatly near-physiological replication provided by hiPSC-CMs and adverse hERG mutation types but also to specific mutations located at different positions throughout the full-length hERG channel structure. Point mutations in the pore domain of the hERG channel cause a more severe clinical phenotype than those in the N- or C-terminal and other transmembrane segments and are not easy to be corrected, according to functional studies (16). The evidence shows that LUM can correct A561V, G604S, and N633S located in the pore domain but not T634S, which is also in the same location (**Figure 1**, **Table 1**). Furthermore, the effect of LUM has not been evaluated for the same mutation location in different cell types. Therefore, attributing this selectivity to the different locations of diverse point mutations in the hERG channel is very difficult. The most plausible explanation is that the conformation of the hERG protein produced by certain individual mutations has such subtle differences that LUM can identify specific mutants while selectively maintaining protein structure. Taken together, the selectivity of LUM may only depend on the exposure of drug-binding sites of protein conformation induced by particular mutations, which is influenced by point mutations at different locations and intracellular environments.

In general, the intracellular mechanism by which LUM promotes the expression of misfolded proteins is unclear. The pharmacological mechanism of LUM has yet to be fully revealed, even in the case of CFTR, and the few studies in LQT2 are much less likely to give a persuasive and comprehensive insight into illuminating its pharmacological mechanism. LUM is generally thought to function primarily through co-translation with folding intermediates (17). As a typical protein conformational disease, mutated CFTR indeed provides a referenceable and available research model for others. In CFTR, indirect evidence suggests that LUM binds directly to the misfolded protein to stabilize its conformation, and then facilitates its escape from the strict cellular protein quality control, such as retention in the endoplasmic reticulum and degradation through the ubiquitin-proteasome system (18). The stability of the conformation enhances the anti-trypsin digestion ability of the full-length channel protein; that is, at the same time, the mutant protein is retained more under the action of LUM (10). Besides, LUM may weaken the main cytoplasmic stress pathways induced by mutation proteins, such as heat shock response (HSR), and thus reduce the expression of related molecular chaperones Hsp70, Hsp90, and others (19). LUM accomplishes this by competing with the most important intracellular protein folding factors, molecular chaperones, and preferentially binding to the misfolded hERG protein. These explanations, however, are only based on circumstantial evidence because there is no visual evidence for the intracellular binding of LUM to hERG proteins, let alone specific binding sites and binding timings. A cryo-electron microscopy structure of CFTR in complex with LUM supports a mechanism in which the correctors stabilize the first transmembrane domain (TMD1) at an early stage of biogenesis, preventing its premature degradation, and thereby allosterically rescuing many disease-causing mutations (20). We expect similar findings of the binding of LUM to hERG-specific domains.

Lumacaftor (LUM) needs to test the consequences of more variants in LQT2 induced by hERG mutations.

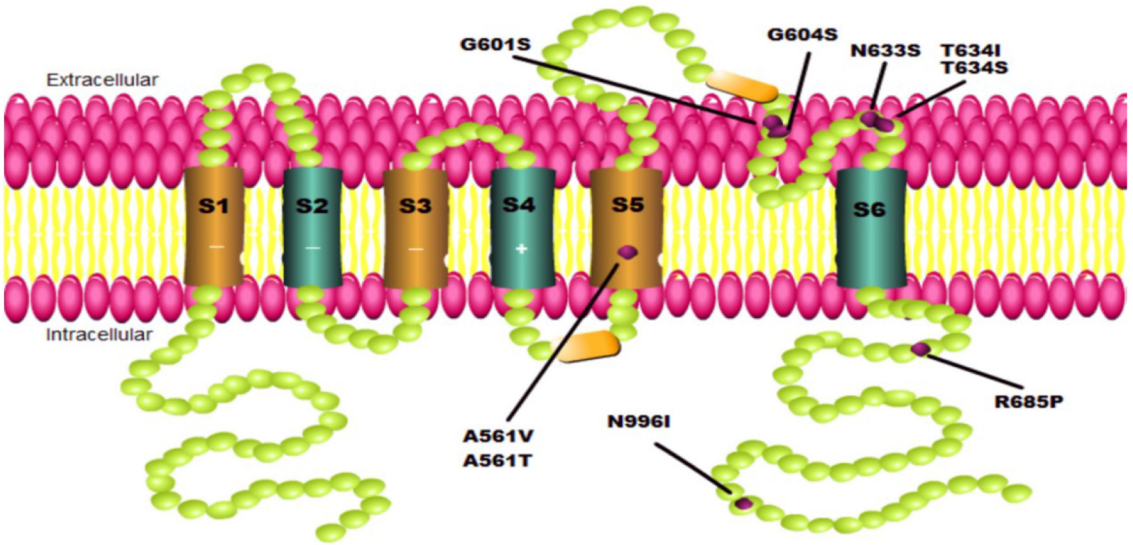

FIGURE 1 | Schematics of *KCNH2* mutations involved in this paper. Each green ball represents an amino acid. Each purple point represents one mutation located on the pore domain to cause a hERG channel trafficking defect.

TABLE 1 | The effect of the chemical chaperone Lumacaftor on different mutation sites of hERG full-length channel protein.

Mutations	Location	Generation	Model	Effect of Lumacaftor	References
A561V	Pore domain	Disease-specific patients	hiPSC-CMs	Correction of phenotype	(7)
G604S N633S R685P	Pore domain Pore domain C-terminal	Disease-specific patients	hiPSC-CMs	Prolonged APD90 (G604S) Correction of phenotype	(6)
A561T N996I	Pore domain Cytoplasmic tail	CRISPR-Cas9	hiPSC-CMs	Correction of phenotype	(8)
T634S	Pore domain	Transfection	HEK-293	No significant	(9)
T634I	Pore domain	Transfection	HEK-293	No test	(9, 16)
G601S	Pore domain	Transfection	CFBE41o*	No significant	(11)

**CFBE41o, Cystic fibrosis human bronchial epithelial cell line.*

Additionally, there are still problems in interpreting the result, making the translation from experiment to clinical practice difficult. According to the researchers, using gene-editing tools such as the Dual Integrase Cassette Exchange (DICE) or clustered regularly the interspaced short palindromic repeats (CRISPR)/Cas system in conjunction with high-throughput electrophysiological testing platforms, such as microelectrode array (MEA), to evaluate the role of LUM in multiple single variants of LQT2 may be efficient and beneficial. Understanding what determines the stereo-selectivity of LUM, on the other hand, may be more useful for developing novel specific chemical chaperones and achieving precision medicine. Together, considering the various phenomena presented by LUM, at least the following conclusions can be drawn:

1. Lumacaftor (LUM), as a chaperone for substrate proteins with such a broad stereo-selectivity, could have an impact on other protein conformation disorders.
2. For the same mutation, using two different cell platforms (HEK293 vs. hiPSC-CMs) may lead to different results in terms of translation and transcriptional effects.
3. Lumacaftor (LUM) has been proved to be effective against heterozygous mutations of the *KCNH2* gene. If the prolongation of APD90 of the G604S mutation can be explained by a strong dominant-negative effect, LUM is also effective for homozygous mutations.
4. The intracellular mechanism of LUM's rescue for various mutations in the hERG gene may be involved in the interaction factors during the maturation of hERG protein rather than only depend on mutation specificity.

5. Lumacaftor's (LUM's) selective rescue of different mutants of the same substrate protein reminds us that we should detect the effect of the drug on the hERG mutations as much as possible.

We thank O'Hare et al. for their further contribution to understanding in this regard.

AUTHOR CONTRIBUTIONS

ZZ: conceptualization, data curation, writing—original draft, software, and resources. YS: writing—review and editing. JL: conceptualization, writing—review and editing, and supervision. All authors contributed to the article and approved the submitted version.

FUNDING

This work was supported by the National Natural Science Foundation of China [Grant Number 81870255] and the Natural Science Foundation of the Zhejiang Province [Grant Number LY21H020001].

REFERENCES

1. Hartl FU, Hayer-Hartl M. Molecular chaperones in the cytosol: from nascent chain to folded protein. *Science.* (2002) 295:1852–8. doi: 10.1126/science.1068408
2. Yadav K, Yadav A, Vashistha P, Pandey VP, Dwivedi UN. Protein misfolding diseases and therapeutic approaches. *Curr Protein Pept Sci.* (2019) 20:1226–45. doi: 10.2174/1389203720666190610092840
3. He S, Moutaoufik MT, Islam S, Persad A, Wu A, Aly KA, et al. HERG channel and cancer: a mechanistic review of carcinogenic processes and therapeutic potential. *Biochim Biophys Acta Rev Cancer.* (2020) 1873:188355. doi: 10.1016/j.bbcan.2020.188355
4. Delisle BP, Anson BD, Rajamani S, January CT. Biology of cardiac arrhythmias: ion channel protein trafficking. *Circ Res.* (2004) 94:1418–28. doi: 10.1161/01.RES.0000128561.28701.ea
5. Smith JL, Anderson CL, Burgess DE, Elayi CS, January CT, Delisle BP. Molecular pathogenesis of long QT syndrome type 2. *J Arrhythm.* (2016) 32:373–80. doi: 10.1016/j.joa.2015.11.009
6. O'Hare BJ, John Kim CS, Hamrick SK, Ye D, Tester DJ, Ackerman MJ. Promise and potential peril with lumacaftor for the trafficking defective Type 2 Long-QT syndrome-causative variants, p. G604S, pN633S, and pR685P, using patient-specific re-engineered cardiomyocytes. *Circ Genom Precis Med.* (2020) 13:466–75. doi: 10.1161/CIRCGEN.120.002950
7. Mehta A, Ramachandra CJA, Singh P, Chitre A, Lua CH, Mura M, et al. Identification of a targeted and testable antiarrhythmic therapy for long-QT syndrome type 2 using a patient-specific cellular model. *Eur Heart J.* (2018) 39:1446–55. doi: 10.1093/eurheartj/ehx394
8. Brandão KO, van den Brink L, Miller DC, Grandela C, van Meer BJ, Mol MPH, et al. Isogenic sets of hiPSC-CMs harboring distinct KCNH2 mutations differ functionally and in susceptibility to drug-induced arrhythmias. *Stem Cell Reports.* (2020) 15:1127–39. doi: 10.1016/j.stemcr.2020.10.005
9. Al-Moubarak E, Zhang Y, Dempsey CE, Zhang H, Harmer SC, Hancox JC. Serine mutation of a conserved threonine in the hERG K channel S6-pore region leads to loss-of-function through trafficking impairment. *Biochem Biophys Res Commun.* (2020) 526:1085–91. doi: 10.1016/j.bbrc.2020.04.003
10. Van Goor F, Hadida S, Grootenhuis PD, Burton B, Stack JH, Straley KS, et al. Correction of the F508del-CFTR protein processing defect in vitro by the investigational drug VX-809. *Proc Natl Acad Sci U S A.* (2011) 108:18843–8. doi: 10.1073/pnas.1105787108
11. Veit G, Xu H, Dreano E, Avramescu RG, Bagdany M, Beitel LK, et al. Structure-guided combination therapy to potently improve the function of mutant CFTRs. *Nat Med.* (2018) 24:1732–42. doi: 10.1038/s41591-018-0200-x
12. Ma J, Guo L, Fiene SJ, Anson BD, Thomson JA, Kamp TJ, et al. High purity human-induced pluripotent stem cell-derived cardiomyocytes: electrophysiological properties of action potentials and ionic currents. *Am J Physiol Heart Circ Physiol.* (2011) 301:H2006–17. doi: 10.1152/ajpheart.00694.2011
13. Brandao KO, Tabel VA, Atsma DE, Mummery CL, Davis RP. Human pluripotent stem cell models of cardiac disease: from mechanisms to therapies. *Dis Model Mech.* (2017) 10:1039–59. doi: 10.1242/dmm.030320
14. Karakikes I, Ameen M, Termglinchan V, Wu JC. Human induced pluripotent stem cell-derived cardiomyocytes: insights into molecular, cellular, and functional phenotypes. *Circ Res.* (2015) 117:80–8. doi: 10.1161/CIRCRESAHA.117.305365
15. Schwartz PJ, Gnecchi M, Dagradi F, Castelletti S, Parati G, Spazzolini C, et al. From patient-specific induced pluripotent stem cells to clinical translation in long QT syndrome Type 2. *Eur Heart J.* (2019) 40:1832–6. doi: 10.1093/eurheartj/ehz023
16. Anderson CL, Kuzmicki CE, Childs RR, Hintz CJ, Delisle BP, January CT. Large-scale mutational analysis of Kv11.1 reveals molecular insights into type 2 long QT syndrome. *Nat Commun.* (2014) 5:5535. doi: 10.1038/ncomms6535
17. Okiyoneda T, Veit G, Dekkers JF, Bagdany M, Soya N, Xu H, et al. Mechanism-based corrector combination restores ΔF508-CFTR folding and function. *Nat Chem Biol.* (2013) 9:444–54. doi: 10.1038/nchembio.1253
18. Okiyoneda T, Barrière H, Bagdány M, Rabeh WM, Du K, Höhfeld J, et al. Peripheral protein quality control removes unfolded CFTR from the plasma membrane. *Science.* (2010) 329:805–10. doi: 10.1126/science.1191542
19. Yanda MK, Liu Q, Cebotaru L. A potential strategy for reducing cysts in autosomal dominant polycystic kidney disease with a CFTR corrector. *J Biol Chem.* (2018) 293:11513–26. doi: 10.1074/jbc.RA118.001846
20. Fiedorczuk K, Chen J. Mechanism of CFTR correction by type I folding correctors. *Cell.* (2022) 185:158–168.e11. doi: 10.1016/j.cell.2021.12.009

Conflict of Interest: The authors declare that the research was conducted in the absence of any commercial or financial relationships that could be construed as a potential conflict of interest.

Publisher's Note: All claims expressed in this article are solely those of the authors and do not necessarily represent those of their affiliated organizations, or those of the publisher, the editors and the reviewers. Any product that may be evaluated in this article, or claim that may be made by its manufacturer, is not guaranteed or endorsed by the publisher.

Advantages of publishing in Frontiers

OPEN ACCESS
Articles are free to read for greatest visibility and readership

FAST PUBLICATION
Around 90 days from submission to decision

HIGH QUALITY PEER-REVIEW
Rigorous, collaborative, and constructive peer-review

TRANSPARENT PEER-REVIEW
Editors and reviewers acknowledged by name on published articles

Frontiers
Avenue du Tribunal-Fédéral 34
1005 Lausanne | Switzerland

Visit us: www.frontiersin.org
Contact us: frontiersin.org/about/contact

REPRODUCIBILITY OF RESEARCH
Support open data and methods to enhance research reproducibility

DIGITAL PUBLISHING
Articles designed for optimal readership across devices

FOLLOW US
@frontiersin

IMPACT METRICS
Advanced article metrics track visibility across digital media

EXTENSIVE PROMOTION
Marketing and promotion of impactful research

LOOP RESEARCH NETWORK
Our network increases your article's readership